Sheffield Hallam University

A Sheffield Hallam University thesis

STRUCTURE AND PROPERTIES

OF

CARBON FIBRE REINFORCED
AROMATIC THERMOPLASTICS

A thesis submitted to the Council for National Academic Awards

in partial fulfilment of the requirements for the degree of

DOCTOR OF PHILOSOPHY

by

GARETH CHARLES McGRATH

Collaborating Establishment:

ICI plc,
Wilton Works,
Middlesbrough,
TS6 8JA.

Sponsoring Establishment:

Department of Metals and
   Materials Engineering,
Sheffield City Polytechnic,
Sheffield,
S1 1WB.

SEPTEMBER 1988

PREFACE

All the work reported in this thesis was carried out during the period for which the candidate was registered for a higher degree. No part of this has been submitted for a degree at any other polytechnic, university or college.

During the period 1986-87 the following modules of the postgraduate course 'Metallurgical Process and Management' were attended:

1. Numerical Methods and Programming

2. Corrosion and High Temperature Resistant Materials

3. Heat Treatment of Steels

4. Stainless Steels

A one day conference on Fracture Mechanics was attended on 4 December 1986 at the Kelvin Conference Centre, Glasgow.

In 1986 a seminar was presented on this work to staff and research assistants of the Sheffield City Polytechnic.

In 1988 a paper based on this work was published:

G. C. McGrath, D. W. Clegg and A. A. Collyer, 'The mechanical properties of compression moulded recon-stituted carbon fibre reinforced PEEK (APC-2)'. Composites 19,3,(May 1988) 211-215.

(See Appendix 3 for copy).

ACKNOWLEDGEMENTS

provide the foundations of my education; and their ever-present support over the years.

Finally, to Elaine my wife, without whom this work would still be on the drawing board, all my love.

STRUCTURE AND PROPERTIES OF CARBON FIBRE REINFORCED AROMATIC THERMOPLASTICS

G. C. McGrath

ABSTRACT

In common with all composite materials, Aromatic Polymer Composite-2 (APC-2) is inherently expensive and as such any reclaimed material is potentially extremely valuable. In this work, pieces varying from 6.35-25.4mm square (0.25-1.0inch) were cut from APC-2 single ply prepreg of thickness 0.125mm and compression moulded into panels 150mm square, with the thickness controlled to meet the requirements of subsequent characterisation. Further work was carried out on panels of the same dimensions moulded from squares cut from 8 ply preconsolidated APC-2, the size of these squares ranging from 10-25.4mm square. The flexural, tensile and compressive mechanical properties, fracture and impact toughness, and creep behaviour of these composites were determined, as a function of particle size. Finally, the potential for moulding was assessed. Results from tensile and flexural tests show that the variations in the tensile and flexural moduli of the composites increase linearly with particle size. Using suitable modifications of planar reinforcement theory to produce a quasi-isotropic theory, an accurate prediction of the experimental values is possible, from the Modulus Reduction Factor [MRF]. A similar approach with respect to the experimental strength can only be made if the mode of failure is known. The fracture toughness of the composite moulded from single ply prepreg was found to be greater than that of continuous fibre reinforced APC-2 and increased with decreasing particle size over the size range examined. Fractographic analysis of this phenomenon revealed several toughening mechanisms: Polyetheretherketone (PEEK) rich zones act as crack arresters; fibre bundle and particle bridging of the crack increase the work to fracture. Impact toughness is greatly enhanced over injection moulded composites for similar reasons. The creep property profile is very promising and shows retention of the creep resistance of PEEK and carbon fibre. The formability shows a possible opportunity for component manufacture otherwise impossible at present.

C O N T E N T S

STRUCTURE AND PROPERTIES OF CARBON FIBRE
REINFORCED AROMATIC THERMOPLASTICS

INTRODUCTION

Over the past few years there has been a significant advancement in the development of thermoplastic polymers as matrix materials for continuous fibre reinforced composites.[1-7] This has been prompted by the many potential advantages that thermoplastics offer when compared with thermosets as a composite material.

The advantages of thermoplastic polymers can be defined in four major groups. Firstly, linear chain polymerisation produces a prepreg of indefinite shelf life. Secondly, the thermoplastic phase is in many cases extremely tough, and conveys enhanced damage tolerance to the final product. Thirdly, a degree of crystallinity will promote excellent environmental resistance. Finally, being a thermoplastic polymer, shorter cycle times, improved repairability and scrap reclaim are all distinct advantages which translate to an economic and versatile component.

In order to utilise fibre reinforced thermoplastic composite materials to their full potential, the performance characteristics of such materials during their entire service life must be known. This requires analytical and experimental methods which predict changes in mechanical, physical, thermal and chemical properties caused by exposure to service conditions.

Initial attempts to utilise thermoplastic polymers as composite matrices involved amorphous thermoplastics such as the polysulphone family.[8] Continuous reinforcing fibres were readily solution impregnated to form a preimpregnated tape, usually termed prepreg. However, this initial advantage rapidly turned sour as a composite

structure manufactured from the prepreg was severely attacked by the same solvents as were used in the initial fabrication.[9,10] It is unlikely that any such amorphous thermoplastic will exhibit sufficient chemical resistance properties for use in the rigorous environments required of high performance composite. Also, reinforcing a crystalline thermoplastic matrix gives a greater enhancement of properties than reinforcing an amorphous matrix.[11] Table 1.

The latest developments have therefore been towards semi-crystalline thermoplastic polymers such as polyphenylene sulphide (PPS) and polyether ether ketone (PEEK), which have been examined for their potential as matrices for continuous fibre reinforcement.[4,5,10,12] Unfortunately, the chemical resistance of these polymers prevents conventional solution impregnation techniques to produce prepreg.

One impregnation method that has proved successful with semi-crystalline polymers is a film stacking method.[1,7] This is a method for impregnating fibres with thermoplastic by compression moulding. Fibre impregnation with PPS film has been very promising owing in part to its sharp melting point.[10]

In 1982, ICI introduced Aromatic Polymer Composite APC-1 based on 60% by weight of continuous carbon fibre reinforcement in a PEEK matrix; to be followed in 1982 by APC-2 based on 68% by weight of continuous carbon fibre reinforcement in a PEEK matrix. Impregnation technology is applied to produce a prepreg which is about 0.13mm thick containing highly collimated, high strength carbon fibres.[13,14] The prepreg tapes are then laid up and moulded to form sheets suitable for processing by hydrorubber forming, press forming, roll forming, diaphragm shaping or vacuum forming.

From these processes scrap is generated and it is with a view to

reclaiming and utilising this scrap that the following work is undertaken.

1. LITERATURE

In the early 1970's, aerospace companies began to consider and evaluate carbon fibre reinforced thermoplastics as carbon fibre reinforced epoxy matrix composite replacements for selected components. The anticipated improvements which motivated the programmes were increased toughness, scrap reclaim, unlimited shelf life and rapid cycle times.

The initial evaluations with amorphous polysulphones showed considerable promise,[1,2,8] as they were easily incorporated as the matrix in prepregs via solvent impregnation. Unfortunately, it was the solubilities of the polymer in certain solvents which led to the downfall of these materials and significantly delayed the appearance of carbon fibre reinforced thermoplastic products. Parts made with carbon fibre reinforced polysulphones are susceptible to solvent attack by cleaners and lubricants such as methylene chloride and aircraft hydraulic fluids.

Polyetherimide (PEI) is a relatively new addition to the range of amorphous thermoplastics, but is still susceptible to solvent attack. The combination of PEI with carbon, glass and aramid continuous fibres could realise a breakthrough for composites in the field of general engineering if sensitivity to solvents is not critical. PEI meets the requirements for fast fabrication at low cost for large scale transport, marine and mechanical applications.[15,16] Clean processing, indefinite shelf life and cohesive bonding offer additional advantages.

- 3 -

When the poor fracture resistance and damage tolerance of all high

performance thermoset matrix carbon fibre composites was generally

recognised in the late 1970's, the search for tougher matrix

systems was resumed. Unfortunately, the known routes to improve

the toughness of thermosets all introduce weaknesses such as

reduced performance temperature range and lower compression pro-

perties induced by lower matrix modulus. Hence a renewed interest

in thermoplastics as significantly tougher composite matrices.

1.1 CRYSTALLINE THERMOPLASTICS

Recently, semi-crystalline thermoplastic polymers such as poly-

phenylene sulphide (PPS) and polyether ether ketone (PEEK) have been

studied for their potential as matrices for continuous fibre rein-

forcement. Unfortunately, the chemical resistance characteristics

of these thermoplastics prevents conventional solution impregnation

techniques. Thus, the advantage of chemical resistance of semi-

crystalline thermoplastics has been a disadvantage in developing a

process for intimate wetting and impregnation of continuous fibres.

The development of thermoplastics has prompted extensive research

into toughened thermoset systems and such composites are at present

under extensive evaluation within the aerospace industry.

1.1.1 POLYPHENYLENE SULPHIDE

The structure of PPS consists of a polymer backbone of alternating

disubstituted aromatic rings and divalent sulphur atoms.
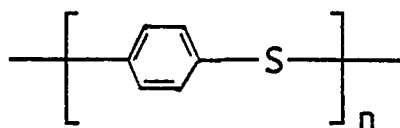
The molecular weight can be systematically increased in a controlled

manner by heating the polymer powder in air at a temperature below

285°C, the melting point. The mechanism for the molecular weight

increase is complex and involves both cross linking and chain

extension.[17]   This ability to increase the molecular weight of PPS leads to the production of a variety of resin products which permit its use in applications ranging from corrosion resistant coatings to high performance fibre filled injection mouldings. However, the continuous use temperature is only around $150^{\circ}C$[12] and the presence of sulphur is undesirable when considering toxic gas emission on burning.

1.1.2 POLYETHER ETHER KETONE

The development, by ICI, of a process to produce carbon fibre rein-forced thermoplastic PEEK undirectional prepreg has attempted to meet the demands of an aerospace industry where there is a growing need for new polymers which have higher service temperature, better chemical resistance and improved fire and smoke performance. These demands are becoming more pronounced with the ever-increasing legislative pressures and public opinion.

The continuous use rating of PEEK is $200^{\circ}C$,[18] far more acceptable to the aerospace industry than previous thermoplastic matrix compo-sites.   As it is crystalline in nature[19] it is resistant to acids, alkalis and organic solvents, and responds very well to rein-forcement with such fibrous material as carbon or glass, with conse-quent further enhancement of properties[20].

The excellent matrix properties of PEEK can be used to good effect in the production of composite materials based on glass or carbon fibre reinforcements.   Those composites based on carbon fibres are unique because of the extent to which the theoretical properties of this particular fibre can be exploited and utilised to maximum advan-tage.

The structure of PEEK is:

- 5 -
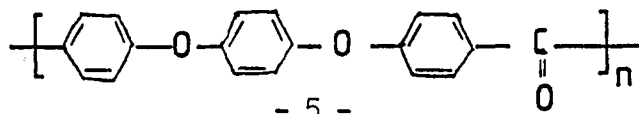
From these developments aromatic polymer composites have evolved which are available as preimpregnated tapes, from which laminates may be constructed.[14]

1.2   AROMATIC POLYMER COMPOSITE

Aromatic polymer composite, APC-2, is prepared as a preimpregnated tape containing 60% by volume, 68% by weight of continuous collimated, high strain carbon fibre impregnated with PEEK, and therefore APC-2 has all the advantages offered by the PEEK matrix, plus the exceptional degree of reinforcement afforded by the carbon fibre reinforcement.

However, aromatic polymer composite materials are not just a mixture of reinforcing fibres and polymer.   The fibres must be evenly distributed in the polymer matrix with strict control of the interface between the fibre and the polymer.[21]

The choice of PEEK as the polymer phase is important because, of all thermoplastic polymers PEEK has a unique balance of properties with particular reference to:

(a) Environmental Resistance - the only common solvent to attack PEEK is concentrated sulphuric acid, and PEEK is resistant to all solvents commonly found in the aerospace industry.[18,22]

(b) Temperature Resistance - PEEK shows a melting point of 343°C, with continuous use rating at 200°C.   However, in common with all crystalline polymers it shows a glass transition below the melting point which causes the reduction in properties around 140°C. Such properties are satisfactory for the majority of aerospace applications, although higher duty applications may require the introduction of systems with a higher transition temperature.   It is important to note that with crystalline polymers valuable properties remain beyond the transition temperatures, unlike the

thermosetting and non-crystalline thermoplastics where prope

rapidly fall to zero once the decomposition or transition te

ature respectively is exceeded.[18]

(c) Resistance to creep, fatigue, impact and thermal ageing.[18,23,24]

(d) Resistance to burning, with low smoke emission.[14,18]

(e) Resistance to weathering and erosion.[18]

(f) Improved fracture toughness.[25]

(g) Adhesion, as PEEK is a good hot melt adhesive.[13]

In APC-2 the fibres are sufficiently wetted by the polymer and the

interface incorporates an element of epitaxial crystallisation such

that the polymer appears as a natural extension of the fibre, and

the bond between the polymer and the fibre is a vital factor in the

production and property profile of APC-2.

1.3 THE PRODUCTION OF APC-2

In order to appreciate fully how APC-2 is produced, it is instructive

to examine the way in which its constituents are processed. As

previously stated APC-2 is a composite of carbon fibres and PEEK.

1.3.1 THE CARBON FIBRE

It is more than twenty years since high performance carbon fibres

were developed to meet the important needs of the aircraft industry

which was demanding a lightweight construction material, stronger

and stiffer than the metal alloys then available. Since then

applications of carbon fibres have become much more widespread,

extending into the sports and leisure and general industrial

scene.[26,27]

1.3.1.1 Requirements

Graphite has a hexagonal close packed crystal structure which in

the two directions of the basal plane is strong and stiff, while

in the third direction (perpendicular to the basal plane) it is

weak and compliant. High performance carbon fibres must therefore make use of the strong and stiff directions without suffering from the poor properties of the weak direction.

The graphite layer planes must be aligned parallel to the fibre axis if high strength and modulus are to be achieved, but this would accentuate the poor shear and tensile strength between planes. A strong fibre microstructure would most likely consist of small elongated grains, and a great deal of valuable research has shown that fibres basically consist of small wrinkled ribbons aligned approximately parallel to the fibre axis.[28]

A simple idealised composite is schematically represented in Figure 1. This shows a single high modulus fibre in a more ductile matrix, the parallel lines acting as strain markers.

If the sample is now stressed uniaxially in tension, both the fibre and the matrix dilate, but because of a mismatch in moduli, concentric shear stress gradients are generated and three initial modes of failure are possible:

(a) failure of the matrix in tension

(b) failure of the fibre in tension

(c) fibre-matrix interfacial debonding via shear failure.

It is the third mode of failure which is of greatest concern in the manufacture of composite systems because a low maximum shear stress at the interface is indicated; and also the interfacial bond strength determines the sensitivity of a component to flaws. So, when manufacturing the carbon fibres this problem must be overcome.

A measure of the tendency to fail in interfacial shear is achieved by the short beam shear strength test.

1.3.1.2 Manufacture

Carbon fibres are prepared by a variety of methods, from numerous

starting materials, and the production route determines their ultimate character.[29]

However, most high performance fibres are manufactured from polyacrylonitrile textile precursor by a process involving controlled pyrolysis in discrete stages: (Figure 2)

(a) Oxidation at 200-250°C.

(b) Carbonisation at 1,000°C or above in a non-oxidising atmosphere to produce a high strength fibre.

(c) Graphitisation at 2,500-3,000°C in a non-ozidising atmosphere to produce a high modulus fibre.

(d) Surface treatments to modify the fibre surface by carefully controlled oxidation to promote good interfacial bonding with the PEEK in subsequent production. It is important to optimise this bond strength, because if the bond is too good the advantages of fibre reinforcement are lost as the composite tends to become brittle.

The properties of the fibres are determined by the precise temperature used in the manufacturing process. Stiffness or modulus increases continuously with manufacturing temperature, whereas strength reaches a peak then decreases as the process temperature is increased beyond this point as shown in Figure 3.

This behaviour gives rise to two types of fibre:

Type I, heated to 2,600°C and having the higher modulus (380 - 448 GPa) and somewhat lower ultimate tensile strength (1330 - 2070 MPa),

and Type II, heated to approximately 1,500°C which have a higher tensile strength (2410 - 3100 MPa) and a somewhat lower modulus (240 - 310 GPa).

- 9 -

The inverse relationship between modulus and strength can be modified by high temperature stretching, as practised in the U.S.A.

Therefore, it is possible to produce a family of fibres with properties tailored to the application.

The surface treatment is all important to the production of APC-2 and for successful production four major observations need to be considered.[30]

(a) The original, as formed, carbon fibre surface appears to be weak under shear loading. Interfacial failure within the outer fibre surface layers is predominant.

(b) Surface treatments are effective in increasing the shear loading capability of the fibre through a two part mechanism. The surface treatments remove the existing surface, leaving behind a layer more structurally sound and capable of sustaining shear loading, as well as adding surface groups, primarily oxygen, which interact with the polar groups in the matrix. The type of treatment that is most effective depends on the fibre, and the matrix materials and the chemical mechanisms by which a good coupling is achieved are of great importance and subject to. much commercial secrecy. The difference in the mechanical properties of the same composites produced by different manufacturers is often due to variations in the fibre treatment.

(c) Increases in surface area do not occur with surface treatments.

(d) Fibre treatments change the mode of interfacial failure from weak frictional sliding to matrix interfacial failure.

1.3.2 POLYETHER ETHER KETONE, PEEK

PEEK, chemically identified as poly (oxy-1, 4 phenylene-oxy-1, 4-phenylene-carbonyl-1, 4-phenylene)[31] is a melt processable aromatic polymer.

1.3.2.1 Viscosity

In polymer science it is not the absolute viscosity of a solution or solvent that is of particular interest, but the increase in viscosity attributable to the dissolved polymer. Therefore, in the viscometry of polymeric solutions, it is some expression of relative viscosity that is useful. The relative viscosity, ηr, is defined as the quotient of the viscosity of the solution, ηs and the viscosity of the solvent, ηo:

$$\eta r = \eta s / \eta o$$

Another measure of the increase in viscosity by a high molecular weight solute is the specific viscosity, ηsp:

$$\eta sp = \eta r - 1$$

Two additional quantities useful in viscometry are the reduced viscosity, ηred, defined as $\eta sp / C$ and the inherent viscosity (IV), defined as $\ln \eta r / C$. C being the concentration and thus the relative viscosity of a polymer solution is concentration dependent, so that a useful viscosity value is the limiting one when either $\eta sp / C$ or $\ln \eta r / C$ is extrapolated to zero concentration. This quantity is termed the intrinsic viscosity, or the limiting viscosity number, $[\eta]$. Since the relative viscosity is dimensionless, the units for $[\eta]$ are those of reciprocal concentration.

1.3.2.2 Historical Development

The first synthesis of a wholly aromatic polyether ketone was reported by Bonner,[32] who obtained a polymer of low molecular weight (inherent viscosity, IV, 0.18) by Friedel-Crafts polycondensation (1), using

nitrobenzene as a solvent and aluminium chloride as a catalyst.

(1) [reaction scheme: diphenyl ether + ClOC–⟨⟩–COCl → [—⟨⟩–O–⟨⟩–CO—]]
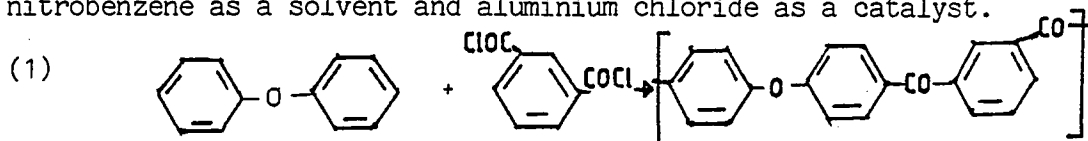
Goodman[33] and his co-workers obtained similar products by analagous

reactions and were the first to report a polymer of structure A,

synthesised by the reaction (2), using methylene chloride as the

solvent.   The inherent viscosity, IV, being 0.5.

(2) [reaction scheme: ⟨⟩–O–⟨⟩–COCl → [—⟨⟩–O–⟨⟩–CO—] A]

Another synthesis of this same polymer was by Iwakura,[34] who also

observed that the polymer was insoluble in all the usual organic

solvents.

This insolubility, being highly desirable in the final product, presents

a serious synthesis problem, because the molecular weights that can

be obtained in such solvents is limited.   This is because the growing

chains crystallize out from the polycondensation systems as shown by

Attwood and his co-workers,[35] who also produced Table 2, which inter-

relates the various viscosity terms.

Iwakura used phosphoric acid as the solvent for reaction (3), which

presumably dissolved the polymer by protonation of the carbonyl groups.

(3) [reaction scheme: ⟨⟩–O–⟨⟩–CO₂H → [—⟨⟩–O–⟨⟩–CO—] A]
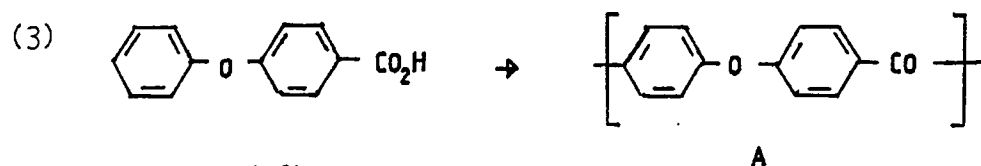
However, Marks,[36] devised a more effective acid solvent system in

that liquid hydrogen fluoride was found to be an excellent solvent

for polyarylether ketones generally and these solutions are yellow,

which indicates protonation.   Simultaneously the BF_3HF complex was

an excellent catalyst for polycondensation (1) or (2).

This synthesis produces polyarylether ketones of high molecular weight,

with IVs in the range 1.02-2.76. Dahl[37] has extended this synthesis emphasising the importance of molecular weight, while demonstrating that for polymers like A, an IV $\geqslant 0.8$ was essential to develop a useful degree of toughness in partially crystalline specimens made by conventional melt fabrication techniques.

An alternative synthesis is in principle provided by the polyarylether synthesis put forward by Johnson and his co-workers.[38] Unfortunately they did not obtain polymers of high molecular weight due to the premature crystallization from the dipolar aprotic solvents such as dimethyl sulphoxide or sulpholane. This type of solvent was chosen because protic solvents cannot be used for polycondensations (4) or (5), thus accentuating the solvent problem.

(4)

(5)
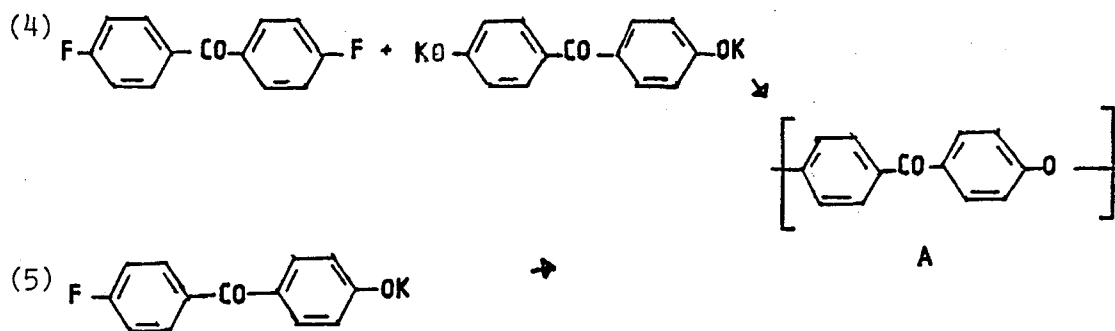
They reported a family of crystallizable polymers prepared in sulpholane or dimethyl sulphoxide. These tended to be brittle unless obtained in the amorphous form, a clear indication that the polymers made in this way, such as some of the polyether ketones, which develop substantial crystallinity were of low molecular weight.

The problems of preparing polyarylether ketones of high molecular weight can be overcome by the use of specific diaryl sulphones as the polycondensation solvents at temperatures close to the polymers melting point, as reported by Attwood and his co-workers.[35]

1.3.2.3   Synthesis of polyether ether ketone

Atwood and his co-workers,[35] found that tough polyarylether ketones

- 13 -

can be obtained by the polycondensation of bis-4-halogenophenyl ketones with the potassium salts of bis-4-hydroxyphenyl ketones at 280-340°C using certain diaryl sulphones as solvents for the poly-condensation (4). Under the same conditions, complications arose in polycondensation (5).

1.3.2.3.1 Polycondensation (4). The partially dehydrated bis-potassium salt is mixed with the required amount of diphenyl sulphone with agitation. This mixture is then heated to 200-240°C in a nitrogen atmosphere while stirring, and evacuating the vessel to 30mm Hg to produce a slurry of dehydrated bis-phenoxide. A slight excess of bis-4-fluorophenyl ketone is added with the remainder of the solvent to control the molecular weight and the mixture heated to 335°C for 2-3 hours. The polymer is isolated as below.

1.3.2.3.2 Polycondensation (5). The fluorophenoxide plus a small amount of bis-4-fluorophenyl ketone, to control the molecular weight, and sufficient diphenyl sulphone to produce the desired concentration of polymer (generally 30-50%) is heated with stirring under a nitrogen atmosphere at 335°C for 2-3 hours.

1.3.2.3.3 Isolation. Upon cooling, the viscous melt sets hard. The product is powdered and extracted with boiling methanol, boiling water and methanol, and repeated three times round this cycle. The polymer is dried in an oven overnight at 140°C, to produce yields of about 98% theoretical.

Although there is no evidence for structural anomalies in the poly-ether ketone made, synthesis by the latter route, i.e. by the polycon-densation of the fluorophenoxide, gave products containing some gel and soluble polymer in which the chains appear to be branched.

Attwood and his co-workers[35] report several different polyaryl ether ketones, giving almost identical x-ray diffraction patterns,

and in the unit cells of these polymers ether and carbonyl linkages are interchangeable. The series was built up by the reaction of 4, 4'-difluorobenzophenone or 1, 4-bis (fluorobenzoyl) benzone, with the potassium derivatives of several bis-phenols in diphenyl sulphone.

Polyether ether ketone, PEEK, is prepared from 4, 4'-difluorobenzophenone and the potassium derivative of the bis phenol,

$$HO \quad - \hspace{-2pt}\langle\rangle\hspace{-2pt} - \quad OH$$
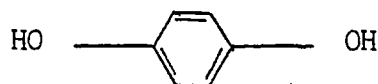
1.3.3 APC-2

The major problem to be overcome is the impregnation of the carbon fibre with PEEK to produce a prepreg which will allow industry the versatility it demands at a cost effective level, permitting these composites to be considered as aerospace alternatives. The technical problems have been approached from many angles: solution impregnation,[39] powder impregnation,[40] and melt coating,[41] have all been attempted.

The first commercial continuous fibre thermoplastic prepreg was introduced in 1982[42] from ICI, based on carbon fibre impregnated with PEEK and designated APC-1[43]. This was superseded in 1984 by APC-2 [44] in which the carbon fibre content was increased to 68% by weight from 60% by weight.

The process is a proprietary fibre impregnation technology technique[45] capable of giving a fully impregnated product with fibres from 5mm in length to continuous.

The most obvious properties of composite materials derive from the reinforcing fibres. The PEEK phase is present principally as a means of transferring loads from the structure into the fibres. The efficiency with which the PEEK phase can perform this duty depends

on the nature of the interface between the PEEK and the reinforcement, and it is the specially developed interface science together with the impregnation process that results in negligible void content. This optimisation of the microstructure promotes the maximum utilisation of matrix properties within the composite.

Thus, the reinforcing carbon fibre and PEEK matrix form a symbiotic relationship with the fibre taking the load and the PEEK protecting the fibre.

1.4   THE MACROSTRUCTURE OF APC-2

The main consideration here is orientation of the layers of fibres within a structure.

The orientation of each layer of laminated structure is easily defined with respect to a control axis. To identify the construction of such a laminate it is necessary to indicate the ply orientation with respect to the control axis and the number of such laminates. Thus 0_4 indicates that four plies are laid up with their axes parallel to the control axis. By contrast 90_4 indicates that the four plies have axes perpendicular to the control axis.

A set of brackets indicates a repeated sequence, the numerical suffix being the number of times that sequence is repeated. A further suffix, s, indicates that the lay up is symmetrical about the central axis, e.g. $(0, 90)_{2s}$ expands to

0, 90, 0, 90, | 90, 0, 90, 0

Symmetry about a central axis is essential when constructing laminates from the anisotropic prepreg, otherwise buckling may result from the thermally generated residual stresses.

In the case of a symmetric lay up with an odd number of plies, the central ply which is not repeated is indicated by a bar, e.g. $(0, 90, \bar{0})s$

expands to

$$0, \ 90, \ 0, \ 90, \ 0$$

The quasi-isotropic laminate is popular, having approximately uniform properties in all directions in the plane of the sheet, e.g. $(+45, \ 90, \ -45, \ 0)_{Ns}$ or $(0, \ 90, \ +45, \ -45)_{Ns}$ where N is any number.

For convenience a woven cloth is identified as 0/90 or ±45.

1.5   THE PROPERTIES OF APC-2

The properties of APC-2 are well established and tabulated in Appendix 1.   They are indicative of a composite system that has a very high efficiency of fibre wetting.

1.5.1.   STIFFNESS

For engineering design purposes a simple study of stiffness at short time scales and ambient temperatures is insufficient.

Based on Dynamic Mechanical Analysis studies[13] it is possible to deduce that the stiffness of APC-2 does not vary significantly in the temperature range $-160 - +120^{\circ}C$.   However, because PEEK undergoes a glass transition at $143^{\circ}C$, above that temperature the stiffness falls significantly in a lay up such as $(+45, \ -45)_N$, where the properties are resin dominated.   Despite this significant drop, the stiffness of a uniaxial (and thus fibre dominated) lay up is not greatly affected and because the PEEK is semi-crystalline, a very good balance of properties is retained until close to the melting point (Figure 4).

1.5.2   STRENGTH

It is easy to visualise how fibres provide strength in tension, but in compression there is a natural tendency for the fibres to buckle unless they are supported by a stiff resin.   Indeed, the very ability of the resin to yield, while enhancing the toughness of the composite may slightly compromise the compressive strength.   Therefore the

compressive strength is generally lower than the tensile strength.

1.5.3 CREEP IN THERMOPLASTICS

Creep is an important engineering problem, and thermoplastic resins are not renowned for good creep resistance, particularly the early plastic materials which were not developed principally as structural materials, e.g. polyethylene and polypropylene.

There is not a method available at present which is capable of predicting long term behaviour from the properties and composition of the constituents,[46] and despite its immense practical importance, the connection between creep and fracture initiation has received very little attention.

However, Hartness[4] has shown that carbon fibre reinforced PEEK has superior creep resistance to the 'state-of-the-art' carbon fibre reinforced epoxy systems.

APC-2 demonstrates virtually no creep at ambient temperatures when axially loaded, and even when loaded transverse to the fibre axis, the most susceptible configuration, the creep response is low.[47]

1.5.4 TOUGHNESS

Toughness and durability are the most critical properties of any material with respect to confidence in it for structural components and yet they are not easy to define.

The need for a laboratory test has produced the Instrumented Impact Test and many authors have documented the developments.[48-56]

During recent years instrumentation has been developed significantly; two reasons are clear for motivating this activity.

First, the relative ease and low cost in using a computer for handling and analysing large amounts of data.

Second, the technical understanding of toughness for thermoplastics remains imperfect.

The instrumented falling weight impact test does provide much additional information. The force-time curves are often complex and encompass several deformation and fracture events. Hence the previously adopted total energy measurement fron non-instrumented tests,is seen to be attributable to many events, not all of which relate to material behaviour.[56]

In keeping with other experimental work in this report, the system employed was that of ICI, as described by Hooley and Turner,[57] which gives a peak force, corresponding to the first breaking of fibres on the back surface; the initiation energy for failure and finally failure energy.

A more detailed examination of samples, subjected to low energy impacts, using ultrasonic C-scan techniques coupled with microscopic examination indicates that some damage is caused within the sample before the peak force is reached. This damage consists of cracks in the transverse plies and delamination between the plies. There are two aspects of delamination to be considered:

(a) If a sample suffers extensive delamination a large increase in surface area occurs which requires significant energy, so high delamination and high energy absorption are inter-related. Thus, increasing the delamination and debonding of the fibres is a good method to enhance energy absorption in a composite designed as a one shot absorber.[58]

(b) Alternatively, any partial delamination seriously affects the subsequent strength, which is particularly relevant when designing structures to resist accidental damage and many tests have been developed to measure this residual strength, usually in compression.[59]

Figure I of Appendix 1 being produced to illustrate the properties of APC-2.

1.5.5 FRACTURE TOUGHNESS

In respect of damage tolerance it is therefore the resistance to delamination which is of major importance and this has been the basis of research founded on tests such as the double cantilever beam,[60] where the energy required to propagate a crack between two plies can be measured directly.

Original work by Hartness[4] and Carlile and Leach[24] on carbon fibre reinforced PEEK produced results for the interlaminar strain energy release rate which were an order of magnitude greater than for the epoxy systems.   These results have since been substantiated by Donaldson.[23]   The resistance to delamination appears to be associated with the ductile character of PEEK.

Carlile and Leach[24] indicate that the high resistance to crack propagation is one reason for the good damage tolerance as exemplified by the retention of compressive strength after impact.

Although the matrix may be tough, this toughness is not always realised in the composite, indeed short fibre additions to a tough matrix may result in a moulding which will shatter upon impact.[61]   The most pronounced problems are the geometry of the resin phase and the con- straints imposed upon the resin by the fibres.

Fracture mechanics suggests that the thin layers will be tougher than the thick ones, which prompted a hypothesis of a criterion for toughness in composites.[19]   This is based upon comparing the plastic zone size of the resin phase with the characteristic thickness of the resin. However, the criterion is beset with difficulties as these thin layers are subject to thermal stresses induced during fabrication causing warp in an unbalanced layup.

The double cantilever beam (DCB) test is basically the controlled propagation of a pre-positioned crack by means of Mode I stressing. Data so collected can be used to assess G_{IC}, the critical strain energy release rate; there are numerous data reduction methods put forward and the most important are reviewed here.

1.5.5.1   The Area Method

This method is based on the definition of G_{IC} proposed by Irwin.[62]

$$G_{IC} = -\frac{1}{b} \frac{du}{da} \qquad (1.1)$$

where   u is the total strain energy stored in the test specimen

   b is the crack width

   a is the crack length

   du is the change in strain energy due to crack extension from a to a + da, is the area between loading and unloading curves (dA) on a load displacement plot from the DCB test.

$$- du = dA = \tfrac{1}{2} (Pd\delta - \delta dP) \qquad (1.2)$$

where P is the applied load,

   δ is the resultant deflection

Combining (1.1) and (1.2):

$$G_{IC} = \frac{1}{b} \frac{dA}{da} = \frac{1}{2b} \left(\frac{Pd\delta}{da} - \frac{\delta dP}{da} \right) \qquad (1.3)$$

This same approach is also applicable to the case of finite crack extension and provides the basis for a straightforward data reduction scheme.

A typical DCB plot is presented in Figure 5(a), at P, the crack starts extending, simultaneously the load falls off to P_2, whereupon the beam is unloaded, the crack having grown from a to a + Δa.   The loss of strain energy due to this crack extension is the area, Δ A, between the loading and unloading curves.   For cases in which the load

- 21 -

deflection curve during crack propagation can be approximated by a straight line one can determine the critical strain energy release rate, G_{IC}, from the relationship.

$$G_{IC} = \frac{1}{b} \frac{\Delta A}{\Delta a} = \sum_{i=1}^{N} \frac{1}{2b\Delta a} (P_1 \delta_{2i} - P_2 \delta_{1i}) \qquad (1.4)$$

An average value of G_{IC} can be determined by measuring P_1, P_2, δ_1 and δ_2 for a series of N crack extensions of length Δa. Thus:

$$G_{IC} = \frac{1}{2bN\Delta a} \sum_{i=1}^{N} (P_{1i} \delta_{2i} - P_{2i} \delta_{1i}) \qquad (1.5)$$

Therefore, in the case of Figure 5(b), where the crack has propagated by cleavage, the load decreases instantaneously, with no increase in deflection.

$$G_{IC} = \frac{1}{2b\Delta a} [\delta(P_1 - P_2)] \qquad (1.6)$$

When the loading and/or unloading curves are non linear then the G_{IC} values can be determined by measurement of the area between the two curves.

1.5.5.2 Compliance Method based on Linear Beam Theory

As discussed by Wang[63] this method only applied if the material is linear elastic and the beam displacement is small.

The theory assumes that each cracked half behaves as a conventional beam as illustrated in Figure 6 and therefore:

$$\delta = BPa^3 \qquad (1.7)$$

where B is a constant defined by:

$$B = \frac{64}{E_x^b bh^3} \qquad (1.8)$$

where E_x^b is the effective bending modulus in the axial direction of a cantilever beam of thickness h/2.

Combination of (1.3) and (1.7)

$$G_{IC} = \frac{3BP^2a^2}{2b} = \frac{3P\delta}{2ba} \qquad (1.9)$$

Therefore, for stable crack growth, as is usually found in displacement controlled tests on ductile materials, G_{IC} is given by:

$$G_{IC} = \frac{3BP_c^2a^2}{2b} \qquad (1.10)$$

or

$$G_{IC} = \frac{3P\delta_c}{2ba} \qquad (1.11)$$

where P_c is the critical applied load

δ_c is the critical displacement.

It is also possible to incorporate shear deformation into the calculation; this is of particular interest when considering orthotropic materials such as unidirectional reinforced composites.

Applying the beam theory of Timoshenko[64] equation (1.7) becomes:

$$\delta = BPa^3 (1 + S) \qquad (1.12)$$

where S is the expression for shear deflection

$$S = \frac{3E_x^b h^2}{32G_{xz}a^2} \qquad (1.13)$$

where G_{xz} is the interlaminar shear modulus relative to the xz plane.

Substitution into (1.3)

$$G_{IC} = \frac{3BP^2a^2}{2b} (1 + S/3) \qquad (1.14)$$

This requires a knowledge of E_x^b and G_{xz}. However, a precise value of these laminate properties is difficult to obtain, the ratio E_x^b/G_{xz} can be estimated allowing estimation of S. If this is the case a more conventional form of G_{IC} can be obtained by combination of (1.12) and (1.14).

$$G_{IC} = \frac{3P_c\delta_c}{2ba} \left(\frac{1 + S/3}{1 + S} \right) \qquad (1.15)$$

An estimated value of S allows use of a data reduction scheme as described in conjunction with (1.11).

Large deflections complicate the analysis and equations (1.10) and (1.11) are no longer valid.

Devitt[65] proposes a non linear beam analysis method.

1.5.5.3 Generalised Empirical Analysis

Once again this is based upon compliance, and a generalised form of equation (1.7):

$$\delta = RPa^n \qquad (1.16)$$

where R and n are constants determined experimentally from the relationship:

$$\log(P/\delta) = -\log R - n \log a \qquad (1.17)$$

A least squares fit to equation (1.16) for a series of loading and unloading curves, as shown in Figure 7 allows R to be determined. Obviously, if n = 3 beam theory is recovered.

Substitution into (1.3) of equation (1.16) produces:

$$G_{IC} = \frac{n R P_c^2 a^{n-1}}{2b} \qquad (1.18)$$

$$\text{or} \quad G_{IC} = \frac{n P_c \delta_c}{2ba} \qquad (1.19)$$

This method was successfully applied by Chai[66] to DCB results on graphite epoxy laminates with different lay ups. Values of n ranged from 2.74 - 2.97. Using the same method, Whitney[60] obtained a value for n of 3.74 for a different unidirectional epoxy system. This large value probably due to damage at the crack tip.

Wang[63] compared these methods and put forward an alternative reduction method based on a non linear analysis. This method is applicable to non linear load displacement curves and large displacements. The geometrically non linear analysis was based on the Ritz

method.[67] The derivation is complex and its inclusion not relevant here.

$$G_{IC} = -2 \left(\frac{\partial u}{\partial a} \right)_\delta \quad \delta = \text{constant} \qquad (1.20)$$

This comparison produced Figure 8, showing a higher value of G_{IC} from the non linear method, which Wang believes gives a much better indication of G_{IC}. The higher value is obtained because of the larger deflections which are involved giving rise to a non linear curve including a small hysteresis loop for each loading and unloading cycle. This loop was present in a few of the particulate APC-2 samples tested.

Wang believes non linear conditions largely invalidate the area and linear compliance methods, and speculated that the differences in G_{IC} values for the same method may be due to difficulty in measuring crack length and visco elastic effects. The problems of visco elasticity are discussed by Devitt.[65]

Whitney also compared the data reduction systems as presented in Table 3, and it is seen that the area method, empirical analysis and centre notch method (which is not a DCB, but included for comparison) are in relative agreement. For this reason, Whitney chose the area method for ease of manipulation. He also qualifies its use, indicating application only when the loading and unloading curves are identical in two sequential cracks and assuming all energy is used in delamination.

The data reduction system employed by Carlile[24] for APC-2 is the area method.

1.5.5.4   Previous DCB tests on Composite Materials
There have been a number of studies on the Mode I delamination fracture toughness of continuous fibre composites. Carlile[24], Whitney[60], Devitt[65] and Chai[66] were in agreement that a DCB

is suitable for studying the interlaminar fracture toughness of continuous fibre reinforced composite systems.

Wang[63] and Bascom[68] also employed DCB methods to study random short fibre and woven composites respectively.

Only the approach of Bascom was markedly different, in that he used a width tapered beam, maintaining a constant crack length to width ratio. The general expression for G_{IC} is:

$$G_{IC} = \frac{P^2}{2b} \frac{dc}{da} \tag{1.21}$$

where for ideal elastic beams:

$$\frac{dc}{da} = \frac{24 \, a^2}{E_B h^3 b} \tag{1.22}$$

where E_B is the bending modulus of the composite

     h is the beam height

If the specimen is width tapered for a constant ratio of a/b, the G_{IC} can be determined from P_c and E_B alone, being independent of crack length because:

$$G_{IC} = \frac{12P^2 \, a^2}{E_B h^3 \, b} \tag{1.23}$$

This avoids the problem of accurate crack length measurement. However, to offset this advantage, a knowledge of E_B is required. Also more material is needed and fabrication problems are encountered with fibre reinforced composites as directionality is critical.

Barlow[69, 70] presents an interesting variation in the approach to DCB theory. A razor blade was forced into the composite normal to the fibre axis, thus creating a split and so a cantilever beam. G_{IC} is given by:

$$G_{IC} = \frac{3 \, E_B \, d^3 \, h_b^2}{8(a')^4} \tag{1.24}$$

where h_b is the blade thickness

   d is the section thickness

   a' is the effective crack length

$$E_B = E \left(\frac{a^2}{a^2 + 3d^2} \right)$$ (1.25)

The measured crack length, a, is related to the effective crack length a' by a graphically determined factor:

$$c' = c + \Delta c$$ (1.26)

where Δc is material dependent and may be positive or negative

This work is particularly important because it highlights the need for an optimised matrix for maximum fracture toughness.

The results from this and others are presented in Table 4. These are mean values because all workers have reported large variations in their results, which can be explained in a number of ways.

Chai,[66] for example, found that in the quasi-isotropic material he tested, the fibre orientation made considerable differences to the G_{IC}.

Wang[63] found that the different beam thicknesses played a considerable part in the value of G_{IC}, ranging from 875 Nm^{-1} for 5mm beams to 2,000 Nm^{-1} for 14mm beams. He proposes this difference to be a result of variation in lateral constraints and the likelihood of different properties due to longer curing times etc. for thicker beams. Even when measuring the G_{IC} for a constant beam thickness, calculated values differed considerably, e.g. for a beam thickness of 11mm, the mean G_{IC} value was 1,700 Nm^{-1}, the standard deviation being 672 Nm^{-1}.

Devitt[65] also reported a variation in results. (A range of G_{IC} from 500-1,000 Nm^{-1}).

This demonstrates the inherent problems of characterising composites,

as properties may vary from one batch to another. This is particularly true of the semi-random fibres studied herein, as it is more probable that the fibre lay up, and so properties, will vary throughout the composite.

As expected the fracture toughness of thermoplastic matrix composites is higher than that of corresponding thermoset matrix composites. Also highlighted in Table 4 is the higher value of G_{IC} for thermoset system with elastomers added. Bascom[68] presents the toughening mechanism in detail, this operates by dispersing a fine particulate phase, which has a greater elasticity than the thermoset matrix in which it is embedded. These particles tend to deform elastically, absorbing energy without fracturing.

Two types of fracture are evident in the load displacement plots presented by these workers. Firstly, a 'saw tooth' type where cracks propagated in uncontrolled steps representing brittle failure. Secondly, a steady crack growth where the load falls steadily with crack extension representing ductile failure. Both types of failure are evident in APC-2.

Of particular relevance to this work are the higher values for woven fibres and short fibres. This is reported by Harkness,[4] Whitney[60] and Wang.[63] Mechanisms for this will be discussed later.

1.5.6 TRIBOLOGICAL PROPERTIES

The wear rates and friction coefficients of PEEK/fibre composites have been measured under various tribological conditions.[71] Since the measured tribological property is a function of microstructure, the investigation of structure-property correlations will lay the foundation for the fabrication of the desired product.

An increase of fibre content generally decreases the wear rate due to

the increase of E thus:

$$W_s = K \frac{\mu}{E} \frac{1}{\varepsilon_w} \frac{1}{\tau} \qquad (1.27)$$

where W_s is the specific wear rate

K is a constant

E is the elastic modulus

ε_w is the fracture strain

τ is the interlaminar shear strength

μ is the friction coefficient

As the carbon content increases, μ, the coefficient of friction decreases, largely due to the increasing amount of carbon. This is explained by:

$$F = \alpha E^2 (V_s/V_c) \varepsilon_w W_s \qquad (1.28)$$

where F is the friction force

α is a constant

V_s is the sliding velocity

V_c is the crack propagation velocity

The carbon fibre induces a low W_s and ε_w to override the rising E value, as the carbon fibre content increases. Morphologically, the easy slipping of the carbon structure can induce a low frictional force.

With reference to these equations, the friction coefficient increases as the sliding velocity increases.

Finally, the adhesively worn surface, microstructurally reveals a third layer; of material transfer, where the recrystallisation of the deformed matrix is assumed to occur.

1.5.7 ENVIRONMENTAL RESISTANCE

The properties of the composite must be maintained in use, particularly

in the hostile environments they are likely to encounter within the aerospace industry.

Hartness[4] and BA[72] have demonstrated that PEEK has excellent resistance to all reagents of interest in the aerospace industry and the only common solvent to attack PEEK is boiling concentrated sulphuric acid. Even paint strippers have no detectable effect on the carbon fibre reinforced PEEK systems.[22]

Like most other materials, PEEK can be consumed by flame, but it has a high char yield, is self-extinguishing, with low toxic gas evolution, [14] all vital when considering aerospace applications.

APC-2 is also slower to heat up and burn through than aluminium because of the lower thermal conductivity.

1.6 THE PROCESSING OF APC-2

By their very nature, thermoplastics offer new scope for high rate, efficient fabrication technology, the development of which may be regarded as a key step in enabling high performance fibre reinforced plastics to become a mass production industry and thereby reduce fabrication costs. In this review, the current processing strategies under investigation and research are outlined.

Compared with the thermoset composites, APC-2 possesses the inherent advantage of thermoformability and reprocessability.

APC-2 is supplied as pre-impregnated tape (or prepreg), tow feedstock and pre-consolidated sheet feedstock.

Brewster and Cattanach[73] suggest two major classes of fabrication strategy are applicable to this type of material: automated layup and adaptions of metal working technology.

The processing may then be sub-divided, dependent upon the starting material.

(a) Processes using pre-consolidated sheet feedstock

> Hydro-rubber forming
>
> Roll forming
>
> Diaphragm shaping
>
> Matched die moulding

(b) Processes using pre-impregnated tape and tow feedstock

> Filament winding
>
> Tape laying
>
> Braiding and weaving
>
> Pultrusion
>
> Autoclave and vacuum bag moulding
>
> Diaphragm moulding

1.6.1 GENERAL CONSIDERATIONS TO PROCESSING

Carbon fibres have an extremely low coefficient of thermal expansion so that the dimensional changes associated with temperature changes reflect the anisotropy of the end product. Typical values for coefficients of linear thermal expansion for uniaxial APC-2 are presented in Table 5.

The anisotropy of thermal expansion means that it is desirable to balance the arrangement of plies within a moulding if warp is to be prevented. Even with such a lay up, the difference between the thermal contraction in layers of different orientation will give rise to thermal stresses within a moulding and these must be minimised.

Cattanach and Cogswell[74] state that in the initial stages of the cooling process, these stresses are readily dissipated but that they start to lock at $220^{\circ}C$. As such, the level of thermal stresses induced in APC-2 mouldings is comparable with those in conventional high temperature curing thermosetting resin systems except that, being a tough matrix PEEK does not permit stress relaxation through transverse ply cracking.

(a)   Processes using pre-consolidated sheet feedstock

       Hydro-rubber forming

       Roll forming

       Diaphragm shaping

       Matched die moulding

(b)   Processes using pre-impregnated tape and tow feedstock

       Filament winding

       Tape laying

       Braiding and weaving

       Pultrusion

       Autoclave and vacuum bag moulding

       Diaphragm moulding

1.6.1   GENERAL CONSIDERATIONS TO PROCESSING

Carbon fibres have an extremely low coefficient of thermal expansion so that the dimensional changes associated with temperature changes reflect the anisotropy of the end product.   Typical values for coefficients of linear thermal expansion for uniaxial APC-2 are presented in Table 5.

The anisotropy of thermal expansion means that it is desirable to balance the arrangement of plies within a moulding if warp is to be prevented. Even with such a lay up, the difference between the thermal contraction in layers of different orientation will give rise to thermal stresses within a moulding and these must be minimised.

Cattanach and Cogswell[74] state that in the initial stages of the cooling process, these stresses are readily dissipated but that they start to lock at 220°C.   As such, the level of thermal stresses induced in APC-2 mouldings is comparable with those in conventional high temperature curing thermosetting resin systems except that, being a tough matrix PEEK does not permit stress relaxation through transverse ply cracking.

Even in a quasi isotropic lay up, the thermal expansion is low. Care
must be taken when using matched steel moulds, because the moulding will
not release without the use of a suitable mould release agent to prevent
adhesion.

APC-2 is a very good black body absorber and can be heated rapidly in a
number of ways. The most effective of these is the use of quartz infra
red heaters, ideally simultaneously from both sides, using 75 kWm^{-2}
energy density.[14] (Figure 9).

Any forming has to be carried out above the melting point of the matrix
PEEK, i.e. 343°C and ideally the whole sheet should be at 400°C.

PEEK does, however, exhibit super cooling as presented in Figure 10 and
some shaping is possible for a very short time after the APC-2 has fallen
below the melting point by around 20°C.

PEEK is an excellent hot melt adhesive and will bond firmly to itself and
other materials, under only contact pressure, providing both surfaces are
at or above the melting point. An optimum tool temperature is 180-200°C
to give immediate solidication, optimum crystallization and minimise
bonding to the tool.

The carbon fibres are inextensible and therefore any shaping process
has to be capable of accommodating fibre movement. One of the main
mechanisms in sheet shaping is interply slip which is possible above
the melting point of PEEK. (Figure 11).

1.6.2   HYDRO AND RUBBER BLOCK FORMING

These are similar processes where sheet material is formed to the shape
of a single sided mould, by either a hydraulically pressurised rubber
diaphragm (hydroforming) or by a mechanically pressurised and deformed
rubber block. This allows the necessary interply slip to prevent
fibre wrinkling in stretched areas and some thickening by fibre bunching

in areas being compressed. A more gradual folding and feeding action during shaping is achieved than with matched metal moulds and because of the even pressure over the surface, from a compliant medium, fibre damage is minimised.

1.6.3 ROLL FORMING

Adaptations of metal rolling machinery provide a potential for high rate manufacture of sections such as top-hat or z-stiffeners.

Selected masking of the APC-2 blank is an aid when using infra red heating, to produce colder and therefore stiffer areas to promote correct alignment and feed to the forming rolls.

At least five roll stands are required to form a top-hat section, four to form the section and one which reproduces the final shape and cools the section. To restrict excessive interlayer slip, a drive to top and bottom rolls is necessary, together with alignment and support devices.

1.6.4 DIAPHRAGM SHAPING

This process involves simultaneously heating, maintaining, consolidation and shaping between two plastically deformable diaphragms. Positive pressure is applied to the outside of the diaphragms (or a vacuum between) to consolidate the plies and maintain the consolidation whilst the whole sandwich is heated to 400°C and moulded to the required shape. The diaphragms help to prevent splitting or wrinkling of the APC-2 during shaping, by providing elastic tear resistant surfaces. (Figure 12).

1.6.5 MATCHED DIE MOULDING

Although this process is undoubtedly feasible, at this stage it is a complication which continuous fibre reinforced composites can do without,[18] because of the anisotropy of the composite and the widely

differing coefficients of thermal expansion with respect to the composite and metal. This causes pronounced difficulty in component ejection.

1.6.6 FILAMENT WINDING

The tow is heated to $400^{\circ}C$ immediately prior to winding on to a mandrel. Consolidation pressure may be applied through tension or pressure rollers. Both surfaces need to be above the melting point of PEEK at contact, but cooling is rapid because of the low thermal capacity of the heated area.

1.6.7 TAPE LAYING

A continuous process where consecutive layers of prepreg are ironed onto a mould surface. Consolidation pressure is maintained for a few seconds while the tape cools, and further plies welded to previously consolidated material. Once again both surfaces need to be above the melting point of PEEK, but because the heat capacity of the thin tape being laid is small compared to the mould and previous layers, cooling to solidification occurs rapidly.

This process allows predetermination of fibre direction and optimisation of properties in a chosen direction.

1.6.8 BRAIDING AND WEAVING

The tow is stiff and cannot be bent back on itself without snapping, therefore, special techniques have been developed. The braided and woven forms exhibit a limited degree of drape, which should assist in shaping double curvatures, etc.[75]

1.6.9 PULTRUSION

The APC-2 prepreg tape can be reformed into other cross sections by pultruding through a hot die which heats the APC-2 to $400^{\circ}C$, whilst at the same time gradually changing the cross section as the tape

proceeds through the die. As the carbon fibre is incompressible, and there is little excess PEEK to flow at, the APC-2 composite is incompliant. Some compliance has to be incorporated into the die, in order to maintain a constant pressure.

To avoid die wipe the fibres in the outer layer should run in the direction of the pultrusion; 90, +45 and -45, orientations being in the core.

It is thought that braided APC-2 prepreg tow would provide a good basis for the core.[75]

1.6.10 AUTOCLAVE AND VACUUM BAG MOULDING

Standard techniques well developed for the production of thermoset composite components can easily be adapted for APC-2. The principal changes are the bagging and sealants to accommodate $400^{\circ}C$.

The processing methods are thereby established for APC-2 and Jones, Leach and Moore[76] conclude that for successful engineering applications, certain choices must be made correctly:

(a) Conditions should be specified for the application, particularly in terms of stress or strain, time under load, temperature and geometry.

(b) An appropriate stress analysis should be made so that a link can be made between loading conditions, geometry and material properties.

(c) The mechanical properties required should be known, where to find such properties and how to interpret them in the light of the above stages.

1.7   THE APPLICATION OF REINFORCED PEEK

The previously discussed parameters have aroused considerable interest because of the combination of high mechanical strength and potential

for low cost processing.   PEEK is particularly attractive because even when unreinforced, the heat distortion temperature is 155°C[77] and when reinforced this value is raised considerably.   Carbon fibre reinforced PEEK is in fact currently under evaluation for various internal engine components.   Indeed, the latest version of the Ferrari Formula 1 racing engine employs carbon fibre reinforced PEEK for the oil pump, and the inlet and impeller of the turbo charger.[78]

Other major potential areas of interest are aerospace parts both in the US and Europe[79, 80] including antennae, radomes,[72] space station parts,[81] and seating and structural parts.   However, because of the relative infancy of the technology, these applications are jealously guarded secrets in many instances.   Boeing[82] have achieved thirty per cent weight savings and ninety per cent cost savings by replacing aluminium with glass reinforced PEEK for fairings that stream-line the engine mountings for the 757-200.   The key properties that ensure these fairings will withstand high levels of moisture, sonic vibration and high air speeds are indicated by ICI.[83]   The fairings, two on each wing, streamline the air flow around the strut assembly used in mounting two Pratt and Whitney 2037 jet engines.   A joint development programme between Boeing, Vaupell Industrial Plastics Inc. and ICI Advanced Materials in Wilmington, USA, led to the material selection.

Interest has also been generated in helicopter technology and the Westland 30-300 has been fitted with a demonstrator tailplane pro-duced from APC-2 and short fibre reinforced PEEK[84, 85] and Westland are confident that the advent of high performance fibre reinforced thermoplastic composites such as APC-2 will provide significant improvements in helicopter structural technology.

Orthopaedic applications have been promoted because of the resistance to chemical attack.[86] APC-2 possesses advantages over conventional orthopaedic alloys. Weight is one such consideration, but more importantly bone has a Young's Modulus of around 20 GPa; the Young's Modulus of conventional Co-Cr-Mo alloys is ten to twenty times this, and so the majority of the stress is taken by the artificial joint and not by the bone. This tends to lead to a weakening of the bone due to lack of use. APC-2 can overcome this because its Modulus is more comparable to that of bone.

The first of a new generation of Victrex high performance polymers specially designed for bearing applications was launched by ICI in 1984.[87] This composite is based on PEEK, solid lubricants and carbon reinforcing fibres which are claimed to optimise the very properties of friction wear and limits PV (applied pressure x surface velocity) at high speeds and under considerable loads. This composite has a lower friction coefficient than bearing materials such as porous bronze graphite, resin impregnated carbon or polyimide/graphite; an average figure of 0.14 compares with at least 0.20 for these competing materials. The wear factor is also extremely low.

Naval applications appear to be forestalled at present because of the high prohibitive costs[88] but as technology advances the use of such composites may become viable.

Carbon fibre reinforced PEEK, both as APC-2 and injection mouldings, is therefore scheduled for protracted use in applications where damage cannot be avoided. Damage can be of two kinds:
(a) delamination, where although the fibre structure remains continuous the strength, particular in torsion or compression, is compromised;
(b) holes where the fibres are broken.

It is possible to repair this damage by remoulding the component either in situ or by the removal of the component and return to the mould, depending upon the degree of damage. For simple delaminations, the full original property spectrum can be recovered, while for fibre· breakage two-thirds of the original strength is possible after repair.[42]

Of course, the ideal repair operation is full remoulding of the sample, but it is possible to envisage a field repair kit consisting only of a tool similar to a soldering iron.

1.8   SCRAP GENERATION

The construction of elegant and optimal designs from continuous fibre prepreg inevitably means waste of some material, and while the industry may learn from the skills of tailors and dressmakers in the art of pattern making, the utilisation of material in the continuous fibre form will probably not exceed 75% efficiency.[89]

As the carbon fibre reinforced thermoplastics industry expands, so the scrap generated could represent an embarrassment. In the case of APC-2 this problem can be turned to an economic advantage, since the scrap can be granulated, diluted with additional resin and used as an injection moulding compound, a high value material in its own right.[42]

Further to this idea it should be possible to compression mould granulated scrap into preconsolidated sheet stock, providing the properties so achieved can be predicted, and it is with this prediction in view that the present research has been undertaken.

2. MORPHOLOGY AND CRYSTALLIZATION OF APC-2

The morphology and crystallinity of aromatic polymers and their composites have been studied by various workers.[19, 90-96]

Since the morphology of the semi-crystalline thermoplastic matrix determines the final properties of the composite, it is essential that the crystallization behaviour associated with APC-2 be characterised. Furthermore, by understanding the basic morphology of the thermoplastic matrix, the processing parameters can be adjusted to optimise the mechanical properties of the end product.

The presence of reinforcing carbon fibres in the PEEK matrix significantly increases the rate of crystallization compared with that of unreinforced PEEK processed under identical conditions.[92]

The heat distortion temperature gives a direct measure of the temperature limit, at which a material can still bear the load. This temperature is dramatically increased by glass fibre reinforcement in crystalline polymers but only marginally for amorphous polymers.[97] In 1971 Krautz[98] reported that the heat distortion temperature response of crystalline polymers is unique to glass fibre reinforcement. A satisfactory explanation was not available at the time. However, since this observation, carbon fibres have been developed for use as reinforcing fibres and a similar improvement in the heat distortion temperature has been observed when a thermoplastic polymer is reinforced by smooth carbon fibres. This rise in heat distortion temperature can be explained by the ability of a locally smooth surface, such as glass and some PAN-based carbon fibres, to induce polymer matrix self-alignment and crystallization in crystallizable polymers (but not in inherently amorphous polymers which cannot be crystallized or nucleated). The ordered matrix polymer has elasticity to resist flow and deflection under load; even at temperatures

where the same disordered polymer will deform by viscous flow. This explains why carbon fibre, if it has a smooth (and active) surface can raise the heat deflection temperature as much as glass fibre does in crystallizable PEEK,[99] and which gives only marginal heat deflection temperature rises in amorphous polyetherimide and polyether-sulphone.

PEEK has been investigated using Fourier transform infra red reflection-absorption spectroscopy (FT-IR-RAS).[100] This study was of the interfacial interactions between cast films of PEEK and the basal plane of graphite single grystals. For randomly orientated polymer chains (quenched films) preferential orientation with respect to the substrate was not observed. When the polymer films were crystallized via annealing, however, the preferred orientation of the chains was found to be perpendicular to the substrate. One possible explanation for the normal orientation of the crystalline polymer chains on the basal plane of graphite single crystals is that the intermolecular interaction is stronger than the interaction between the chains and the substrate.

The excellent creep performance is probably not only a result of the inherent resin performance, but may relate to the internal crystalline substructure within the spherulites, relative interstitial dimensions and crystallite size,[18] and this internal structure is in itself very complicated, having many facets. However, many of these, such as crystallinity and crystal lamellar thickness, tend to be correlated with each other and are mainly determined by the temperature at which crystallization takes place.

One of the most important properties of PEEK matrix is its excellent solvent resistance, which is to be reproduced in APC-2. In order to optimise this property a certain degree of crystallinity is essential[101]

and with this in mind, Small,[102] Wakelyn,[103] Seferis[104] and Blundell et al[105] have all developed methods for assessment of the crystalline/amorphous ratio of PEEK in carbon fibre composites.

Each of these methods has its advantages and the selection of technique is related to necessary fabrication constraints.

A sideline to this work was the discovery by Seferis[104] that there is a strong exothermic reaction between PEEK and copper powder at $340^{\circ}C$ and this produced voids within the samples. Although the mechanism of this reaction has not been fully established, a breakdown of the polymer chains producing a phenol is a strong hypothesis at present.

2.1 CRYSTALLIZATION BEHAVIOUR DURING COOLING

Isothermal crystallization behaviour, although convenient for characterising the overall crystallization behaviour, does not relate directly to the practical moulding conditions, where the crystallization usually occurs during a cooling cycle. This situation has been simulated by differential scanning calorimeter (DSC) cooling scans.[92, 93, 106-108]

The crystallization process occurs over a band of temperatures which is typically about $20^{\circ}C$ wide. For convenience Blundell and Osborn[93] characterised the whole process with a single parameter T_C, which was the temperature at which the peak crystallization occurred. The results are shown in Figure 13.

As the cooling rate is increased, the crystallization temperature range is decreased. At the faster cooling rates a lot of small crystallites are formed around a large number of nucleation sites, giving a lower degree of crystallinity. Slow cooling produces fewer, larger crystallites.

Furthermore, as the carbon fibre content is increased, the supercooling

necessary to induce crystallization decreases. The repeated melting of the same PEEK sample produces a reduced number of nuclei for crystallization.[107] At equivalent thermal histories PEEK containing carbon fibres has a higher nucleation density than unreinforced PEEK. The surface of carbon fibres and nuclei in the PEEK matrix compete for crystallization growth. As the holding time in the melt is increased then the number of matrix spherulites formed on cooling decreases, and so a more pronounced transcrystalline region forms.

Correspondingly, the composites preheated in the melt for a hundred minutes show about twice the transverse tensile strength and strain to failure of those preheated for only thirty minutes.[107] The relevant tensile fracture surface shows that the former samples had a greater matrix adhesion to the carbon fibre than the latter although this is not necessarily an advantage as this is offset by loss of impact strength[13] because of the inherent rigidity.

2.2   THE RELATIONSHIP OF THE CRYSTALLIZATION BEHAVIOUR TO FINAL MORPHOLOGY

Crystallinity depends primarily on the combined effects of nucleation and growth of the spherulitic entities in the thermoplastic matrix. The primary process being terminated when the radially growing spherulites impinge upon their neighbours such that the matrix space is enclosed within the spherulitic boundaries as depicted schematically in Figure 14.

The much smaller lamellar crystals are the internal entities which take part in the growth process of the spherulites. The thickness of the lamellae and weight fraction of the spherulites (i.e. the crystallinity) are greatly influenced by the crystallization temperature and to a lesser extent by time at that temperature. Both the thickness of the lamellae and crystallinity tend to increase with higher temperature.[19]

When attempting to relate the crystalline morphology to the crystallization rate characteristics and cooling rate during the fabrication of APC-2, two issues are important:

(a) The temperature, T_c, at which peak crystallization occurs as this determines many of the details of the morphology. (Figure 13).

(b) The extent to which the primary spherulite growth process has been completed. This is particularly relevant when very fast cooling rates are involved with a possibility that a portion of the thermoplastic matrix will be unoccupied spherulites as in Figure 14A. This situation must be avoided in order to retain the full solvent resistance of APC-2.

Thus, at faster cooling rates the completion of the spherulitic growth process is more important than the degree of crystallinity within the spherulites.

The crystallization process in APC-2 at extremely high cooling rates cannot be studied with laboratory DSC instruments as the cooling rates are too great. However, these rates may be achieved under certain moulding conditions. Blundell and Osborn[93] therefore extrapolated their experimental data with a crystallization model based on the Avirami equation[109] and concluded that in order to achieve the required level of crystallization, APC-2 should be fabricated so that the cooling rates from the melt do not exceed about 700°C/minute. If a fabrication route is chosen where the cooling rate exceeds this figure, then the APC-2 moulding will need to be post annealed to achieve the necessary crystallinity. Cebe[108] states that for non-isothermal studies amorphous films were crystallized by heating or cooling rates from 1°C min^{-1} to 50°C min^{-1}. A large percentage of crystallinity develops from this secondary process.

Blundell and Willmouth[110] propose a model to predict the cooling

rate as a function of composite thickness, tool temperature and degree of heat transfer to the tool. This information can be combined with crystallization behaviour data to estimate the level of crystallinity attained during fabrication and to outline conditions necessary to ensure adequate crystallinity. For many situations, cooling rates through the temperature zone of crystallization are fairly uniform across the thickness, giving uniform crystallinity in the matrix.

2.3 ELECTRON BEAM IRRADIATION

The post processing effect of high energy electron irradiation on semi-crystalline PEEK has been examined by Yoda.[111] He derived the crystallite size and lattice distortions in the chain direction from the analysis of 002, 006 and 008 Bragg reflections. The application of the paracrystalline model revealed the average crystallite size is reduced by fifteen per cent, whereas the lattice distortion parameter and unit cell dimension of the c-axis are little affected upon irradiation with 5,000 M rad. It was also shown that the long period observed by small angle x-ray scatterings does not change on irradiation up to 5,000 M rad.

A slight decrease in the crystallite size in the polymer chain direction is observed, and the degradation of the crystal possibly occurs in the vicinity of the crystalline/non-crystalline interface.

Sasuga and Hagiwara[112, 113] studied molecular motions of non-crystalline PEEK, and mechanical relaxation of crystalline PEEK under the influence of electron irradiation, by measurement of dynamic visco elastic properties.

Three different molecular processes are overlapped in the γ relaxation of unirradiated non-crystalline PEEK, i.e. molecular motion of water bound to main chain (peak temperature at -100°C), local motion of main

chain (at -80°C) and the one at -40°C arises from molecular motion of an aligned and orientated part having close conformation to the crystal structure. The β relaxation connected with the glass transition temperature occurred at 150°C, and shifted to higher temperatures by irradiation. The α' relaxation, which can be attributed to rearrangement of molecular chains due to crystallization, was observed in unirradiated PEEK (at about 180°C) and its magnitude decreased with the increase in irradiation dose. This effect indicates the formation of structures inhibiting crystallization such as cross linking and/or short branching during irradiation.

A new relaxation, β', appeared in the temperature range of $40-100^\circ$C by irradiation and its magnitude increased with dose. This relaxation was attributed to rearrangement of the molecular chain (from loosened packing around the chain ends, which were introduced into the non-crystalline region by chain scission under irradiation) to more rigid packing.

From these results Sasuga and Hagiwara[112] propose that deterioration in mechanical properties of non-crystalline PEEK by high energy electron beam irradiation was brought about by chain scission and structural changes such as cross linking and/or branching in the main chain.

Non-crystalline PEEK shows a higher resistance than semi-crystalline PEEK to electron irradiation of high dose rate.[112]

The difference in radiation susceptibility between non-crystalline and crystalline chains would result partly from a different freedom of molecular motion between the phases, because suitable molecular motion is required for chain scission and/or cross linking. In the crystalline phase, molecular motion is largely restricted by the

crystal lattice so that the probability of chain scission and cross linking is less than in the non-crystalline phase. Therefore the chains in crystallites can be considered to be less susceptible to irradiation than those in a non-crystalline phase. Application of this concept suggests that semi-crystalline PEEK should be more resistant than non-crystalline PEEK to irradiation. However, experimental research shows the reverse order of radiation stability, as evaluated by degradation of mechanical properties.

The lower radiation resistance of semi-crystalline PEEK seems to be influenced by the irradiation susceptibility of molecules in another region, for example, the interface between crystalline and non-crystalline phases.[113]

When considering semi-crystalline PEEK,[113] irradiation caused the glass transition temperature (β relaxation) to shift upwards, and β' relaxation, related to loosened chain packing, to appear just below the glass transition temperature. Also, a small shoulder appearing at -40°C to 0°C on the δ relaxation peak, which disappeared in the first scan after irradiation, reappeared in the second scan.

This shoulder on the δ relaxation peak was assigned to segmental motion of the chains at the crystalline/non-crystalline interface.

The inferior radiation resistance of semi-crystalline PEEK with respect to non-crystalline PEEK is thought to be a result of preferential disintegration of tie molecules between crystalline and non-crystalline phases.

3.   FAILURE MECHANISMS IN COMPOSITE MATERIALS

PEEK, reinforced with thirty weight per cent short carbon fibre exhibits a fatigue crack growth rate four to six times lower; and a tensile strength fifty per cent higher than unreinforced PEEK. However, the fatigue crack growth rate and tensile strength of PEEK reinforced with thirty weight per cent short glass fibres are similar to those of unreinforced PEEK.   These superior properties in carbon fibre reinforced PEEK are attributed to the optimisation between the carbon fibre and PEEK matrix.[114]

Unfortunately, the inherent heterogeneities in composite materials, especially short fibre materials, means that the application of a classical fracture mechanics approach as applied to metals is not always relevant.   Kanninan[115] reports composite fracture research can be categorised broadly into two divisions:

(a) A continuous analysis for homogeneous anisotropic linear elastic material containing an internal or external flaw of known length. This pays no attention to the heterogeneous nature of composites.

(b) A semi-empirical analysis of the micro-mechanical details of the crack tip region in an undirectional composite.   This being more applicable to composite materials.

Wang[116] utilised this latter approach to analyse, by fracture mechanics techniques, based upon conservation laws of solid mechanics, the notch-tip stress intensities in the specimens.   This data provides information on fracture characterisation of the composite and is useful in the design and analysis of the composite.

During tensile fracture composites can fail in one of two ways:

(a) fibre breakage,

(b) fibre pull out.

Folkes[61] and others highlight that for optimised performance, maximum fibre breakage in a failure is necessary.

To prevent fibre pull out the fibre must be sufficiently long for the frictional energy of pull out to exceed the energy for fibre breakage.

The length at which these two energies are equal is called the critical fibre length, l_c. Blumentritt[117] gives:

$$l_c = \frac{\sigma_{uf} \cdot r}{\tau} \qquad (3.1)$$

where l_c is the critical fibre length

σ_{uf} is the ultimate fibre strength

r is the radius of fibre

τ is the composite shear strength

When the critical fibre length is exceeded, then the major fracture mechanism should be caused by fibre fracture. In practice fibre pull out still exists at lengths three to four times that of the critical length[118] due to anomalies in the bonding of the fibre to the matrix. A detailed insight into the mechanisms of fibre pull out is given by Folkes[61], Cooper[119] and Piggot.[120]

Although short fibres tend to be deleterious to the strength properties of the composite, it was found that they improved the toughness of the composite.[61, 117] This is due to the work required firstly to debond the fibre from the matrix, and then the frictional work required to pull the fibres from the matrix.

These contributions to failure are discussed by Harris.[118]

3.1   DEBONDING

As the load on the composite is increased, matrix and fibre at the crack tip attempt to deform differentially and a relatively large

local stress begins to build up in the fibre. This stress causes
the local Poisson contraction which, aggravated by lateral concentra-
tion of tensile stress (normal to the interface) ahead of the crack
tip may initiate fibre/resin decohesion, or debonding as presented
in Figure 15(c). The interfacial shear stress resulting from the
fibre/matrix modulus mismatch will then cause extension of the debond
along the fibre in both directions away from the crack plane. This
will permit further opening of the matrix crack beyond the fibre, and
the process will be repeated at the next fibre. An upper limit to
the energy of debonding is given by the total elastic energy that will
subsequently be stored in the fibre at its breaking load, i.e. $\sigma_f^2 / 2E_f$
per fibre per unit volume, or with N fibres bridging the crack:

$$W_{debond} = \frac{N \pi r^2 \sigma_{fy}'}{2E_f} \qquad (3.2)$$

where W_{debond} is the energy of debonding

$\quad$ r is the radius of the fibre

$\quad \sigma_f'$ is the breaking stress

$\quad E_f$ is the modulus of the fibre

$\quad$ y is the mean debonded length

Debonding may lead to large scale deviation of the crack tip parallel
with the fibres, resulting in an effective blunting of the crack.
Cracking may then proceed on some other plane, remote from the original
crack plane, with a resultant increase in the complexity of the fracture
face and increase in composite toughness.

3.2 FRICTIONAL WORK FOLLOWING DEBONDING

After debonding, the fibre and matrix move relative to each other as
crack opening continues and work must be done against frictional
resistance during the process. The magnitude of this work is hard
to assess because the level of frictional force is not accurately

known.   One estimate, assuming that the interfacial frictional force,

λ , acts over a distance equal to the fibre extension, suggests

that this contribution may be given by:

$$W_{friction} \quad = \quad N \lambda \pi r y^2 E_f \qquad (3.3)$$

where E_f is the fibre failure strain, and this contributes substantially

to the toughness of composites.

3.3   FIBRE PULL-OUT

After debonding a continuous fibre is loaded to failure over a 'gauge

length' and it may break at any point within this region as presented

in Figure 15(d) presumably with a strength statistically characteristic

of that gauge length.   The broken ends will then retract and regain

their original diameter, and they will be gripped by the resin.   In

order to permit further opening of the crack and ultimately separate

the two parts of the sample, these broken ends must be pulled out of

the matrix, Figure 15(e).   Further frictional work is needed to accom-

plish this, and the resulting fracture surface will often have a

'brush-like' appearance characteristic of many fractured composites.

Approximate estimates for the work of pull-out, $W_{pull-out}$ is given by:

$$W_{pull-out} \quad = \quad \frac{N \lambda \pi r l_c^2}{6} \qquad (3.4)$$

where l_c is the critical length

The distance over which the fibre end is pulled out is approximately

$l_c/4$.   It can be shown that in aligned, short fibre reinforced com-

posites the work of pull-out (and consequently, the work of fracture)

will be a maximum when the reinforcing fibres are exactly of the

critical length.[119]   If the fibres are at an angle to the crack

face, brittle fibres will fail prematurely without pull-out but

plastically deformable ones will undergo extra work of shearing as

they pull out, contributing extra toughness.   These two effects of fibre length and fibre orientation are presented in Figure 16 from the work of Harris.[118]

During delamination a composite can fail in three ways:

(a)   fracture through the matrix,

(b)   fracture through the fibre-matrix interface,

(c)   fracture of fibres.

The energy for fracture of fibres is much higher than other fracture types, and composites which have good fibre matrix adhesion are more likely to fail through the matrix.

This was demonstrated by Barlow[69] who presented an optimised matrix where PEEK particles and waves were clinging to the fibres and failure was through the matrix.   The non-optimised matrix, however, revealed a clean surface;   indicating substantial fibre matrix debonding and failure along the fibre matrix interface.

Chai[66] reports that both types of failure may occur in the same fracture, mainly because of different fibre orientations but also partially caused by a variation in thickness of the matrix layer between the fibres.

Chai also reports that in multi-directional composites the direction of wave markings, characteristic of brittle fracture, tended to be across the fibre direction regardless of the main delamination direction.

The reason for the brittle fracture mode, Chai proposes is the inter-ference of fibres on the ductile matrix.   This was also presented by Bascom[68] for woven fibres, which also tend to have a greater fracture toughness than unidirectional equivalents.   This is thought to be because of the more complicated crack path.

Bascom also observed resin rich areas at crossover points in the weave, which with a tough matrix improved fracture toughness, but with a brittle matrix, had a deleterious effect.

Wang,[63] demonstrated the fibre bridging effect often found during delamination of random short fibre composites. The bridge took the form of fibres, or bundles of fibres, bridging the gap between the two cracked halves, tending to retard crack growth so increasing fracture toughness. Fracture toughness was also increased through the fibre pull-out mechanism.

Wang also reported sub-critical cracks in front of the main crack. This subsequently leads to exaggerated fibre bridging and so to considerable increases in energy absorption. It was suggested that the sub-critical crack formations may be related to multi-axial stresses induced by the main crack and local microscopic weak spots in the composite.

Thus, the fracture mechanism for uni-directional composites stressed in the fibre direction is substantially different to the mechanism for delamination between fibre layers.

The semi-randomly orientated particles used to construct specimens in this work will display both types of fracture. Although the overall particle plane is the same as the delamination plane, some particles will intercept adjacent planes. Thus the fibres in this particle will need to be pulled out in an off axis tensile fashion and this means a knowledge of failure mode will be critical when predicting characteristics of composites fabricated thus.

4. THE THEORY OF REINFORCEMENT

The success of fibre reinforced thermoplastics is due to the synergy between fibres and matrix. Having discussed the requirement to obtain an optimised matrix, it is necessary to discuss the form of reinforcement.

There are three categories of reinforcing particle; continuous,[13] short fibre[61] and planar.[121] With a view to expanding the planar reinforcement theory to accommodate a carefully controlled APC-2 offcut particle size, the theory is reviewed.

The two schools of thought on the subject are:

(a) the Halpin-Tsai equations,[122-125]

(b) a series of equations which are applied to take account of the mode of failure. This was proposed by Padawer and Beecher.[126]

By appropriate mathematical manipulation of these two theories, a theory has been developed to produce an applicable mathematical model.[121]

4.1 PLANAR REINFORCEMENT

The main disadvantage of fibre reinforcement is that the mechanical properties are highly directional. In order to achieve multi-directional high strength, comparable to a quasi-isotropic lay up, the planar reinforcement concept was originated. Planar reinforcements include flakes and ribbons.

For planar isotropic composites it might be expected that flakes would be superior to fibres[127, 128] since suitably orientated flakes can stiffen a material in two dimensions rather than in just one. However, some of this advantage is offset because of interactions between nearest neighbours in the three-dimensionally packed structure. This can be explained by considering stress transfer situations. Piggot[128]

- 53 -

and Riley[129] have discussed in detail the stress distributions associated with flakes and fibres respectively.

4.1.1 STRESS DISTRIBUTION

Fibres and flakes are similar in the 1-2 plane, but in the 2-3 plane, the flake has two nearest neighbours with which to share stress as compared with the fibre, which has six nearest neighbours. (Figure 17).

Maximum stress occurs in a reinforcing element where an adjacent element ends, and thus the six nearest neighbours in fibre reinforcement allow a higher average stress in the fibres, whereas the two nearest neighbours in flake reinforcement must take three times the amount of stress transferred compared with the situation in fibre reinforcement.

The only difference between fibre and planar reinforcement should be a numerical factor to allow for the different geometry and the effect of stress transfer between different planes of flakes. The theory of mechanisms for planar reinforcement is based on fibre reinforcement theory, flake reinforcements being analogous to short fibres, and ribbon reinforcement being analogous to long fibre.

In the following discussion, it is understood that except for the longitudinal ribbon direction, the property relations are similar for flake and ribbon composites.

4.1.2 ELASTIC PROPERTIES

A typical arrangement of flakes is presented in Figure 17, and Figure 18 presents the elastic moduli of planar reinforced composites aligned in this manner. Such a composite is anisotropic and requires six moduli to describe its stiffness characteristics:[130]

E_{11}, which is its Youngs modulus parallel to ribbon length; this corresponds to Youngs modulus for continuous fibre reinforcement,

E_{22} and G_{12}, which are in plane moduli, and are

greatly enhanced for planar reinforcement compared

with fibre reinforcement,

E_{33}, G_{13} and G_{23}, which are the remaining composite

moduli, these values in planar reinforcement are not

greatly enhanced over fibre reinforcement.

Any useful theory, therefore, must predict the quantities E_{11}, E_{22}

and G_{12}.

In order to calculate the tensile modulus of a composite it is possible

to use the 'rule of mixtures'. This ignores any interaction between

the constituents of the composite and is normally sufficient for

engineering practice. When applying it to planar composites, however,

it is wrong to disregard interactions between flakes.

In flake and ribbon reinforced composites, the non-uniform size and

random distribution of the reinforcing elements add complications to

the analysis and in the derivation of the following equations, the

following assumptions have been made:

    (a)   rectangular flakes,

    (b)   no voids,

    (c)   no flake imperfections,

    (d)   ideal flake matrix adhesion, and

    (e)   uniform flake distribution.

Padawer and Beecher[126] produced an analytical model of planar

reinforcement based on the rule of mixtures, but also containing a

Modulus Reduction Factor [MRF] defined by:

$$MRF = 1 - \frac{\ln(u+1)}{u} \qquad (4.1)$$

$$\text{where } u = \alpha \left\{ \frac{G_m \phi_f}{E_f(1-\phi_f)} \right\}^{1/2} \qquad (4.2)$$

where α is the aspect ratio = width/thickness,

G_m is the matrix shear modulus,

ϕ_f is the volume fraction of the flake, and

E_f is the Young modulus of the flake.

The MRF factor is a fraction, less than or equal to one, approaching unity with increasing flake aspect ratio, reinforcement volume fraction and matrix shear modulus. Figure 19 presents two families of curves, typical of the extremes associated with flake reinforcements. The upper family of curves is for E_f/G_m equal to 25, typically representative of ceramic flake/aluminium matrix systems. The lower set is for E_f/G_m equal to 500 typical of ceramic flake/plastic resin systems.

Introducing the MRF to the rule of mixtures gives:

$$E_c = \phi_f E_f [MRF] + (1 - \phi_f E_m) \qquad (4.3)$$

E_c may be taken in either direction (longitudinal or transverse); thus values of E_{11} and E_{12} respectively are obtained.

To predict values for G_{12}, the Halpin-Tsai equations have been derived, [122, 124, 125] which are based upon the self consistent micromechanics method developed by Hill.[131]

$$\frac{G_{12}}{G_m} = \frac{1 + \rho \eta \phi_f}{1 - \rho \eta \phi_f} \qquad (4.4)$$

$$\text{where } \eta = \frac{G_f \backslash G_m - 1}{G_f \backslash G_m + \rho} \qquad (4.5)$$

where ρ is a measure of reinforcement depending upon the boundary conditions, and

G_f is the flake shear modulus.

The appropriate value of ρ required for G_{12} has been shown to be:[129,130]

$$\log \rho = \sqrt{3} \log \alpha \qquad (4.6)$$

4.1.3   TENSILE STRENGTH PROPERTIES

As claimed by Riley,[129] the disturbing effects caused by mutual interactions of the flake edges mean that discontinuous reinforced composites can only attain 50-80% of the strength of continuous reinforced composites, depending on the aspect ratio.

For planar composites with a linear elastic matrix, equations have been derived[126, 132, 133] for tensile strength based on the rule of mixtures, assuming:

(a)   uniformly spaced flakes parallel to the plane,

(b)   ideal matrix/flake adhesion,

(c)   matrix and flake linearly elastic to failure, and

(d)   no interactions between reinforcement extremities.

The validity of these equations depends on the failure mode, (i.e. flake fracture or flake pull-out), which itself depends on aspect ratio and interfacial shear strength, τ [134]

$$\frac{W_c}{t} = \frac{\sigma_f}{\tau} \qquad (4.7)$$

where t is the flake thickness

σ_f is the rupture strength, and

W_c is the critical flake width

Only if the flake width is greater than W_c will the composite fail by fracture of the reinforcements, otherwise a lower level flake pull-out occurs without full utilisation of the reinforcement, because the flakes are too small to effect transfer of their breaking strength.[129]

4.1.4   FLAKE FRACTURE

The strength reduction factor accounts for the discontinuous nature of the reinforcement.

$$\sigma_c = \Phi_f \sigma_f \, [SRF] + \Phi_m \sigma'_m \qquad (4.8)$$

- 57 -

where SRF $= \left\{ \dfrac{1 - \dfrac{\tanh(u)}{u}}{1 - \mathrm{sech}(u)} \right\}$ (4.9)

where u is given by equation (4.2), and

σ'_m is the tensile strength in the matrix at rupture,

$$\sigma'_m \sim \sigma_m / 3$$

(σ_m being the tensile strength of the matrix).

4.1.5   FLAKE PULL-OUT

Failure of the matrix results in pull out of the flakes and there is little effective strength given to the composite by the reinforcement.

The [MPF] Matrix Performance Factor characterises this type of failure.

$$\sigma_c = \phi_f \, \tau_m [\text{MPF}] + \phi_m \, \sigma''_m \qquad (4.10)$$

where MPF $= \dfrac{\alpha}{u} \left\{ \dfrac{1}{\tanh(u)} - \dfrac{1}{u} \right\}$ (4.11)

where τ_m is the shear rupture stress of the matrix or interface whichever is the lower, and

σ''_m is the tensile strength in the matrix at rupture.

In this mode of failure σ''_m approximates to σ_m.

4.1.6   TOUGHNESS

Planar reinforced thermoplastic materials have not been examined in detail for toughness, but soft metal/hard metal laminates have been examined extensively.[135]   Figure 20 shows the two configurations found to be most effective.

Figure 20(a) has the crack front perpendicular to the laminae, and crack propagation in the hard laminae is inhibited by the soft laminae.

Figure 20(b) has the crack front parallel to the laminae; the laminae tend to separate just ahead of the crack, reducing the stress concentration and diverting the crack.

Toughness is considerably improved in both cases. Aligned flakes are subject to similar processes but the exact toughening effect is difficult to quantify.

4.1.7 PARTICLE SHAPE

Theory predicts[128, 135, 136] that there will be a difference in strength of a composite reinforced with round platelets as opposed to square platelets, and also a difference in strength of composites reinforced in a regular arrangement compared with irregularly filled composites. This is because of the degree of overlap and therefore the amount of flake stress transfer associated with the different packing systems. In practice, owing to the inherently irregular flakes associated with the materials involved, these variations are not always apparent. It is therefore vital that the offcuts of APC-2 are cut into precise squares to optimise use of the theory. Circles are not used because they would incorporate varying fibre lengths into the particular reinforcement system under investigation.

4.2 APC-2 SCRAP RECOVERY

When designing to take full advantage of the properties of APC-2, offcuts are inevitable and the quality assurance required for demanding applications may also lead to the rejection of some parts. The ability to remould parts will assist in reducing waste. However, as the industry expands, large quantities of high cost material will be scrapped. With APC-2 it is possible to reclaim this scrap either by injection moulding or compression moulding, but such mouldings must have predictable mechanical properties if they are to be of greatest benefit to the consumer in reducing cost.

So far only limited scrap reclamation work has been undertaken, and this is now examined in conjunction with the theory of fibre reinforcement.

4.3   THEORETICAL PREDICTION OF THE MECHANICAL PROPERTIES OF APC-2

4.3.1   STIFFNESS

The carbon fibre used in APC-2 has a mean tensile modulus of 230 GPa, while PEEK has a tensile modulus of 3.8 GPa.

In a tensile test, with the loading along the fibre axis, the PEEK and fibre share the load applied in parallel.   The law of mixtures determines the potential axial stiffness of a fibre reinforced composite along the fibre axis:

$$\text{Axial tensile stiffness} = \sum_i \phi_i E_i$$

where ϕ_i is the volume fraction of the i component, and

E_i is the modulus of the i component.

All elements are subject to the same strain.

Thus, the theoretical tensile modulus of APC-2 along the fibre axis is 142 GPa and this theoretical value should be achieved if each fibre is thoroughly wetted and connected to its neighbour so that it can share its proper proportion of the load.

By contrast, if the load is applied transverse to the fibre axis, a first approximation may be made of the components being in series, and each element is subject to the same stress.
Then:

$$\text{Transverse tensile compliance} = \sum_i \phi_i J_i$$

where J_i is the compliance of each component.

From this, an approximate tensile stiffness for APC-2, normal to the fibre axis, of 8 GPa can be deduced.[13]

This approximation ignores the very severe constraints under which the thin compliant layers of PEEK are placed, and a slightly higher value should actually be recorded.

4.3.2   STRENGTH

The carbon fibre used in APC-2 has a tensile strength of 3,620 MPa, while the tensile strength of the PEEK is 95 MPa.   The concept of strength is rather less amenable to fundamental analysis than the theoretical arguments about stiffness except in the case of tensile strength of a uniaxially aligned fibre, where the law of mixtures should apply.   According to this, the tensile strength of APC-2 should be 2,245 MPa.

By comparing these theoretical values with the published data in Appendix 1, a very high efficiency of wetting is concluded.

This conclusion is of particular importance, since it permits use of the carefully constructed theoretical models proposed.

5.   APC-2 SCRAP RECOVERY

With APC-2 it is possible to reclaim scrap by diluting with additional resin and injection moulding or by compression moulding diced APC-2 scrap.

5.1   INJECTION MOULDING

Initial investigations on APC-2 by ICI[13, 18, 42] produced very promising results.   The scrap was reclaimed by granulation and then diluting with additional PEEK and processing to form a fully shaped article using conventional injection moulding technology.   Such mouldings can be stiffer and stronger than those made from conventional carbon fibre reinforced PEEK injection mouldings because in standard injection moulding compounds, no matter what length of fibre is used, the fibres rarely exceed 0.5mm in length.   A properly wetted continuous fibre reinforced thermoplastic may be chopped to length and fed through an injection moulding process with little attrition because the individual fibres are protected from abrading each other by the viscous resin

between them. Thus it is possible to injection mould a product with enhanced properties, especially with respect to impact resistance and notch sensitivity.[45]

This investigation was extended to APC-2,[14, 137] to produce injection mouldings of the scrap at fibre loadings up to 50% by weight although this loading is not thought to be commercially practical.[138] The results, shown in Table 6, also show enhanced mechanical properties compared with conventional carbon fibre reinforced PEEK injection mouldings.

The fibre length of such mouldings will be random and impractical to analyse theoretically. Compression moulding of regular particle sizes would permit such an analysis.

5.2   COMPRESSION MOULDING

Scrap prepreg, cut into squares, can be compression moulded at 400°C with fibre loadings in excess of 50% by weight of carbon fibre. This produces a moulding which has random in-plane reinforcement. The initial particle size of 3mm square produced mouldings of disappointing mechanical properties,[13] and the particle size was subsequently increased to 12.7mm to improve these properties. Results of these mouldings are shown in Table 7.

However, the large standard deviations apparent in certain properties suggest that a good deal more work is necessary to perfect the moulding technique before results will be obtained which can be analysed theoretically.

6.   MATHEMATICAL ADAPTATION OF PLATELET REINFORCEMENT THEORY

The theory is based around three factors which are dependent upon:

(a)   Matrix Performance

(b)   Strength Reduction

(c)   Modulus Reduction .

These variables will also dominate the reinforcement system which will be the product of compression moulding regular shaped APC-2 scrap particles.

Consequently, these factors need to be assessed by experimental work and then modified to account for the anisotropy of the APC-2 particles which constitute the moulding.

7.   MATERIALS

7.1   MATERIALS SELECTION

APC-2 prepreg, a composite which contains 68% by weight of Hercules Magnamite AS4 carbon fibre in a PEEK matrix was the material selected for investigation because of the excellent potential which it offers to the aerospace industry.

The strategy of dilution of APC-2 with additional PEEK resin necessitates a source of additional PEEK resin and this is available in two forms, i.e. either powder or transparent film.

7.2   MATERIALS PREPARATION

It was necessary to cut the APC-2 prepreg into smaller particles of known dimensions.   The nominal thickness of the supplied prepreg tape was 0.125mm, and therefore this dimension was invariable, so the only dimensions which could be varied were length and width.

A granulated prepreg tape was available from ICI, which had been through a fragmentation process, achieved by a Mono Muncher.[139]   This process was based on two parallel, inwardly rotating shafts each fitted with intermeshing cutting teeth.   The shafts rotated at different speeds so that as well as nip by the teeth there was tearing and shearing action between the opposing teeth.   The fragments were ragged and of

variable length and very little regularity, which was necessary for mathematical modelling, was achieved. This material was found to be invaluable in solving the initial processing problems as it was available in large quantities.

When these processing problems had been overcome and moulding techniques perfected, the prepreg tape was cut into square particles 6.35-25.4mm (0.25-1.00 inch) in size.

The PEEK film was cut to match the outline and dimensions of the matched metal mould, so that an alternate layer sequence of PEEK film and APC-2 particles could be prepared, thus diluting the APC-2.

7.3   MATERIAL CHARACTERISATION

The glass transition temperature, Tg, and melting point, Tm, of the supplied materials were determined using a Differential Scanning Calorimeter with the following conditions:

$$\text{Starting temperature} \quad : \quad 0^{\circ}\text{C}$$
$$\text{Rate} \quad : \quad 10^{\circ}\text{C min}^{-1}$$
$$\text{Final temperature} \quad : \quad 450^{\circ}\text{C}$$

The mechanical properties of APC-2 were determined in accordance with ASTM D3039, IITRI, and ASTM D-790 for tensile, compressive and flexural properties respectively.

The impact properties were determined as described in detail by Hooley and Turner.[57]

Fracture toughness measurements were made by use of a double cantilever beam technique described in detail in section 9.7.

Isochronous creep data was generated and subsequently long term results were compiled within the timescale available, at a load based upon the isochronous data.

Finally, having produced a fully characterised chipboard type product

from the offcuts, it was thought useful to assess the potential of this material for moulding components and such a programme was undertaken.

8.   EXPERIMENTAL PROCEDURE

8.1   MOULDING

Initial samples were manufactured by the method described by White[137] where a matched metal mould was used in conjunction with a 12" Moore's press at 390°C.

However, initial trials suggested improved properties and surface finish could be achieved by increasing the consolidation pressure to 5.5 MPa, from 3 MPa, and these suggestions were confirmed by the ICI APC-2 Development Laboratory.[140]

8.1.1   DETAILS OF PROCEDURE

The following steps were followed in the preparation of moulded plaques:

1.   It is important that the pressure and mould faces are parallel and flat, because depressions as small as 7 microns can adversely affect the surface quality of the pressed sheet, and so the Moore's press was carefully aligned.   The mould was examined to ensure negligible distortion and surface irregularity.

2.   High temper aluminium sheet was cut to the outline and dimensions of the matched metal mould, and both the mould and aluminium sheet pretreated with Freekote FRP mould release, applied as recommended by the manufacturer.

3.   Unless otherwise stated, the pieces of cut prepreg were scattered by hand into the mould, which had a piece of the previously prepared aluminium sheet on each face.   This procedure should approximate to a random fibre direction and so produce an isotropic sheet.

- 65 -

4. The matched metal mould was then placed between the hot
    platens of the press, which controlled the temperature between
    a maximum of $390^{o}C$ and a minimum of $370^{o}C$. Contact pressure
    of only 0.2 MPa was applied at this stage, sufficient to ensure
    good heat transfer without stressing the fibres before the
    PEEK matrix was soft enough to be compliant. PEEK melts at
    $343^{o}C$.

5. At $345^{o}C$, the pressure was increased to 1.0 MPa, and maintained
    until thermal equilibrium was achieved at $380^{o}C$, whereupon a
    consolidation pressure of 5.5 MPa was applied and maintained
    for ten minutes.

6. Post consolidation cooling was effected by an air quench
    through the platens at $7^{o}C$ min^{-1} to $300^{o}C$, followed by a water
    quench at $40^{o}C$ min^{-1} to $70^{o}C$. The pressure was not allowed to
    decrease with cooling.

7. Samples were removed from the mould at $70^{o}C$.

However, production of double cantilever beam samples (DCB) was more
involved than this and required extensive technique development before
the commencement of testing.

The object was to produce a flat sheet 5mm thick, with an internal
fold of aluminium to form a pre-crack through the centre of the sheet
thickness, up to 35 mm from one end of the sheet.

It is important that the orientation of the aluminium is central and
parallel with respect to thickness. This permits the crack to propa-
gate down the centre of the sample, so both halves of the cracked sample
are of equal thickness, giving true cantilever beam conditions. In
the case of continuous fibre reinforced samples, this presents few
problems, as the prepreg naturally orientates the foil correctly in a
single moulding operation. However, the small squares which were

being used as base material here presented many problems and numerous systems were attempted to establish a successful moulding technique as follows:

(a)   A single moulding operation was carried out in which 100g of Mono Munched material was added to the mould and levelled.   The fold of aluminium was placed on top of this and the final 100g placed on top of this and moulding carried out in the previously described manner. A cross-section through the sheet revealed an unsatisfactory pre-crack which was neither straight nor central.

(b) In an attempt to prevent excessive wandering, 70g of Mono Munched material was given a standard moulding cycle.   A further 30g was then added and levelled before the aluminium fold was positioned and covered with 30g of material before a second moulding operation. Finally, a further 70g of material was added and a final moulding operation carried out.   Obviously this was very time consuming and showed very little improvement in the orientation of the pre-crack.

(c)   To utilise the stiffening effect of continuous fibres, method (b) was repeated using 0° orientated fibres to construct the top and bottom layers of 70g.   Such a moulding was sampled and placed under test, but the crack migrated to the continuous layer interface and thus any such testing would be unrepresentative of the composite under evaluation.

(d)   100g of Mono Munched material was moulded, the aluminium fold placed directly on top of this and the final 100g of material added before a second and final moulding.   It was thought that the flat moulded surface would act as a former, preventing the foil from move-ment, so holding it true and central, and this was achieved to some degree.   Two samples were taken from such a moulding and tested. The first showed different degrees of bending in each half and thus a loss of the required DCB conditions.   The second sample was reinforced

by glass fibre epoxy strips glued to the outside in an attempt to
minimise bending, but this was unsuccessful because the adhesion
interface failed after very little displacement.   It was thought
that a contributory factor to the problem could be that some parts
of the moulding were receiving two or more cycles while others
received one.   consequently, a final moulding technique was attempted
in order to eliminate this, as described in (e).

(e) Finally, 100g of Mono Munched material was moulded and removed
from the mould.   Another 100g was moulded.   The adjoining faces
were degreased and the first sheet moulded onto the second with the
aluminium fold inserted between the two prior to final moulding.
The resultant sheet contained a very straight pre-crack and this was
the moulding technique employed for subsequent DCB specimen prepara-
tion.

The moulding procedure was thus defined, and with this a range of seven
particle sizes varying from 6.35 - 25.4 mm were taken and samples pro-
duced destined for the mechanical testing procedures outlined later.
The particle size was increased by equal increments between samples,
and thus a complete range of the particle size effect could be accumu-
lated.

When injection moulding APC-2 offcuts, dilution of the fibre volume
fraction was necessary, in compression mouldings, this presented a
problem with the distribution of the additional resin.

The dilution was attempted using PEEK granules without any success
because the PEEK granules migrated to the bottom of the mould, leaving
APC-2 in the upper regions, thus producing a distinct two part
moulding.

Eventually, dilutions of 55, 60 and 65% PEEK by weight were achieved
by stacking alternate layers of PEEK film with 12.7mm square APC-2

particles within the mould to achieve the predetermined dilution.

Another alternative which it was thought may offer useful theoretical evidence was to produce an ordered lay up of particles within the moulding. This effect was created in mouldings with 25.4mm square particles stacked to produce lay ups with fibre orientations of $(0)_{16}$, $(90)_{16}$ and $(0,90)_8$. The system of particle arrangement was a regular pattern as presented in Figure 17 and thus approaching the theoretical situation.

Other particle effects could prove interesting such as:

(a) The effect of combining two particle sizes in one moulding. The two sizes chosen initially were 25.4mm and 12.7mm square.

(b) The effect in a woven product. A mould was made of woven 12.7mm wide strips in eight mats.

(c) The effect of elevated temperature. Flexural testing at $200^{\circ}C$ was used to ascertain this.

(d) The effect upon final properties if the base material for the moulding was preconsolidated sheet stock. Pieces were cut from 8 ply preconsolidated material and moulded as previously described to establish this.

(e) The effect of extended time at moulding temperature upon the material properties, because if mouldings were made from offcuts and scrap parts, then APC-2 would be subjected to longer times at the moulding temperature. Mouldings were made, holding at temperature for up to eight hours to establish this.

9.   MECHANICAL TESTING

A series of samples were thus ready for evaluation. The properties under investigation were flexure, tensile, compression, damage tolerance, impact toughness, fracture toughness, creep, and finally

formability. The test methods outlined generally follow the recommendations of ASTM and The Composites Research Advisory Group, CRAG, wherever possible and, where necessary, testing was performed at ICI Wilton (APC Development Laboratory).

9.1   INITIAL PREPARATION

The quality of samples was determined prior to all mechanical testing, by ultrasonic C-scanning at ICI. Details of this method may be found in Appendix 2. Samples were cut to size using diamond impregnated tooling, with a suitable fluid to provide lubrication and cooling. Where sample fixtures were required, the following procedure was carried out:

(i)   The use of end tabs necessary for the tensile and compression testing of composites and these were made from a woven cloth/ epoxy laminate sheet. The tabs were prepared with a length of 54mm and a taper of 30°, and positioned adjacent to the gauge length. It was important to apply the tabs in a uniform manner.

(ii) For DCB samples, it was necessary to use 25mm square blocks machined with a 13mm diameter hole through the centre.

The fittings were applied in the manner outlined below:

(a)   Surfaces were degreased with 1.1.1. trichlorethane.

(b)   Surfaces to be bonded were shot blasted to give uniform abrasion over the area to be bonded.

(c)   Loose particles were removed from the abraded surfaces by a short immersion in an ultrasonic cleaning bath containing 1.1.1. trichloroethane.

(d)   The surfaces were bonded together in accordance with the manufacturers procedures and recommendations of temperature, pressure and time to achieve optimum bonding.

(e)   The surfaces were bonded with a suitable adhesive system.

Redux 319A, Araldite 2007, Araldite 2005 and Araldite epoxy

resin were all found to be suitable. The bonding procedure

applicable to the particular adhesive being employed was

followed.

Specimen dimensions may be found in Table 8.

9.2   FLEXURAL MEASUREMENTS

The advantages of flexure as compared with tension for strength measure-

ments on brittle materials are that the results are less sensitive to

slight misalignment of the specimen-apparatus assembly, and the stress

field is such as to limit the region in which a failure is likely to

initiate.

The appropriate classical elasticity formula can be used and the

maximum stress, σ is given by:-

$$\sigma \; = \; \frac{3PL}{2bd^2} \qquad\qquad (9.1)$$

where L is the span

b is the width

d is the thickness and

P is the maximum force recorded during the test.

The modulus of elasticity or flexural modulus, E_F, is the ratio

within the elastic limit of stress corresponding to strain.   This

can be calculated by drawing a tangent to the steepest initial straight-

line portion of the load deflection curve and:

$$E_F \; = \; \frac{L^3 \, m}{4b \, d^3} \qquad\qquad (9.2)$$

where m is the slope of the tangent to the initial straight-line portion

of the load deflection curve.

The width and thickness were measured at the centre of the specimen to

an accuracy of 0.01mm, and testing carried out under the following conditions:

Support span	:	101.6mm
Nominal span thickness	:	50:1
Loading nose diameter	:	6.35mm
Support nose diameter	:	6.35mm
Test rate	:	5mm min^{-1}

9.3   TENSILE MEASUREMENTS

Tensile testing machines seldom apply an accurately axial stress to the specimen at low elongations, as are experienced with APC-2. This means that some bending is usually superimposed on the tension and the maximum stress in one face of the specimen is therefore greater than the recorded average stress.[141]   A brittle specimen therefore breaks at a recorded stress that is lower than that which actually initiated the failure.

There is evidence to show that the measured tensile strength can be increased[141] if specimens are aligned in appropriately designed clamps with special precautions.   Such precautions are expensive and difficult to implement, and so flexure is a popular alternative deformation mode because it enables many of the difficulties to be avoided.

The tensile strength, σ_u, can be calculated for the specimens from:

$$\sigma_u = \frac{P}{bd} \qquad (9.3)$$

The modulus of elasticity or tensile modulus, E_T, being given by:

$$E_T = \frac{ml}{bd} \qquad (9.4)$$

where l is the gauge length of the extensometer.

The width and thickness were measured at five positions on the specimen,

as in Figure 21, to an accuracy of 0.01mm.

The axial strain was measured using a 50mm gauge length extensometer, at a test rate of 1.0mm min^{-1}.

9.4 COMPRESSIVE MEASUREMENTS

Because, as for other engineering materials, APC-2 is needed for compressive applications as well as for tension and flexure, there has been interest in the compressive strength. For continuous fibres aligned in one direction, it has been found that the strength under compression in one direction is less than under tension. The basis of the failure when it occurs has been attributed to shear yield in the resin, debonding of the fibres, voids and differential effects arising from differences in Poissons ratio.[142]

The test method used for compressive strength was Illinois Institute of Technology Research Institute (IITRI) Test Method,[143] and a sketch of the test arrangement is shown in Figure 22.

Longitudinal compression strength is given by:

$$\sigma_{LC} = \frac{P}{bd} \qquad\qquad (9.5)$$

Since the stress versus strain graphs were non linear compression modulus values are not quoted from this data, and only a secant modulus may be calculated.

The width and thickness were measured at one position on the specimen to an accuracy of 0.01mm and testing carried out at a rate of 1.0mm min^{-1}.

9.5 DAMAGE AREA

The ability of APC-2 to withstand impact damage is vital to its success as an aerospace material, but results are notoriously difficult to produce consistently,[141, 142, 144] and results were not expected

- 73 -

to produce significant differences between the samples produced from different particle sizes, but the work was carried out for a complete characterisation of the samples.

The thickness was measured at nine positions on the specimen to an accuracy of 0.01mm and experimental conditions of:

Support ring diameter	:	50.0mm
Impactor diameter	:	16.0mm
Impactor energy	:	7 and 10 J
Drop height	:	480.0mm

The specimen was ultrasonically C scanned after impacting and the damaged area measured using an Optomax image analyser.

9.6   INSTRUMENTED FALLING WEIGHT IMPACT

Instrumentation of falling weight apparatus has to be a compromise between conflicting demands and as a result, several methods of instrumentation have evolved, each with its own particular merits and disadvantages.[48-56]   A major consideration is the requirement for speed and convenience in operation, since impact testing often involves large numbers of specimens.   The method employed herein is that described by Hooley and Turner[46] and developed by ICI at Wilton.

The standard specimen support is an annular ring of internal diameter 50mm and the specimen either square or circular in shape.   The support can be changed as necessary for other specimen geometries and even for whole mouldings.   The impactor, usually 100N, is released from a height such that the impact velocity is either $3ms^{-1}$ or $5ms^{-1}$. With this combination of force and drop height, there is sufficient energy to break virtually any specimen without the impactor being appreciably decelerated.   A force transducer is connected to the impactor, which produces a record of force acting on the specimen as

it is being deformed by the impact.

The information is stored in a transient recorder and displayed on a storage oscilloscope as a force time curve. The information is processed by a computer to present force deflection and absorbed energy.

The force deflection curve identifies the type of failure, and how the energy is partitioned between crack initiation and crack propagation, thus differentiating between the extremities of brittle and ductile failure in a quantifiable manner.

As the impactor strikes the surface, the force begins to rise in an approximately linear manner, from which an assessment of stiffness can be obtained. For a brittle material, failure occurs in this linear portion and the force falls abruptly to zero. For a ductile material the curve shows a peak, falling off in force as the material deforms, corresponding to a yield. As the force decreases the material is drawing around the nose of the impactor until penetration occurs. The force, deflection and energy at this final break point are computed, together with the same information at the yield point.

A special case for this type of curve is the fibre reinforced composite which fails in two modes, represented by an initial linear portion followed by an abrupt fall off in force corresponding to the breakage of fibres on the back surface of the composite. This fall off is not, however, to zero and the composite continues to fail by crack propagation through the lamina and this is represented by the remaining portion of the force deflection curve. Total failure is when the force becomes zero.

The computer calculates the energy for the initiation of failure and the deflection at this point, the energy to total failure and deflection

at this point.   The initial gradient of the force deflection plot
is also given.

The experimental testing was carried out under the following conditions:

> Support ring diameter   :   50.0mm
>
> Impactor diameter   :   12.7mm
>
> Impactor velocity   :   5.0 ms^{-1}
>
> Impactor weight   :   100.0 N

9.7   FRACTURE TOUGHNESS

The subject of fracture toughness has developed from the basic concept
of Griffith[145] that the strength of a brittle material,is governed
by small defects that act as stress concentrators.

If an artificial crack is introduced, a measurement of the strength
should allow the fracture surface energy to be calculated, but the
experimentally derived values for many materials are orders of magni-
tude higher than would be expected from calculations based on atomic
or molecular constants.   Cracks growing in normally brittle plastics
seem to be associated with fracture surface energies of about 1 KJm^{-2}
whereas estimates based on assumptions of chain scission would be in
the region of 1 Jm^{-2}.   This discrepancy, coupled with the presence of
red and green coloured regions on the fractured surface of PMMA, led
Barry[146] to postulate that there is appreciable plastic flow at the
tip of a crack growing in a polymer in its glassy state.   This promotes
the formation of a plastic zone at the crack tip which toughens the
material in three ways:

(a)   it dissipates the high local stresses to some degree,

(b)   it absorbs more energy than would be required for growth of a
      brittle crack of the same length, and

(c)   it dissipates energy, because energy absorbed in the plastic
      zone is not recoverable as it would be from elastic deformation,

and therefore this energy is not available to support further crack growth.

Aluminium blocks were attached as previously described to produce a final sample as shown in Figure 23. To facilitate crack observation the edges of the specimen were coated with typewriter correction fluid.

The DCB specimens were tested on an ESH hydraulic test machine at a test rate of 1.0mm min^{-1}.

The specimen was loaded in tension by means of the aluminium blocks until the crack in the sample preformed by the aluminium fold was propagated. The loading was then stopped and the aluminium fold cut.

The crack tip was marked with a scalpel on both sides of the specimen and the beam unloaded.

The beam was loaded again until a further crack was propagated, whereupon the loading was stopped, the crack extent marked as before and the beam unloaded. The average change in crack length was then measured using a vernier caliper and this procedure repeated until the specimen failed.

An X-Y recorder was on line to record plots of displacement against load.

9.8 CREEP

Tension is the deformation mode for a large proportion of the creep experiments reported in the literature. The main reasons for its predominance over other modes are that:

(a) most molecular relaxation mechanisms are associated with the shear mode and therefore shear and tension are the modes of greatest interest at macroscopic level,

(b) tension specimens constitute a simple system in which the stress

is uniform over the whole cross section.   One measurement technique

will suffice for the whole strain range of practical interest, and

(c)   elastic design formulae are usually expressed in a form that

requires a knowledge of Youngs modulus, and no purpose would be

served by substituting a different system for plastics.

The satisfactory evaluation of this property generally requires very

long tests for every material, under different stress and temperature

conditions, and because of this Franceschi, Momo and Campagna have

evaluated the possibility of predicting creep deformation by the use

of shorter run tests.[147, 148]   They conclude that the use of a

time-stress equivalence approach may be successfully applied.   This

equivalence can be defined by stating that a highly stressed sample

of polymeric material creeps in an identical, but accelerated way as

a moderately stressed sample.

Since the materials are usually non linear visco elastic, creep tests

are generally carried out at several stress levels, at constant

temperature, and the basic presentation of data is a family of curves

showing the variation of strain with the logarithm of elapsed time at

each stress level.

There are several other ways in which the stress-strain-time dependence

can be displayed.   Extraction of data may be easier using one of these

alternative methods of presentation.   The most important cross-plots

are presented in Figure 24.

Plotting the applied stress level against strain at a pre-determined

time produces an isochronous stress-strain cross plot.   The non

linearity of the material response (i.e. lack of proportionality of

stress and strain) is immediately apparent from such a plot.

Alternatively, a strain level can be selected and stress plotted

against the log of time to reach this strain level. This isometric stress-log time cross-plot is often taken as a first approximation to the stress relaxation behaviour of the material, although the data has been derived from a creep experiment.

By dividing the time-dependent stress by the fixed strain level chosen for the isometric cross-plot, an isometric modulus-log time graph may be produced.

Two types of data plot are presented here, conventional extended time plots at constant stress, and isochronous plots.

The specimen is shown diagrammatically in Figure 25, and Figure 26 shows the arrangement of this specimen in the clamps on the creep machine.

Initially, the region around the hole was shot blasted to reduce the tendency to slip in the clamps supporting the specimen within the creep machine.

Isochronous plots were constructed at a 100 second time period using electro mechanical extensometers to measure the strain. These were attached to the specimen through knife edge clamps at either end of the gauge length. The contact pressure was sufficient to ensure mechanical stability of the extensometer and eliminate the possibility of slip, while at the same time causing a minimum of damage to the surface of the sample.

In between each stress level strain measurement the specimen was unloaded and allowed to relax. The plots presented are the mean of three specimens.

With this data to hand, extended time plots were constructed at a constant stress value, considered to be relevant from the isochronous information. This value of stress was 80 MPa and, as before, applied

by mechanical loading through an amplification factor of ten using a pivot arrangement. The force acted along the axis of the specimen to eliminate bending stresses.

9.9   MOULDING OF THE TEST COUPON

A curvature particularly difficult to form in continuous fibre reinforced thermoplastics is one which has three dimensional curvature. It was thought that the material under investigation may provide an ideal compromise between standard injection mouldings and continuous fibres, whether woven or not.

The specimens were heated in an oven at $400^{\circ}C$ for 5 minutes, then transferred to a press within ten seconds and a pressure of 2.0 MPa was applied to form them into shape over the forming tool. Typically the cooling of blanks proceeded over an 8-10 second transport from the oven to forming tool, and a 4-12 second contact with the cold metal tool, followed by free exposure to ambient air.

Petroleum jelly was used to lubricate the alloy/silicon rubber mould tools, and two radii of curvatures were examined.

This constituted a qualitative assessment of blank moulding and the results were tabulated accordingly.

10. RESULTS

10.1 PEEK CHARACTERISATION

The DSC results on PEEK film gave a glass transition temperature, T_g, of $147^{\circ}C$ compared with the published value of $143^{\circ}C$.

However, it is necessary to achieve a T_g of this order in APC-2 itself if total success if to be achieved in the application of APC-2. To verify this a 30mg sample of APC-2 which had been quenched according to section 8.1.1, was used in the DSC pan. The weight was increased from 10mg because the PEEK content of APC-2 is only 32% and an inflexion of sufficient magnitude is necessary for accurate assessment of the T_g and this inflexion depends on the PEEK content, not the carbon fibre content. The data obtained from this system gave a T_g of $154^{\circ}C$, so it appears that the T_g has not significantly been affected by the addition of carbon fibres to the PEEK matrix.

10.2 APC-2 MECHANICAL CHARACTERISATION

The mechanical properties of APC-2 were determined for the relevant macrostructural configurations and these are presented in Table 9, with standard deviations quoted in brackets.

This data was used to compare quasi isotropic values with the results contained in this section.

10.3 THE EFFECT OF PARTICLE SIZE

10.3.1 GENERAL CONSIDERATIONS

The overall aim was to compare the properties of the material form under investigation with the parent material and thus to predict the particle size at which quasi-isotropic properties could be expected.

10.3.2 FLEXURAL PROPERTIES

The flexural strength of a series of mouldings with increasing particle size is presented in Figure 27, the plot is apparently linear and by

using linear regression analysis the gradient was found to be 3.78 MPa mm^{-1}. Extension of this analysis suggests that at a particle size of 69.6 mm square, quasi-isotropic flexural strength (616 MPa) will be attained.

The flexural modulus also increases linearly with particle size, as presented in Figure 28. The best fitting line has a gradient of 0.26 GPa mm^{-1} and a quasi-isotropic modulus (40.9 GPa) is predicted at a particle size of 47.7 mm square.

10.3.3 TENSILE PROPERTIES

The tensile strength of a series of mouldings with increasing particle size is presented in Figure 29. Once again, an apparently linear plot is evident, but the actual strength is considerably reduced compared with the flexural strength. The gradient is 2.86 MPa mm^{-1} and a quasi-isotropic tensile strength property (704 MPa) is predicted at a particle size of 170.8 mm square, somewhat greater than the previously predicted particle size, when studying flexural properties.

The tensile modulus increases linearly with particle size, as presented in Figure 30. The best fitting line has a gradient of 0.26 GPa mm^{-1} and a quasi-isotropic tensile modulus (48.6 GPa) is predicted at a particle size of 48.3 mm square.

The tensile strain at failure vs. particle size is also a linear relationship (Figure 31). The gradient being 0.0175% mm^{-1} predicts quasi-isotropic strain (1.69%) at a particle size of 78.0 mm square.

10.3.4 COMPRESSION PROPERTIES

The compression strength of a series of mouldings with increasing particle sizes is presented in Figure 32. The plot is apparently linear, the gradient of the best fitting line being 5.05 MPa mm^{-1}, with the quasi-isotropic compressive strength (361 MPa) being exceeded at a particle size of 12.3 mm square, presumably because of

the orientation effect within the greatly reduced gauge length as compared with the flexural and tensile specimens.

10.3.5   DAMAGE AREA

The damaged areas of a series of mouldings with increasing particle sizes are shown in Figure 33.

Two impact energies were examined, i.e. 7 and 10J.   The lower level energy impact plot suggests a sharp fall off in damage tolerance below a particle size of about 9mm square.   This was supported by a visual examination of the failures, the moulding made from particles of 6.35mm square being the only sample which was penetrated totally.

The higher level energy impact plot suggests no such critical point, merely a gradual increase in damage tolerance as the particle size of the moulding is increased.

10.3.6   IMPACT TOUGHNESS

The energy absorbed to initiate failure, and the total energy absorbed during falling weight impact testing are presented together in Figure 34.   Both plots are apparently linear with a good agreement of prediction for attainment of quasi-isotropic properties.

The energy absorbed to initiate failure of the carbon fibres in the back face increases much slower than the energy for total failure increases, although both properties are approximately 50% of the quasi-isotropic values for a particle size of 6.35 mm square.

The energy absorbed to initiate failure increases at 0.1 Jmm^{-1} leading to a prediction of a quasi-isotropic value (6.0J) at a particle size of 34.8 mm square.

The total energy absorbed during failure increases at 0.357 Jmm^{-1} predicting quasi-isotropic properties (20.0J) at a particle size of 33.7 mm square.

- 83 -

10.3.7 FRACTURE TOUGHNESS

In order that direct comparison of previous work by Carlile[24] on continuous fibre reinforced APC-2 could be made, the data reduction method selected was the area method. Whitney[60] supports the use of this method and recommends its accuracy.

Because of the original nature of this moulding technique and relative infancy of DCB testing, preliminary discussion of technique and analysis of results is necessary.

The use of the area method meant that the variables which needed to be recorded during the test were crack length, load and displacement. Load and displacement were easily recorded continuously on an X-Y recorder with little error.

However, the measurement of crack length did present difficulties. The beams all fractured in cleavage, except the APC-2 reference which exhibited mixed mode failure. The change in crack length as the DCB was loaded was required and, being an instantaneous fracture it amounted to a 'jump' of the crack.

Thus after each progression the crack had to be measured, necessitating stopping the displacement and locating the crack tip with a travelling microscope and marking with a scalpel in the white edge of the sample. This was done on both sides of the sample and the mean taken, measurement was by a digital vernier.

This technique is the source of several errors, not necessarily just with respect to the measuring process. Observations during fracture and subsequent examination of the fractured surface revealed that the crack was not always straight in the particulate samples, with the crack tending to follow particle boundaries and interfaces across the beam.

The difficulty in determining an accurate crack length represents a major flaw in the use of the parallel beam DCB test and could produce substantial variation in the calculation of G_{IC}, and particular attention is paid to statistical analysis of these results.

Some beams produced only one propagation before failure, limiting the number of results, and for this reason it is vital to establish that G_{IC} does not vary with total crack length, i.e. down the length of the beam.

The results so produced are presented in Table 10, with the mean value for each beam and overall mean value tabulated. Table 11 presents the mean with respect to standard deviation and 95% confidence limits for each particle size.

The 95% confidence limits were calculated from:

$$\text{Predicted range for} \quad \mu = \bar{x} \pm \frac{Sx}{\sqrt{n}} t \qquad (10.1)$$

where μ is the population mean value,

$\bar{x}$ is the sample mean,

Sx is the standard deviation,

n is the number of samples, and

t is a statistical modification from tables.

This data is presented with respect to particle size and G_{IC} on Figures 35 - 42. From these figures it can be seen there is not a definite trend relating crack length to G_{IC}.

Examination of the effect of particle size on the strain energy release rate, G_{IC} is presented in Figure 43. There is an apparently linear relationship between particle size and G_{IC}, although this slope is now negative and has a value of -79.2 (Nm^{-1}) mm^{-1} with continuous fibre properties (2068 Nm^{-1}) being predicted at a particle size of 33.5mm square.

Also included on the figure are the 95% confidence limits and these appear to converge as the particle size increases, which suggests less difficulty in data recording of crack length due to fewer particulate boundaries. Linear regression is used to predict the best fitting slope.

10.3.8 CREEP

Isochronous data plots are presented in Figures 44 - 50. These figures relate the stress and strain with respect to particle size and from these the data for Figure 51 were extracted, showing the effect of particle size upon strain levels at a high and intermediate levels of stress; 130 MPa and 80 MPa respectively.

It is readily seen that at intermediate levels of stress the strain remains constant over the particle size range examined, whereas at higher levels of stress the smaller particle constructed material becomes progressively more susceptible to exaggerated levels of strain.

Figures 52 - 58 present long term creep behaviour of the material. When comparing the increasing particle size, a general reduction in gradient is highlighted by Table 12. All these plots are at a stress level of 80 MPa and compare favourably with the creep data presented in Appendix 1 for $\pm$ 45 APC-2 at 23°C.

10.3.9 FORMABILITY

Although this can only be a very qualitative assessment of the material under investigation, it is perhaps the most significant to the consumer of APC-2, because if it were possible to mould a component otherwise unattainable then not only would scrap be self supportive but the overall cost of APC-2 would be reduced. Thus, two significant commercial aspects would be satisfactorily concluded simultaneously.

The general comments on mouldings carried out within this work are

presented in Table 13, and representative mouldings are presented in Figures 59-63.

It was evident that blanks containing smaller particles produced better finished mouldings, with a reduced tendency to tear and wrinkle. Also, the more pronounced the corner, the greater the tendency to result in poor mouldings. To overcome this, an alternative moulding technique is necessary.

10.4 THE EFFECT OF PEEK CONTENT

The flexural properties of diluted APC-2 are presented in Figures 64 and 65. The dilution effect is apparently linear over the dilution range examined, both with respect to strength and modulus.

Diluting the APC-2 for compression moulding is a laborious and, from the results obtained, unrewarding activity. For this reason, and after consultation with the Aromatic Polymer Group at ICI, the investigation was not extended to other properties or dilutions.

As previously discussed in Section 5.1, APC-2 has been successfully diluted and injection moulded[14, 137] to give superior properties compared with a standard injection moulding, but this advantage does not materialise in the compression moulding system. Indeed, by comparing the data from Appendix 1, at 40% PEEK, with Figures 64 and 65, the flexural modulus of compression moulded material is 57% of the comparable injection moulded system and the flexural strength only 30% by the same comparison.

10.5 THE REGULAR LAY-UP

Particular attention was paid to the flexural properties for the reasons outlined in Section 9.3; and the tensile properties would be extremely suspect in a $(90)_{16}$ lay-up because of a tendency to fail at the grips.[13]

These properties are presented in Table 14 where the $(90)_{16}$ lay-up

is readily seen to have approximately the same properties as the

continuous reinforcement system, within experimental error.

This suggests that the moulding technique is producing a moulding with

good interfacial bonding, so nothing is lost by the bonding between

particles.

10.6   THE COMBINATION OF PARTICLE SIZES

The commercial production of mouldings from APC-2 precludes the granu-

lation of offcuts so produced being cut into carefully controlled

particle sizes; because of the nature and complexity in shape of the

individual plies.   Thus, it is necessary to be able to predict the

properties of a moulding which contains particles varying in size.

Presented in Table 15 are the properties of a moulding with 50% 25.4mm

square particles thoroughly mixed with 50% 12.7mm square particles.

Included in the table are characterisation details of the 'Mono Munched'

scrap, this being an attempt to identify its position on the mechanical

property vs. particle size plots.

The moduli properties of the 'Mono Munched' material are disappointing,

and in order to try and improve this situation the Mono Munched material

was sieved and fine particles, smaller than 3mm, were removed. Although

other mechanical properties were improved, the moduli were still

disappointing.

10.7   THE WOVEN PRODUCT

The idea of a woven moulding has been examined in detail by Measuria

and Cogswell.[75]   Presented in Table 16 are a series of properties

for a woven matting product produced from 12.7mm wide scrap strips.

As with the square particle reinforcement system, the tensile strength

value is particularly disappointing, although all other properties show

great promise for a reinforcement system if the scrap available is suitable for utilisation in this manner.

10.8   TEMPERATURE CAPABILITY

The maximum quoted continuous use rating of APC-2 is 200°C.[18]   At this temperature, approximately 80% of the flexural properties of a unidirectional laminate are retained with respect to the properties at 23°C.   However, because this temperature is above the glass transition temperature, in a lay-up where the properties are matrix dominated the modulus reduces significantly.

At this temperature, 200°C, the flexural strength of a moulding containing 12.7mm square particles is 159.6 (11.8) MPa, this being 40% of the flexural strength at 23°C for a similar moulding.   The flexural modulus of such a moulding at 200°C is 16.1 (0.05) GPa, this being 47% of the modulus at 23°C.

10.9   THE EFFECT OF USING PRECONSOLIDATED SHEET AS BASE MATERIAL

10.9.1   GENERAL CONSIDERATIONS

A possible source of second generation material for processing would be mouldings of components which had failed in service or by quality control rejection.   With a view to examining these materials a series of mouldings was constructed for different particle sizes of 8-ply preconsolidated sheet stock.   The properties of such mouldings were evaluated in similar manner to the single ply series of Section 10.3.

10.9.2   FLEXURAL PROPERTIES

The flexural strengths of a series of mouldings with increasing particle size is presented in Figure 66, a best fitting straight line produces a gradient of 4.46 MPa mm^{-1} and quasi-isotropic properties (616 MPa) are predicted at a particle size of 80.0mm square.

The flexural modulus also increases linearly with particle size, as

presented in Figure 67. The best fitting line has a gradient of 0.59 MPa mm^{-1} and quasi-isotropic material properties (40.9 GPa) predicted at 48.3 mm square.

10.9.3   TENSILE PROPERTIES

The tensile strength of a series of mouldings with increasing particle size is presented in Figure 68. Once again, an apparently linear plot is evident but the actual strength is considerably reduced compared with the flexural property. However, the gradient is somewhat greater, so the tensile strength increases much more rapidly with respect to particle size than does the flexural strength in this particular instance, with quasi-isotropic properties (704 MPa) being predicted at 88.4 mm square, via a gradient of 7.5 MPa mm^{-1}.

The tensile modulus increases linearly with particle size, as presented in Figure 69. The best fitting line having a gradient of 0.59 MPa mm^{-1} and quasi-isotropic properties (48.6 GPa) predicted at a particle size of 56.7 mm square.

The tensile strain at failure vs. particle size is also a linear relationship as presented in Figure 70. The gradient being 0.0175% mm^{-1} predicts quasi-isotropic strain to failure (1.69%) at a particle size of 67.7 mm square.

10.9.4   COMPRESSIVE PROPERTIES

The compression strength of a series of mouldings is presented in Figure 71. The plot is apparently linear, the gradient of the best fitting line being 8.08 MPa mm^{-1}, with quasi-isotropic compressive strength (361 MPa) being exceeded at a particle size of 21.6 mm square, presumably as in Section 10.3.4 because of the orientation effect within the greatly reduced gauge length as compared with tensile and flexural properties.

10.9.5   IMPACT TOUGHNESS

The energy absorbed to initiate failure, and the total energy absorbed during failure are presented together in Figure 72.   Both plots are apparently linear with a good agreement of prediction for attainment of quasi-isotropic properties.

As previously recorded in Section 10.3.6 the energy absorbed to initiate failure increases much slower than the energy for total failure increases, but now both properties are approximately 50% of the quasi-isotropic values at 19.0 mm square when compared with 6.35mm square in the previous examination of single ply particles.

The energy absorbed to initiate failure increases at 0.13 J mm^{-1} and leads to a prediction of quasi-isotropic value (6.0J) at a particle size of 42.4 mm square.

The total energy absorbed during failure increases at 0.39 J mm^{-1} predicting quasi-isotropic properties (20.0J) at a particle size of 44.7 mm square.

10.9.6   FRACTURE TOUGHNESS

Having established the basic principles in Section 10.3.7, the effect of particle size is presented in Figure 73.   There is an apparently linear relationship between particle size and G_{IC} and this slope is again negative with a value of - 123.5(Nm^{-1}) mm^{-1}, with continuous fibre properties (2068 Nm^{-1}) being observed at a particle size of 17.9 mm square.   The 95% confidence limits are also included because of the large deviations observed previously.

10.10   THE EFFECT OF PROLONGED TIME AT ELEVATED TEMPERATURE

As presented in Figures 74 and 75, there is little effect upon the flexural properties of the mouldings by holding at the moulding temperature of 400°C and no conclusive evidence is seen of a reduction

in properties.

A polymer may become brittle after a long time at elevated temperature
but this is not so in the case of PEEK as indicated by Figure 76 which
presents the impact toughness properties of a moulding tested under
these conditions.

11.   DISCUSSION

Some indication has already been given as to the nature of failure in
polymer composites (Section 4.1.4) and it is of interest to have a
closer look at the actual fracture process.   Whenever it occurs,
whether by tension, compression, flexure, peel or impact, it is for
one or more of the following reasons:

(a)   cohesive failure of the matrix,

(b)   cohesive failure of the reinforcement, or

(c)   adhesive failure at the interface or interfacial region.

Reinforcement failure occurs when the stress in the direction of the flake
axis exceeds a certain value and usually precedes total failure in
which matrix cracking or interfacial debonding takes place.   In some
cases it is believed that the origin of failure is through microcracks
produced by differential expansion effects during cooling after
moulding, or in subsequent thermal cycling.

Some idea of the mode of failure can often be gained from the appearance
of the broken specimen.   For example, if fracture takes place at the
interface, then flakes are pulled out and have little or no polymer
adhering to them.   On the other hand, in the case of matrix failure,
the flake may be again pulled out, but this time there will be an
indication of the presence of polymer on the flakes.   In cases where
there is a strong interface, flake fracture may be observed, with

very few exposed fibre lengths being visible.

The work contained herein is based upon two different types of material as sources for moulding the specimens. The initial work involved pieces of single ply thickness and the work was thereafter carried out on specimens constructed from eight ply base material, which had a quasi-isotropic lay-up of $(+,-,90,0)_s$ in order to substantiate the theoretical modelling system.

In the case of continuous fibre reinforcement all the fibres work at maximum efficiency, with the average strain in the fibre being equal to that in the matrix. In discontinuous reinforced composites this is not so. Figure 1 shows the state of deformation around a short fibre. The fibre restricts the deformation of the surrounding matrix because it is stiffer than the matrix material. The load is transferred from the matrix to the fibre via the interfacial shear stresses. The calculation of the variation of the shear and tensile stresses along a short elastic fibre in an elastic matrix was carried out by Cox.[149]

The shear stress is greatest at the ends of the fibre and decays to zero somewhere along it. The tensile stress is zero at each end of the fibre and reaches a maximum at the centre. If the fibre is just not long enough, the maximum tensile stress reaches the tensile stress in the matrix. The ratio $(L/D)_c$ that occurs under these conditions is called the critical aspect ratio (L being the fibre length and D its diameter). For values of L/D less than $(L/D)_c$ the tensile stress in the fibre is always less than that in the matrix, and clearly under these conditions the transfer of load from the matrix to the fibre is poor and the mechanical properties of the fibre are not fully utilised. If L/D is greater than $(L/D)_c$, the tensile stress at the interface remains at a maximum over a greater proportion of the fibre length. Here, the

transfer of stress from the matrix to the fibre is very efficient
but the average tensile stress in the fibre is always less than that
in the matrix because of the reduced tensile stress at the ends of
the fibre. The efficiency of stress transfer is, therefore, never
100%.

In order to accommodate this change in reinforcement efficiency with
fibre length, the term ψ_L is included in the rule of mixtures. This
is the fibre length correction factor and has a value less than unity.

$$E_c = \psi_L E_f \phi_f + E_m \phi_m \qquad (11.1)$$

where E_c is the Youngs modulus of the composite,

   E_f is the Youngs modulus of the fibre,

   E_m is the Youngs modulus of the matrix,

   ϕ_f is the volume fraction of the fibre, and

   ϕ_m is the volume fraction of the matrix.

The theory developed by Cox[149] gives:

$$\psi_L = \left[1 - \frac{\tanh (\beta L/2)}{(\beta L/2)} \right] \qquad (11.2)$$

where L is the fibre length and

$$\beta = \left(\frac{H}{E_f A_f} \right)^{\frac{1}{2}} \qquad (11.3)$$

where A_f is the area of the fibre, and

$$H = \frac{2 \pi G}{\ln(r_1/r_o)} \qquad (11.4)$$

where r_1 is the mean separation of fibres normal to their length,

   r_o is the fibre radius, and

   G is the shear modulus of the fibre.

If $\beta L/2$ is large the value of ψ_L approaches unity but if $\beta L/2$ is
small then ψ_L tends to zero. It is therefore necessary to consider
the expression:

$$\frac{L}{2} \cdot \left[\frac{H}{E_f A_f} \right]^{\frac{1}{2}}$$

In order to analyse this expression Cox[149] assumed hexagonal packing of the fibres and:

$$\frac{2\pi r_o^2}{\sqrt{3}\, r_1^2} = \text{relative fibre density} = \frac{\text{actual fibre density}}{\text{specific gravity of fibre}}$$

The specific gravity of AS4 carbon fibre is 1.8.

Hence $\dfrac{r_o}{r_1} = 0.39 \, (\text{actual fibre density})^{\frac{1}{2}}$

For a PEEK composite of specific gravity 1.6[42] containing 39% of resin of specific gravity 1.32[15], the actual fibre density is:

$$1.6 - (0.39 \times 1.32) = 1.0852$$

Hence $\dfrac{r_o}{r_1} = 0.406$

and $H = 6.97 \, G$

The shear modulus, G, of PEEK is 1.3 GPa, Youngs Modulus, E, of AS4 carbon fibre is 235 GPa.

Hence $\dfrac{L}{2} \left[\dfrac{H}{E_f A_f} \right]^{\frac{1}{2}} = \dfrac{L}{2 r_o} \left(\dfrac{6.97 \times 1.3}{\pi \times 235} \right)^{\frac{1}{2}}$

$$= 0.055 \, (L/r_o)$$

Therefore, in conclusion, $\beta L/2$ is equal to 0.11(L/d), where d is the fibre diameter.

The diameter of AS4 carbon fibres is 8×10^{-3} mm and the fibre lengths of this work vary from 6.35 - 25.4mm, and calculation of the fibre length correction factors, ψ, for such aspect ratios results in values from 0.9885 to 0.9971. This implies very little reduction of modulus with respect to the continuously reinforced unidirectional composite.

However, the composite under examination is not unidirectional, and so

requires a further modification,[121] ψ_o , to account for the variation in orientation that is a consequence of attempts to achieve random distribution.

$$E_c = \psi_o \, \psi_L \, E_f \, \phi_f + E_m \, \phi_m \qquad (11.5)$$

$$\text{where} \quad \psi_o = \sum_{i=1}^{K} a_i \cos^4 \theta_i \qquad (11.6)$$

where a_i is the fraction of fibres orientated at an angle θ to the direction in which the value of E_c is required, and

K is the number of intervals of angle into which the fibre orientation distribution is divided.

Assuming the angles of distribution approximate to a quasi-isotropic situation $(+,-,90,0)_s$:

$$\psi_o = 0.375$$

Thus, the overall modification factors have values from 0.3707 to 0.3739, producing tensile moduli predictions of 54.7 - 55.2 GPa respectively for 6.35mm square particles and 25.4mm square particles. This situation is not in operation by consideration of the experimental tensile moduli as presented in Figure 30.   Clearly, the other moduli will not be predicted any more accurately, because the values of the overall modification factors are approximately equal in value.

Thus, flake reinforcement theory as discussed in Section 4, is adopted for the analysis of the data.

11.1   ANALYSIS OF THE MATERIAL CONSTRUCTED FROM SINGLE PLY PARTICLES

By consideration of the moduli and strengths presented in Figures 27 - 32, it is possible to assess the correlation between the mechanical properties that are under examination, i.e. tension, flexure and compression.

The two graphs of modulus versus particle size have uniform gradients

of 0.26 GPa mm^{-1}, so it is reasonable to assume that a very definite relationship exists between particle size and modulus.

However, the graphs of strength versus particle size, although having similar gradients, are not as clearly defined because of the mode of failure. This observation is highlighted by the particle size at which quasi-isotropic strengths are predicted from linear regression analysis of the graphs. This particle size varies from 12.3mm square for compression strength to 170.8mm square for tensile strength.

The variation of strength within the moulding may be thought of in terms of:

$$\text{Strength } \alpha \quad \frac{\text{Particle size}}{\text{Test piece length dimension}}$$

and when the particle size and test piece dimensions are approximately equal, then the test approaches a quasi-isotropic situation and properties of a quasi-isotropic laminate may be expected.

This is an important design criteria for the optimum reclamation of APC-2 offcuts, because if the critical dimensions of the component to be manufactured contain particles of APC-2 that are of similar dimensions, then quasi-isotropic properties may be achieved without the use of expensive prepreg material. Although such a system could not be envisaged for primary aerospace structures, many automobile components could be formed in such a manner.

11.1.1   MODULUS MEASUREMENTS

11.1.1.1   Tensile Modulus

The calculation of the appropriate factor depends upon successful and relevant interpretation of its various constituent components. The factor under consideration here is the Modulus Reduction Factor (MRF) and the particular components under consideration are the constituents of u, a constant for a constant aspect ratio and material properties:

$$u = \alpha \left\{ \frac{G_m \, \phi_f}{E_f (1 - \phi_f)} \right\}^{\frac{1}{2}}$$

The matrix shear modulus of PEEK, G_m is 1.3 GPa, so this term is constant; α, the aspect ratio varies only with the particle size; the modulus, E_f, of the flake does, however, vary with angle of orientation to the direction in which the value of E_c is required. There are two possible alternative approaches to this:

(a) To analyse the data using simple volume fractions and to assume the modulus of a unidirectional reinforcement system. If this is so:

$$u = \alpha \left\{ \frac{1.3 \times 0.68}{134 \times 0.32} \right\}^{\frac{1}{2}}$$

$$u = \alpha \, (0.1436)$$

(b) Alternatively, a novel approach would be to propose that E_f takes account of the anisotropy within the flake and to use the modulus of either a quasi-isotropic, $(+,- 0,90,)_s$, or a $(90,0)_s$ lay-up; such an arrangement would mean that $\left(\phi_f / 1 - \phi_f \right)$ was unity.

quasi-isotropic,
$$u = \alpha \left\{ \frac{1.3}{48.6} \right\}^{\frac{1}{2}}$$

$$u = \alpha \, (0.1636)$$

or $(0,90)_2$,
$$u = \alpha \left\{ \frac{1.3}{71.8} \right\}^{\frac{1}{2}}$$

$$u = \alpha \, (0.1346)$$

These predictions are presented in Figure 77, and they suggest that the most applicable approach to the problem is the quasi-isotropic prediction.

It is readily observed that it is virtually impossible for the reinforcement theory based on a unidirectional lay-up to be effective as this predicts a modulus greater than the quasi-isotropic lay-up, at a particle size of less than 6.35mm square. This is proven not to be so by the work undertaken herein and confirmed by White.[137]

Of the other two possible approaches, it is suggested that the $(0,90)_s$ predictions are more relevant to an ordered lay-up, as presented in Table 14. This is discussed in more detail later.

This leaves the analysis of a quasi-isotropic property profile prediction. In order to assess this more fully the practical results are superimposed onto Figure 77. The outcome of this exercise confirms that this approach is applicable to modulus predictions over the particle size range under consideration, the theoretical plot being well within the $^{+}_{-}5\%$ error band.

To substantiate this proposal the flexural modulus must be analysed in the same manner.

11.1.1.2 Flexural Modulus

The three relevant values of u are:

$$\text{unidirectional,} \quad u = \alpha \left\{ \frac{1.3 \times 0.68}{130 \times 0.32} \right\}^{\frac{1}{2}}$$

$$u = \alpha \, (0.1458)$$

$$\text{quasi-isotropic,} \quad u = \alpha \left\{ \frac{1.3}{40.9} \right\}^{\frac{1}{2}}$$

$$u = \alpha \, (0.1783)$$

$$(0,90)_s, \quad u = \alpha \left\{ \frac{1.3}{68.8} \right\}^{\frac{1}{2}}$$

$$u = \alpha \, (0.1375)$$

The subsequent predictions are presented in Figure 78. Once again, the unidirectional modulus predictions suggest that the quasi-isotropic modulus would be exceeded at a particle size of less than 6.35 mm square, so the approach is subsequently abandoned.

Consequently, the quasi-isotropic predictions would appear to be experimentally justified, as once again these predictions are virtually within the $^{+}_{-}5\%$ error band.

11.1.2 STRENGTH

The micromechanical analysis of the mechanical behaviour in terms of the separate contributions of the two components to the mechanical properties is complicated. This complication arises not only from the fairly straightforwardly recognised complexities of reinforcement concentration, but also from uncertainties in the magnitude of interaction, especially as this might itself vary as the polymer and reinforcement are mechanically forced into greater contact during fabrication. In addition there are uncertainties in reinforcement distribution, complicated by any agglomeration, and to what extent void formation has occurred during fabrication, and the related problem of imperfect interfacial contact between the matrix and reinforcement. Nevertheless, predictions from theory are essential for the successful design of composite structures.

An analysis of the prediction of strengths of discontinuously reinforced composites is dependent upon reinforcement concentration, aspect ratio and constituent properties. However, implicit in these equations are the following assumptions that:

(a)   there are uniformly spaced flakes parallel to the plane,

(b)   there is ideal matrix/flake adhesion,

(c)   both matrix and flakes are linearly elastic to failure, and

(d)   there are no interactions between reinforcement extremities.

These conditions are extremely difficult to attain in discontinuous reinforced composites. Failure is assumed to be by flake fracture or flake pull out, and never by a combination of the two.

However, the quantity relating to the strength of the interface is determined by both the degree of wetting and the adhesion between the flakes and matrix. These in turn are subject to the conditions under which the composite was fabricated and may be adversely or beneficially

affected.   If the dispersion of flakes is not uniform, cracks may easily propagate parallel to the flake direction, regardless of the stress direction.

Finally, composite failure may occur through moulding flaws or the presence of excessive voids.[126, 130]   Thus, the complete picture is considerably more complicated than that predicted from the idealised equations of composite mechanics, and the predicted strengths are very much higher than actual strengths.

This phenomenon has been examined by several researchers,[150-155] who found severe stress concentrations around fibre discontinuities, with magnitudes dependent upon the size and nature of the end gap, fibre length, resin shrinkage and resultant inter-fibre resin paths.   The concentration of stress between fibre ends and of interfacial shear stress can cause matrix or interfacial yielding at low overall stress levels.

Although a stiffer matrix tends to result in composites of higher strength, because of increased efficiency of stress transfer, it also gives rise to higher matrix and interfacial shear stresses, thus increasing the probability that a crack, initiated at a fibre end, will propagate through the matrix and cause premature composite failure.[156]

In composite materials, fracture behaviour is complex.   Fibres and flakes are strong, but usually brittle, while matrices are weak but generally tough.   Whereas fibre and flake properties are desirable for strength and stiffness, matrix properties control the toughness of the composite.   In discontinuous reinforced composites fibres and flakes act both to initiate cracks and to inhibit crack propagation.   Discontinuities are the predominant structural flaws which initiate cracks in these composites but, since cracks must often travel around fibres or flakes in the crack path, the reinforcements act to inhibit crack

propagation.

As a consequence of the perturbation effect, described by Chen,[157] caused by the mutual interactions of the extremities of the reinforcements, discontinuous reinforced composites are inherently much weaker than continuous fibre composites.

These reductions can be expressed via two factors dependent upon the failure mode. Where flake fracture occurs, the Strength Reduction Factor [SRF] (equation 4.9) applies:

$$[SRF] = \left\{ \frac{1 - \frac{\tanh(u)}{u}}{1 - \mathrm{sech}(u)} \right\}$$

If flake pull out is the cause of failure, then the Matrix Performance Factor (equation 4.11) applies:

$$[MPF] = \frac{\alpha}{u} \left\{ \frac{1}{\tanh(u)} - \frac{1}{u} \right\}$$

The analysis of u is obviously vital and thus the quasi-isotropic theory that has been proposed needs expansion to include strength predictions.

The three strength parameters which have been examined in a theoretical model are presented in Figures 79-81. There are two very significant observations to be made from these figures:

(a) The predicted strengths are generally very much higher than the actual strengths. The reasons for this are as discussed previously and can be accounted for as proposed by Padawer and Beecher[126] using a constant within equation (4.8) such that:

$$\sigma_c = \phi_f \, \sigma_f \, [SRF] \, K + \phi_m \, \sigma'_m \qquad (11.7)$$

K is less than one and represents the strength loss due to material inhomogeneities and fabricating defects. Equation 4.8 thus represents an upper bound.

(b) The predicted increase in strength with particle size is considerably less than the actual gradient of the strength against particle

size plots.

This can be explained by consideration of the failure mode. When mouldings are made from small particle sizes, flake pull-out predominates and the [MPF] is applicable. Conversely, at larger particle sizes, flake fracture predominates and the [SRF] is applicable.

Consequently, the failure is not uniform, but consists of a combination of flake fracture and flake pull-out, with the predominant failure mode changing from flake pull-out at small particle sizes to flake fracture at larger particle sizes.

This was confirmed by microscopic and macroscopic examination of the fractures, which revealed partial flake pull-out and flake fracture. Figure 82 presents a microscopic section showing both systems.

If the [MPF] is being considered then a constant must also be employed in equation (4.10) such that:

$$\sigma_c = \phi_f \tau_m [MPF] K + \phi_m \sigma_m'' \qquad (11.8)$$

To analyse the strength of the particulate composite with these equations, the proposed quasi-isotropic theory for modulus prediction is employed. This suggests that all relevant mechanical properties are contained in the appropriate factor of equations 11.7 and 11.8. The factor accounts for the matrix and fibre properties; the orientation of the flake is contained within the quasi-isotropic material properties that are employed in the calculation of the factor. This is because quasi-isotropic properties approximate to the properties of an isotropic composite, which would contain fibres aligned in all directions, and the particulate composite approaches this alignment also, since the flakes are randomly distributed in all directions of the plane of the composite.

11.1.2.1   Tensile Strength

As reported by White,[137] the tensile strength of the reclaimed APC-2 is very disappointing, the value of K being 0.42 from experimental data.   Figure 79 suggests that by the use of this value of K, the initial failures are predominantly flake pull-out, and with increasing particle size, the failure becomes progressively more dominated by flake fracture.   This phenomenon was observed by microscopic examination of the tensile specimens over the particle size range examined. Possible explanations of the poor tensile strengths are discussed in Section 9.3.

11.1.2.2   Flexural Strength

Lusis, Woodhams and Xanthos[132] report that flexural strengths are generally much higher than tensile strength values of the same specimens and this observation is supported by the experimental value of K for the flexural strength prediction of particulate APC-2, which is 0.73.

A similar effect to that within tensile predictions is presented in Figure 80, where initial failure is a result of flake pull-out which becomes progressively more dependent on flake fracture as the particle size increases.

Once again this phenomenon was observed by micro examination of the specimens.

11.1.2.3   Compression Strength

Padawer and Beecher[126] reported that the mode of failure in compression was due to a kink type local instability.   Compressive strength was generally higher than tensile strength, and this is certainly supported by the results herein.

The compression strength of the reclaimed APC-2 is presented together with the theoretical predictions in Figure 81.   Because the compression

strength is compromised by the ability of PEEK to yield,[13] values of continuous reinforced composite compression strength are very much reduced compared with other strength properties.

However, this effect is not observed here, possibly a result of the short gauge length (15.0mm). Thus at a particle size approximating to this, quasi-isotropic strengths should be achieved.

Since the particle sizes under consideration are within this size range, this is virtually the examination of continuous fibre reinforced composite and the [SRF] predicts a good approximation of the compression strength over the range 6.35 - 12.3 mm, 12.3 mm square being the particle size with predicted quasi-isotropic compression strength.

Rosen[158] predicts a relationship of the form:

$$\sigma_c = \frac{\tau_m}{(1-\phi_f)} \qquad (11.9)$$

where σ_c is the strength of the composite,

τ_m is the shear rupture stress of the matrix or interface, whichever is the lower, and

ϕ_f is the volume fraction of the flake,

but as Sheldon[142] states, this gives low values for the compression strength.

Thus when designing components the [SRF] must be used together with a consideration of the gauge length/particle size relationship.

11.1.3 DAMAGE AREA

As suspected, there is very little difference in the damaged area with respect to particle size. However, a marked difference between the areas associated with the two energies employed is noted and so an interesting effect is evident, but requires further evaluation by a

more sophisticated technique - the Instrumented Falling Weight Impact Technique.[48-57]

The importance of the results obtained from this technique is that the inherent toughness of PEEK has been reproduced in the moulding of reclaimed APC-2 particles.   As discussed previously it is possible that the simple addition of short fibres or flakes to an inherently tough thermoplastic matrix will produce a moulding which will shatter upon impact in a brittle manner.   This is partially due to the many factors, such as fibre-matrix bond quality, fibre length and orientation, and the ductility of the polymer matrix, which influence the composites general performance.[159]

11.1.4   IMPACT TOUGHNESS

Computer analysis of the force-time curve permits a number of parameters to be calculated.   Two of these are of particular interest;   the energy absorbed to initiate a specific failure (i.e. yielding or the initiation of a crack) and the total energy absorbed by the specimen for complete fracture.

Jones, Leach and Moore[76] report experiments upon various forms of PEEK, including short carbon fibre reinforced PEEK, with 30% by weight of carbon fibre.   Fracture of such composites occurs by crack initiation[55] and is followed by crack propagation.   Consequently total energy comprises initiation and propagation components (both of which are dependent upon geometry).   They report that the component of energy required to initiate a crack is small compared with the total energy to failure, particularly above -20°C and thus crack propagation would be expected to be the dominant energy absorbing process.   Below this temperature, crack propagation energy decreases with respect to initiation energy, and this is coincident with the ductile-brittle transition, suggesting that the crack initiation process in short fibre

reinforced PEEK is fibre dominated, whilst the propagation process is matrix dominated. Therefore, when the matrix is tough, crack propagation is the major energy absorbing process; but when the matrix is brittle, crack initiation energy is the dominant energy absorbing process.

Continuous fibre reinforced PEEK exhibits a different impact behaviour[76] because, although the initial failure is cracking, followed by subsequent propagation, observation of the fractured specimens shows that the overall area of impact damage is restricted to the damage zone around the impact (i.e. long crack propagation is prevented by the quasi-isotropy of the lay-up). This energy to initiate and propagate failure is much greater for APC-2 than for the injection moulded composite, and the total energy of failure does not fall markedly below -20°C. This suggests that the fibres dominate the process for APC-2 as well as the initiation of failure.

Cogswell,[13] Leach[47] and Jones et al[76] report that both initiation and failure energies vary with thickness, such that empirically:

$$\text{initiation energy} \quad \alpha \quad \text{thickness}^{1.42}$$
$$\text{total energy} \quad \alpha \quad \text{thickness}^{1.47}$$

and from this, the initiation energy of 2mm thick injection moulded short carbon fibre reinforced at 20°C is approximately 0.9J, whilst the total energy to failure is approximately 4.4J.

From Appendix 1, the same values for APC-2 are 6 and 20J respectively.

Presented in Figure 34 are the corresponding values for a series of particulate, compression moulded APC-2 mouldings and it is readily observed that these values fall between the two previously reported sets of figures, tending towards APC-2, as the particle size increases.

It is suggested that the type of failure mode in operation is largely

that of the continuous reinforced PEEK because examination of the damage zone reveals restriction of the zone to the region of impact as previously discussed.

Furthermore, extrapolation of the graphs to predict the impact properties of shorter fibre reinforced composites produces predictions of 100% in excess of the actual values for 30% by weight short carbon fibre rein- forced PEEK reported by Jones and his co-workers.[76] They hypothesise that toughness may actually be reduced by increasing the fibre volume fraction. Also, Friedrich and his co-workers[160] report that no general enhancement in toughness is achieved by the increase of fibre content.

These impact toughness properties are very promising indeed and detailed microscopic and macroscopic analysis of fracture toughness reveals possible mechanisms for this enhanced toughness.

11.1.5 FRACTURE TOUGHNESS

From the results gained, the first thing of note is their marked scatter. This problem of scatter was also experienced by other workers investi- gating the strain energy release rate of composites.[63, 65, 66, 161, 162]

As previously discussed this may in part be a result of recording errors, especially the crack length. A sophisticated technique to overcome this has recently been developed by ICI[163] involving electronic measurement of the crack length. Unfortunately, this technique was not available for use here. These recording difficulties were compounded in this work with randomly orientated particles within the samples, because the crack tended to follow the particle boundaries. This leads to a jagged crack front of varying length, a problem not so evident in continuous fibre composites.

The scatter may, however, be a result of the inherent heterogeneity of

the samples. As the particles are random, so the alignment of possible fracture paths is random, with brittle and tough fracture paths occurring simultaneously in the beam. The variation in approach of the crack front to these paths, and hence further crack propagation, will produce vastly different results from the same DCB.

The presence of the brittle and tough paths is a major difference between the particulate composites and continuous unidirectional fibre composites, in these composites the crack follows a simple interlaminar path with the fibre direction running normal to the crack front. Therefore, when the crack and fibres are parallel, this presents the weakest path for the fracture to follow.

It is readily apparent that no such path is available for the crack front to follow in the particulate composite, and to facilitate crack observation a travelling microscope was employed upon the crack tip. This was ideal for observations but presented long time problems with focussing and lighting when photography was necessary. Because of the lack of specialised photographic equipment for use in conjunction with the ESH machine, an improvisation of an optical travelling microscope and automatic exposure Olympus camera was employed. Unfortunately, this was focussed by moving the whole rig and thus bad lighting gave 'hot spots' on the film.

The tendency of the crack to wander more when travelling through particles running across the crack direction is shown in Figures 83 and 84. This presents a much more difficult path for the crack to follow, thus increasing the likelihood of propagating into the short transverse direction. This is demonstrated particularly in Figure 83. The crack was originally in a particle with fibres running across its path, but for ease of continued growth it strayed upwards and ran into a particle with fibres running with the crack. This allows the

crack to take a much easier path, so it runs much straighter.

By contrast Figure 84 shows the original crack again in a cross fibre region but instead of moving up into the parallel fibre region, a secondary crack has started and moved into a less favourably orientated region and so takes a more jagged path.

This secondary crack opening is an important factor when explaining the higher fracture toughness of the particulate composites. This is because G_{IC} is defined as the strain energy release rate per unit area of new fracture surface created, the new fracture surface created would include the main crack plus the secondary crack. However, the actual measured crack length would only account for the longest, or main, crack. Therefore, although enough energy is needed to propagate both cracks, the crack length for calculation purposes may give the appearance that the longer crack has taken all the energy to propagate it. This will produce a higher value of G_{IC}. This secondary crack phenomenon was evident in all samples. The value gained is not a false value, because although there is a larger area, this beam is not more likely to fail because of the presence of the short crack, a view supported because ultimate failure does not occur at these points of secondary cracking, unless they are edge effects.

Further examples of secondary cracking are presented in Figures 85 to 88.

Also evident are cracks opening in front of the main crack, subsequently leading to particle bridging of the beam, as with large secondary cracks. This bridging also contributes markedly to the fracture toughness as the fibres tend to cross the gap between the two halves of the DCB and then need to be broken or pulled out of one half. They are almost invariably pulled out, this in itself leading to an increase in toughness.

This helps to explain why, in some samples, the fracture toughness appears higher for longer crack lengths. There is more surface area available for particles to bridge the opened crack, thus increasing the energy required to break the bond.

The appearance of secondary cracks ahead of the main crack may be because the main crack is not travelling in exactly the same direction as the primary stress direction as a result of the orientation of the fibres. Thus, multiaxial stresses are compiled just ahead of the main crack. Localised weak spots just ahead of the crack may also contribute to the crack opening.

The appearance of secondary cracks behind the crack front occurred when the main crack found a difficult path, often coinciding with an area where three or more particles met. Under closer examination it was discovered that such regions contained a high concentration of unrein-forced PEEK. The crack blunting effect of these regions is presented in Figure 87. Here the crack has run into a PEEK region and it is clearly evident that the crack has blunted from the presence of the rounded tip. This blunting has set up stresses further along the composite and a crack has emerged transverse to the main crack direction. This is because its path ahead is blocked by a further PEEK rich region.

In order to examine these PEEK rich regions the edge of the sample had to be polished before viewing through a microscope. The results are shown in Figures 89-92. These show well the presence of PEEK rich zones forming at the confluence of three particles.

Presented in Figures 93 and 94 are macrographs of the polished top surface, showing clearly the areas of PEEK around the particles and how certain configurations lead to enlarged PEEK concentrations. Figures 95 and 96 present high magnification micrographs of such PEEK

enriched regions. Clearly visible are flakes of fibre dislodged during moulding.

The PEEK rich region theory may help to explain why the fracture toughness decreases with increasing particle size. Owing to the smaller particle size, there are many more regions where three or more particles come together producing more PEEK rich regions and therefore more crack arresting mechanisms. This, in conjunction with the fact that in the smaller particulate beams, the interlaminar path must be more tortuous, as there are likely to be more particles crossing the delamination path at steeper angles, produces higher G_{IC} values for smaller particle size.

The greater abundance of PEEK rich regions is shown well in Figures 97, 98 and 99. Figure 97, which is from a 25.4mm square particle size, shows far fewer PEEK rich zones than Figure 98, which is from a 6.35mm square particle size. Figure 99 is an oblique light micrograph of the same area as Figure 98 but shows much better contrast between the light PEEK regions and dark APC-2 regions.

A major drawback of secondary crack propagation during the DCB test was that the crack tended to migrate to the edge of the beam causing premature failure. This happened most frequently in the smaller particle size beams. Not surprising because these have a higher percentage of PEEK rich regions causing more secondary cracking. Another reason may be that because of the more frequently changing orientation of the fibres with respect to crack direction, the crack is more likely to experience slight changes in direction as it jumps from one fibre orientation to another.

11.1.5.1 Examination of Fracture Surfaces

The macro fracture surfaces are presented for comparison in Figure 100, and the square particulate nature of the composite is highlighted by the white areas at particle boundaries. This is where the PEEK rich

regions have deformed plastically and drawing has taken place prior to failure[164] in a slow ductile manner.

This phenomenon is further presented in Figures 101 and 102 by oblique light microscopy. Figure 101 presents the boundary region between two particles compared with Figure 102 where several particles meet. Because of the topography of the samples, it is not possible to present a totally focussed region but the central area demonstrates the PEEK enriched region between the particles, and its fracture mode.

These types of surface were studied in greater depth by scanning electron microscopy (SEM). The white appearance is lost but such areas are readily identified by distinctive fracture topography.

Figures 103 and 104 present a particle boundary region at low and high magnifications respectively. From the high magnification micrograph it is clear that the boundary region is PEEK dominated, with only a few short fibres. It also shows quite massive ductile deformation of PEEK, as previously reported by Purslow.[164] Further presentations of this phenomenon are Figures 105 and 106.

Of particular interest are Figures 107, 108 and 109 of 12.7mm square particle beams. Clearly visible are the fibres that have been incorporated into the PEEK enriched zone, and the visibility of fibre ends means the fibres have been pulled through and out of the PEEK matrix, a major toughening mechanism for composites.[61]

Another point of interest is the cleavage mechanism in the composites. Under SEM examination it was noted that the majority of the surface had a structure as presented in Figure 110. Examination at higher magnifications, in Figure 111, reveals that failure is contained within the matrix, suggesting the main failure mode is matrix fracture rather than interface failure. This is interesting because the fracture

toughness of PEEK is approximately four times that of APC-2 and it may be thought that if fracture occurs in the PEEK then the toughness of particulate composites would approach that of PEEK. This does not happen because of the presence of carbon fibres, which have a restricting effect. As presented in Figures 104, 106 and 109, ductile fracture of PEEK gives extensive yielding and drawing, therefore, PEEK must be present in excess to promote a totally ductile failure. However, when the PEEK is encased in carbon fibres as presented in Figure 112, there is reduced deformation.

Other types of fracture were observed in the composite to a lesser extent, an example being presented in Figures 113 and 114. Figure 113 shows again the meeting of two particles, but in this instance the fibres are exposed and the fracture appears to be of a more massive ductile nature, as seen in Figure 114. This is probably a result of a combination of factors.

Firstly, this is a region where the crack has migrated from one fibre orientation to another, which may slow or stop a cleavage crack at this interface.

Secondly, it may also be due to this being the start of a crack where, because of the restraining force in another region of the crack front, the area did not cleave immediately, but built up enough energy to propagate the crack slowly in a ductile fashion.

Alternatively, it may be caused by the orientation of the fibres with respect to the crack front.

Another feature of interest from Figure 100 is the presence of the white areas away from particle boundaries, particularly evident in the continuous fibre sample, but also found in the particulate beams as presented by oblique light microscopy in Figure 115. Such areas coincided with the starting and stopping of the crack and the orientation

parallel to the crack front.   Higher magnification of the region in
Figure 116 shows more extensive drawing and deformation than the
normal cleavage mode as presented in Figure 111.

From these observations it is proposed that at the start of crack prop-
agation the restraining forces of fibre bridging allows slight deforma-
tion of the ductile matrix before the cleavage fracture of the main
crack growth takes place.   This accounts for the orientation of the
regions.   The reason for the initial restraint of the cleavage crack
is probably due to less favourable orientations of particles across
the crack front, such as PEEK enriched zones, stopping the crack from
propagating as a whole until a critical stress is reached.   However,
in local areas of more favourable orientation, the stress may be
sufficient to give a ductile deformation by pulling the fibres from
the matrix.

For continuous fibre reinforced systems the mechanisms would necessarily
be different and the system is discussed in detail by Purslow.[164]   As
delamination proceeds at approximately the same rate across the width
of the beam, the white areas extend the width of the sample, parallel
with the crack front.

The ductile deformation probably proceeds until a critical strain
energy is reached, whereupon the sample fails in a cleavage manner. A
gradual fall off in load was observed in the samples, as coincident
with true ductile propagation and the crack did not visibly grow. This
suggests crazing in front of the crack, but no true fracture.   This
resulted in an increase of load until cleavage fracture caused crack
extension.

An interesting observation from SEM fractography was the appearance of
fibre bundles which had bridged the gap between the two halves of the
DCB.   Figure 117 shows such a bundle.   It can be seen that the matrix

towards the end has undergone massive plastic deformation.   Also relatively clean fibres show that the fibre ends have been pulled from the matrix.   This demonstrates one important toughening mode of the particulate composites, because the matrix is deformed by ductile fracture which requires substantial energy and also the fibre ends are pulled through the matrix before finally breaking the bridge, again an energy absorbing mechanism.

To summarise the fractography studies, the PEEK enriched areas deform in a ductile manner, which requires more energy and it is a more massive form of deformation.   This supports the fact that these areas act as crack blunters and arresters.   The very small fibre flakes in these areas are seen to be pulled from the matrix, thus increasing the toughness with respect to the continuous reinforced system.

The major form of fracture through the main body of the particles was seen to be cleavage crack propagation through the matrix, due to the restraining action of the fibres.   Some interfacial fracture was also observed, leaving exposed fibres, but these fibres still had large particles of matrix adhering to them, demonstrating a good interfacial bond.

Some ductile type fracture was observed at the onset of crack propagation, promoted by the slow speed of testing.   This was caused by favourable particle orientations in the particulate beams coupled with the restraining effects of other less favourably orientated particles along the crack front.

A final observation was the appearance of the fibre bundles bridging the crack, showing ductile deformation of the matrix and fibre pull-out, thus contributing significantly to the toughness of the composite, a mechanism obviously not available in the continuous fibre reinforced composite system.

Chai[66] reports that for continuous fibre composites, the inter-laminar fracture toughness was governed by the matrix polymer and is largely independent of the fibre orientation.

However, for the particulate beams, although fracture is still matrix dominated, particle size, orientation and lay-up were found to be contributary factors to the ultimate fracture toughness of the composite. This is because matrix enriched zones cause toughening in an analogous manner to the rubber particle toughening of expoxies.[165]

11.1.6   CREEP

One of the most fundamental limitations of thermoplastics, to their application as engineering materials is their tendency to creep.

APC-2 does not suffer from this weakness, because of the reinforcement with continuous fibres and the viscoelasticity in the matrix will have little effect on the modulus of the composite in the direction of the fibres, but a large effect on the transverse modulus.   In systems containing flakes, or short fibres, the volume fraction of reinforcement is normally lower and therefore the viscoelasticity of the matrix is translated into time dependence of the composite.   However, contained within the particulate composite is a hybrid of these two general systems, with discontinuous reinforcement at high volume fractions.   The volume fraction is constant by design, but the flake size or aspect ratio is variable.

If decoupling of the flakes from the matrix occurs, either with the passage of time or increase in strain, then this is equivalent to a decrease in the volume fraction of the reinforcing phase;   creep rates then tend to increase, as shown in the isochronous plots, Figures 44-50.   These give an indication of the tendency to decouple at higher stress levels.   The creep rate increases due to slippage at the fibre matrix interface.

The effect of increased aspect ratio is seen to be a reduction of creep highlighted at the higher stress levels as presented in Figure 51. This is because there is less tendency for the larger flakes and hence fibres to become debonded from the matrix, as previously discussed within the considerations of modulus and strength.

It is of relevance to report the work of Ogale and McCullough,[166] where the level of crystallinity was found to have no effect upon creep behaviour below 140°C, or the glass transition temperature of PEEK. This fact, in conjunction with the properties contained herein, suggests a very favourable creep performance for particulate APC.

Figures 52-58 show long term creep property plots for these composites. The slope of these plots is summarised in Table 12 and once again creep rate is seen to decrease generally as the aspect ratio increases.

When compared to the creep data contained in Appendix 1, these presentations are very favourable and then inherent basic creep resistance of pure PEEK[76] is very well reproduced within these particulate composites; an important reproduction because the fibre ends may promote void formation and the composite becomes the matrix with cavities and fibres. This appears to have been avoided.

11.1.7   FORMABILITY

Presented in Figures 59-63 are examples of the mouldings constructed from blanks of these particulate composites. A summary of the various mouldings is presented in Table 13.

With respect to the larger radius of curvature mouldings, as presented in Figures 59, 60 and 61, the smaller the particle size the better the moulding, with wrinkling tending to occur with increasing particle size.

However, when examining the smaller radius of curvature there is an increased tendency to tear, which would seem to be offset by increasing

the particle size, as seen in Figures 62 and 63, the former being manufactured from 0.25 inch square particulate composite, the latter from 0.5 inch square particulate composite. Unfortunately, tearing is not completely overcome with increased particle size and the tendency to wrinkle is still evident.

A more amenable technique is obviously necessary for completely successful production of this component. It should be noted that this component has not been successfully moulded from either continuously reinforced APC-2 or the woven product form introduced to improve drape,[75] so this is a very demanding trial and certainly a good deal of promise is seen within Figures 59, 60 and 61 of the larger radius moulding.

One of the most promising technologies that has been developed for the fabrication of double curvature is based on an extension of super plastic forming. This has been a joint venture between ICI and Superform Metals Limited. To fabricate complex curvature sections with this technology, the APC blank is encased between Supral aluminium sheets. A vacuum is then drawn between the sheets and the ambient temperature raised to 380°C, whereupon the Supral sheets become super-plastic so that the sandwich structure can be shaped by differential pressure into an appropriate mould where it is cooled. This process is subject to patent applications.[74] This process would benefit particulate APC-2 because the aluminium sheets would support the particles in the composite preventing tearing and wrinkling.

11.1.8   THE EFFECT OF PEEK CONTENT

The dilution of particulate APC-2 with additional PEEK would seem to be an unrewarding activity when compression moulding. The loss of mechanical properties is rapid and directly proportional to the amount of PEEK added.

However, if the scrap is to be reclaimed by injection moulding it is not feasible without dilution with PEEK to at least 40% by weight of carbon fibre.[138] This produces a moulding superior to a standard injection moulding compound[14, 18, 137] and therefore, when reclaiming scrap it is vital that the end product be considered, and the manufacturing route be planned meticulously to produce a moulding with the desired properties.

11.1.9 THE REGULAR LAY-UP

The data presented in Table 14 shows that by careful alignment of the flakes, a marked increase in the modulus is possible. The modulus of such systems can be predicted by correct choice of modulus for lay-up under examination. When considering a unidirectionally aligned particulate composite, it is necessary to use the modulus of unidirectional continuous fibre APC-2, and when considering other lay-ups, e.g. $(0,90)_{4S}$, then it is necessary to use the modulus of continuous fibre composite with that lay-up. If this procedure is adopted, then accurate predictions of the modulus are possible, as shown by analysing the data in Table 14 against the modulus predictions of Figure 78, where correct choice of continuous fibre lay-up enables accurate predictions for flexural modulus of particulate composites.

When considering the flexural strengths of $(0)_{16}$ and $(0,90)_{4S}$ lay-ups, the values are considerably increased compared with the random arrangement previously examined. However, they are still only about 50% of a continuous fibre reinforced system, but this is to be expected when considering the specimen dimensions with respect to the moulding.

The practicality of such a lay-up is very doubtful, but the results prove that the moulding technique is reproducing the APC-2 interfacial bonding.

11.1.10   THE COMBINATION OF PARTICLE SIZES

The production of a moulding from varying particle sizes produces mechanical properties based on a combination of the properties of the constituent particle sizes.

In the case of the two particle sizes examined, the mechanical properties are predicted by the application of the 'Rule of Mixtures' theory, once again emphasising satisfactory moulding techniques.

The 'Mono Munched' material produces mouldings that are very disappointing with respect to the modulus property.   This is predominantly because the base particle shape is needle like or rectangular, and the width is therefore considerably reduced.   This lowers the value of the aspect ratio, decreasing the [MRF].

An apparent anomaly observed in the property profile presented in Table 15 is the improved tensile strength, compared with the previously regular particle sized mouldings.

It is suggested this may be because of the grossly irregular nature of the constituent particles providing an interlocking network.   Indeed, upon examination of the base stock, a varying particle size includes flakes of length up to 120mm but only 4mm in width; and a very fine dust.   For this reason the material was given an arbitrary sieve, to include generally only particles greater than 3mm, although this was by no means an exhaustive removal of other particles.   After this treatment the modulus was increased, as indeed were flexural and compression strengths of the particulate composite as presnted in Table 15.   The tensile strength did not show any improvement however, so it is suggested that there may be an optimum combination of angular particles for an idealised property profile.

11.1.11   THE WOVEN PRODUCT

Standard woven products have several disadvantages:

(a) They are usually based on more expensive 3,000 filament tows to ensure a thin uniform sheet.

(b) They involve an additional manufacturing stage.

(c) Because the fibres are kinked, the product cannot be expected to yield its full potential strength.

(d) The options available for anisotropic properties are reduced.

The data presented in Table 16 has been produced from standard tows so overcoming the first disadvantage, but point (c) is highly emphasised when compared to conventional woven products.[75]

Such a system, however, does have advantages:

(a) The kinked fibres tend to deflect interlaminar cracking to give a higher fracture toughness.[4]

(b) The nature of the weave constrains lateral movement, so enhanced uniformity of thickness is possible.

11.1.12   TEMPERATURE CAPABILITY

A reasonable retention of strength and modulus is observed at 200°C, the proposed maximum continuous operating temperature of APC-2[18].

However, the continuous reinforced composite typically retains 70% of the modulus[42] at 200°C, not the 47% reported here, so there has been some loss of temperature capability when scrap material is used, because of the loss of continuous fibres which promote the property retention at elevated temperature.

11.2   ANALYSIS OF THE MATERIAL CONSTRUCTED FROM 8-PLY PARTICLES

To extend the proposed theories, particulate composites constructed from a source of 8-ply quasi-isotropic preconsolidated sheet stock are now evaluated.

11.2.1 MODULUS MEASUREMENTS

To reinforce the quasi-isotropic theoretical application of the [MRF]
proposed in the previous discussion, predictions are made for the
particulate composites. As discussed, the quasi-isotropic properties
are used in this factor (MRF), so in these instances the uni-directional
and $(0,90)_S$ lay-up predictions are omitted.

11.2.1.1 Tensile Modulus

Tensile modulus predictions are presented in Figure 118, where theoret-
ical values based upon quasi-isotropic theory are superimposed upon the
experimental values. Very good agreement is observed between these
plots, but the actual results are extremely disappointing, being far
lower than the tensile modulus of material constructed from single ply
material.

It was thought that an improvement in stiffness may have been achieved
in this case because of extended interlock between plies due to the
increased thickness of individual particles. This was not to be the
case, probably being offset by a marked reduction in isotropy caused
by the presence of enlarged particles; thus reducing the composite
modulus, as the composite becomes increasingly dependent upon the
matrix properties for its overall mechanical properties. This is
because of the increase in deformation at flake boundaries, necessary to
eliminate voids, also results in fibre kinking.

11.2.1.2 Flexural Modulus

Comparable predictions for the flexural modulus are presented in
Figure 119, and once again the predictions are excellent with respect
to the experimental results.

However, the modulus itself is very disappointing compared to the
flexural modulus of material constructed from single ply prepreg,

so reinforcing the proposal of an increased dependence upon the matrix modulus.

There is an increased dependence on the modulus of the matrix as the particles are increased in thickness. This is due to the particles being displaced from the ideal E_{11} orientation, as defined in Figure 18. The efficiency is therefore impaired in this direction, which is the direction of testing.

The predictions of achievement of quasi-isotropic moduli are in very good agreement and the mean value of such a prediction for both tensile and flexural modulus is 50.25 GPa, the standard deviation being 4.3.

11.2.2 STRENGTH

Previous predictions of strength proved to be rather optimistic and the use of a constant, K, was necessary to account for inhomogeneities and fabricating defects. The same value for K was used in conjunction with both the [SRF] and the [MPF]. If the application of [MPF] is valid and to be upheld then this value should not change unduly, for the same composite, with particle thickness as the fundamental concept is aspect ratio.

That being so, values of K are employed as reported in Sections 11.1.2.1 and 11.1.2.2 for tensile and flexural strengths respectively.

11.2.2.1 Tensile Strength

As before, the tensile strength was very disappointing.

Presented in Figure 120 is the superimposition of theoretical predictions from quasi-isotropic theory upon the experimental data. The value of K is 0.42 and at smaller particle sizes flake pull-out is predicted and this is observed macroscopically. As the particle size increases the mode of failure becomes predominantly flake fracture.

This reiterates the findings from single ply particulate composites.

11.2.2.2   Flexural Strength

The flexural strength is once again much better than the tensile strength and Figure 121 presents the prediction of almost total flake fracture failure at all particle sizes.   The value of K is 0.73.   Without this correction initial predictions from [MPF] predict flake pull-out, but this was not observed macroscopically and it is unlikely that the value of K is unity, and so a constant value is taken to predict the mode of failure as flake fracture.

11.2.2.3   Compressive Strength

Because compression properties tend to be matrix dominated in polymer composites, the [SRF] gives a more exaggerated prediction of low compression strength than is necessary, indeed [SRF] predictions are lower than [MPF] predictions.   This is because the inherently low compression strength of composites already accounts for a loss of strength and to compound this further by the use of [SRF] unnecessarily exaggerates the situation.

Once again the dimensions of the test specimen may not necessarily be representative of this type of particulate composite.

The predictions superimposed upon experimental data are presented in Figure 122.

11.2.3   IMPACT TOUGHNESS

The mechanical properties of composites containing 8-ply particles are somewhat disappointing, being lower than the comparable properties for composites containing single ply particles.   However, it has been proposed that PEEK enriched zones and torturous fracture paths enhance fracture toughness within such composites.   The occurrence of such zones will be statistically reduced within 8-ply particle composites because fewer particles are contained within the moulding and the likelihood of convergence of three or more particles is

reduced.

It is therefore to be expected that the impact toughness of this class of composites will suffer. This is confirmed by the results presented in Figure 72 where both the initiation and total energy to failure are lower than those presented for single ply composites as presented in Figure 34.

Extrapolation, to predict the properties of short fibre composites, produces values in the region of those reported in Section 11.1.4 and thus the inference is that the mode of fibre dependence is comparable to short fibre composite failure. This is supported by a more widespread damage zone of the composite, away from the point of impact.

Thus the properties of 8-ply particle composites are not promising; the fracture toughness studies should support these results.

11.2.4 FRACTURE TOUGHNESS

By comparison with the results presented in Figure 43, for single ply particle composites and Figure 73 for 8-ply composites, it is seen that the fracture toughness of 8-ply particle composites is lower than the fracture toughness of single ply particle composites.

This is because of the reduction in frequency of occurrence of enriched pure PEEK zones and easier delamination paths, which would act as toughening mechanisms for the composite.

So the overall property profile for 8-ply particle composites is very disappointing, with mechanical properties being adversely affected by the aspect ratio and reduction of isotropy within the composite.

11.3   THE EFFECT OF PROLONGED TIME AT ELEVATED TEMPERATURE

If commercial use of these composites, constructed from offcuts and previously moulded material, is to be made then the matrix must not

be adversely affected by continued time at temperature, as would be experienced in a continuing recycle situation.

Figures 74, 75 and 76 present flexural modulus, strength and impact toughness of material subjected to up to eight hours at $400^{\circ}C$; no apparent loss of property is visible and it is therefore suggested that the recycling would not adversely affect the property profile.

Consequently, if the economics of press installation are viable as discussed by Morris,[167] the reclamation of APC-2 would be a commercial proposition, although many customers may already operate such a press and thus reduce costs even further.

12.   CONCLUSIONS

1.   The modulus of the reclaimed APC-2 can be predicted by application of the Modulus Reduction Factor [MRF], providing that the lay-up geometries are taken into account.   That is to say, if the moulding approximates to quasi-isotropy, then the continuous reinforcement quasi-isotropic modulus should be employed.   However, if the moulding is ordered, say $(0,90)_{4S}$, then the modulus of continuous reinforced (0,90) material should be employed.

2.   The strength of the moulding is less predictable, and the use of a 'defect factor' must be made.   This allows prediction of the strength providing that the mode of failure is observed, with flake pull-out predominating at the smaller particle sizes, and flake fracture becoming progressively more predominant as the particle size increases.   The tensile strength is considerably less than the flexural and compression strengths.   This is partially overcome by the use of irregular, angular particles, as generated by the Mono Munch technique.

3.   There are not significant differences in the damaged areas,
but below a critical particle size of around 9.0mm square, the
damaged area is enlarged by 50% at moderate impact energies of 7.0J.
This phenomenon is not repeated at 10J impact energy, but would be
a serious design consideration if these composites were used in
impact prone areas.

4.   The impact toughness is very promising with single ply particle
composites, although this is not repeated with 8-ply particle composites.
The reasons for this are encompassed within the following fracture
toughness conclusions.

5.   The fracture toughness exceeds continuous reinforcement fracture
toughness, except for the larger 8-ply particle composites.   This is
because of three major toughening mechanisms in operation:
Firstly, the presence of PEEK rich zones at the particle boundaries act
as crack blunters and arresters, causing secondary cracking.
Secondly, the delamination paths are more tortuous than in continuous
fibre reinforced composites.
Finally, because the fibres were of a finite length they could be
pulled from the matrix after bridging the crack in the beam specimen,
thus requiring extra work to break the bridge.

6.   The reclaimed APC-2 can be diluted, but without any apparent
advantages, unless injection moulding is used as the fabrication
technique.

7.   By arranging particles in a regular manner, the modulus of the
scrap particle mouldings can be made to approach that of the original
continuous reinforced composite modulus; and by comparing the axial
and transverse moduli with the original values, a very high efficiency
of wetting is deduced.   This conclusion is of particular importance
since it permits use of the carefully constructed reinforcement analysis.

8.   Particle sizes can be combined to produce a moulding of mechanical properties which are dependent upon the volume fraction of each particle size.   The smallest dimension, width or length, determines the modulus of the moulding and so lenticular particles, as found within the Mono Munched material, produce disappointing results. This is important when considering the method of granulating the recycled scrap.

9.   A woven product is possible, although the production of this type of moulding from offcuts will depend upon having long thin strips of APC-2.   This would produce a composite with a superior modulus, compared with that of a particulate composite.   The modulus is not, however, as high as non woven continuous fibre reinforced APC-2, but the improvement with respect to the particulate moulding may justify the extra production step, as this would be a possible source for woven prepreg.

10. Elevated temperature capability, although good, is less than that of APC-2, so the reclaimed material may not be used with comparable confidence at the maximum continuous use temperature rating of APC-2.

11. Creep resistance of the particulate composite is excellent at room temperature, retaining the inherent resistance of both the PEEK and carbon fibre to produce a composite of promising creep resistance.

12. The formability is satisfactory, demonstrating promising double curvature moulded ability.

13. The resistance to time at moulding temperature during forming is excellent with no loss of flexural or impact properties after eight hours.

14. Composites made from 8-ply particles have disappointing mechanical properties and if such material were available for recycling it would

need to be carefully monitored and channelled into less demanding applications.

13. FURTHER WORK

Although an exhaustive evaluation would have been ideal, further suggestions are:

1. Creep resistance at elevated temperatures should be evaluated. As there is a loss of flexural properties at 200°C, an increase in the rate of creep must be expected at this temperature.

2. Examination of impact toughness at lower temperature to confirm the dependence of failure mode upon either matrix or fibre.

3. With respect to formability, an exhaustive evaluation of mixed particle size and shape using a superforming process as the processing technique.

4. Analysis and predictions of optimum particle sizes to produce property profiles for engineering applications.

REFERENCES

1. L. N. Philips and D. J. Murphy
    'The Properties of Carbon Fibre Reinforced Thermoplastics
    Moulded by the Fibre Stacking Method'
    R.A.E. Technical Report 76140.

2. L. N. Philips and D. J. Murphy
    'Thermoplastics Materials'
    U.K. Patent 1,570,000 (1980)

3. J. T. Hoggat
    'Thermoplastic Resin Composites'
    20th National SAMPE Conference (1975) 606-617

4. J. T. Hartness
    'Polyether etherketone Matrix Composites'
    14th National SAMPE Technical Conference (Oct 12-14 1982) 26-37

5. J. T. Hartness and R. Y. Kim
    'A Comparative Study of Fatigue Behaviour of Polyether etherketone
    and Epoxy with Reinforced Graphite Cloth'
    28th National SAMPE Symposium (April 12-14 1983) 535-544

6. R. Y. Kim and J. T. Hartness
    'The evaluation of fatigue behaviour of polyether etherketone/
    graphite composite fabricated from prepreg tape'
    29th National SAMPE Symposium (April 3-5 1984) 765-776

7. J. B. Cattanach, G. Guff and F. N. Cogswell
    'The processing of thermoplastics containing high loadings of
    long and continuous reinforcing fibres'
    Journal of Polymer Engineering (1986) 6(1-4) 345-362

8. J. McAinsh
    'The reinforcement of polysulphones and other thermoplastics with
    continuous fibre'
    BPF 8th International Reinforced Plastics Conference (1972) 123-128

9. A. P. Cluley
    'High performance engineering materials - carbon fibre reinforced
    thermoplastics'
    The Metallurgist and Materials Technologist (Nov 1983) 554-558

10. J. E. O' Connor, C. C. M. Ma, A. Y. Lou
    'Polyphenylene sulphide: Resin, Prepreg and High Performance
    Composites'
    Philips Petroleum Co. Paper 11E

11. J. Maxwell
    'The drive for plastics: competing performance'
    Plastics and Rubber International, 8, (April 1983) 45-49

12. J. T. Hartness
    'Polyphenylene sulphide matrix composites'
    25th National SAMPE Symposium Proceedings (May 1980) 376-388

13. F. N. Cogswell
    'Continuous Fibre Reinforced Thermoplastics' Chapter 4
    Mechanical Properties of Reinforced Thermoplastics, Elsevier
    Appl. Sci. (1986)

14. 'Aromatic Polymer Composites'
    ICI Product Bulletin APC-2 (1986)

15. L. Post and W. H. M. van Dreumel
    'Continuous Fibre Reinforced Thermoplastics'
    Progress in Advanced Materials and Processes: Durability,
    Reliability and Quality Control, edited by G. Bartelds and
    R. J. Schiekelmann, Elsevier Science Publishers (1985)

16. W. H. M. van Dreumel and M. de Groot
    'An experimental nose-wheel door of continuous fibre reinforced
    thermoplastic'
    Composites, 18, 5, (Nov 1987) 405-407

17. R. T. Hawkins
    'Chemistry of the cure of poly (p-phenylene sulphide)
    Macromolecules, 9, (March-April 1976), 189-194

18. G. R. Belbin
    'Thermoplastic structural composites - a challenging opportunity'
    Proceedings of Institution of Mechanical Engineers, Vol.198 No.47

19. D. J. Blundell, B. N. Osborn
    'The morphology of poly(aryl-ether-ether-ketone)
    Polymer, 24, (August 1983), 953-958

20. T. C. Stening, C. P. Smith, P. J. Kimber
    'Polyarylether ketone: high performance in a new thermoplastic'
    Modern Plastic International, (March 1982), 54-56

21. F. N. Cogswell
    'Microstructure and properties of aromatic polymer composites'
    28th National SAMPE Symposium (April 1983) 528-534

22. F. N. Cogswell and M. Hopprich
    'Environmental resistance of carbon fibre reinforced polyether
    ether ketone'
    Composites, 14, 3 (1983) 251-257

23. C. K. L. Davies, S. Turner and K. H. Williamson
    'Flexed plate impact testing of carbon fibre reinforced polymer
    composites'
    Composites, 16, 4, (Oct 1985), 277-285

24. D. R. Carlile and D. C. Leach
    'Damage and notch sensitivity of graphite/PEEK composites'
    15th National SAMPE Technical Conference (Oct 1983) 82-93

25. S. L. Donaldson
    'Fracture toughness testing of graphite/epoxy and graphite PEEK
    composites'
    Composites, 16, 2 (April 1985) 103-112

26. E. M. Trewin and R. F. Turner
    'Carbon Fibres - 2 Use in composite materials'
    Engineering (May 1980) I-VIII

27. E. M. Trewin, R. Lucas and M. H. Powell
    'Carbon fibre advances the scope of thermoplastics in engineering
    applications'
    The Plastics and Rubber Conference.   Reinforced Thermoplastics II
    9-10 Nov 1977 paper 15

28. R. J. Diefendorf and E. W. Tokarsky
    'The relationship of structure to properties in graphite fibres'
    AFML-TR-72-133 (1977)

29. E. M. Trewin and R. F. Turner
    'Carbon fibres - 1 Properties and Manufacture'
    Engineering (April 1980) I-VIII

30. L. T. Drzal
    'Composite interphase characterisation'
    28th National SAMPE Symposium (April 1983) 1057-1068

31. X. Jin, M. T. Bishop, T. S. Ellis and F. E. Karasz
    'A sulphonated poly (aryl-ether-ketone)'
    British Polymer Journal, 17, (1985) 4-10

32. W. H. Bonner, U.S. Patent, 3,065,205 (1962)

33. I. Goodman, J. E. McIntyre and W. Russel
    Br.Pat.Appl. 971,227 (1964)

34. Y. Iwakura, K. Uno and T. Takiguchi
    'Synthesis of aromatic polyketones and aromatic polyamide'
    Journal of Polymer Science, A1, 6, (1968), 3345-3355

35. T. E. Attwood, P.C. Dawson, J.L Freeman, L.R.J. Hoy, J.B.Rose & P.A.Staniland
    'Synthesis and properties of polyaryletherketones'
    Polymer, 22, (August 1982) 1096-1103

36. B. M. Marks, U.S. Patent 3,442,857 (1969)

37. K. J. Dahl, Br.Pat.Appl. 1,387,303 (1975)

38. R. N. Johnson, A.G. Farnham, R.A. Clendinning, W.F. Hale & C.N. Merriam.
    'Poly (arylethers) by nucleophilic aromatic substitutions
    I. Synthesis and Properties'
    Journal of Polymer Science, A1, 5, (1967) 2375-2398

39. C. N. Turton and J. McAinsh
    'Thermoplastic Compositions'
    USP 3,785,916

40. R. V. Price
    'Production of Impregnated Rovings'
    USP 3,742,106

41. P. E. McMahon and M. Maximovitch
    'Development and evaluation of thermoplastic carbon fibre prepregs
    and composites'
    Advances in Composite Materials, 2, (Paris 1980) 1662-1673

- 133 -

42. G. R. Belbin et al ·
     'Carbon fibre reinforced polyether ether ketone: A thermo-
     plastic composite for aerospace applications'
     2nd Intercontinental SAMPE conference, Stresa,(June 1982)

43. 'Aromatic Polymer Composites'
     ICI plc, Welwyn-Garden-City

44. F. N. Cogswell and R. Hasler
     'Aromatic Polymer Composites'
     ME Leeds Conference (July 1984)

45. R. L. Addleman, I. Brewster and F. N. Cogswell
     'Continuous fibre reinforced thermoplastics'
     BPF 13th Reinforced Plastics Congress (1982) 71-73

46. J. F. Jansson and H. Sundström
     'Creep and fracture initiation in fibre reinforced plastics'
     Failure of Plastics, Brostow/Corneliussen, Hanser Publishers (1986)

47. D. C. Leach
     'The influence of a thermoplastic on the properties of structural
     composites'
     Institute of Metallurgists Conference at the Royal Society (1982)

48. D. R. Ireland
     'Procedures and problems associated with reliable control of the
     instrumented impact test'
     Instrumented Impact Testing, ASTM STP 563, American Society for
     Testing and Materials, 1974, 3-29

49. L. C. Cessna et al
     'The development of an instrumented projectile impact test:
     data on glass-reinforced and impact-modified polypropylene'
     Polymer Engineering and Science (June 1976) 16, 6, 4 6-425

50. H. J. R. Gonzalez and W. J. Stowell
     'Development of an autographic falling weight impact system'
     Journal of Applied Polymer Science (1976) 20, 1389-1404

51. W. Lubert, M. Rink and A. Pavan
     'Force-displacement evaluation of macromolecular materials in
     flexural impact tests'
     Journal of Applied Polymer Science (1976) 20, 1107-1116

52. T. Casiraghi, G. Castiglioni and G. Ajroldi
     'New developments in the assessment of impact resistance
     evaluation by falling weight method'
     Plastics and Rubber, Processes and Applications (1982) 2,
     353-360

53. M. W. Wardle and E. W. Toxarsky
     'Drop weight impact testing of laminates reinforced with Kevlar,
     aramid fibres, E-glass and graphite'
     Composites Technology Review (Spring 1983) 5, 1, 4-10

54. S. D. Sjverdsma, J. P. H. Boyens and J. J. Mooij
     'Shear deformation under impact conditions'
     Polymer Engineering and Science (March 1985) 25, 4, 250-255

55. D. P. Jones, D. C. Leach and D. R. Moore
    'The application of instrumented falling weight impact
    techniques to the study of toughness in thermoplastics'
    Proceedings of 6th International Conference on Deformation
    Yield and Fracture of Polymers (April 1-4 1985) 27.1-27.4

56. P. E. Reed, S. Turner and M. Money
    'Instrumented Falling Weight Testing'
    Proceedings of 6th International Conference on Deformation
    Yield and Fracture of Polymers (April 1-4 1985) 26.1-26.4

57. C. J. Hooley and S. Turner
    'Mechanical Testing of Plastics'
    Automotive Engineer (June/July 1979), 48-54

58. P. E. McMahon and D. G. Taggart
    'Improved carbon fibre composite performance based on new
    fibre and matrix developments'
    2nd Intercontinental SAMPE Conference, Stresa June 1982

59. B. A. Byers
    'Behaviour of damaged graphite epoxy laminates under compression
    loading'
    NASA contract report 159,293 (1980)

60. J. M. Whitney, C. E. Browning and W. Hoogsteder
    'A double cantilever beam test for characterising mode one
    delamination of composite materials'
    Journal of Reinforced Plastics and Composites, 1, (1982) 297-313

61. M. J. Folkes
    'Short Fibre Reinforced Plastics'
    Research Studies Press, Wiley, N.Y., 1982

62. G. R. Irwin
    'Analysis of stresses and strains near the end of a crack
    traversing a plate'
    Journal of Applied Mechanics (Sept 1957), 24, 361-364

63. S. S. Wang, H. Suemasu and N. M. Zahlan
    'Interlaminar fracture of random short fibre SMC composite'
    Journal of Composite Materials (Nov 1984) 18, 574-594

64. S. D. Timoshenko
    'Strength of Materials' Part 1, 3rd edition
    D. Van Norstrand Co. Inc. 1955

65. D. F. Devitt, R. A. Schapery and W. L. Bradley
    'A method for determining the Mode I delamination fracture
    toughness of elastic and viscoelastic composite materials'
    Journal of Composite Materials, (Nov.1980) 14 270-285

66. H. Chai
    'The characterisation of Mode I delamination failure in non
    woven, multi-directional laminates'
    Composites (Oct 1984) 15, 4 277-290

67. S. H. Crandall
    'Engineering Analysis' McGraw Hill 1956

68. W. D. Bascom, J. L. Bitner, R. J. Moulton and S. R. Siebert
'The interlaminar fracture of organic-matrix, woven rein-
forcement composites'
Composites (Jan 1980) 9-18

69. C. Y. Barlow, M. V. Ward and A. H. Windle
'The influence of microstructure on the toughness of carbon fibre/
plastic composites'
Proceedings of 6th International Conference on Deformation Yield
and Fracture of Polymers (April 1-4 1985) 14.1-14.4

70. C. Y. Barlow, A. H. Windle
'Razor blade test for composites toughness'
Journal of Material Science Letters (1985) 4, 233-234

71. C. Lhymn
'Tribological properties of fibrous PEEK matrix composites'
Advances in Polymer Technology (1986) 6, 2, 203-211

72. 'Domes in search of the delicate balance'
Plastics and Rubber Weekly (July 14, 1984)

73. I. Brewster and J. B. Cattanach
'Engineering with long fibre thermoplastic composites'
European SAMPE meeting (March 1983)

74. J. B. Cattanach and F. N. Cogswell
'Processing with aromatic polymer composites'
Developments in Reinforced Plastics-5. Edited by G. Pritchard
Elsevier Applied Science Publishers (1986) 1-38

75. U. Measuria and F. N. Cogswell
'Aromatic Polymer composites: broadening the range'
SAMPE Journal (Sept/Oct 1985) 26-31

76. D. P. Jones, D. C. Leach and D. R. Moore
'Mechanical properties of poly (ether-ether-ketone) for engineering
applications'
Polymer (Aug 1985) 1385-1393

77. T. J. Brown and Dr. C. J. Hooley
'Thermoplastic composites for high performance applications'
Designing with Plastics Composites - Proceedings of Geneva
Conference (1986) 23-33

78. Ideas in Plastics 'Ferrari wins with PEEK, PSO'
Plastics World (Feb 1986) p.50

79. R. B. Rigby
'High temperature thermoplastic matrices for advanced composites'
27th National SAMPE Symposium (May 1982) 747-752

80. G. A. Owens and D. J. Lind
'Applications of carbon fibre reinforced thermoplastic (PEEK)
composite to aero engine component manufacture'
Liverpool Conference (1984)

81. L. M. Povermo, W. K. Muench, W. Marx and G. Lubin
'Composite beam builder'
SAMPE Journal (Jan 1981) 7-14

82. 'Victrex PEEK specified for Boeing engine farings'
    European Plastics News (April 1987) 14, 4, p.37

83. ICI Engineering Plastics (Winter 1986) 26

84. ICI Engineering Plastics (Winter 1985) 25

85. W. D. Hillier
    'Fibre reinforced thermoplastic fabrication technology for
    helicopter primary structure'
    Polymers in Defence - Proceedings of International Conference,
    Bristol 18-20 March 1987

86. D. F. Williams, A. McNamara and R. M. Turner
    'Potential of PEEK and carbon fibre reinforced PEEK in medical
    applications'
    Journal of Materials Science Letters (1987), 6, 188-190

87. ICI launches PEEK Polymer Plastics and Rubber Weekly (Aug 1984)

88. R. Pegg and H. Reyes
    'Advanced composites: Now they've joined the navy'
    Design News (1986) 42, 17, 77-79

89. F. N. Cogswell and D. C. Leach
    'Continuous fibre reinforced thermoplastics: a change in the
    rules for composite technology'
    Plastics and Rubber, Processing and Applications, 4, (1984)
    271-276

90. P. C. Dawson and D. J. Blundell
    'X-ray data for poly(aryl ether ketones)'
    Polymer, 21 (May 1980) 577-578

91. D. R. Rueda et al
    'X-ray diffraction study of die drawn poly(aryl ether ketone)
    (PEEK)'
    Polymer Communications, 24, (Sept 1983) 258-260

92. J. G. Shukla and W. J. Sichina
    'Thermal behaviour of carbon fibre reinforced polyether ether
    ketone'
    SPE Antec (1984) 265-267

93. D. J. Blundell and B. N. Osborn
    'Crystalline morphology of the matrix of PEEK-carbon fibre
    aromatic polymer composites II.Crystallisation behaviour'
    SAMPE quarterly, 17, (Oct 1985) 1-6

94. N. T. Wakelyn
    'On the sturcture of poly (ether ether ketone) (PEEK)'
    Polymer Communications, 25, (Oct 1985) 306-307

95. S. Kumar, D. P. Anderson and W. W. Adams
    'Crystallisation and morphology of poly (aryl-ether-ether-ketone)
    Polymer, 27, (March 1986), 329-336

96. A. V. Fratini et al
    'Refinement of the sturcture of PEEK fibre in an orthorhombic
    unit cell'   Polymer 27, (June 1986) 861-865

97. D. A. Luippold
     'Role of reinforcing fibre in raising DTUL of crystallizable
     thermoplastic polymers'
     30th National SAMPE symposium (March 19-21 1985) 809-819

98. F. G. Krautz
     'Glass fibre enhances high temperature performance of thermo-
     plastics'
     SPE Journal, (1971) 27,74-79

99. A. A. Collyer and D. W. Clegg
     'Fibre reinforced thermoplastics'
     High Performance Plastics (Sept 1985) 2, 11, 1-4

100. H. X. Nguyen and H. Ishida
     'Molecular analysis of the interface of PEEK and basal plane
     graphite single crystals'
     Makromol.Chem. Macromol. Symposium (1986) 5, 13-149

101. E. J. Stober, J. C. Seferis and J. D. Keenan
     'The characterisation and exposure of PEEK to fluid environments'
     Polymer (Dec. 1984) 25, 1845-1852

102. N. T. Wakelyn
     'Resolution of wide-angle x-ray scattering from a thermoplastic
     composite'
     Journal of Polymer Science: Part A Chemistry (1986), 24,
     2101-2105

103. R. W. H. Small
     'A method for direct assessment of the crystalline/amorphous
     ratio of polyetheretherketone (PEEK) in carbon fibre composites
     by wide angle x-ray diffraction'
     European Polymer Journal (1986), 22, 9 699-701

104. J. C. Seferis
     'Polyetheretherketone (PEEK): Processing - structure and
     properties studies for a matrix in high performance composites'
     Polymer Composites, (June 1986), 7, 3, 159-169

105. D. J. Blundell, J. M. Chalmers, M. W. Mackenzie and W. F. Gaskin
     'Crystalline morphology of the matrix of PEEK-carbon fibre aromatic
     polymer composites I. Assessment of crystallinity'
     SAMPE Quarterly 16, 4 (July 1985) 22-30

106. J. N. Leckenby, D. C. Harget, W. J. Sichina and P. S. Gill
     'Crystallization studies of thermoplastic composites by dynamic
     mechanical analysis'
     Carbon Fibres Technology - Uses and Prospects
     Noyes Publications (1986) 86-89

107. Y. Lee and R. S. Potter
     'Crystallization of polyetheretherketone (PEEK) in carbon fibre
     composites'
     Polymer Engineering and Science (May 1986), 26, 9, 633-639

108. P. Cebe and Su-Don Hong
     'Crystallization behaviour of (polyetheretherketone)'
     Polymer (Aug.1986), 27, 1183-1192

109. B. Wunderlich
'Macromolecular Physics' Vol.2 Chapter 6
Academic Press New York 1976

110. D. J. Blundell and F. M. Willmouth
'Crystalline morphology of the matrix of PEEK - carbon fibre
aromatic polymer composites'
SAMPE Quarterly (Jan 1986), 17, 2 50-57

111. O. Yoda
'The crystallite size and lattice distortions in the chain
direction of irradiated PEEK'
Polymer Communications (Jan 1985) 26 16-18

112. T. Sasuga and M. Hagiwara
'Molecular motions of non crystalline PEEK and influence of
electron beam irradiation'
Polymer (April 1985) 26, 501-505

113. T. Sasuga and M. Hagiwara
'Mechanical relaxation of crystalline PEEK and influence of
electron beam irradiation'
Polymer (June 1986) 27, 821-826

114. P. S. Pao, J. E. O' Neal and C. J. Wolfe.
'Fatigue crack growth in PEEK and PEEK composites'
ACS Polymeric Materials Science and Engineering (Sept 1985) 677-682

115. M. F. Kanninen
'A critical look at current applications of fracture mechanics to
the failure of fibre reinforced composites'
Composites (Jan 1977) 17-22

116. S. S. Wang, E. S. Chin, T. P. Yu and D. P. Goetz
'Fracture of random short fiber SMC composite'
Journal of Composite Materials (July 1983) 17, 299-315

117. B. F. Blumentritt, B. T. Vu and S. L. Cooper
'Fracture in oriented short fibre reinforced thermoplastics'
Composites (May 1975) 105-114

118. B. Harris
'Engineering Composite Materials'
The Institute of Metals 1986

119. G. A. Cooper
'The fracture toughness of composites reinforced with weakened
fibres'
Journal of Materials Science (1970) 5, 645-654

120. M. R. Piggot
'Theoretical estimation of fracture toughness of fibrous
composites'
Journal of Materials Science (1970), 5, 669-675

121. H. W. Rayson, G. C. McGrath and A. A. Collyer
'Fibres, Whiskers and Flakes for Composite Applications'
Mechanical Properties of Reinforced Thermoplastics, Chapter 2,
Elsevier Applied Science Publishers 1986

122. J. C. Halpin and J. L. Kardos
'Moduli of crystalline polymers employing composite theory'
Journal of Applied Physics, 43, (May 1972) 2235-2241

123. J. C. Halpin and N. J. Pagano
'The laminate approximation for randomly orientated fibrous composites'
Journal of Composite Materials, 3, (Oct 1969) 720-724

124. J. C. Halpin and J. L. Kardos
'The Halpin-Tsai equations: A review'
Polymer Engineering and Science, 16, (May 1976) 344-352

125. J. C. Halpin and R. L. Thomas
'Ribbon reinforcement of composites'
Journal of Composite Materials, 2, (1968) 488-497

126. G. E. Padawer and N. Beecher
'On the strength and stiffness of planar reinforced plastic resins'
Polymer Engineering and Science 10, (May 1976) 185-192

127. F. W. Maine and P. D. Sheperd
'Mica reinforced plastics: a review'
Composites, 5, (Sept 1974) 193-200

128. B. G. Glavinchevski and M. Piggott
'Steel disc reinforced polycarbonate'
Journal of Materials Science, 8, (1973) 1373-1382

129. V. R. Riley
'Fibre/Fibre interaction'
Journal of Composite Materials, 2, (Oct 1968) 436-446

130. J. Rexer and E. Anderson
'Composites with planar reinforcements (Flakes, Ribbons) - A Review'
Polymer Engineering and Science, 19, (Jan 1979) 1-11

131. R. Hill
'The theory of mechanical properties of fibre strengthened materials: I. Elastic behaviour'
Journal of the Mechanics and Physics of Solids, 12, (1964) 199-212

132. J. Lusis, R. T. Woodhams and M. Xanthos
'The effect of flake aspect ratio on the flexural properties of mica reinforced plastic'
Polymer Engineering and Science, 13, (March 1983) 139-145

133. P. D. Sheperd, F. J. Golemba and F. W. Maine
'Fillers and Reinforcements for Plastics'
Advances in Chemistry series 1974

134. A. Kelly and G. J. Davies
'The principles of the fibre reinforcement of metals'
Metallurgical Reviews, 10 (1965) 1-77

135. M. R. Piggott
'Load Bearing Fibre Composites'
Pergamon Press, Oxford 1980

136. T. S. Chow
'The effect of particle shape on the mechanical properties of filled polymers'
Journal of Materials Science, 15, (1980) 1873-1888

137. P. White
'APC-2 Scrap Recovery'
APC Development Laboratory, ICI Wilton

138. P. White, By Private Communication

139. Monopumps Ltd., Muncher Division
'Reduce Reclaim Cycle'

140. S. Woodward, ICI Wilton, by private communication

141. S. Turner
'Mechanical Testing of Plastics' 2nd Edition
George Godwin in association with PRI 1983

142. R. P. Sheldon
'Composite Polymeric Materials'
Applied Science Publishers, 1982

143. Hofer et al
'Development of Engineering Data on Mechanical Properties of Advanced Composite Materials'
US Air Force Technical Report AFML-TR-72-205

144. R. M. Ogorkiewicz
'Thermoplastics: Effects of Processing'
London Iliffe Books Ltd.,

145. A. A. Griffith
'The Phenomena of Rupture and Flow in Solids'
Phil. Trans. Roy. Soc. A221 (1921) 163-198

146. J. P. Berry
'Fracture processes in polymeric materials: I. The surface energy of polymethylmethacrylate'
Journal of Polymer Science, 50 (1961) 107-115

147. A. Franceshini and A. Momo
'Time stress superposition in some creep experiments'
Polymer, 21 (1980) 725-727

148. A. Franceshini, A. Momo and P. Campagna
'On feasibility of accelerated creep measurements in some polymeric materials' The role of the polymeric matrix in the processing and structural properties of composite materials.
Ed. J. C. Seferis and L. Nicolais.
Proceedings of a Joint US-Italy Symposium on Composite Materials, 1981, Capri, Italy.   Plenum Press

149.. H. L. Cox
'The elasticity and strength of paper and other fibrous materials'
British Journal of Applied Physics 3 (1952) 72-79

150. M. J. Iremonger and W. S. Wood
'Effects of geometry on stresses in discontinuous composite
materials'
Journal of Strain Analysis 4, 2 (1969) 121-126

151. J. Haener and N. Ashbaugh
'Three-dimensional stress distribution in a unidirectional
composite'
Journal of Composite Materials, 1, (1967) 54-63

152. W. R. Tyson and G. J. Davies
'A photoelastic study of the shear stresses associated with the
transfer of stress during fibre reinforcement'
British Journal of Applied Physics, 16 (1965) 199-205

153. D. M. Schuster and E. Scale
'Fundamental Aspects of Fibre Reinforced Plastic Composites'
Chapter 4
Ed. Schwartz and Schwartz Interscience, New York 1968

154. T. F. MacLaughlin
'A photoelastic analysis of fibre discontinuities in composite
materials'
Journal of Composite Materials, 2, 1 (Jan 1968) 44-55

155. R. A. Isaksen, S. Newman and Q. A. Trementozzi
'Some photoelastic observations of reinforcement with polymeric
fibres'
Polymer Engineering and Science, 7, 2 (April 1967) 94-97

156. B. W. Rosen and E. Friedman
'Whisker Technology' Chapter 7
Ed. A. P. Levitt, Wiley New York 1970

157. P. E. Chen
'Strength properties of discontinuous fibre composites'
Polymer Engineering and Science 11, 1 (Jan 1971) 51-56

158. B. W. Rosen
'Fibre Composite Materials' Chapter 3
American Society for Metals (1965)

159. H. Voss and K. Friedrich
'Fracture and fatigue of short glass-fibre reinforced PTFE
composites'
Journal of Material Science Letters, 5, (1986) 569-572

160. K. Friedrich, R. Walter, H. Voss and J. Karger-Kocsis
'Effect of short fibre reinforcement on the fatigue crack
propagation and fracture of PEEK matrix composites'
Composites, 17, 3 (1986) 205-216

161. S. Mall, G. E. Law and M. Katouzian
'Loading rate effect on interlaminar fracture toughness of a
thermoplastic composite'
Journal of Composite Materials, 21 (June 1987) 569-579

162. R. A. Crick, D. C. Leach and D. R. Moore
      'Interpretation of toughness in aromatic polymer composites
      using a fracture mechanics approach'
      SAMPE Journal (Nov/Dec 1986) 30-36

163. M. Davies, ICI by private communication

164. D. Purslow
      'Matrix fractography of fibre reinforced thermoplastics,
      Part 1. Peel Failures'
      Composites 18, 5 (Nov 1987) 365-374

165. A. C. Garg and Yiu-Wing Mui
      'Failure mechanisms in toughened epoxy resins - a review'
      Composites Science and Technology, 31 (1988) 179-223

166. A. A. Ogale and R. L. McCullough
      'Influence of microstructure on elastic and viscoelastic
      properties of polyether ether ketone'
      Composites Science and Technology 30 (1987) 185-201

167. M. Morris
      'Investment in Machinery for the Recycling of ICI APC-2
      Composite Material - An Economic Assessment'
      Appendix 1 of Ph.D. Thesis 1988 Sheffield City Polytechnic

TABLE 1

PARTLY CRYSTALLINE AND AMORPHOUS THERMOPLASTICS:

BENEFITS OF REINFORCING WITH 30% GLASS FIBRES

MATERIAL	HEAT DISTORTION TEMPERATURE AT 1.82 MPa ($^{\circ}$C)		TENSILE STRENGTH AT 23°C (MPa)	
	MATRIX	COMPOSITE	MATRIX	COMPOSITE
Partly Crystalline				
Nylon 6, 6	95	248	80	180
PEEK	155	300	100	175
Nylon 6	75	212	60	160
Amorphous				
Polyethersulphone	201	216	90	155
Polycarbonate	130	140	64	120
ABS	90	100	50	90

TABLE 2

SOLUTION VISCOSITIES FOR POLYMERS OF STRUCTURE A,

PREPARED BY REACTION (4)

η_{red}^{*}	$[\eta]$	$I.V^{\dagger}$
1.53	1.10	1.08
1.38	0.07	1.05
1.10	0.91	0.89
1.04	0.87	0.85
1.01	0.78	0.77
0.93	0.73	0.72
0.57	0.50	0.49
0.37	0.28	0.29
0.24	0.20	0.20

*For solutions in 98% sulphuric acid containing 1g polymer/100ml
 acid

†For solutions in 98% sulphuric acid containing 0.1g polymer/100ml
 acid

TABLE 3

COMPARISON OF DATA REDUCTION METHODS TO CALCULATE THE

FRACTURE TOUGHNESS, G_{IC}

DATA REDUCTION METHOD	G_{IC} Nm^{-1}
AREA METHOD	140
LINEAR BEAM METHOD	121
EMPIRICAL ANALYSIS	151
CENTRE NOTCH	154

WORKER	REF.	DATA REDUCTION METHOD	TYPE OF COMPOSITE	% Fibre	G_{IC}, NM^{-1}
BARLOW	[69]	Razor blade test	Optimised matrix APC-2	60	3380
"	"	"	Non-optimised matrix APC-2 derivitive	60	460
CARLILE	[24]	Area method	Continuous fibre APC-2 cleavage mode	68	2400
"	"	"	" " ductile mode	68	2900
HARTNESS	[4]	-	Continuous fibre APC-1	60	1400
"	"	-	Continuous fibre woven APC-1	60	2000
WHITNEY	[60]	Area method	Continuous fibre graphite/epoxy	-	140
"	"	"	Continuous fibre woven graphite/epoxy	-	280
"	"	"	Continuous fibre graphite-bismaleimide	-	70
"	"	"	Continuous fibre graphite-polysulphone	-	590
DONALDSON	[25]	Off axis tensile test	Continuous fibre graphite-epoxy composite	-	85
"	"	"	Continuous fibre APC-1	60	960
CHAI	[66]	Generalised Empirical Analysis	Quasi-isotropic continuous fibre graphite/epoxy	-	450
DEVITT	[65]	Non-Linear Beam Analysis	Unidirectional glass/epoxy	-	750
WANG	[63]	Non-Linear Analysis	Random short fibre glass/epoxy	50	1400
BASCOM	[65]	Tapered beam test	Continuous fibre woven glass/epoxy	60	1000
"	"	"	Continuous fibre woven glass/epoxy + elastomer	60	4400
"	"	"	Continuous fibre woven graphite/epoxy	61	600
"	"	"	Continuous fibre woven graphite/epoxy + elastomer	58	4600

TABLE 4:   FRACTURE TOUGHNESS VALUES FOR DIFFERENT FIBRE/MATRIX SYSTEMS

TABLE 5

COEFFICIENTS OF LINEAR THERMAL EXPANSION

FOR UNIAXIAL APC (PER $^{\circ}$C)

COEFFICIENTS OF LINEAR THERMAL EXPANSION FOR UNIAXIAL APC (PER$^{\circ}$C)		
	23°C to 143°C	143°C to 343°C
Along fibre	0.5 x 10^{-6}	1.0 x 10^{-6}
Across fibre	30 x 10^{-6}	75 x 10^{-6}

TABLE 6

MECHANICAL PROPERTIES OF INJECTION MOULDED APC-2:

SCRAP AND STANDARD CARBON FIBRE COMPOUND - 450 CA 30

	'Victrex' PEEK 450 CA30	APC-2 Reclaim and 'Victrex' PEEK 450G	APC-2 Reclaim and 'Victrex' PEEK 450G
Weight % Carbon Fibre	30	30	40
Flexural Modulus/GPa	21	25.6	30.4
Flexural Strength/MPa	343	403	410
Tensile Strength/MPa	197	254	242

TABLE 7

MECHANICAL PROPERTIES OF COMPRESSION MOULDED APC-2:

SCRAP AND STANDARD CARBON FIBRE COMPOUND-450 CA30

	'Victrex' PEEK 450 CA30	3mm square APC-2	12.7mm square APC-2
Weight % Carbon Fibre	30	68	68
Flexural Modulus/GPa	13.1	26	38
Flexural Strength/MPa	-	220	343
Tensile Strength/MPa	210	157	366
Impact-Initiation Energy /J	2	3.2	9
Impact-Total Energy/J	9	7.4	29

SPECIMEN TYPE

	FLEXURE	TENSION	COMPRESSION	DAMAGE AREA	IMPACT TOUGHNESS	DCB	CREEP	MOULDING TRIALS
NOMINAL THICKNESS/mm	2.0	2.0	2.0	2.0	2.0	5.0	2.0	1.0
SPECIMEN LENGTH/mm	140.0	150.0	123.0	70.0	70.0	150.0	150.0	150.0
SPECIMEN WIDTH/mm	10.0	12.5	12.5	70.0	70.0	25.0	15.0	150.0
QAUGE LENGTN/mm	-	50.0	15.0	-	-	-	50.0	-
CRACK LENGTH/mm	-	-	-	-	-	35.0	-	-

TABLE 8: SPECIMEN DIMENSIONS FOR MATERIAL CHARACTERISATION

TABLE 9

CHARACTERISATION OF APC-2

PROPERTY	MACROSTRUCTURE OF THE APC-2			
	$(0)_{16}$	$(90)_{16}$	$(0,90)_{4S}$	$(+45,90, -45,0)_{2S}$
Flexural Strength/ MPa	1,876(49.0)	140(6.4)	1,163(30)	616(34.7)
Flexural Modulus/ GPa	130(1.7)	10.3(0.3)	68.8(2.4)	40.9(2.1)
Tensile Strength/ MPa	2,125(31.0)	80.0(1.6)	1,023(47.0)	704(26.0)
Tensile Modulus/ GPa	135(2.1)	9.3(0.4)	71.8(1.6)	48.6(2.9)
Tensile Strain/%	1.45(0.2)	1.0(0.2)	1.35(0.15)	1.69(0.1)
Compression Strength/ MPa	1,094(46.0)	–	742(29.3)	361(20.1)
Impact energy/J:				
Initiation	–	–	6(0.5)	6(0.4)
Total	–	–	25(1.2)	20(1.1)

	Temperature	Cleavage mode	Ductile mode
Mode I interlaminar Fracture Toughness, G_{IC} /Nm^{-1}	23°C	2,068(667)	2,709(691)

( ) = standard deviation

- 152 -

TABLE 10   STRAIN ENERGY RELEASE RATE, G_{IC}, FOR PARTICULATE BEAMS

SAMPLE Size/No.	G_{IC} Nm^{-1}								$\overline{G}_{IC}$ for each beam
	a_1	a_2	a_3	a_4	a_5	a_6	a_7	a_8	
6.35(2)	3280	2740	4280	8050	4800				4630
6.35(3)	5945	2565	4676						4395
6.35(4)	2300	4310							3305
							Total G_{IC} =		4295
9.5(3)	4240	4710							4475
9.5(4)	4070	5310							4690
9.5(5)	2220								2220
							Total G_{IC} =		4110
12.7(1)	3050	2040							2545
12.7(2)	3260	5400							4330
12.7(4)	2810	2400	3980	4520	5300	2940	3990	4940	3860
12.7(5)	3350	4610							3980
							Total G_{IC} =		3756
15.9(1)	2340	1890	3530	4770					3133
15.9(2)	2580	4920	1900	1970	3630	3890			3148
15.9(3)	2060	3400	3640	5620					3680
15.9(5)	3470	3470	2470	3590					3250
							Total G_{IC} =		3285
19.1(1)	2640	3700	2340	1830	2970	4800			3047
19.1(2)	1550	3610	4580						3247
19.1(3)	1970	3580	3040	2870	3230				2938
19.1(4)	2230	4050	4900						3727
							Total G_{IC} =		3170
22.2(2)	1611								1611
22.2(4)	3230	2030	4510	2110	3510				3078
22.2(5)	3780	2980							3380
							Total G_{IC} =		2970
25.4(2)	2840	1870	2890						2533
25.4(3)	3140	3780							3460
							Total G_{IC} =		2904
CONT(1)	2310	3270							2790
CONT(2)	1430	1630	1720	2050					1708
							Total G_{IC} =		2068

- 153 -

TABLE 11

THE STATISTICAL ANALYSIS OF G_{IC} WITH RESPECT TO PARTICLE SIZE

PARTICLE SIZE (mm)	$G_{IC}(Nm^{-1})$	S	95% C.L.
6.35	4295	1753	$\mp$ 1254
9.5	4110	1161	$\mp$ 1440
12.7	3756	1080	$\mp$ 623
15.9	3285	978	$\mp$ 486
19.1	3170	1028	$\mp$ 593
22.2	2970	990	$\mp$ 828
25.4	2904	689	$\mp$ 855
CONT.	2068	667	$\mp$ 700

TABLE 12

THE RATE OF INCREASE IN STRAIN WITH TIME AGAINST PARTICLE SIZE

PARTICLE SIZE/mm	GRADIENT/% STRAIN $(\text{LOG TIME})^{-1}$
6.35	0.01129
9.525	0.00780
12.70	0.00800
15.875	0.00561
19.05	0.00532
22.225	0.00368
25.40	0.00462

TABLE 13

SUMMARY OF THE MOULDING TRIALS

PARTICLE SIZE	3-D CURVATURE SMALL RADIUS	3-D CURVATURE LARGE RADIUS
1 inch square	TEARING WRINKLING	NO TEARING WRINKLING
0.75 inch square		NO TEARING SLIGHT WRINKLING
0.50 inch square	TEARING WRINKLING	NO TEARING SLIGHT WRINKLING
0.25 inch square	TEARING	
0.125 inch square		VERY GOOD NO TEARING NO WRINKLING
Mono Munched		GOOD NO TEARING LITTLE WRINKLING

TABLE 14

THE EFFECT OF A REGULAR PARTICLE LAY-UP

25.4 mm SQUARE PARTICLES

PROPERTY	MACROSTRUCTURE OF THE MOULDING		
	$(0)_{16}$	$(90)_{16}$	$(0,90)_{4S}$
Flexural Strength /MPa	1,028(48.8)	134.6(5.1)	584.9(19.6)
Flexural Modulus /GPa	75.8(1.3)	10.4(0.4)	56.0(3.0)

TABLE 15

A COMBINATION OF PARTICLE SIZES

	PARTICLE SIZE		
	---	---	---
		Mono Munched Material	
PROPERTY	12.7+25.4mm	Random	>3mm Random
Flexural Strength/MPa	432.6(2.6)	396.2(41.2)	439.0(41.8)
Flexural Modulus/GPa	34.3(1.2)	31.0(2.8)	33.5(2.5)
Tensile Strength/MPa	200.1(3.6)	215.9(11.9)	215.6(11.6)
Tensile Modulus/GPa	40.5(1.6)	37.6(2.1)	40.6(2.3)
Tensile Strain/ %	0.72(0.14)	0.77(0.03)	0.77(0.09)
Compression Strength/ MPa	395.0(10.1)	382.0(15.3)	423.3(15.6)

TABLE 16

THE EFFECT OF WEAVING ON THE PROPERTIES OF THE RECONSTITUTED SCRAP

PROPERTY	MACROSTRUCTURE OF THE MOULDING	
	12.7 mm wide strips in $(0/90)_{4S}$ weave	$(0,90)_{4S}$
Flexural Strength /MPa	817(55)	1,163(30)
Flexural Modulus /GPa	61.4(1.7)	68.8(2.4)
Tensile Strength /MPa	669.9(21.9)	1,023(47.0)
Tensile Modulus /GPa	69.6(2.0)	71.8(1.6)
Tensile Strain / %	0.86(0.10)	1.35(0.15)
Compression Strength/ MPa	605.0(7.1)	742.0(29.3)
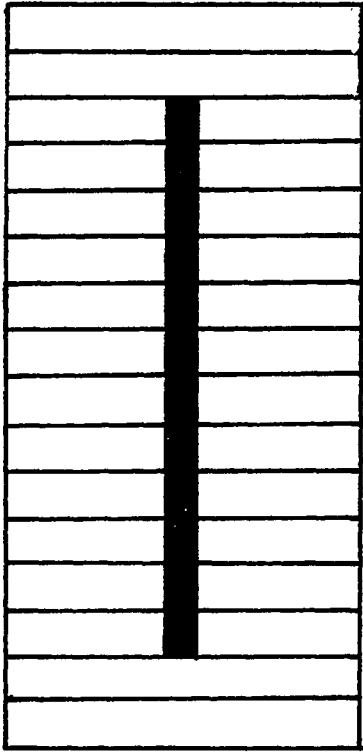
AS CAST

STRESSED

Figure 1

Special acrylic fibre

Oxidation

Inert gas

Carbonisation

Inert gas

Graphitisation

Surface treatment

Continuous fibre flow

Oxidised acrylic tow
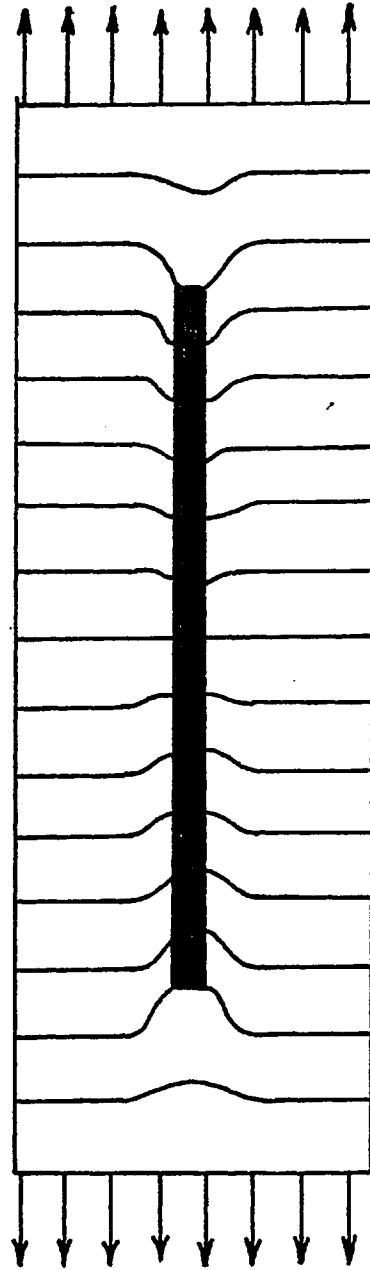
Figure 2 MANUFACTURING PROCESS
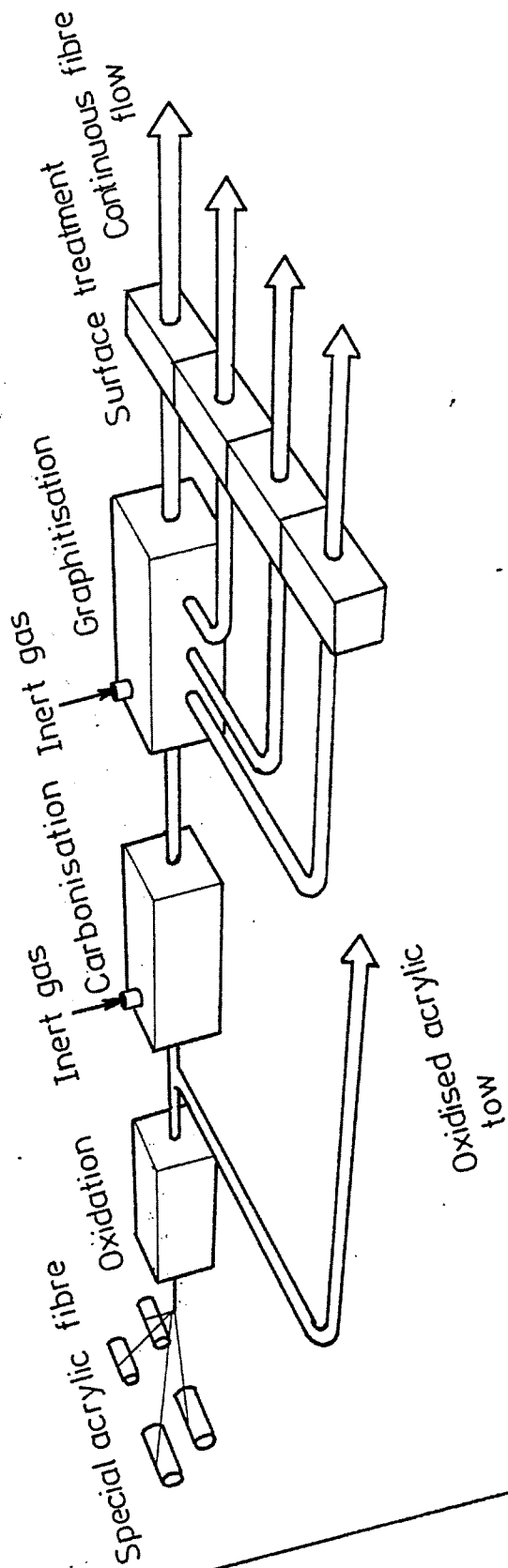
SCHEMATIC DIAGRAM OF THE MANUFACTURING PROCESS

- 161 -
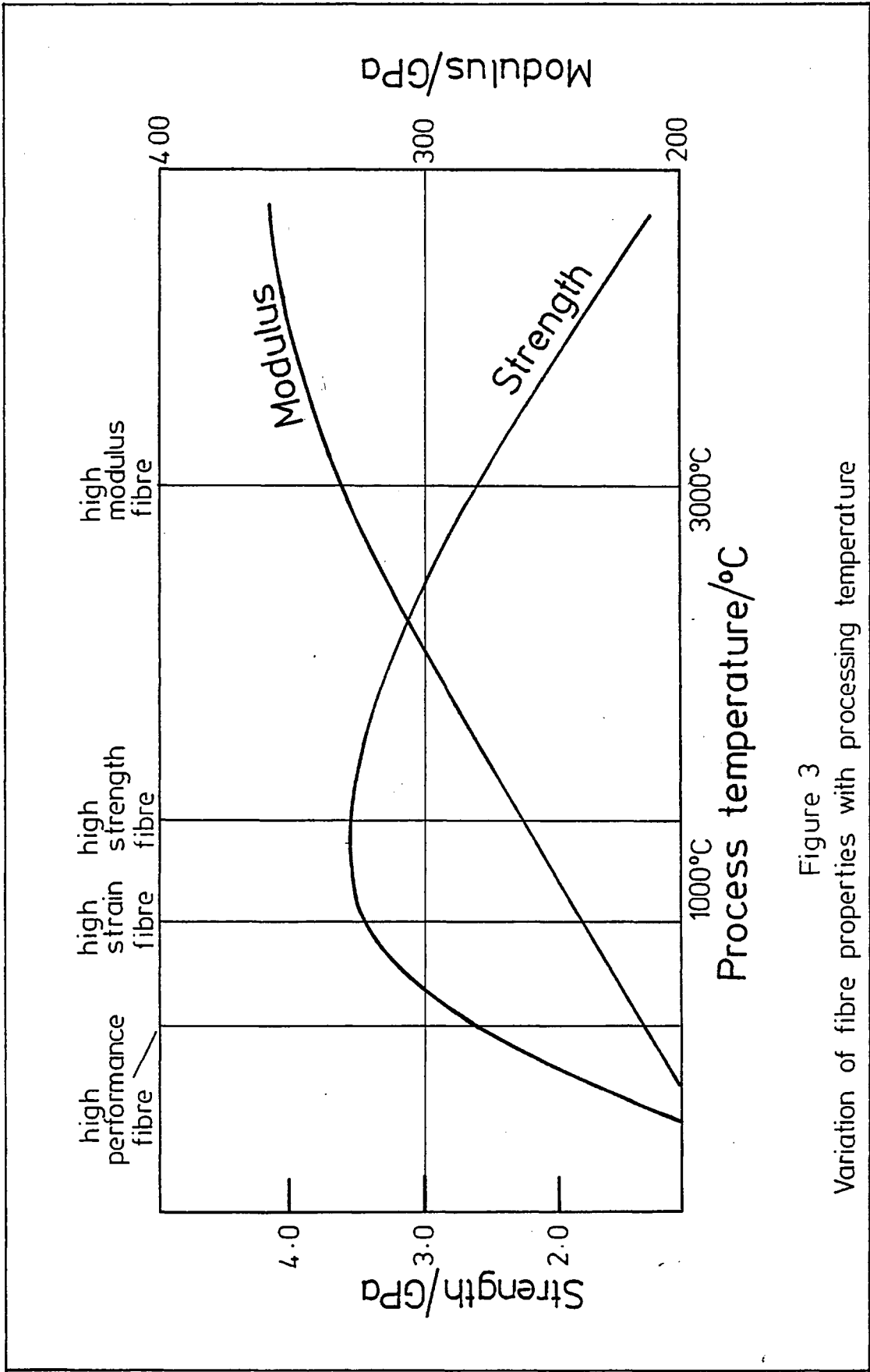
Figure 3

Variation of fibre properties with processing temperature
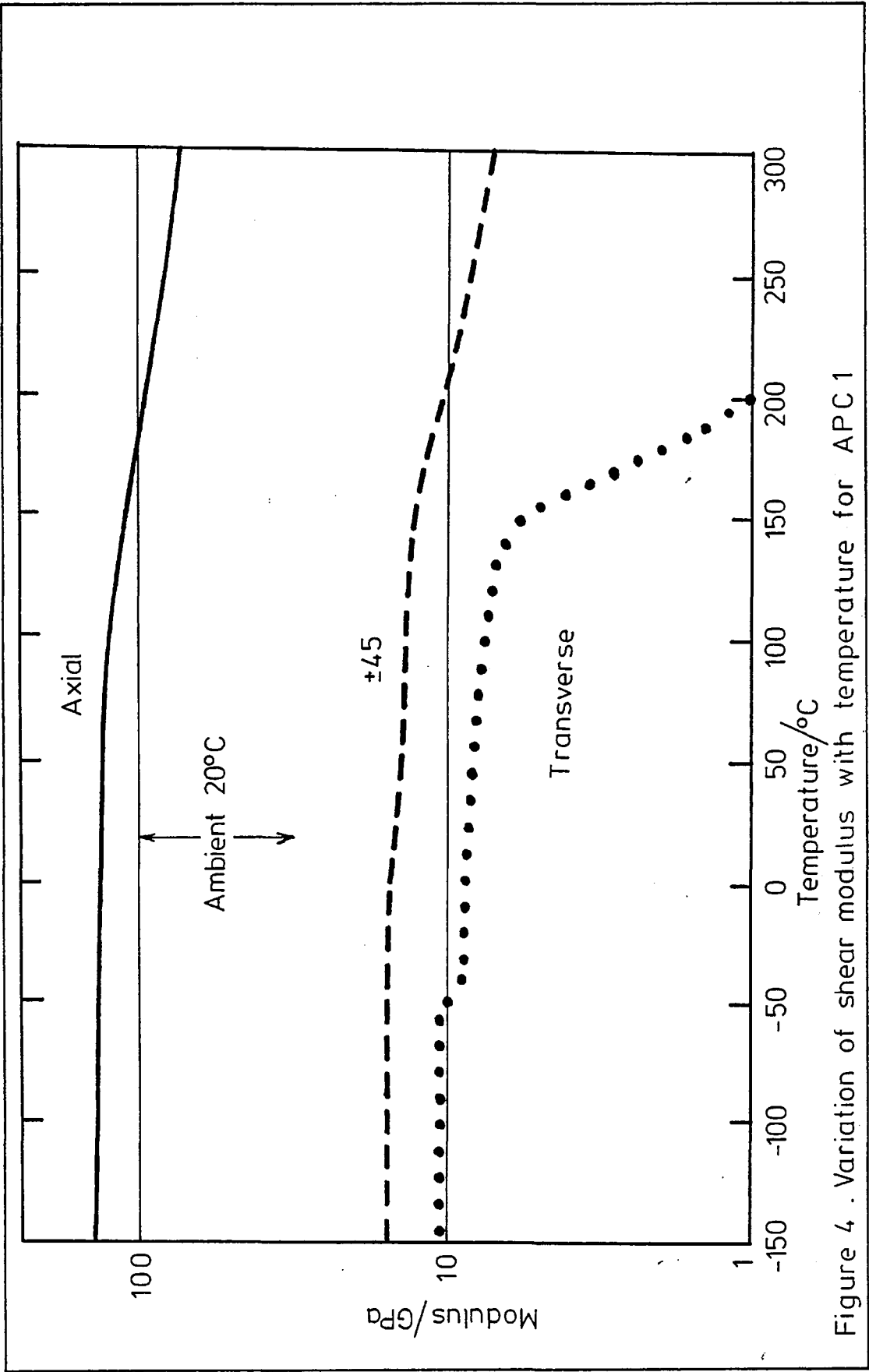
Figure 4 . Variation of shear modulus with temperature for APC 1
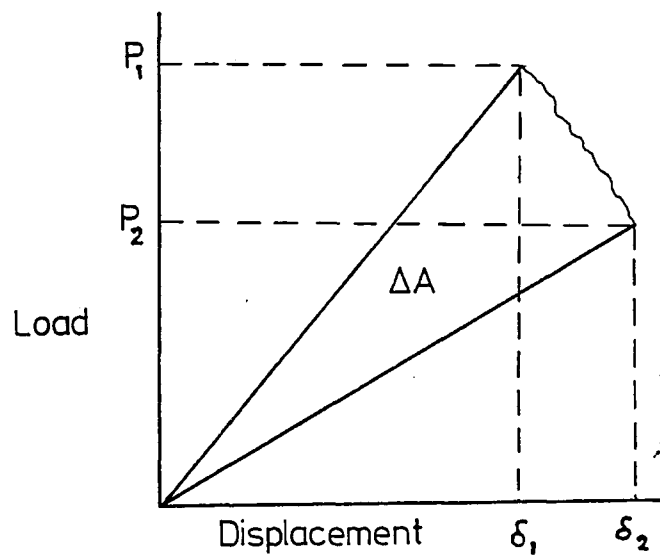
Figure 5a
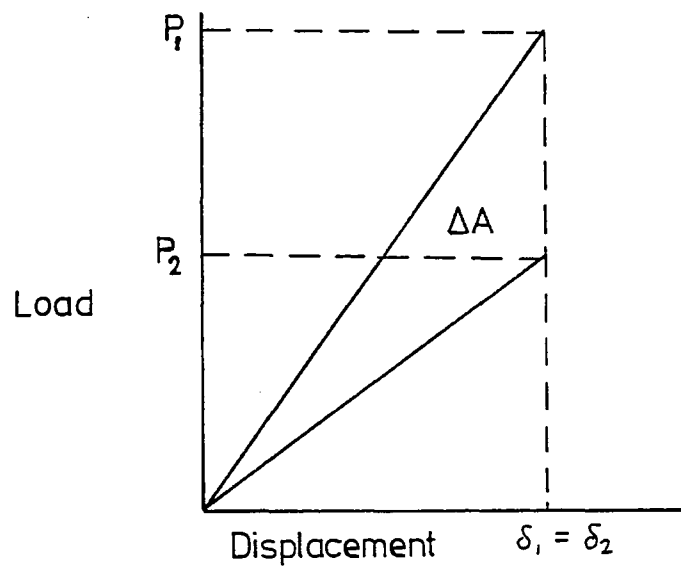
Figure 5b

Diagramatic representation of the
calculation for G_{IC}
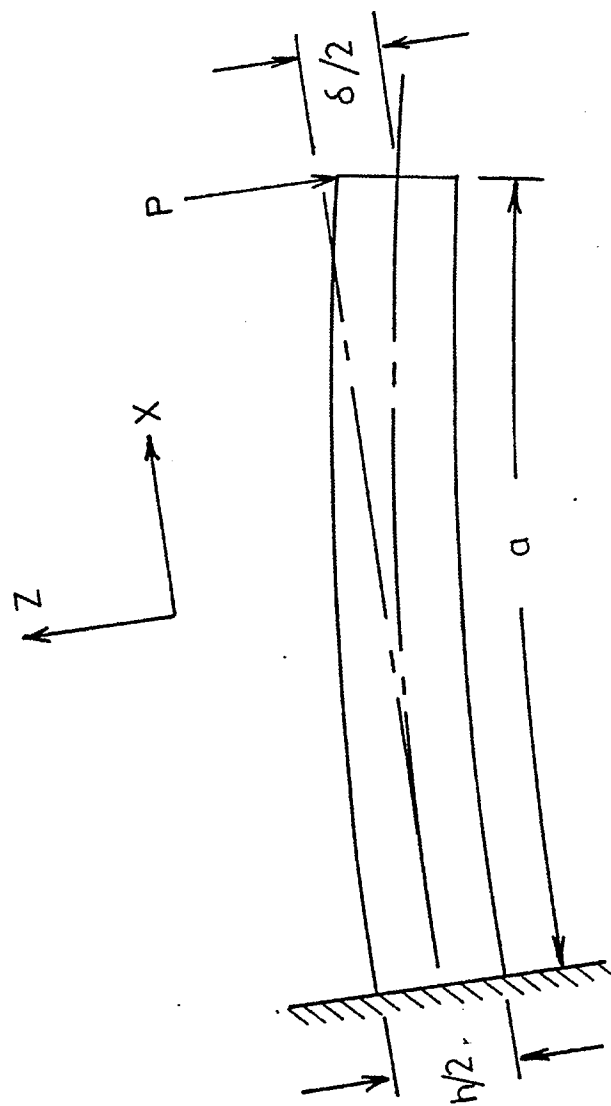
Figure 6

Cantilever beam model for analysis of DCB specimens
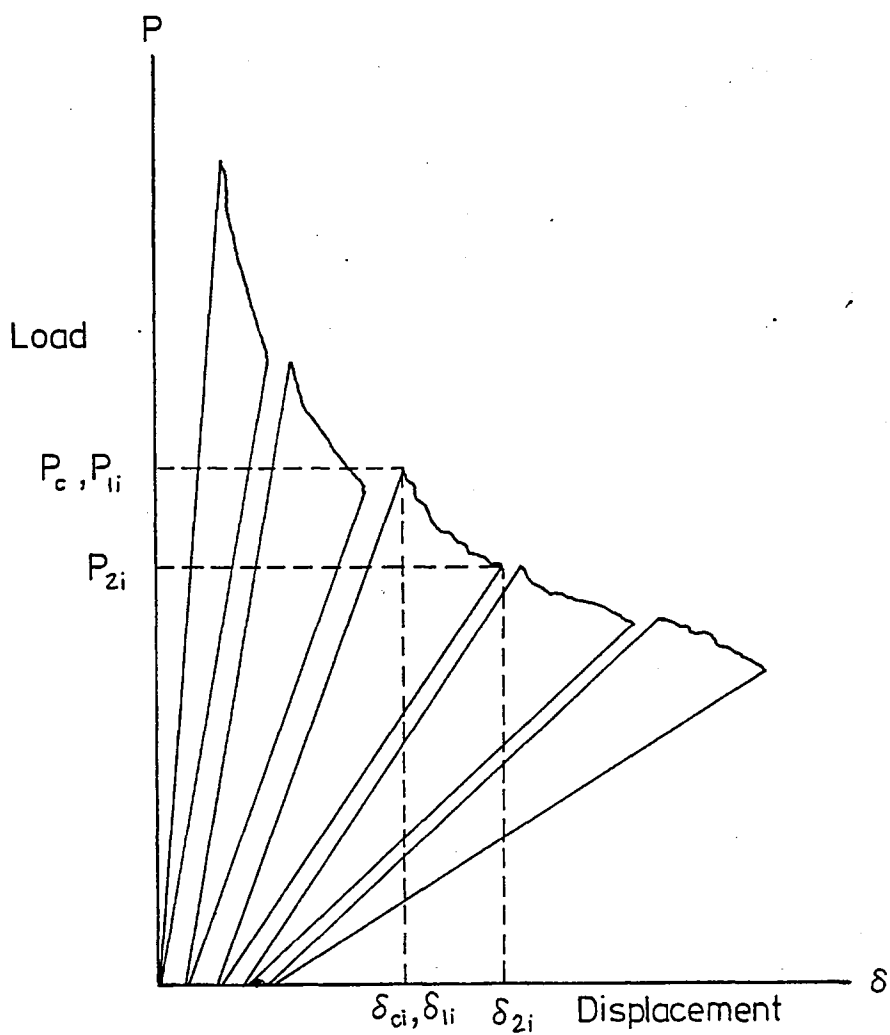
Figure 7

Series of loading and unloading curves used in
determination of G_{Ic}
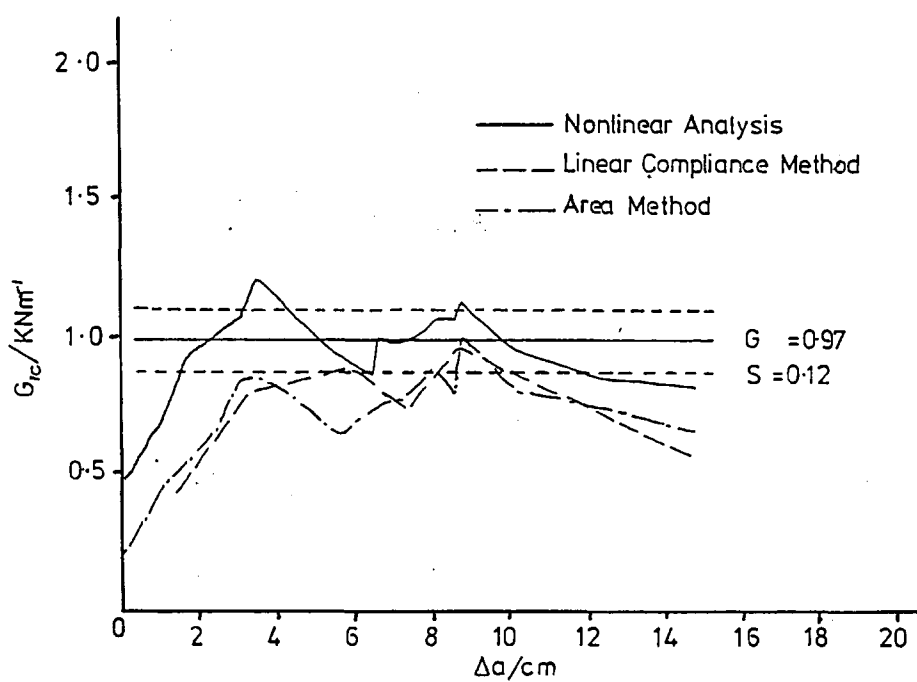
Figure 8

Comparison of data reduction for DCB test
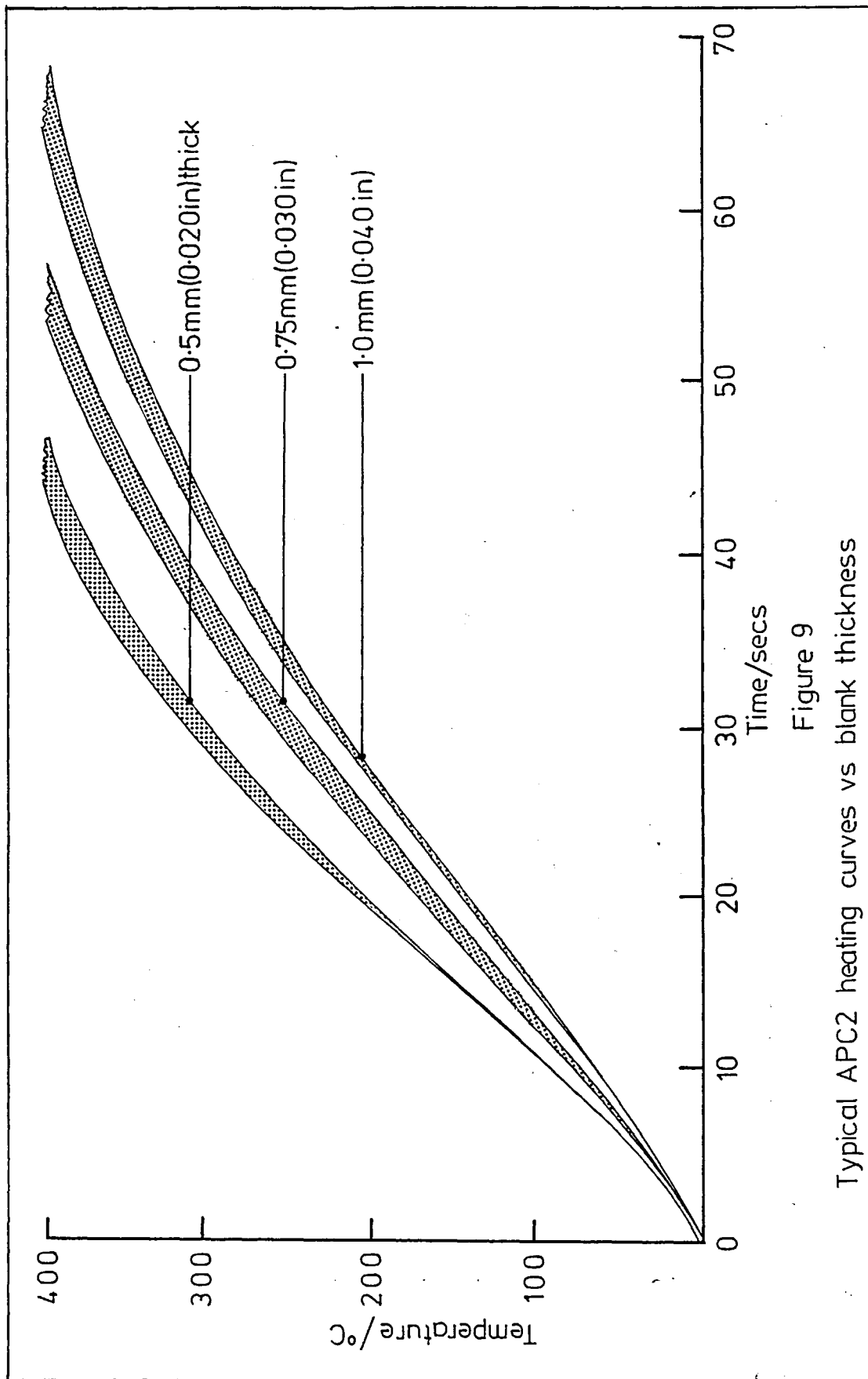
Typical APC2 heating curves vs blank thickness

Figure 9

0.5mm(0.020in)thick

0.75mm(0.030in)

1.0mm(0.040in)

Time/secs
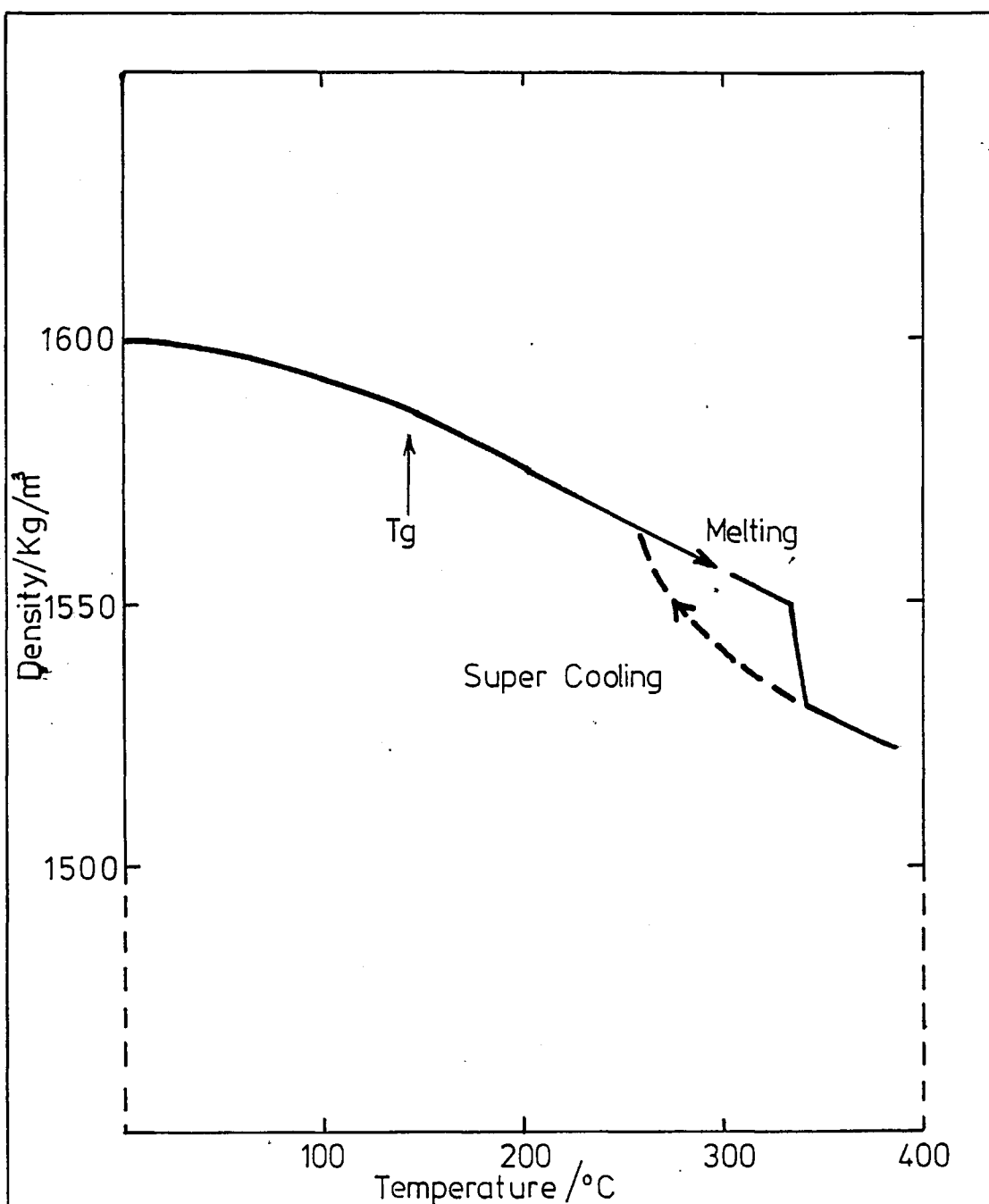
Temperature/°C

Figure 10

Representative plot of density as a function
of temperature for APC2 material. This
graph shows the expected behaviour for
the recommended processing cycle based
on rapid cooling.

Fibre Buckling

No Fibre Buckling

Free Edge

Inter-ply Slip

Adjacent Reverse Bands

No Slip at Free Edge
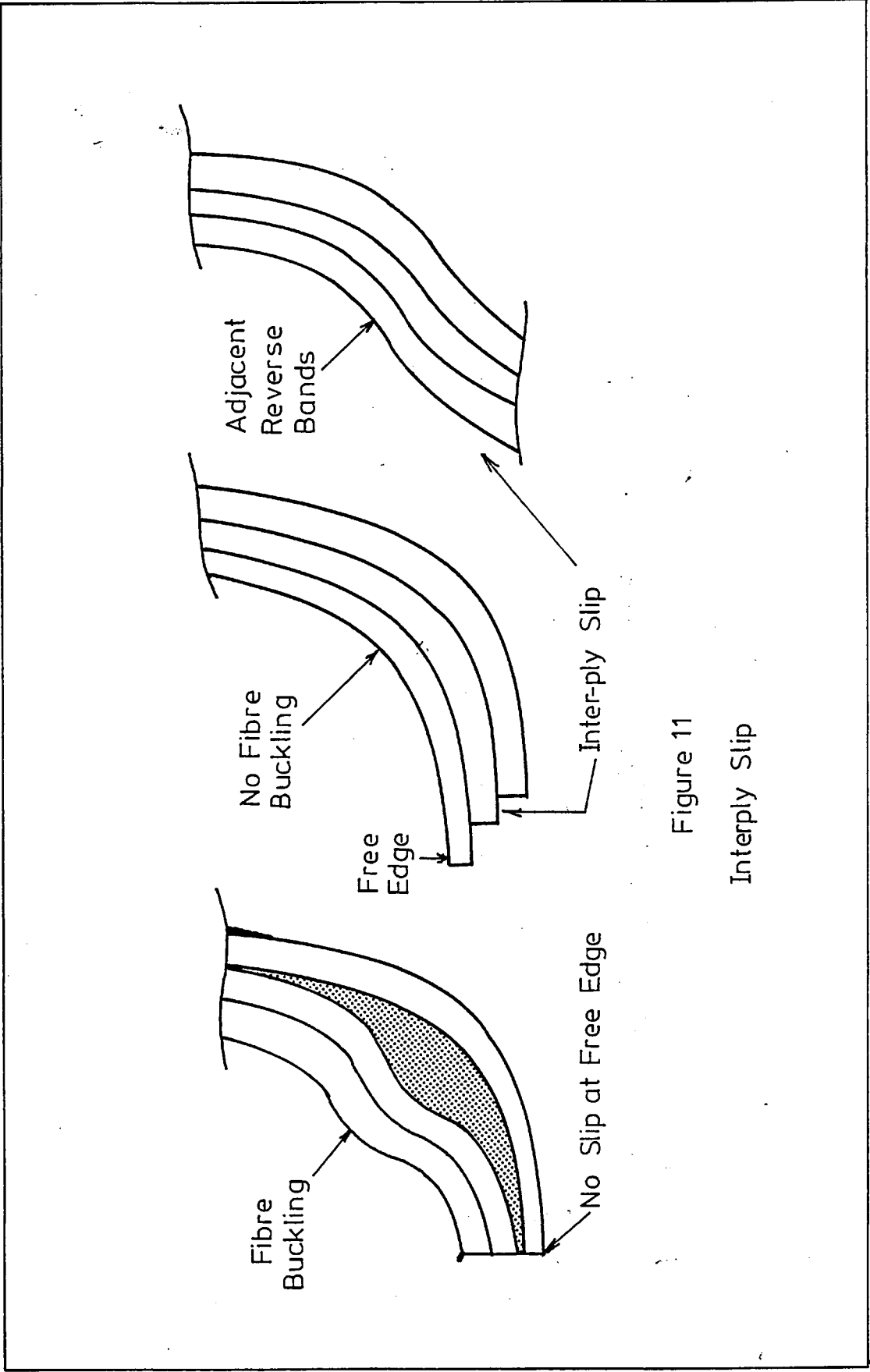
Figure 11

Interply Slip
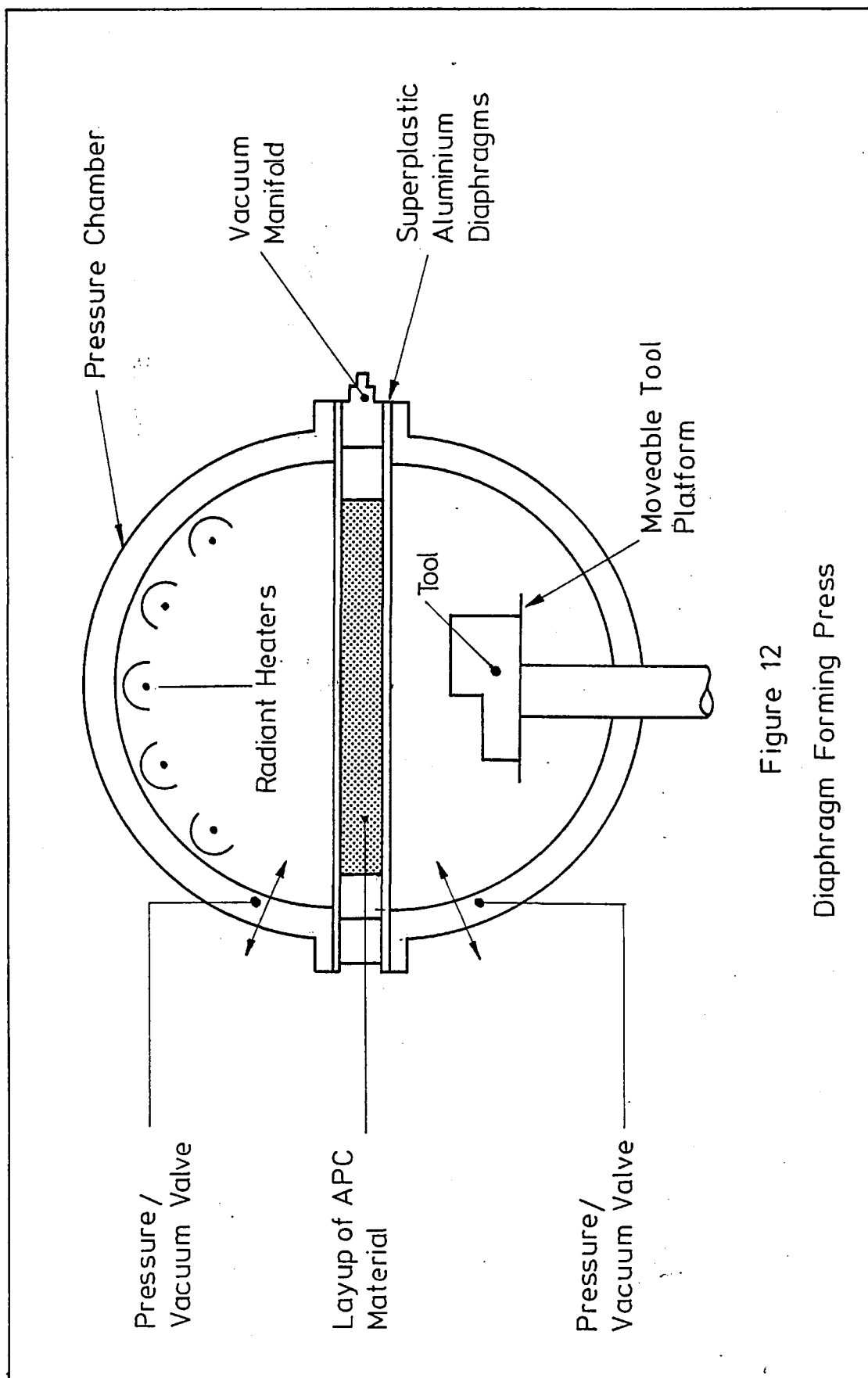
Figure 12

Diaphragm Forming Press

Crystallization behavior
under constant cooling conditions
showing peak crystallization
temperature as a function of cooling
rate. o=experimental data.
The curve shows the predictions based
on the simple crystallization model.
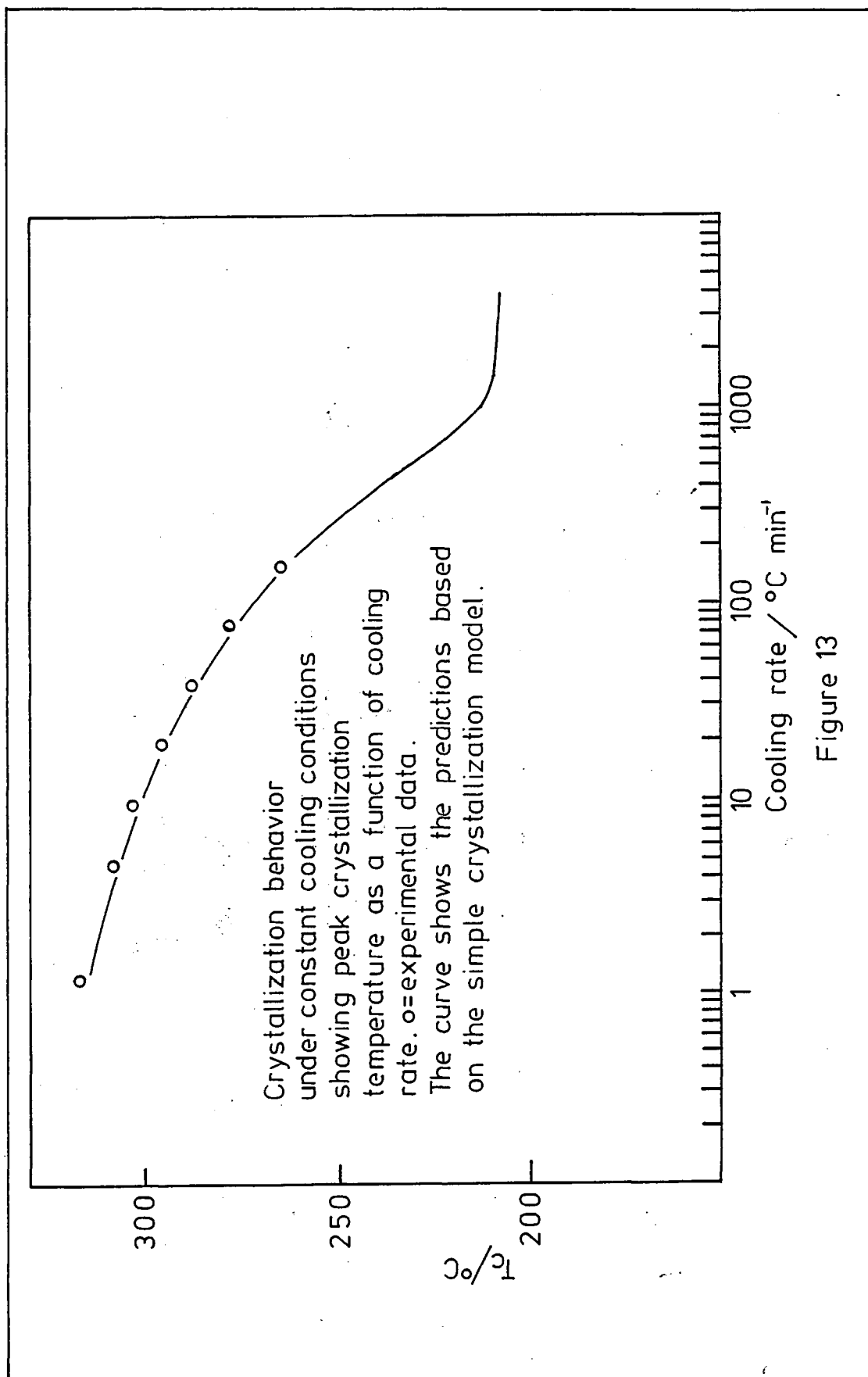
Figure 13
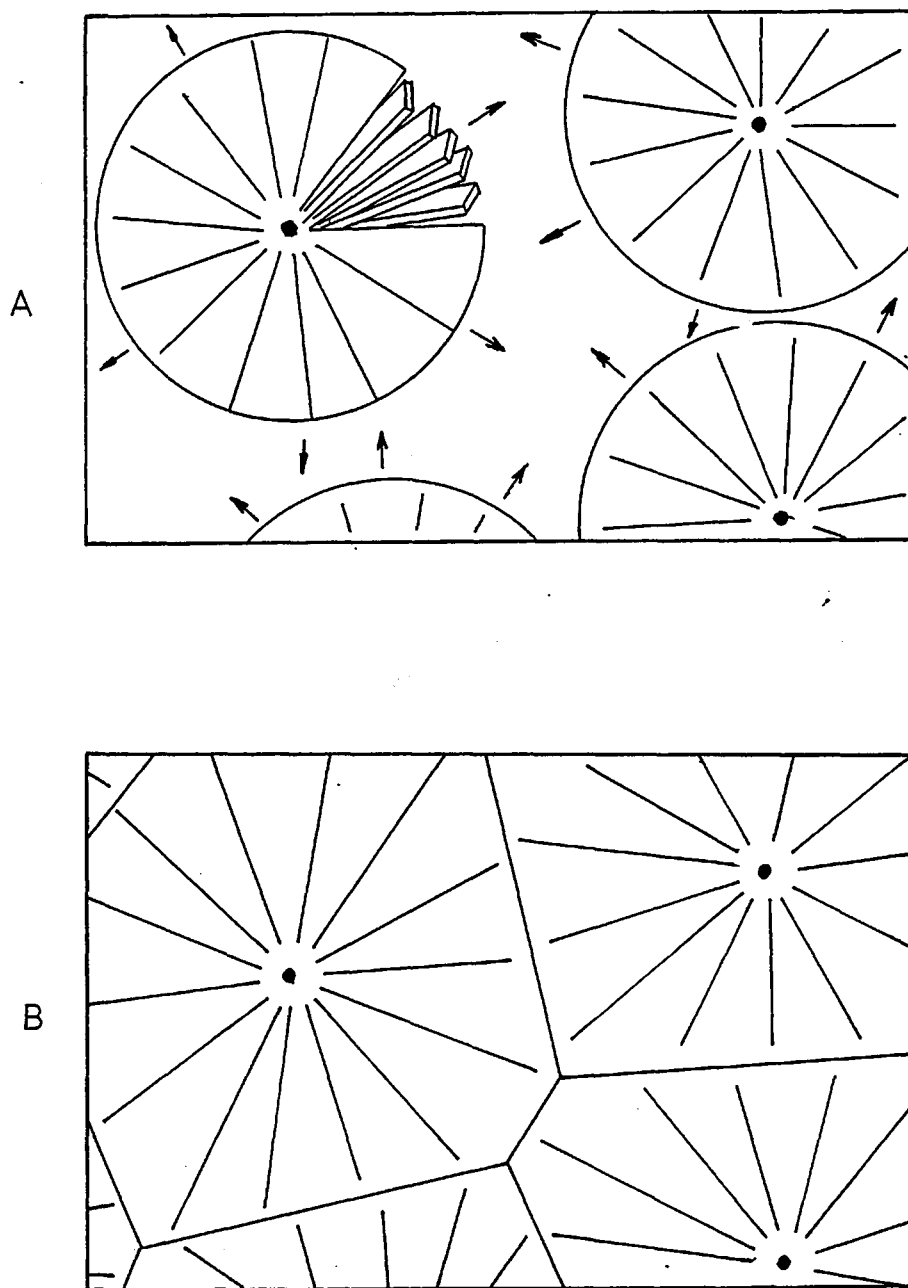
Schematic drawing of spherulites within the PEEK matrix. A, represents an earlier stage of crystallization where there is incomplete coverage by spherulites. The inset depicts the much smaller lamellar crystals [~5nm thick] which make up the larger spherulites [1·10 μm diameter].

B, represents a later stage where the spherulites have fully impinged.

Figure 14
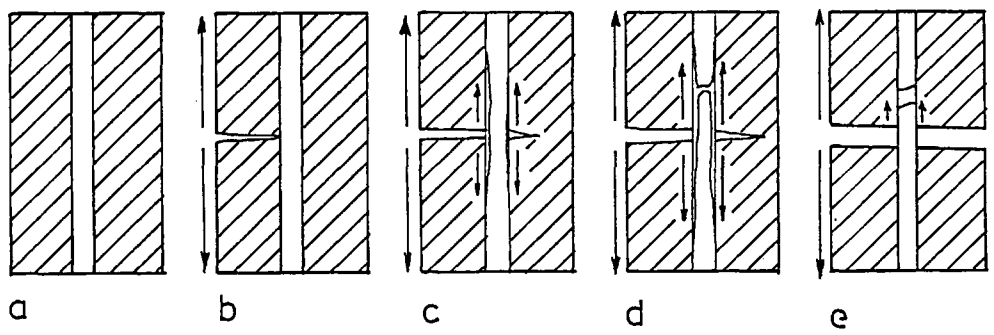
Figure 15

Schematic representation of stages in crack growth
in a fibre composite
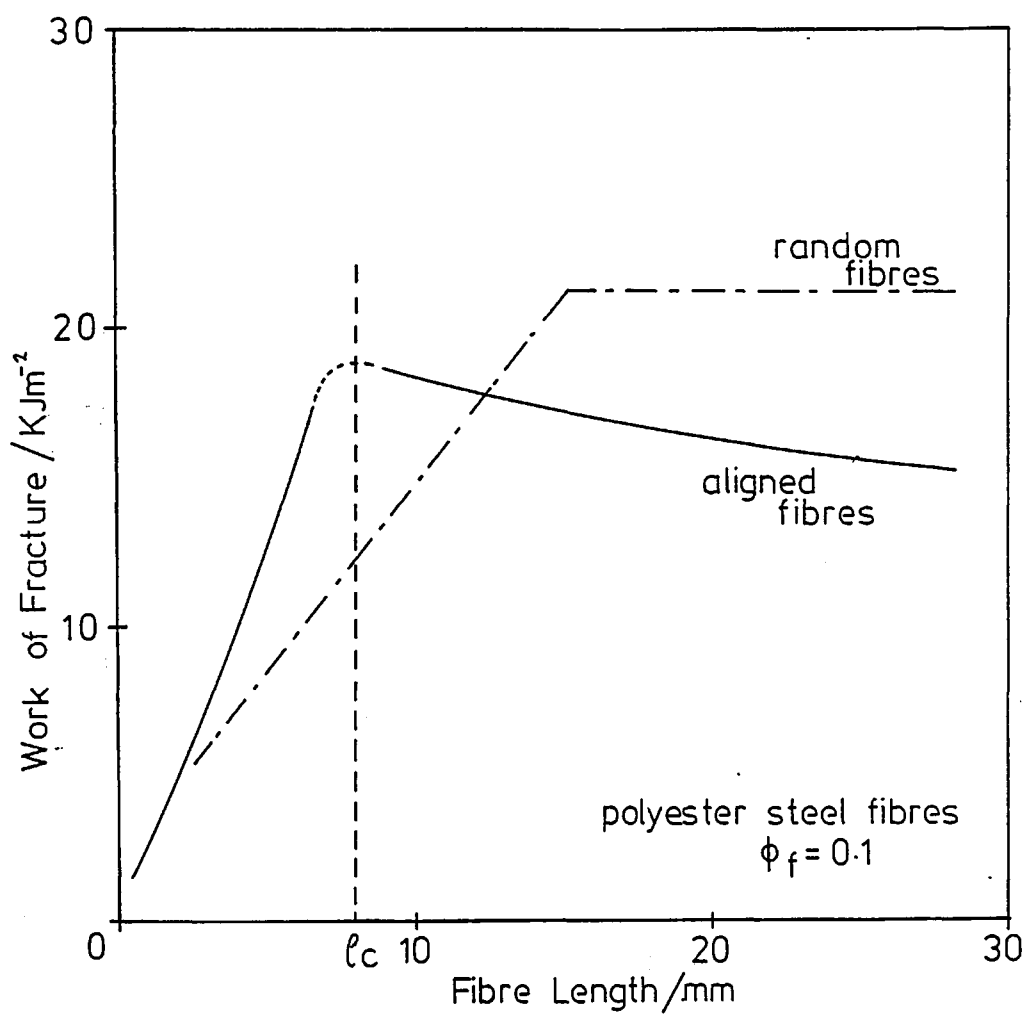
Figure 16

Work of fracture of random
and aligned composites consisting of
chopped steel fibres in a polyester matrix

fibres   flakes

1-2 —— —— ——   1-2 —— —— ——
        —— ——   —— —— ——

2-3   ° °   2-3 —— —— ——
      ° • °   —— —— ——
         ° °   —— —— ——
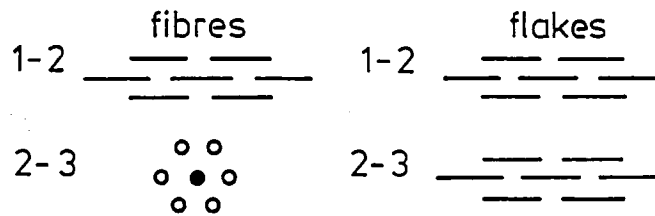
Figure 17

Stress distribution effects in
flakes and fibres.
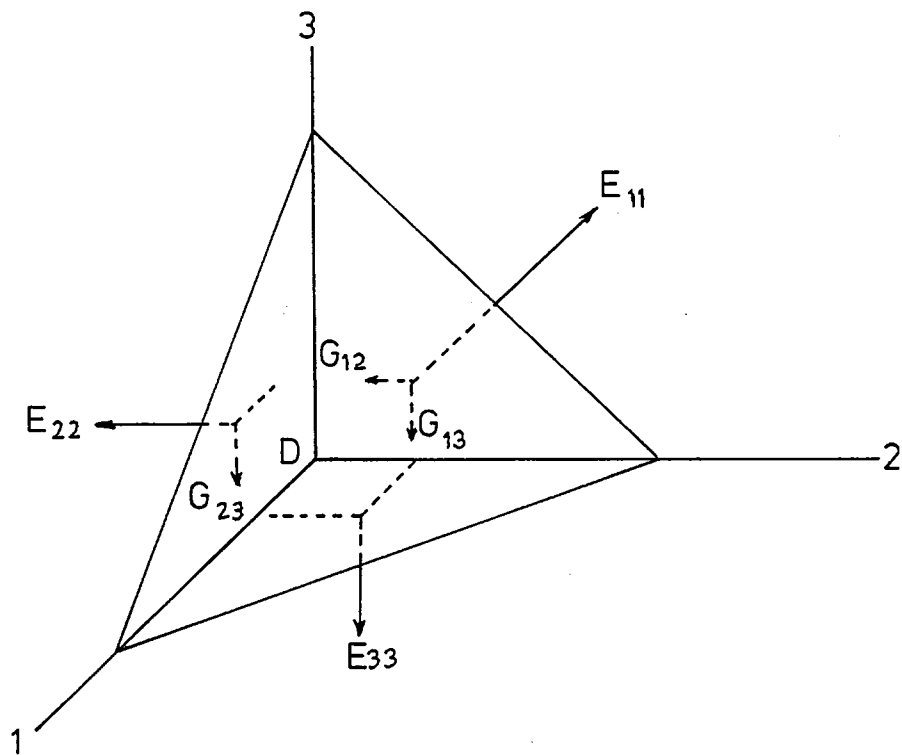
Figure 18
Elastic moduli of planar reinforced
composites.
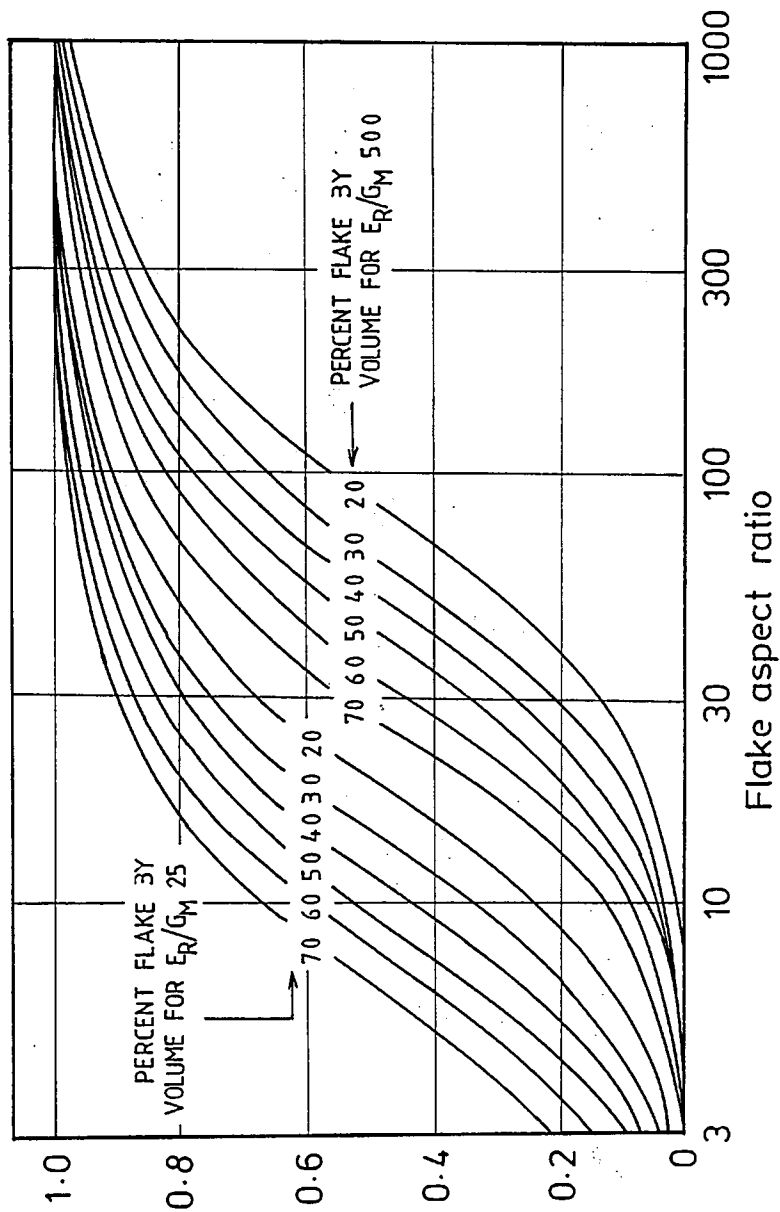
Figure 19

Calculated modulus reduction factor, MRF, v's flake aspect ratio, a, for various laminate parameters.

(a)

(b)
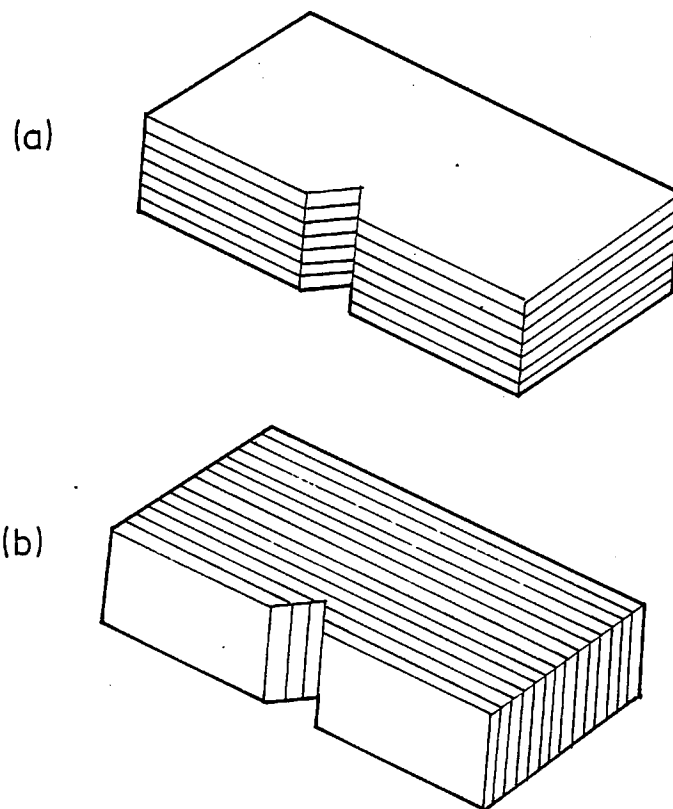
Figure 20
Crack configurations in planar
reinforced composites.
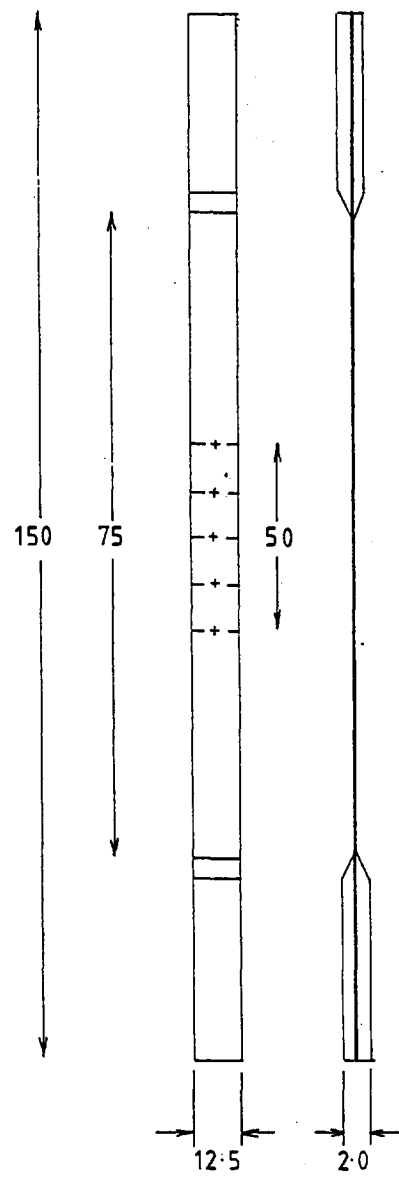
Width measured at : − − −

Thickness measured at : +

Figure 21

The tensile specimen
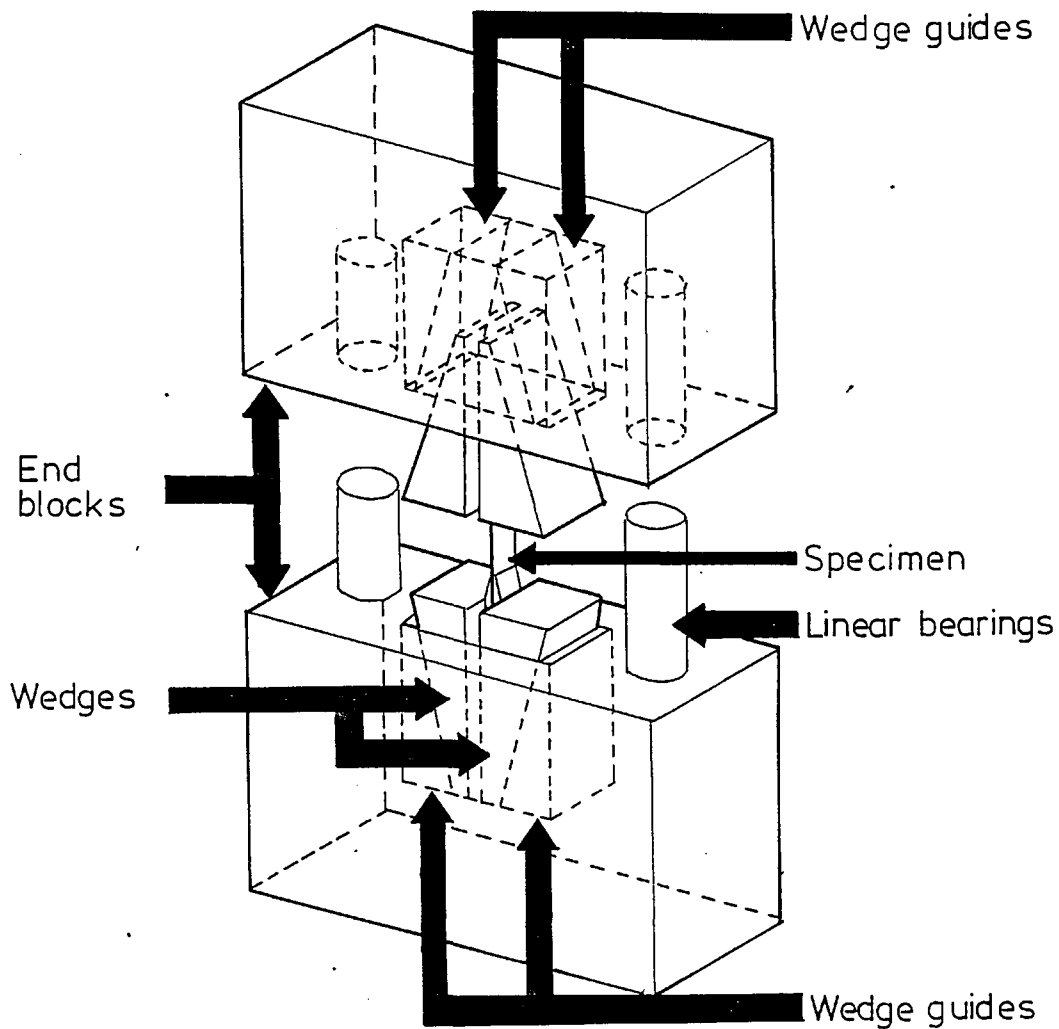
Figure 22

IITRI Compression test
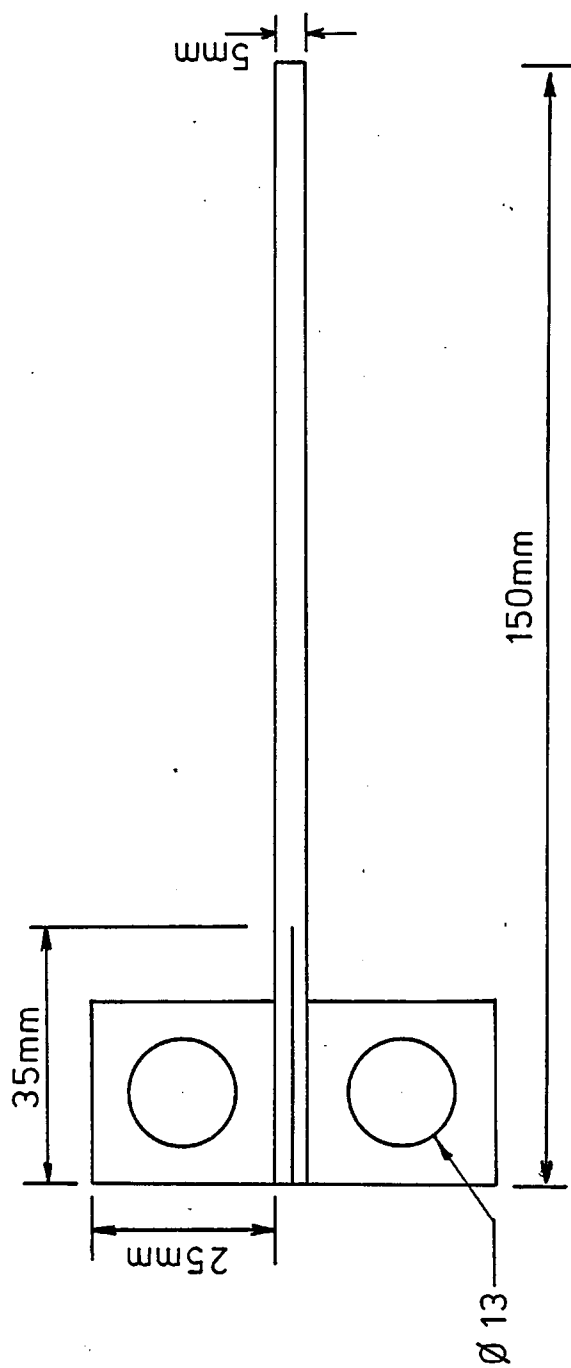
Figure 23

The double cantilever beam specimen
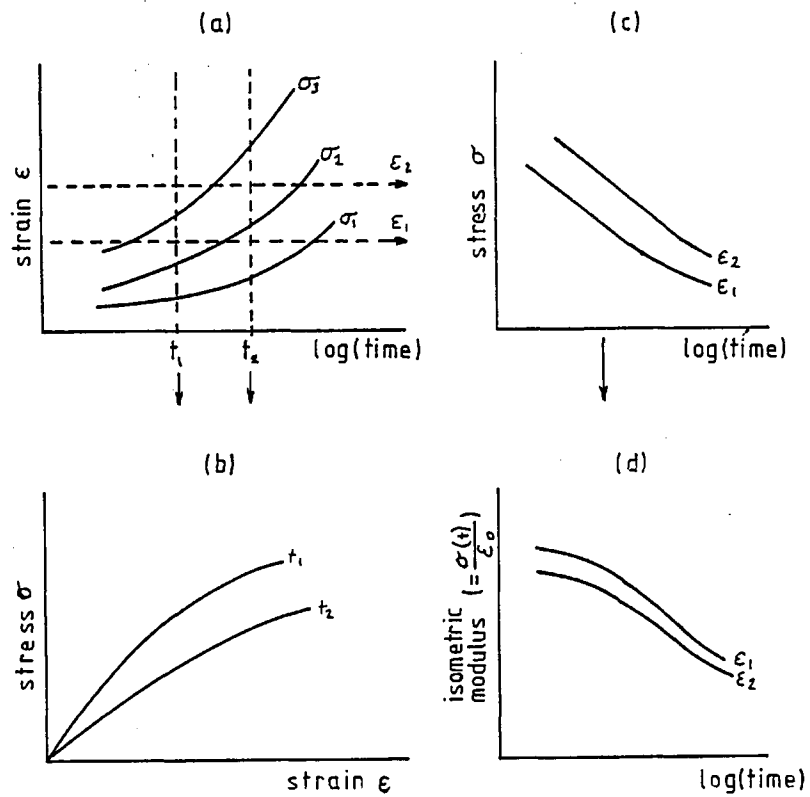
Cross plots of creep data. (a) Basic family of creep curves for a number of stress levels, σ; (b) isochronous stress-strain curves for two selected times, t_1 and t_2; (c) isometric stress-log(time) curves for two selected strain levels, ε_1 and ε_2; (d) isometric modulus-log(time) curves for two selected strain levels ε_1 and ε_2.
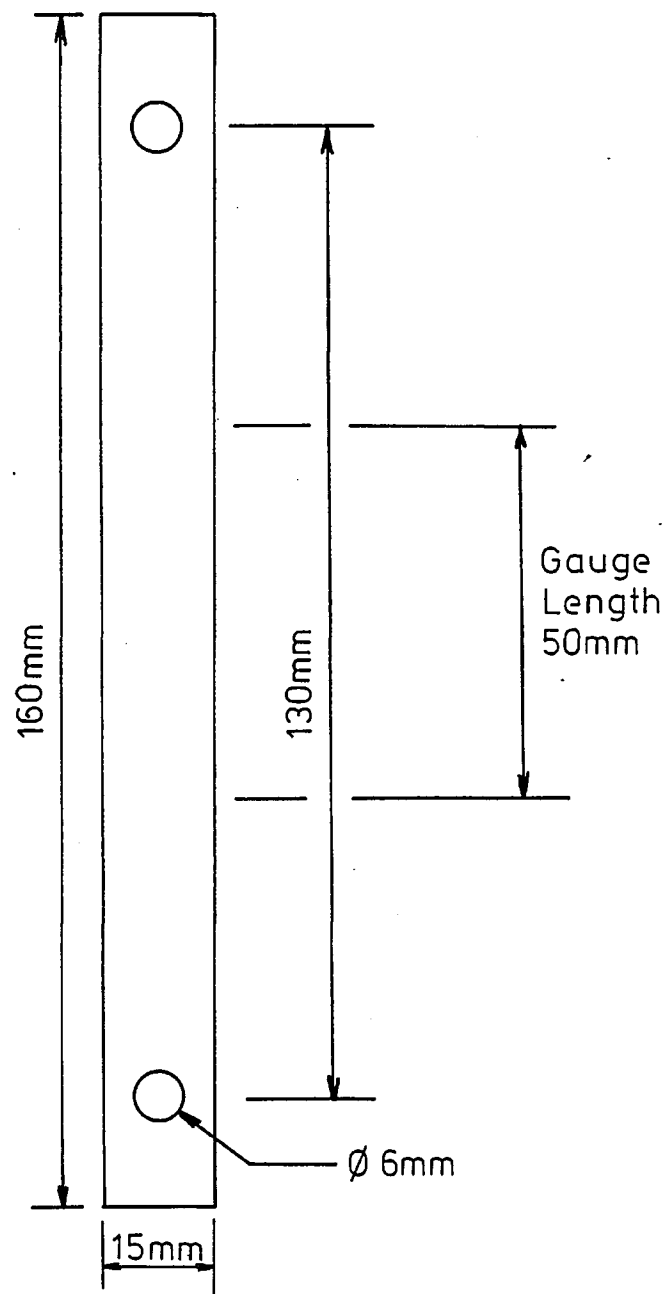
Figure 24

Figure 25

The creep specimen
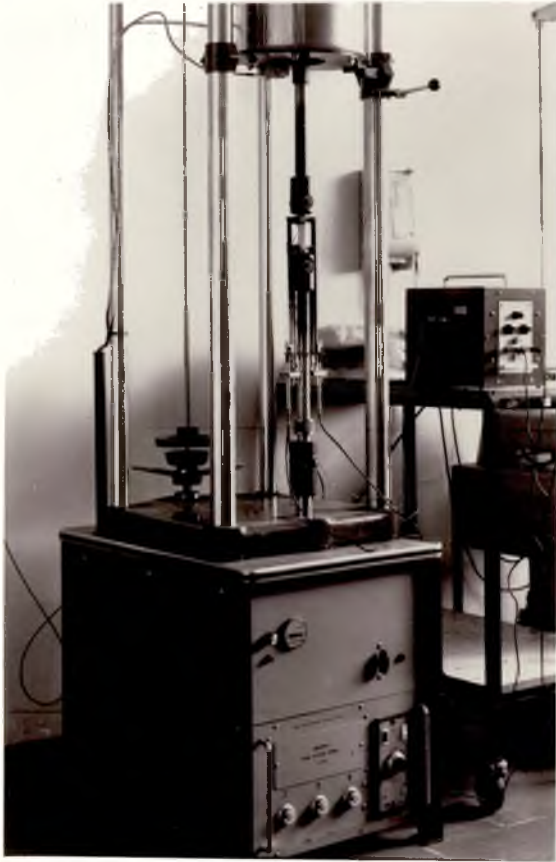
Figure 26
The arrangement of the creep rig.
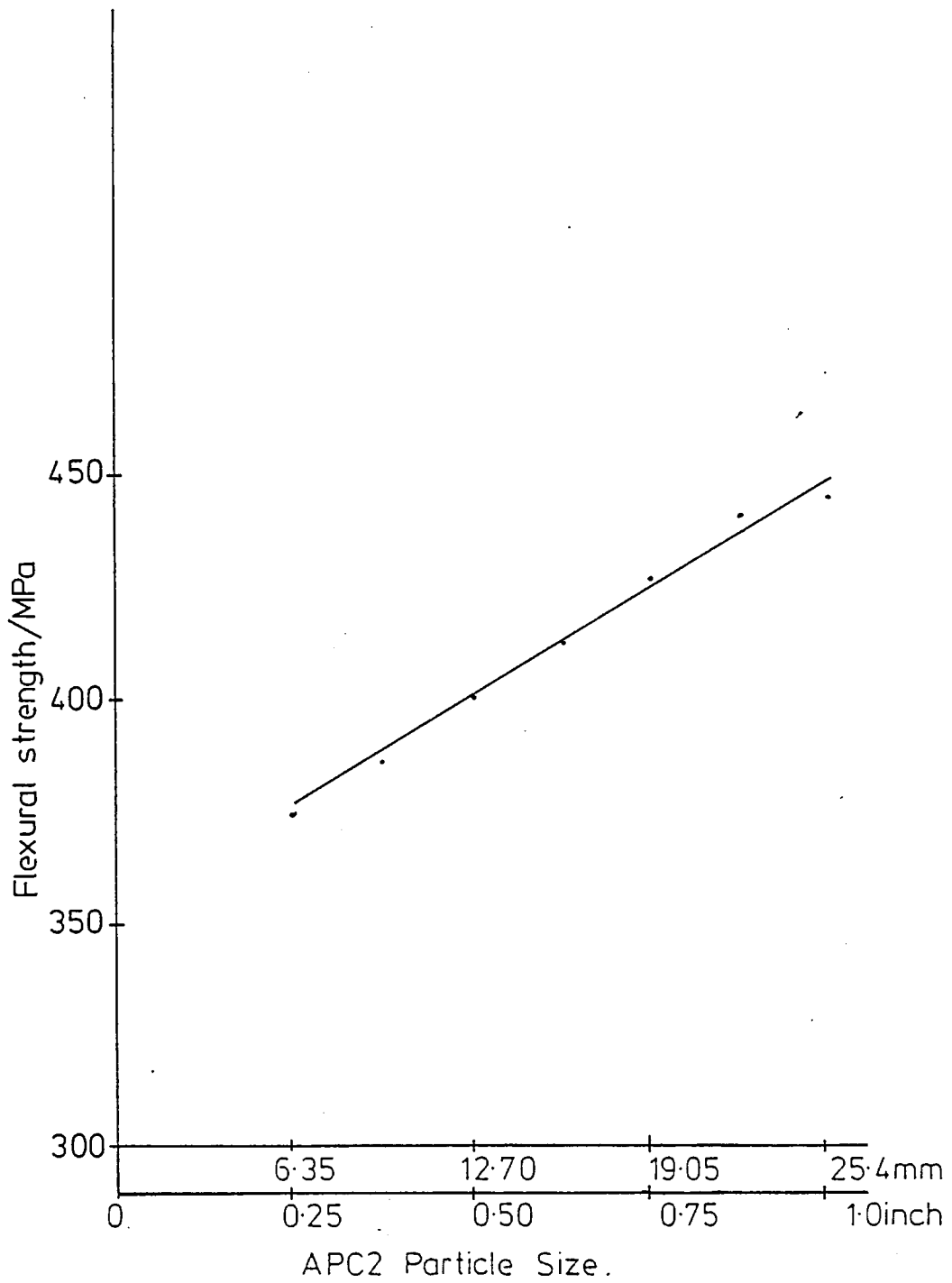
Figure 27
Effect of particle size Flexural strength, mean values

Figure 28

Effect of particle size Flexural modulus, mean values

Figure 29

Effect of particle size Longitudinal tensile strength, mean values
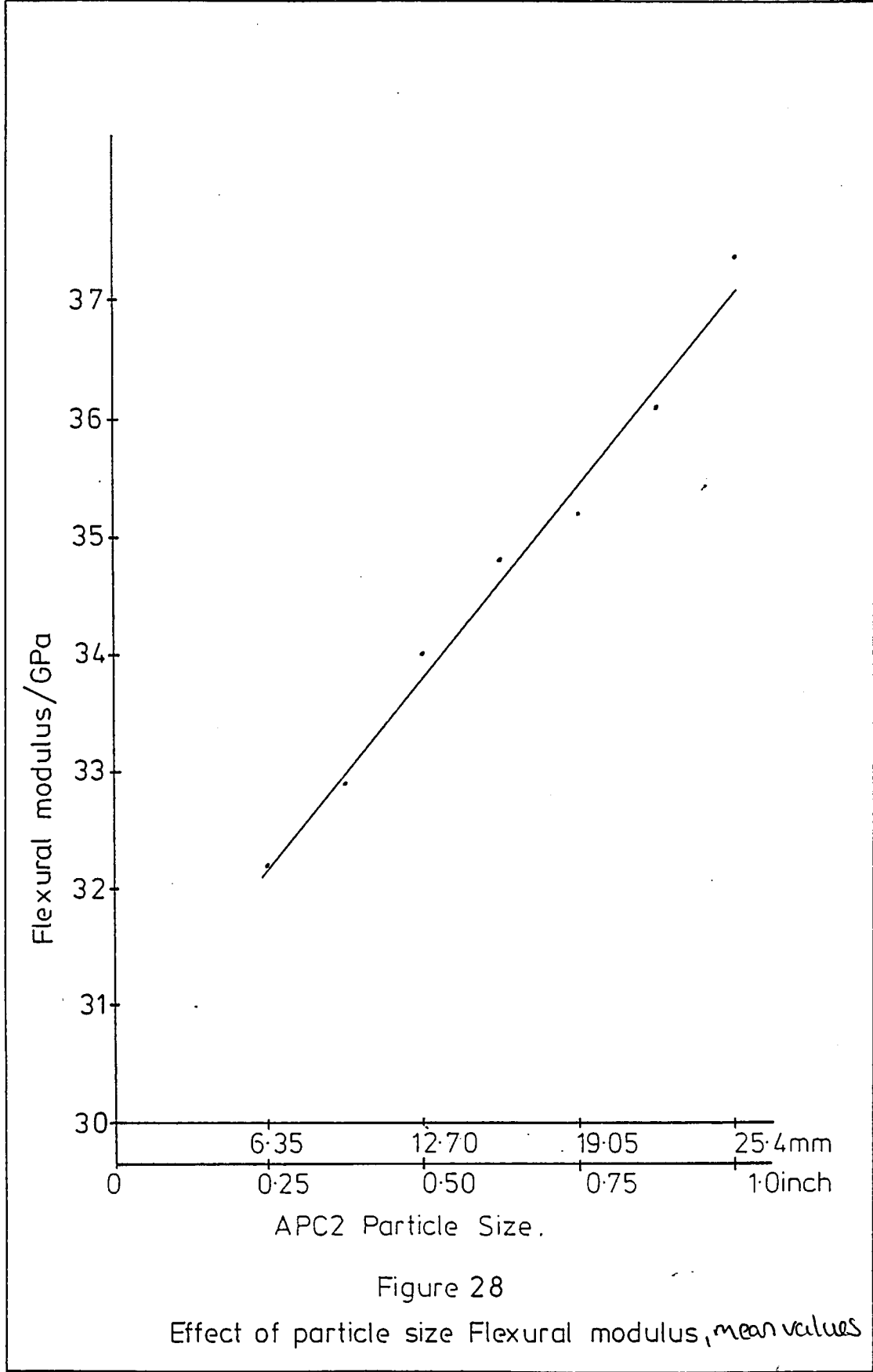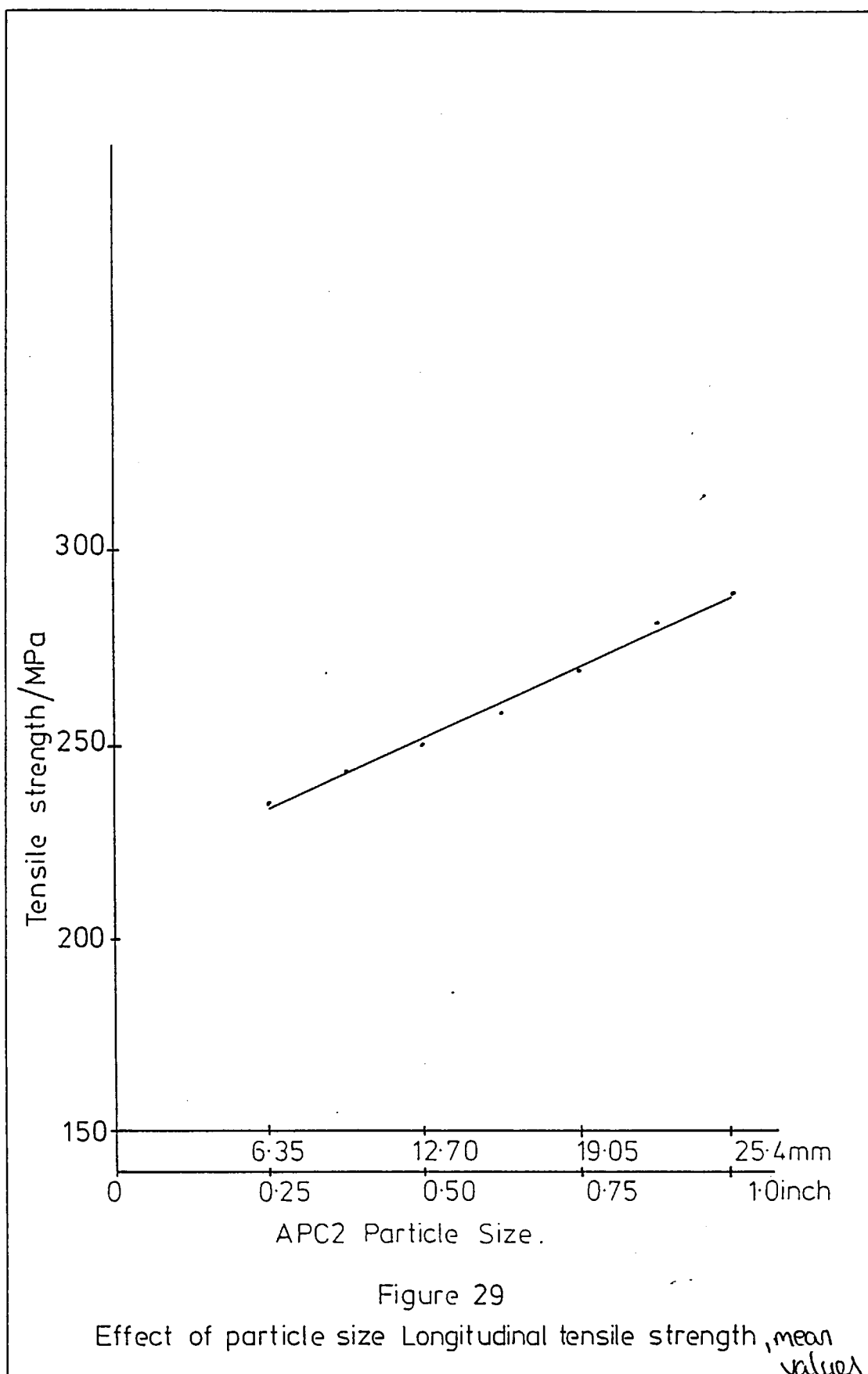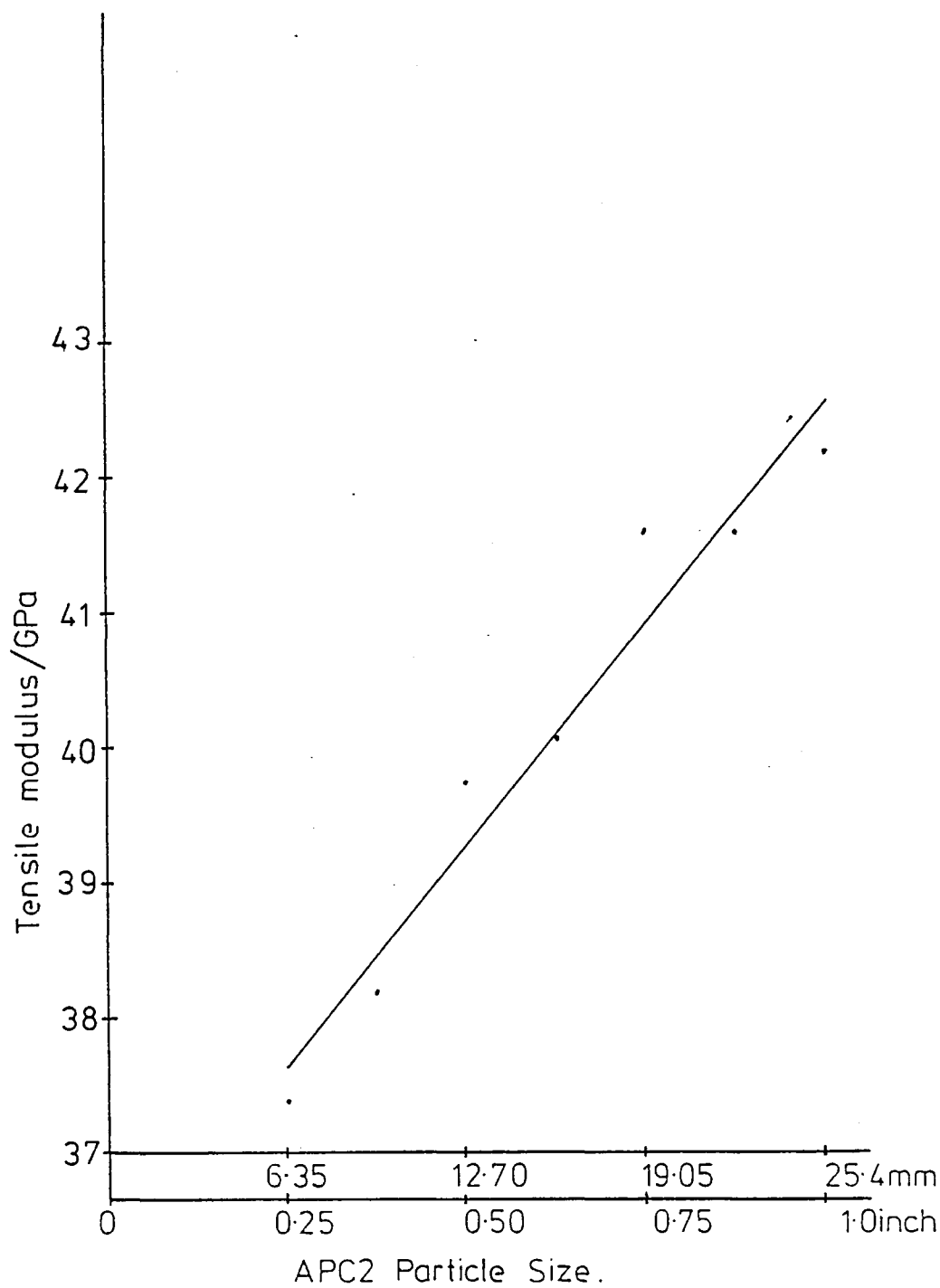
Figure 30

Effect of particle size Longitudinal tensile modulus, mean values
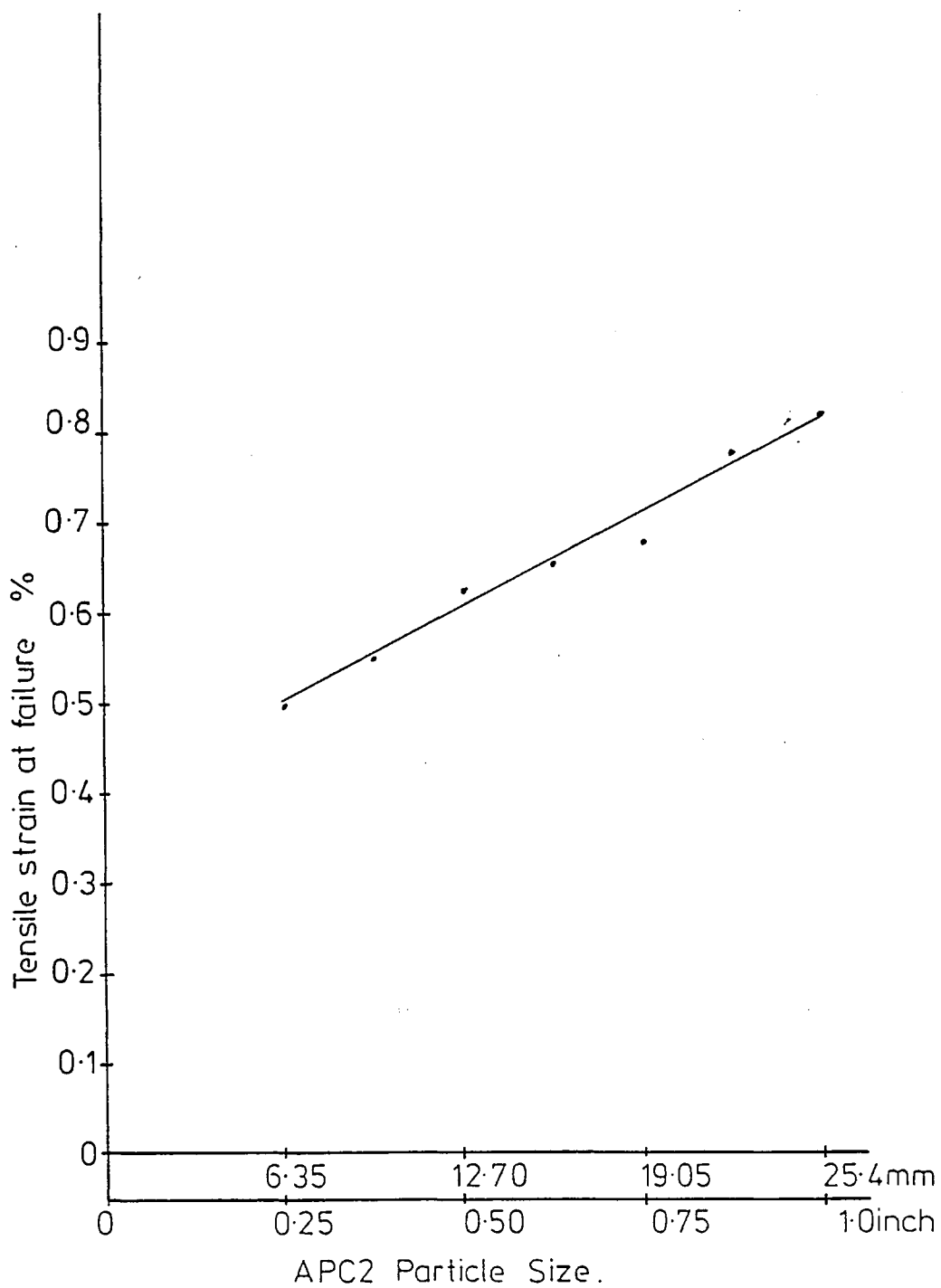
Figure 31

Effect of particle size Tensile strain at failure, mean values
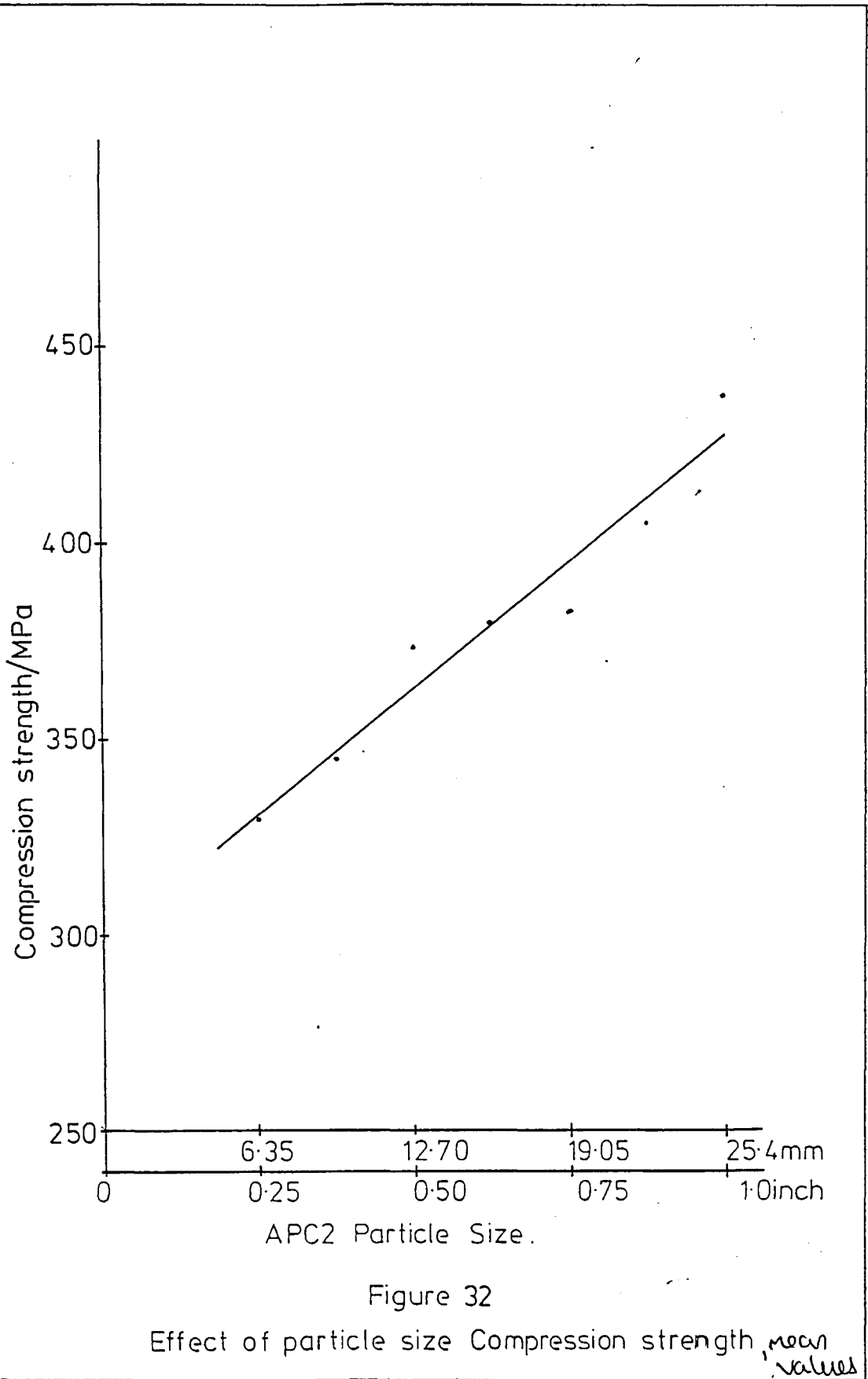
Figure 32

Effect of particle size Compression strength, mean values
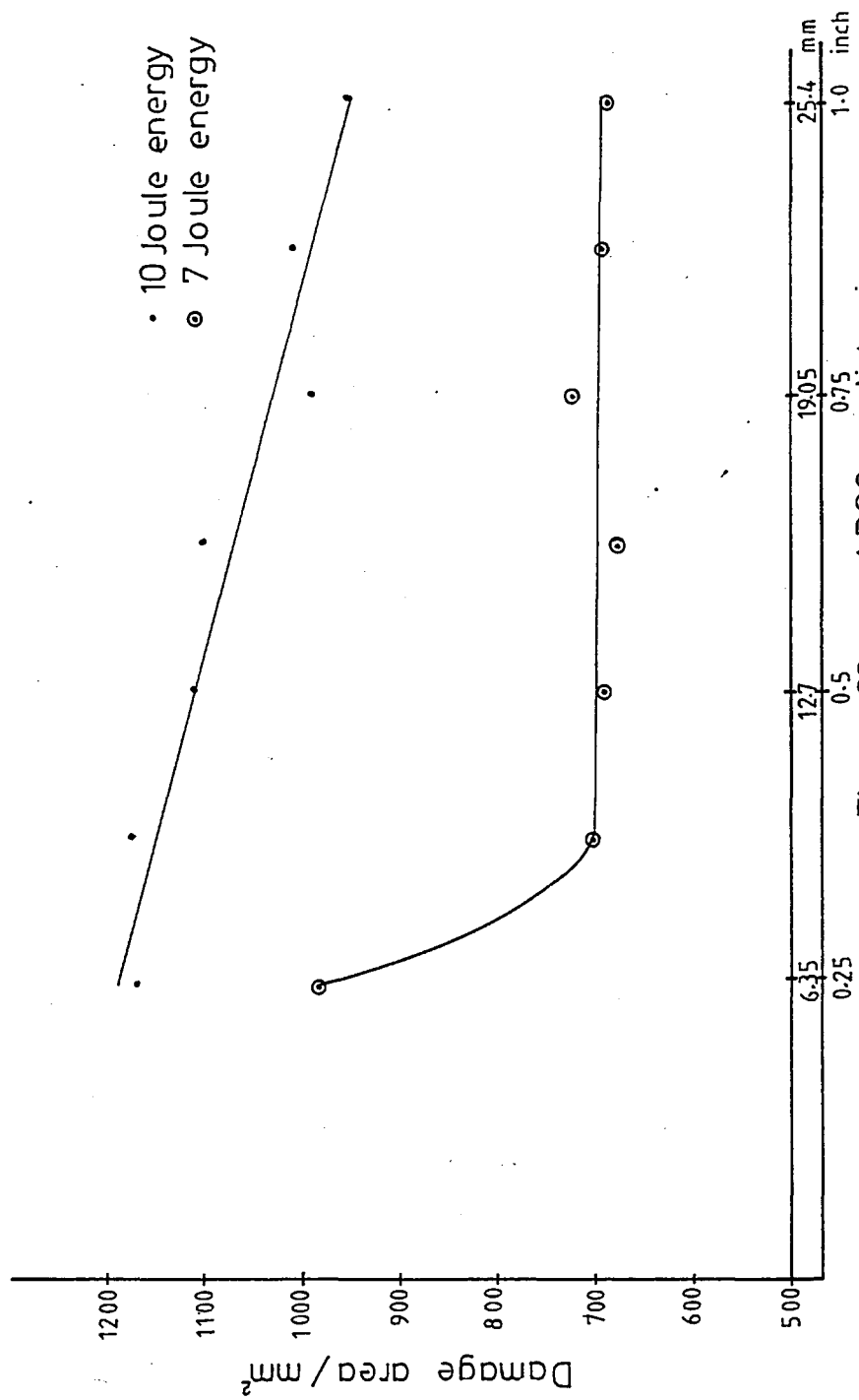
Figure 33   APC2 particle size   Damage area, mean values

Effect of particle size Damage area

Damage area/mm²

- 10 Joule energy
⊙ 7 Joule energy

1200
1100
1000
900
800
700
600
500

6·35 12·7 19·05 25·4 mm
0·25 0·5 0·75 1·0 inch
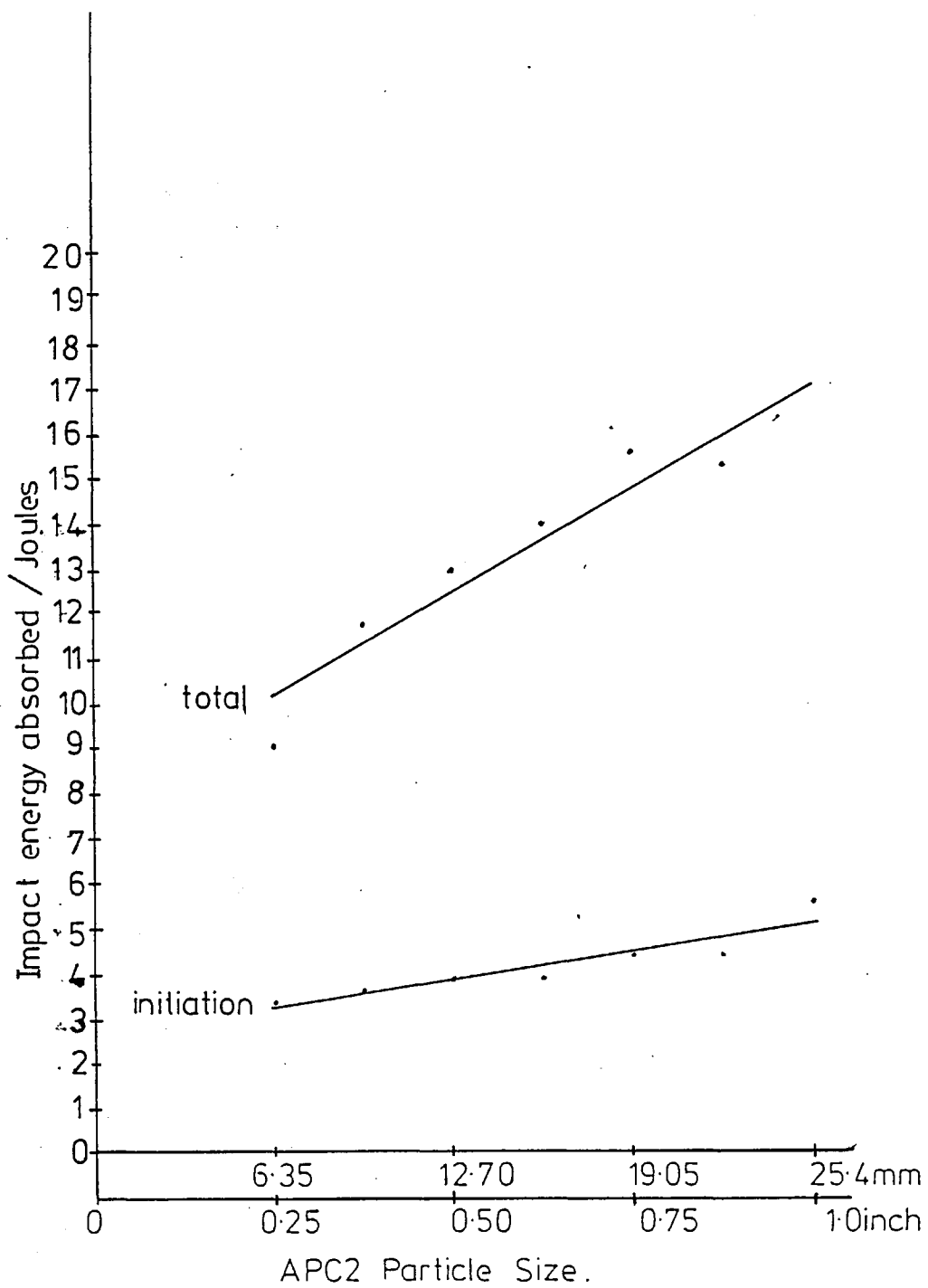
Figure 34

Effect of particle size   Impact toughness, mean values
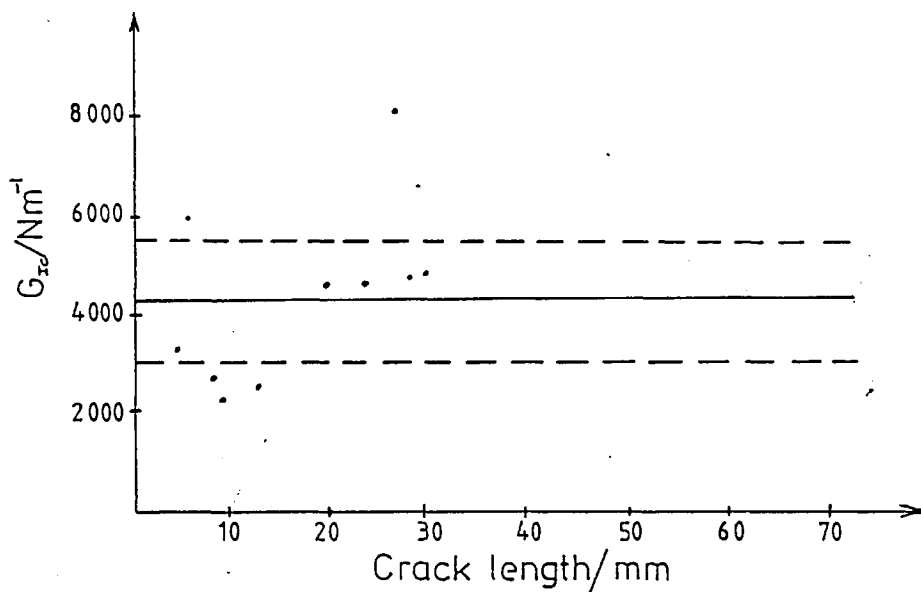
Figure 35

Variation of the strain energy release
rate, G_{Ic} with total crack length
for DC3 with 635mm sq particles.
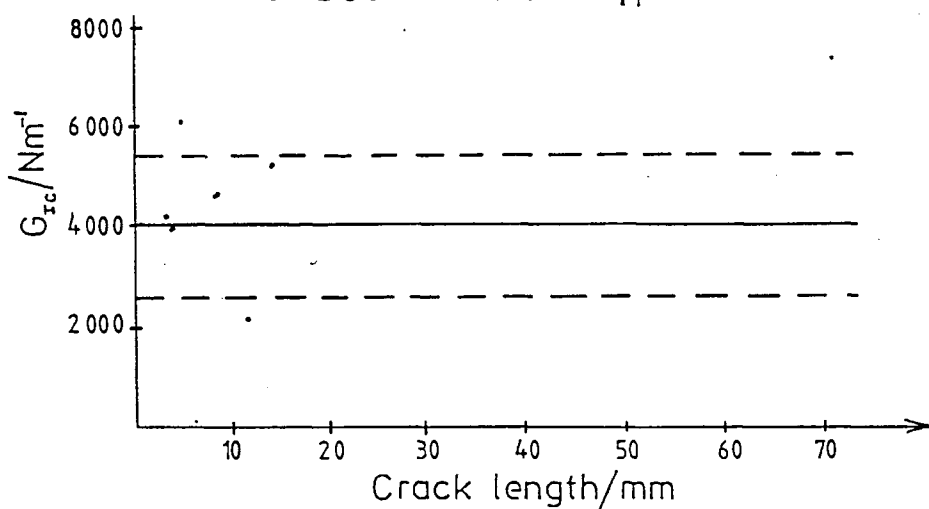
Figure 36

Variation of strain energy release
rate, G_{Ic} with total crack length
for DC3 with 95mm sq particles
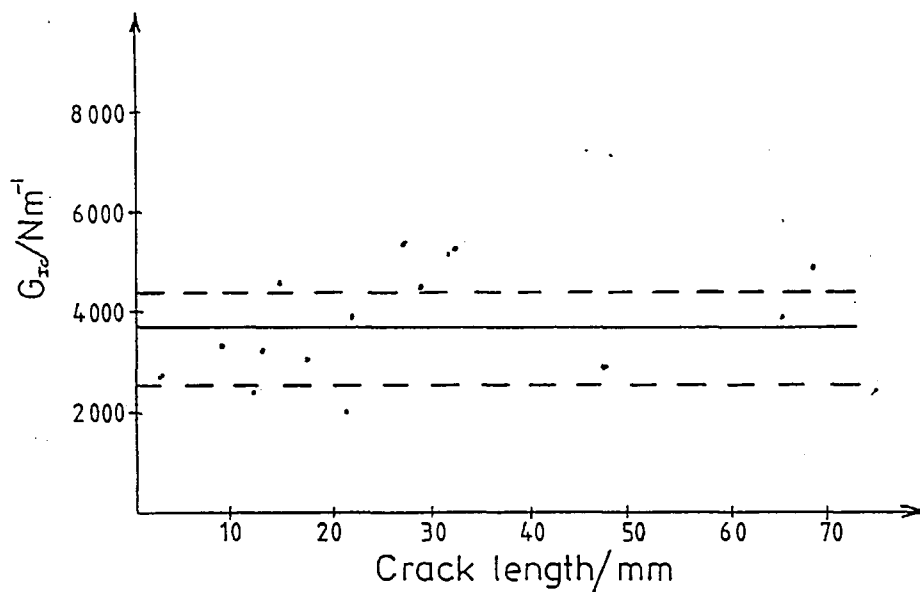
Figure 37

Variation of the strain energy release rate, G_{Ic} with total crack length for DC3 with 12.7mm sq particles.
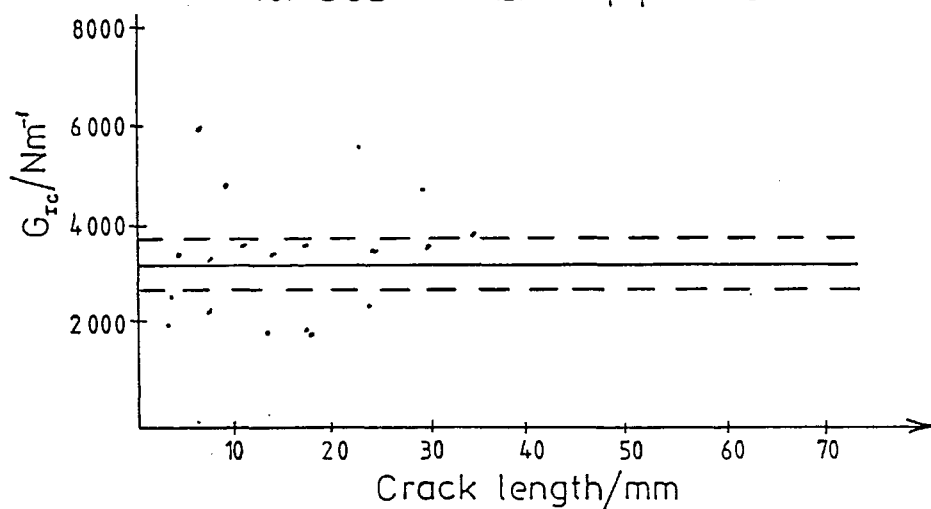
Figure 38

Variation of strain energy release rate, G_{Ic} with total crack length for DC3 with 15.9mm sq particles
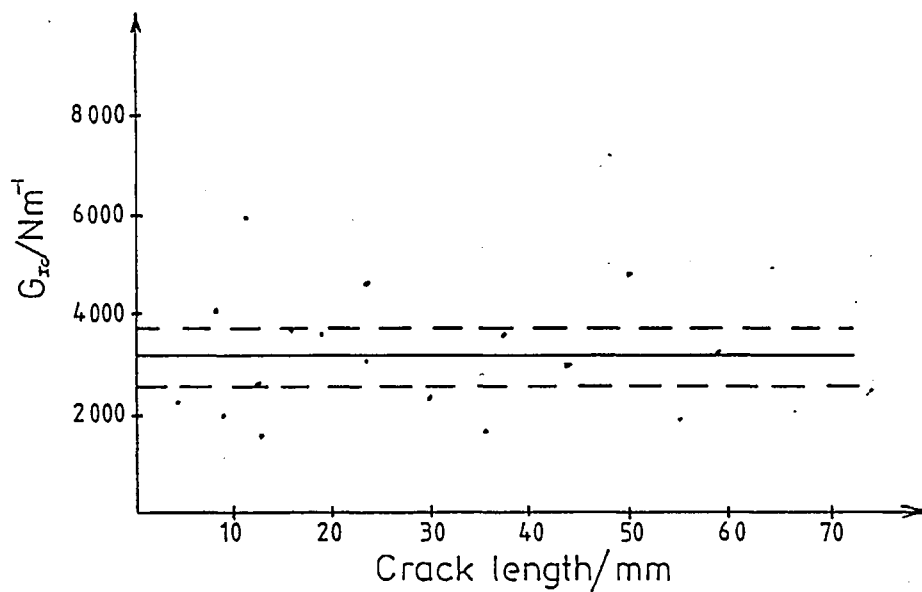
Figure 39

Variation of the strain energy release rate, G_{xc} with total crack length for DC3 with 19·1mm sq particles.
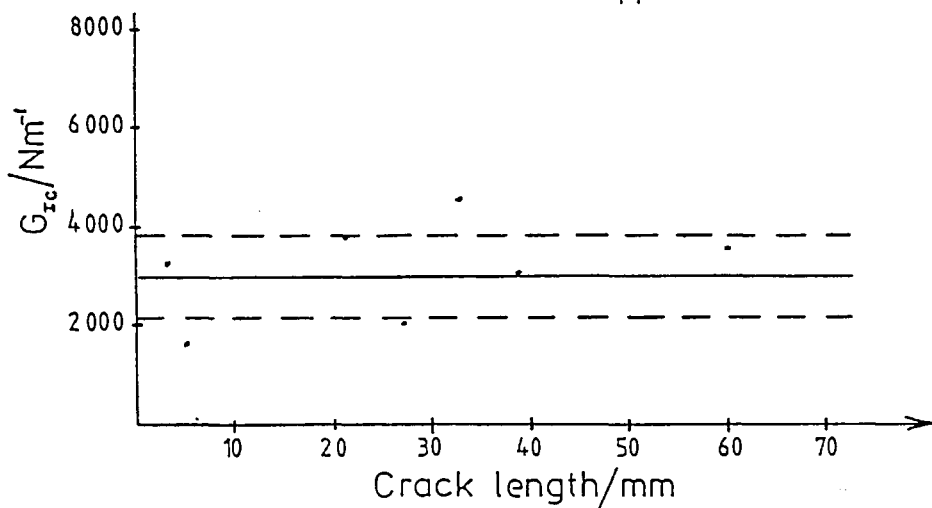
Figure 40

Variation of strain energy release rate, G_{xc} with total crack length for DC3 with 22·2mm sq particles
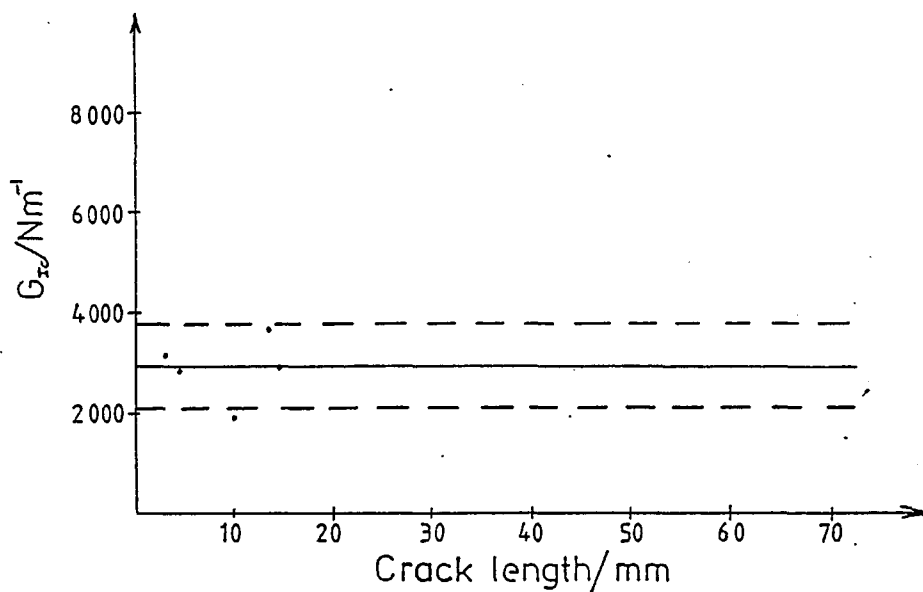
Figure 41

Variation of the strain energy release
rate, G_{Ic} with total crack length
for DC3 with 254mm sq particles
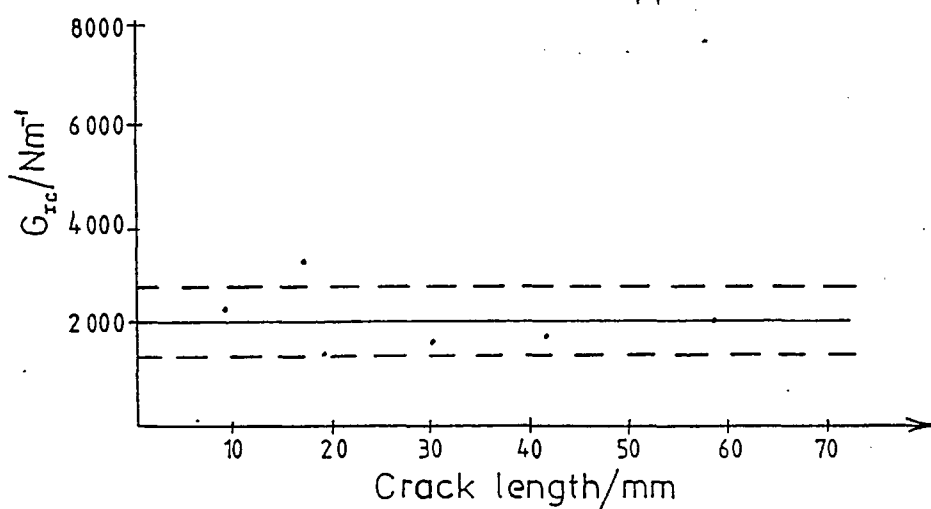
Figure 42

Variation of strain energy release
rate, G_{Ic} with total crack length
for DC3 with continuous fibres

Figure 43
Effect of particle size
Strain energy release rate, G_{Ic}
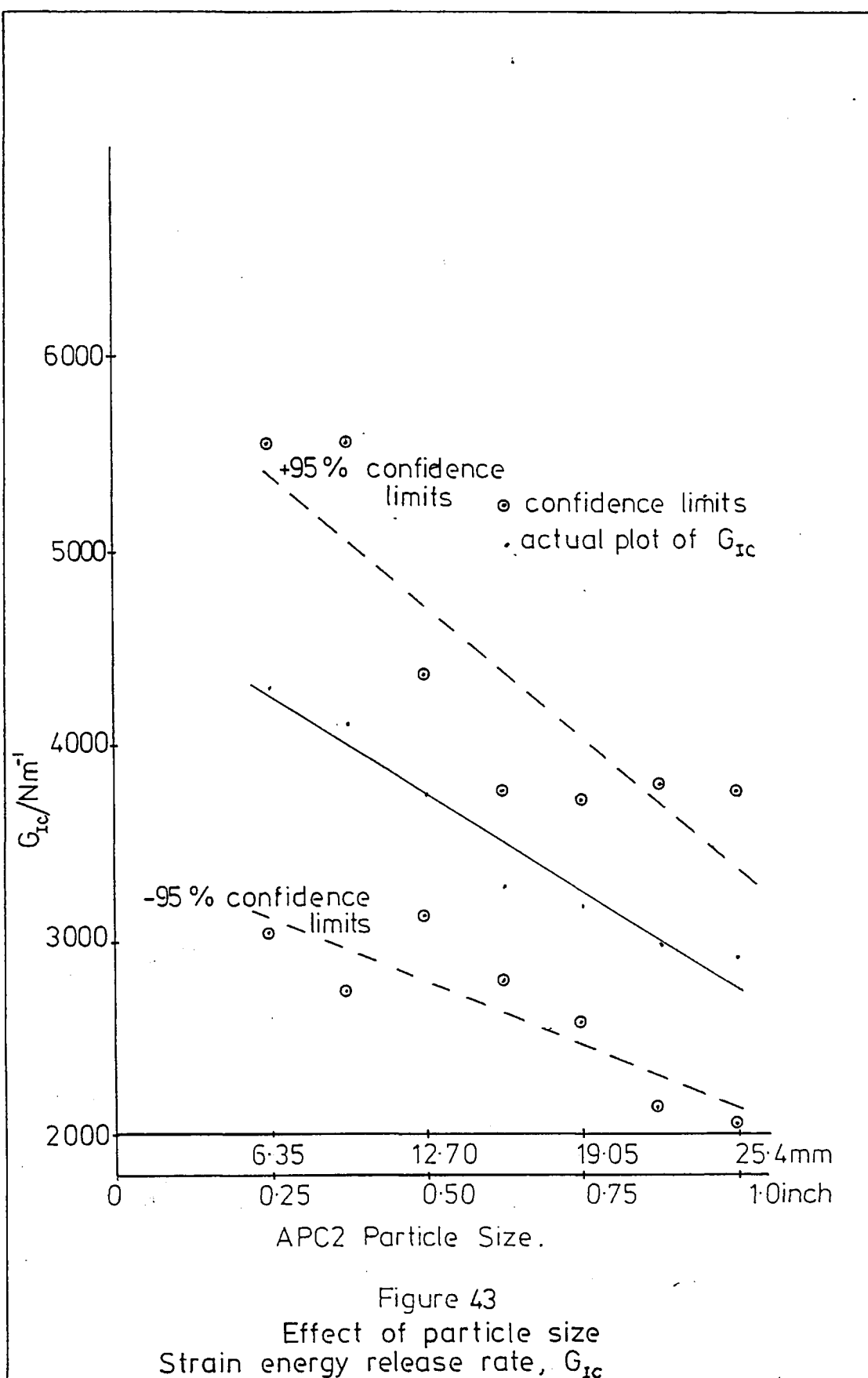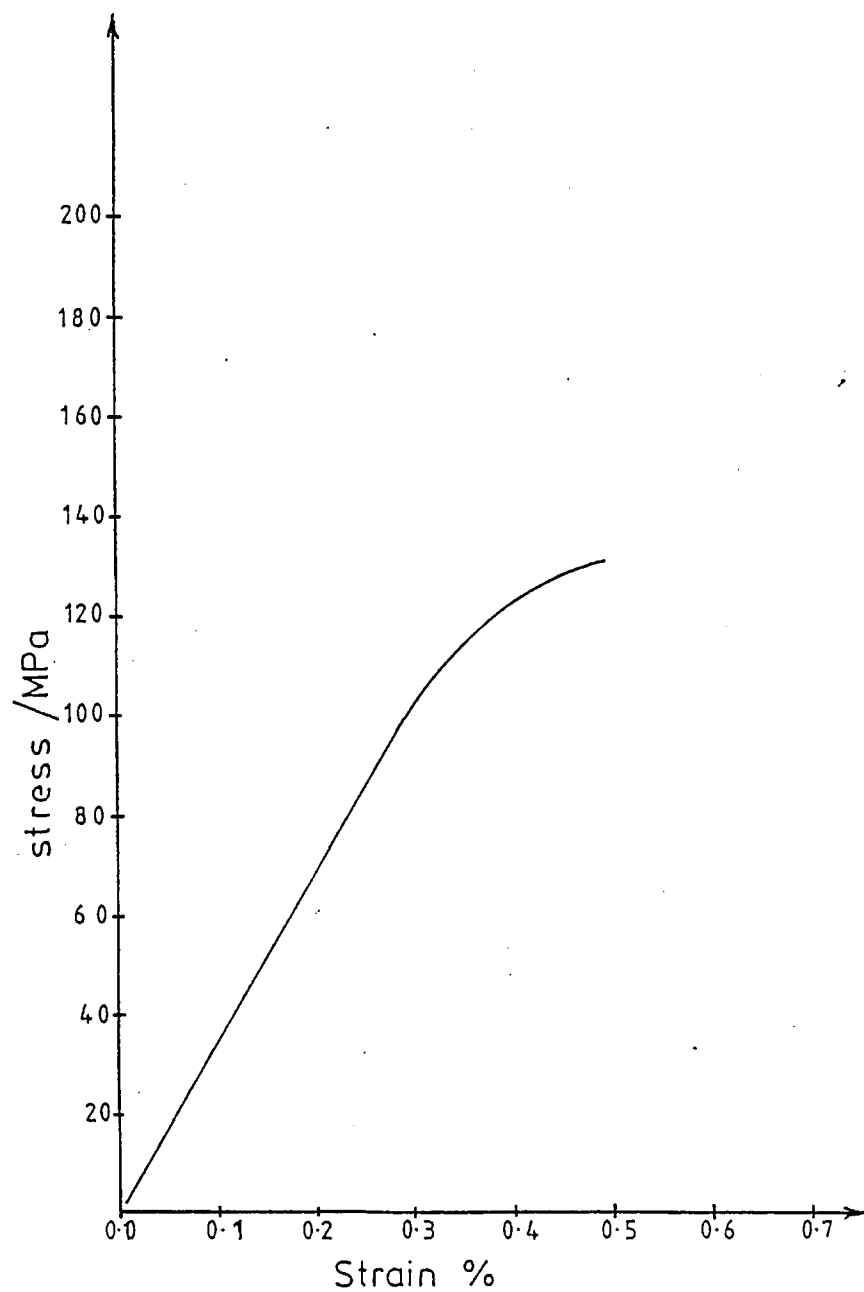
Figure 44

100 second   Isochronous data for APC2
mo u ded from 0.25 inch square
particles.

Figure 45

100 second Isochronous data for APC2 -
moulded from 0375 inch square
particles.
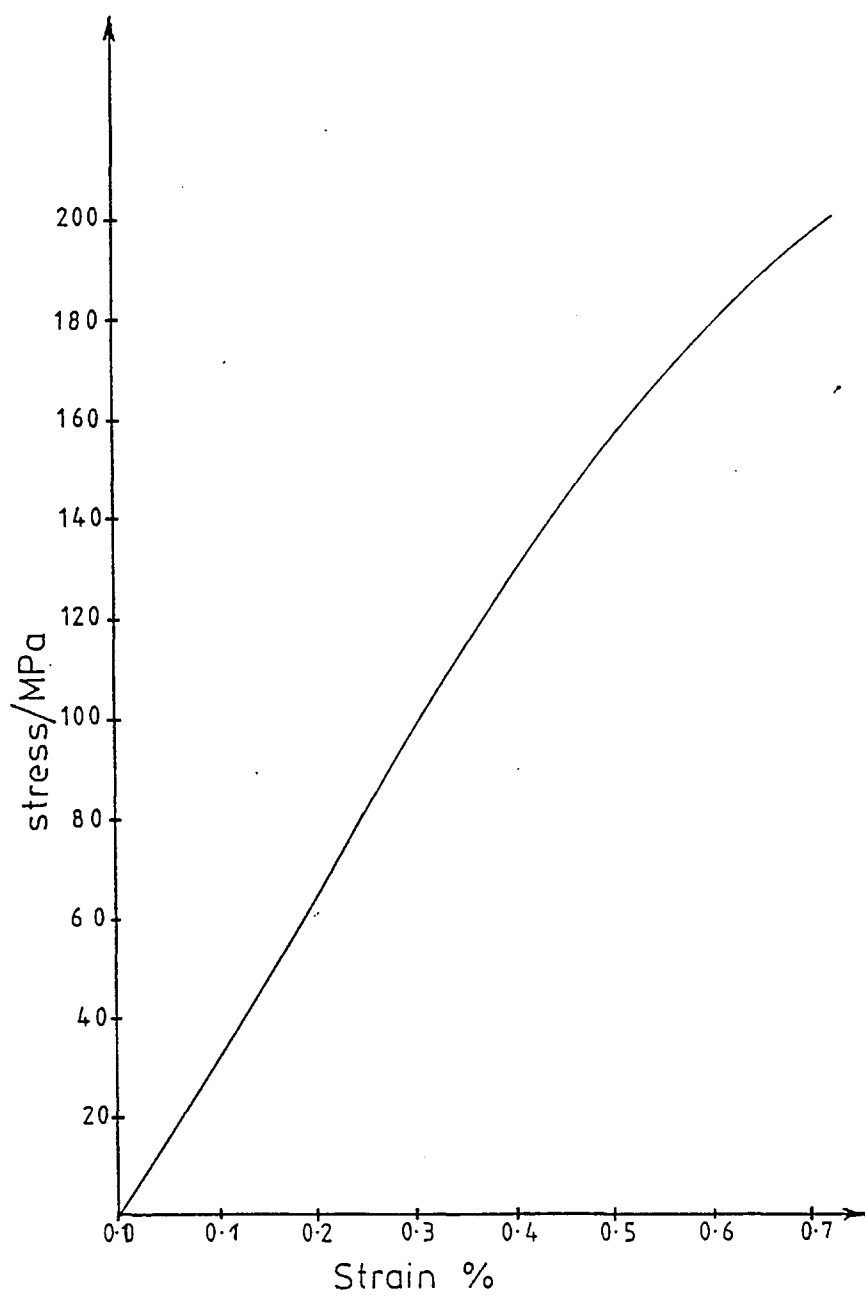
Figure 46

100 second Isochronous data for APC2 moulded from 0.50 inch square particles.
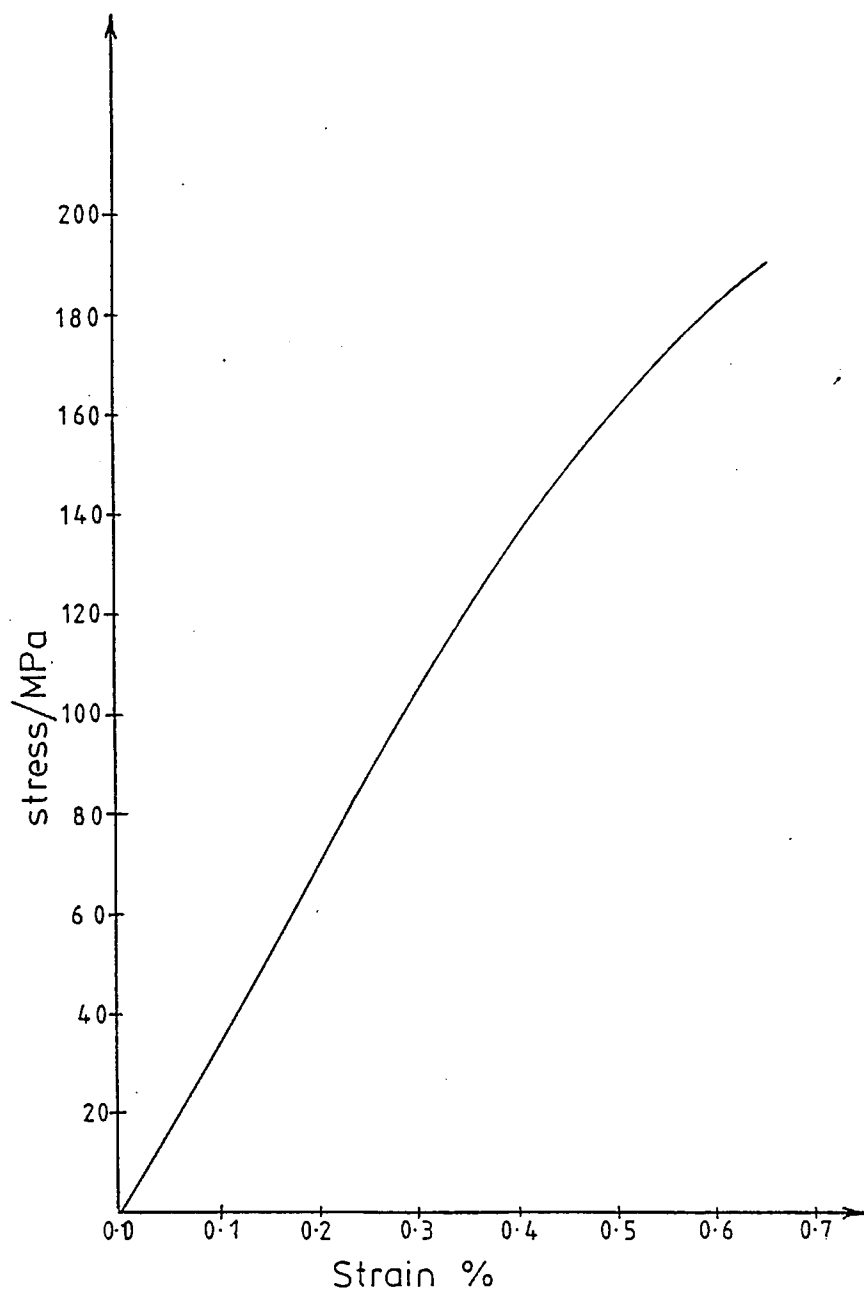
Figure 47

100 second   Isochronous data for APC2
mouded from 0·625 inch square
particles.

Figure 48

100 second Isochronous data for APC2 moulded from 0.75 inch square particles.
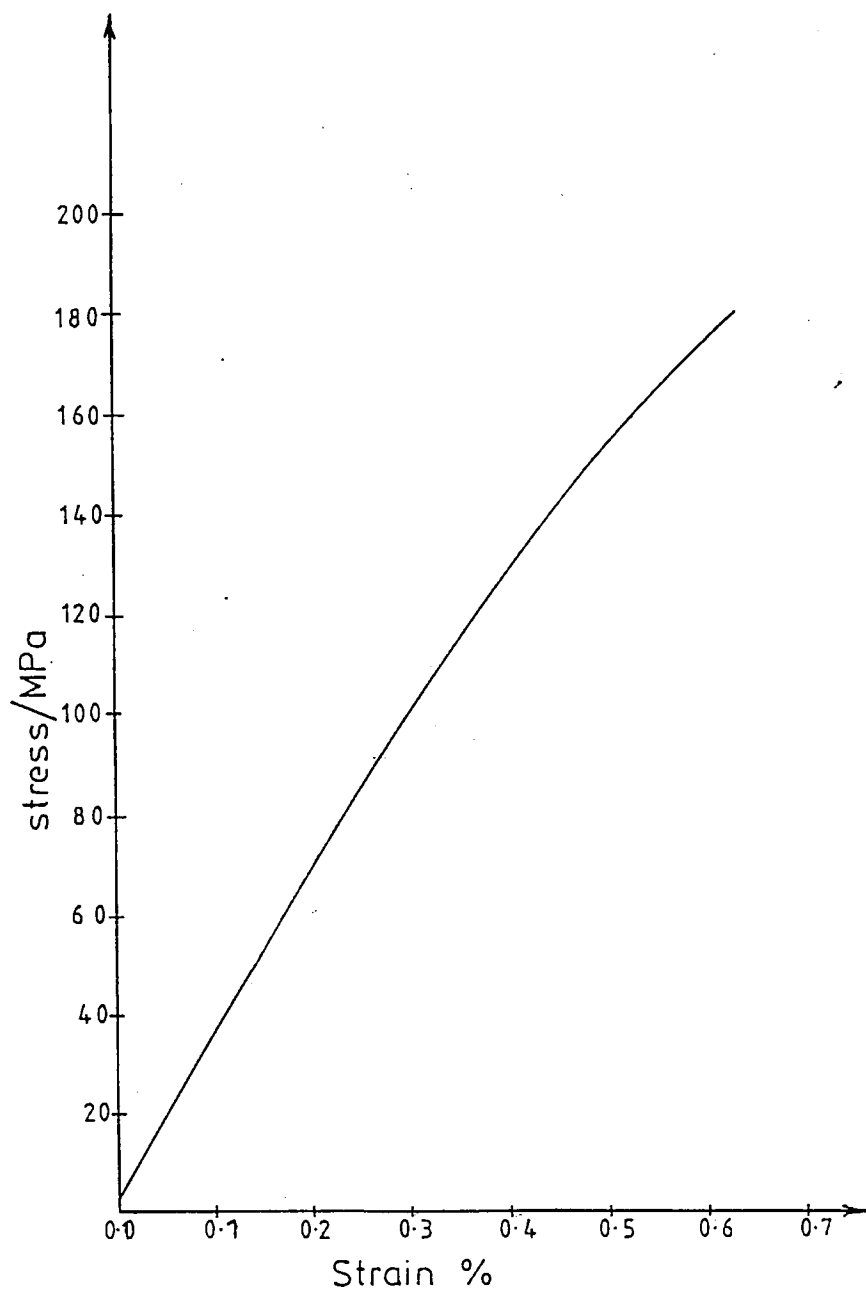
Figure 49

100 second Isochronous data for APC2
moulded from 0·875 inch square
particles.

-203-
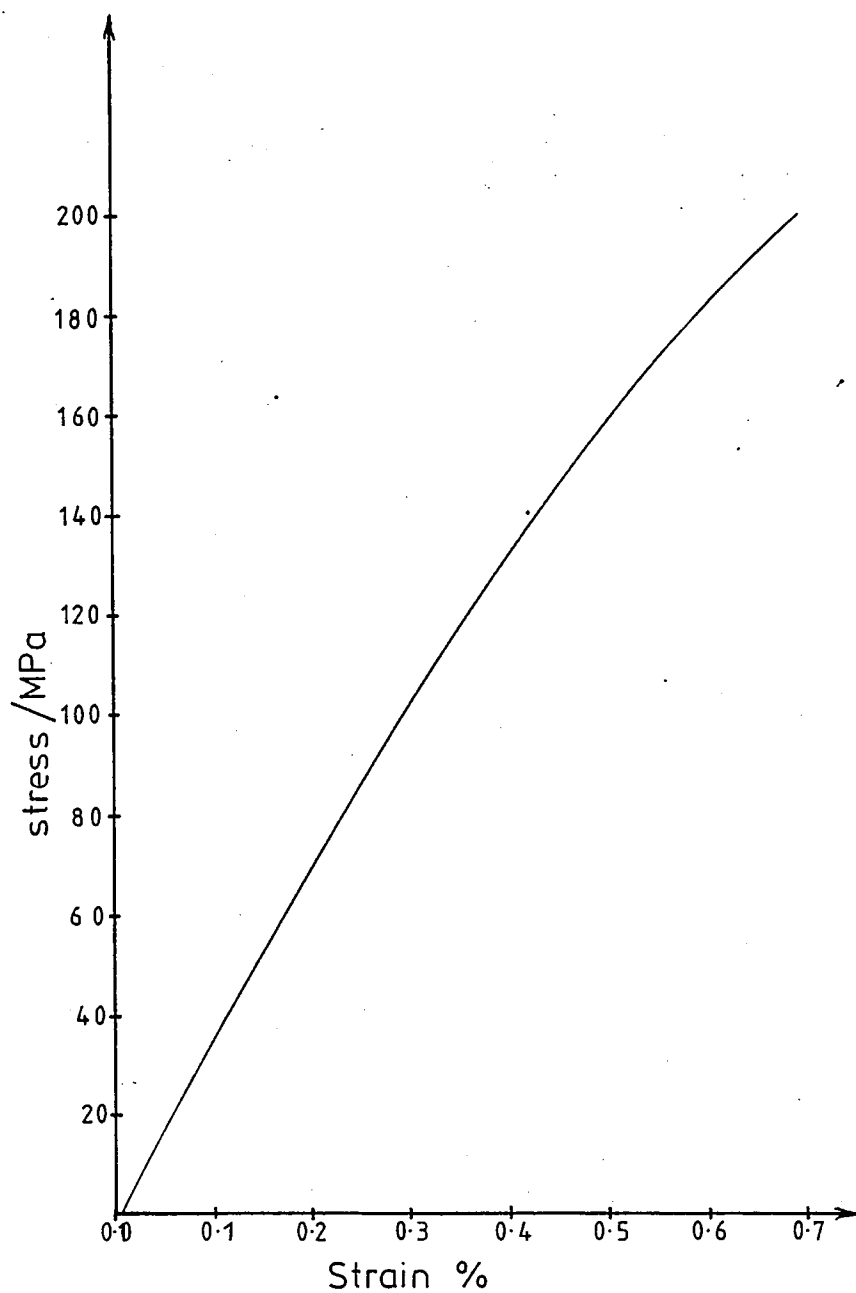
Figure 50

100 second Isochronous data for APC2
moulded from 1·0 inch square
particles.
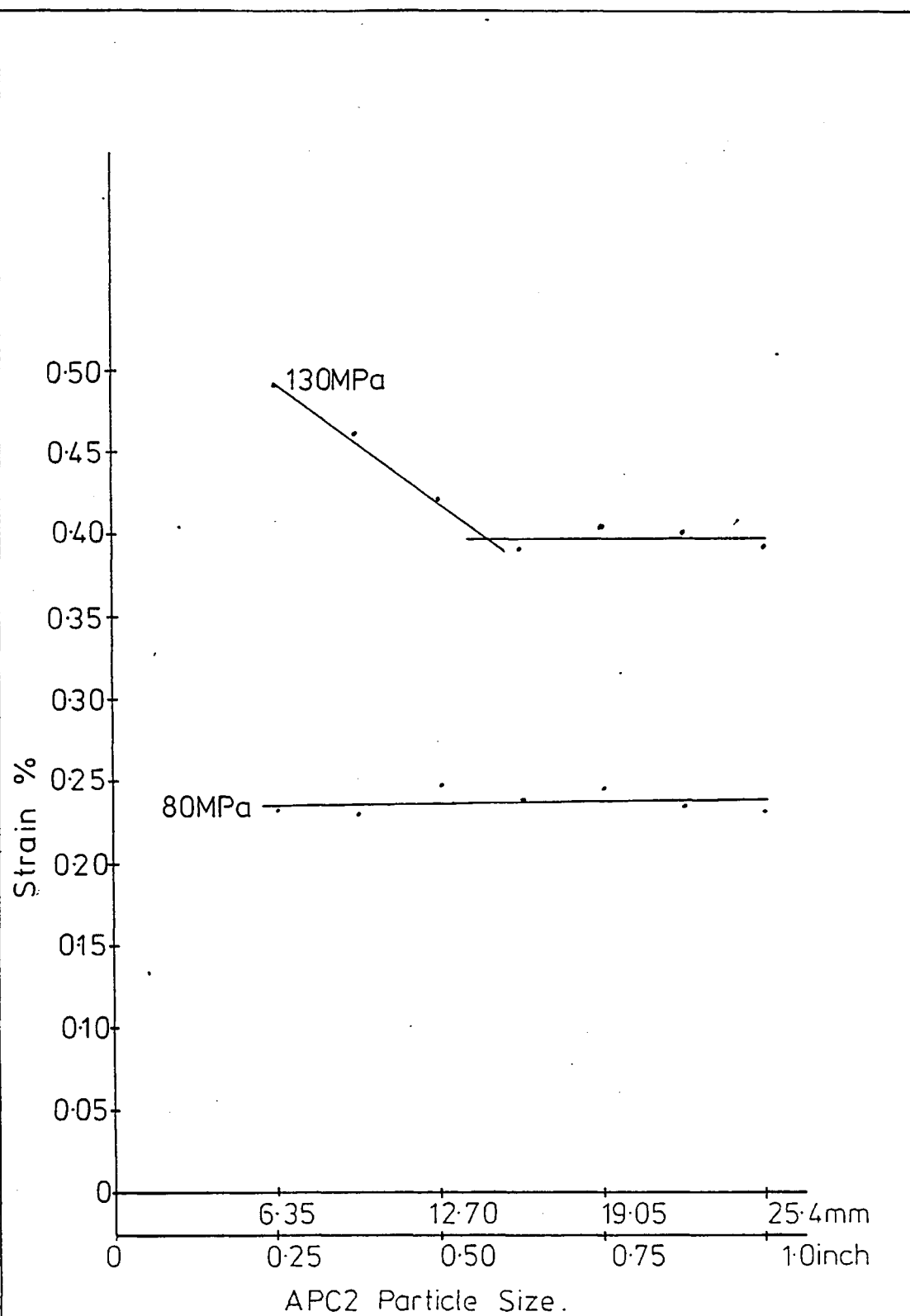
Figure 51
Effect of particle size
Isochronous creep strain at applied stress level stated, 100s
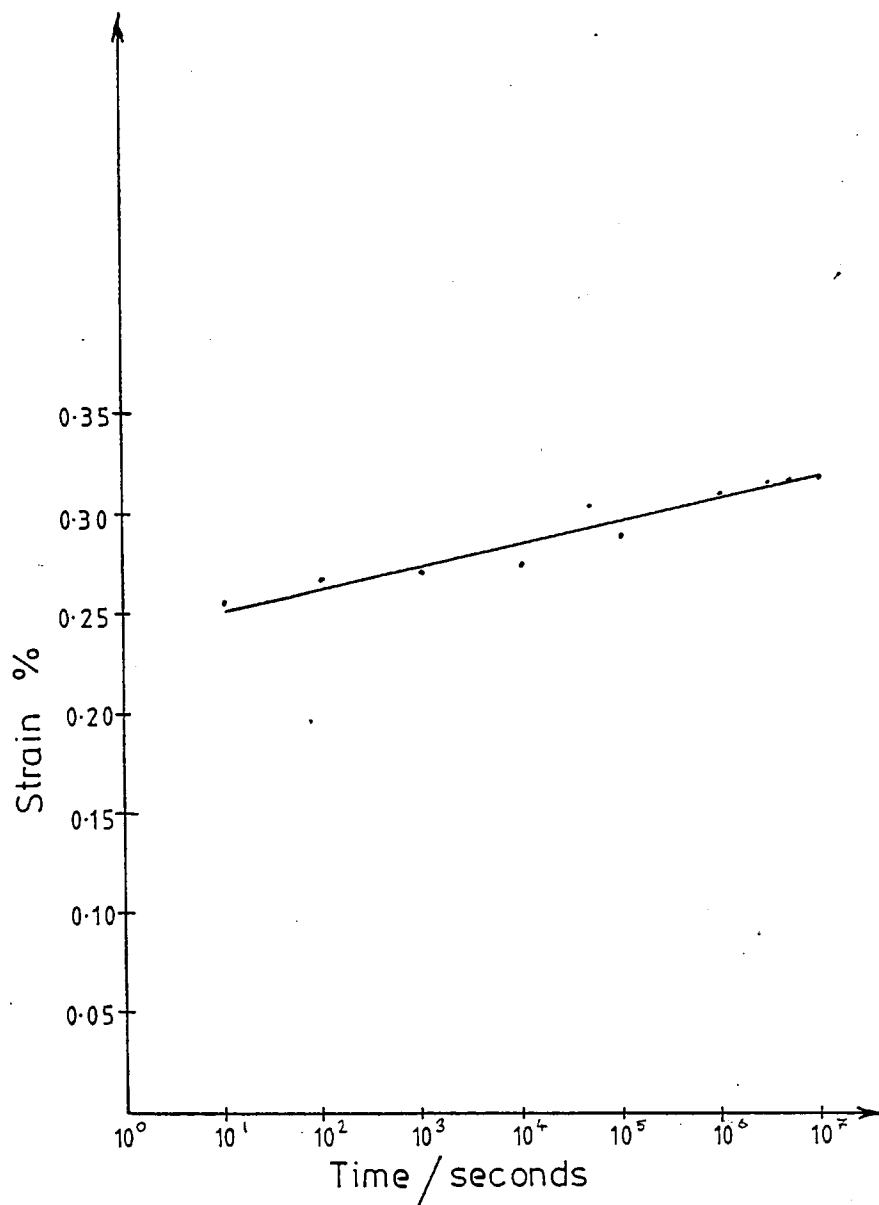
Figure 52
Strain-log(time) creep
curve for APC 2 moulded from
0·25 inch square particles.
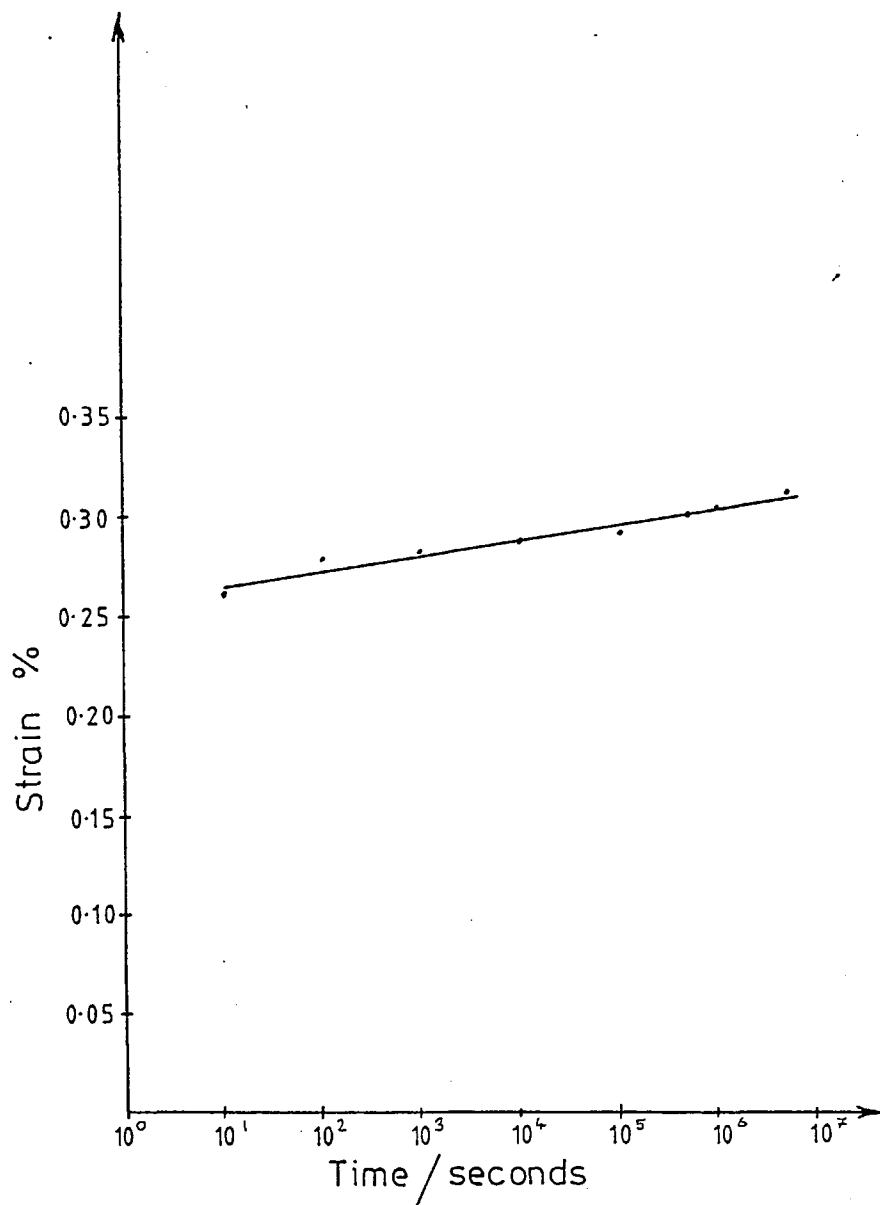
Figure 53
Strain-log(time) creep
curve for APC 2 moulded from
0·375 inch square particles.
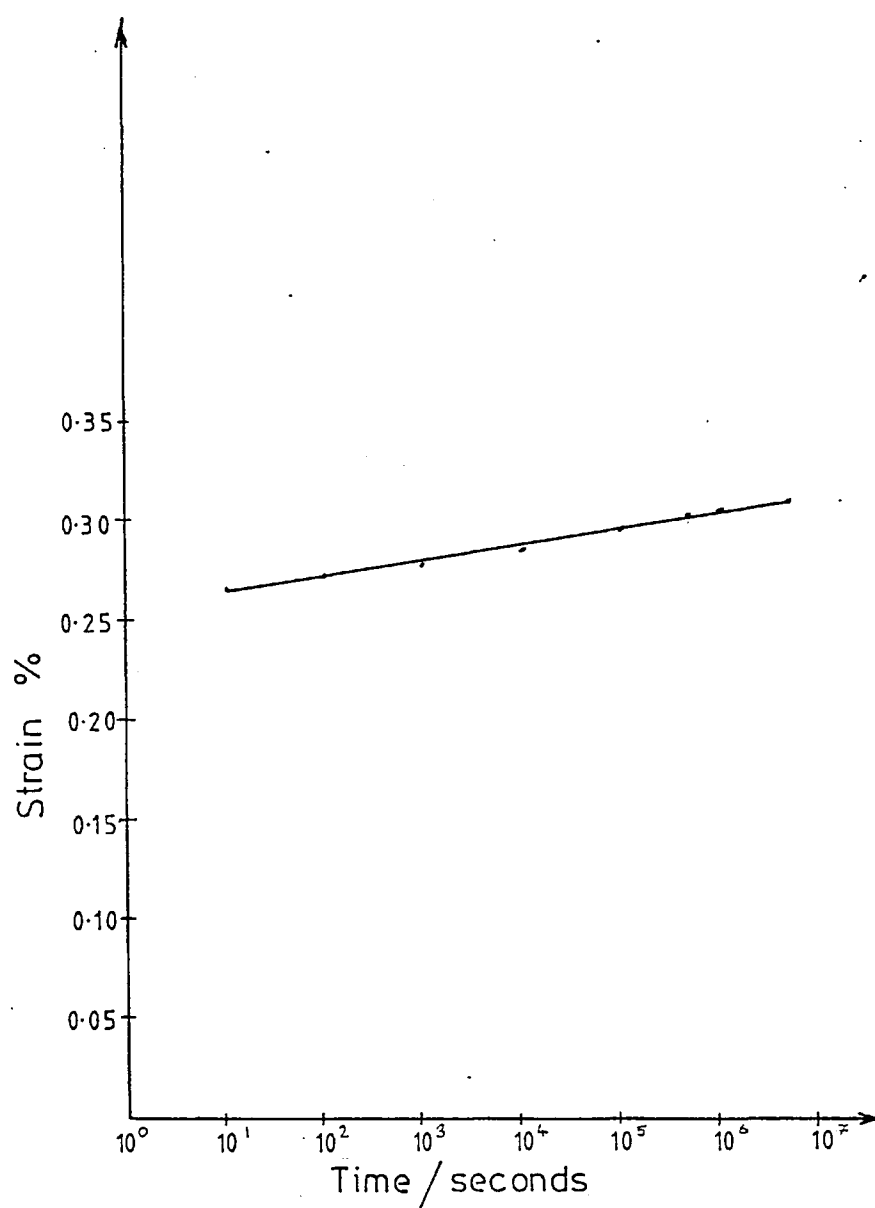
Figure 54
Strain-log(time) creep
curve for APC 2 moulded from
0·50 inch square particles.
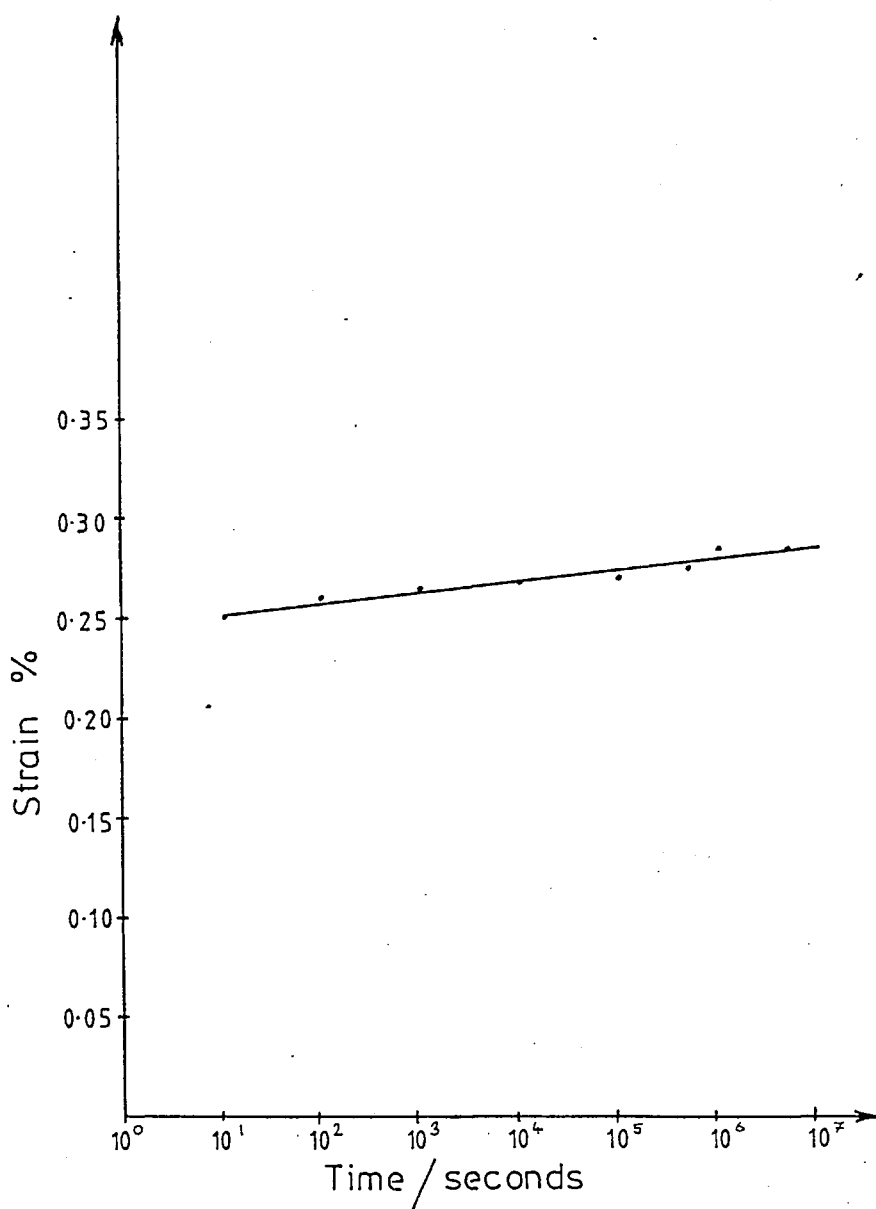
Figure 55
Strain-log(time) creep
curve for APC 2 moulded from
0·625 inch square particles.
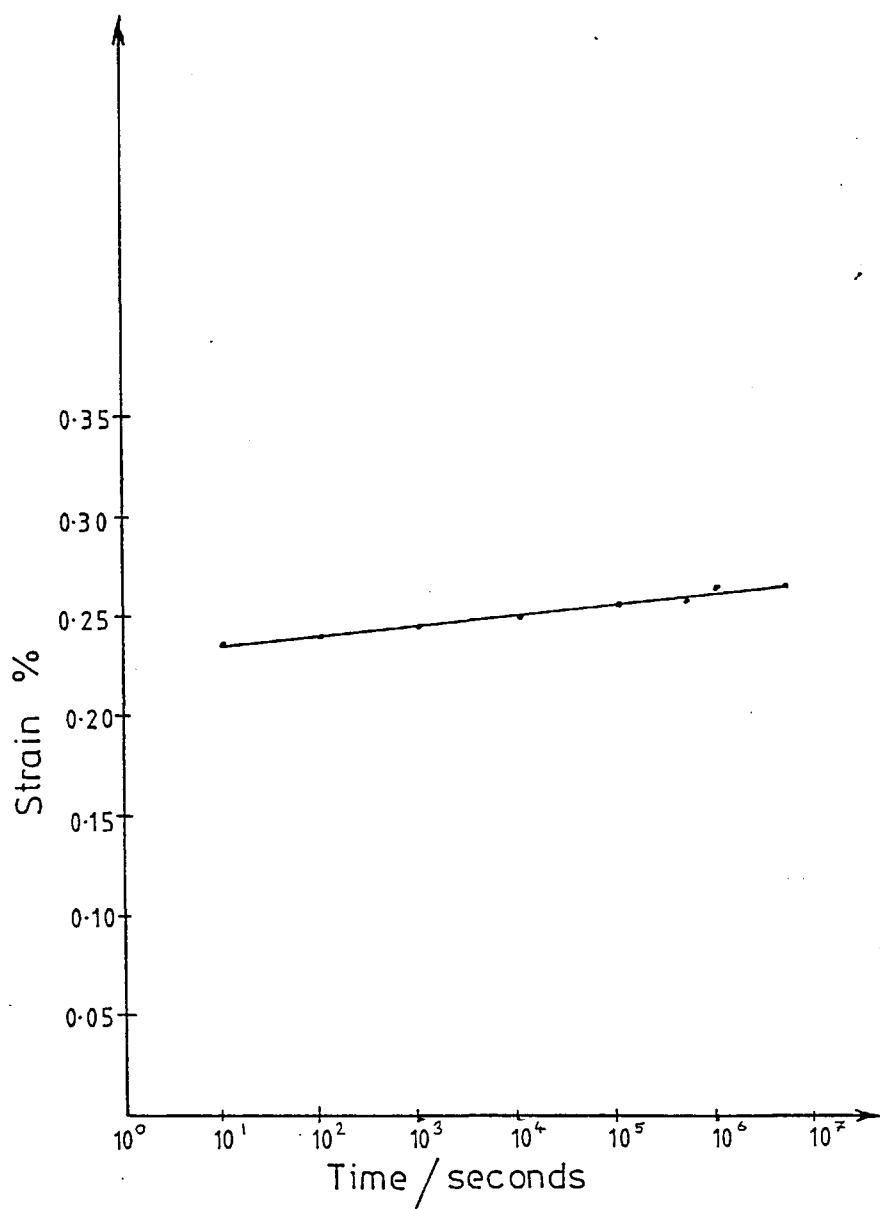
Figure 56
Strain-log(time) creep
curve for APC 2 moulded from
0.75 inch square particles.
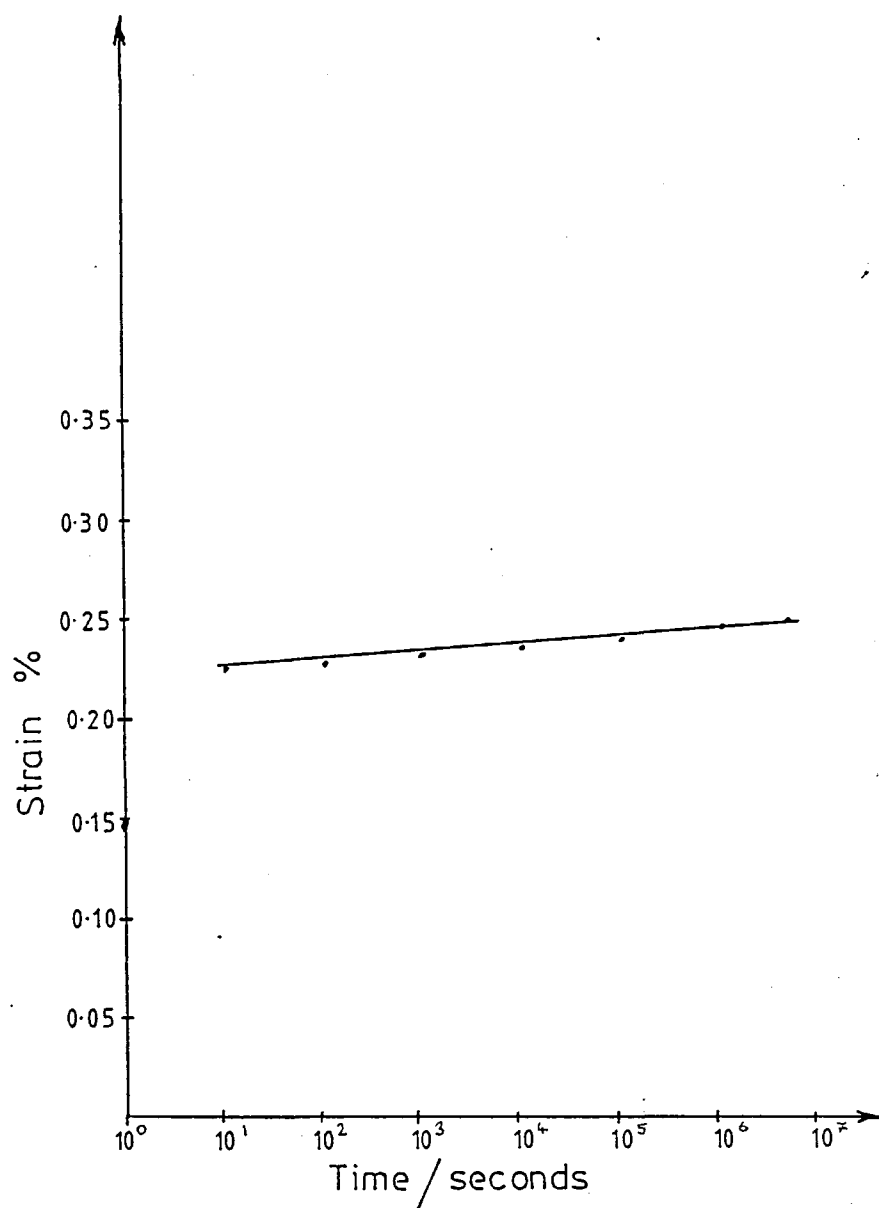
Figure 57
Strain-log(time) creep
curve for APC 2 moulded from
0·8 75 inch square particles.
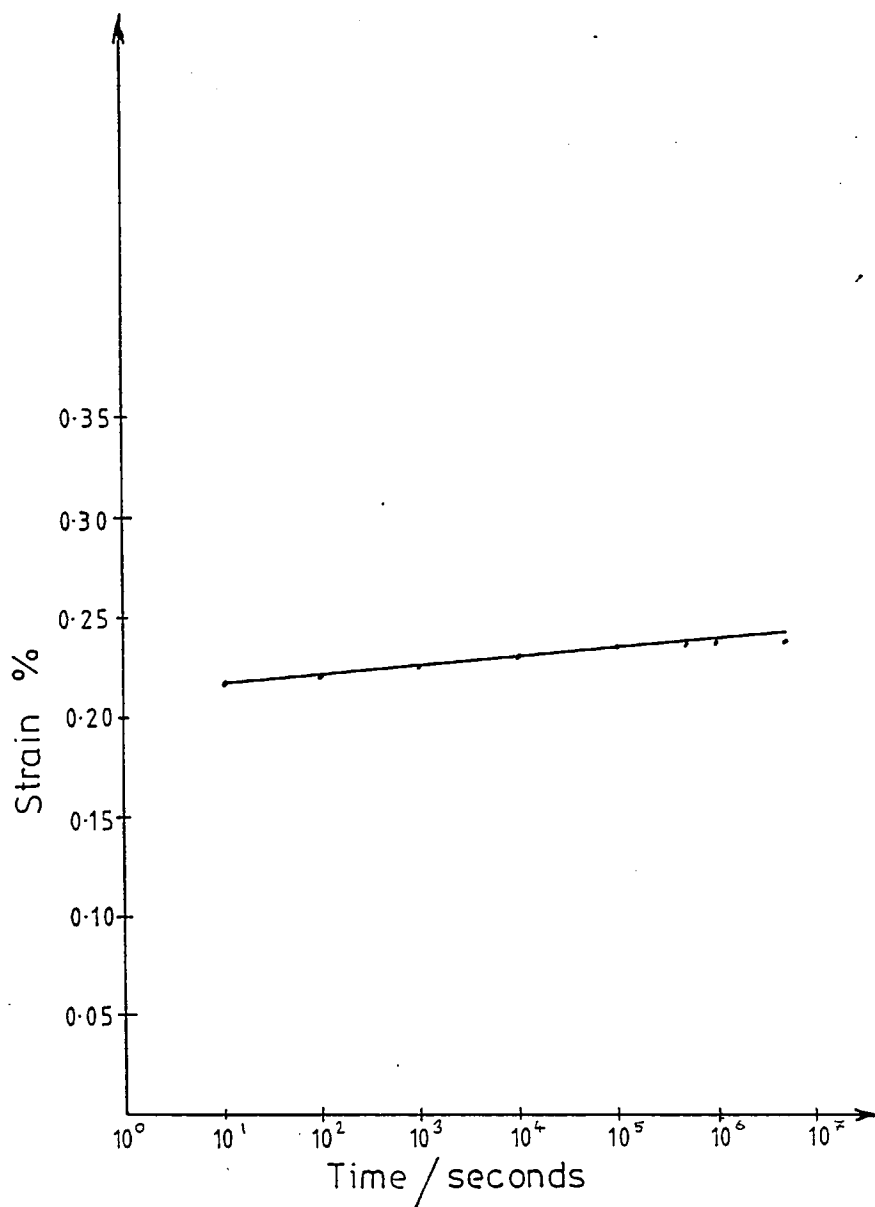
Figure 58
Strain-log(time) creep
curve for APC 2 moulded from
1·0 inch square particles.

Figure 59
A moulding with a large radius of curvature
containing 0·125mm square particles, without
tearing or wrinkling.

Figure 60
A moulding with a large radius of curvature
containing Mono Munched particles, without
tearing but slight wrinkling.

Figure 61
A moulding with a large radius of curvature
containing 25·4mm square particles, without
tearing but a large degree of wrinkling.
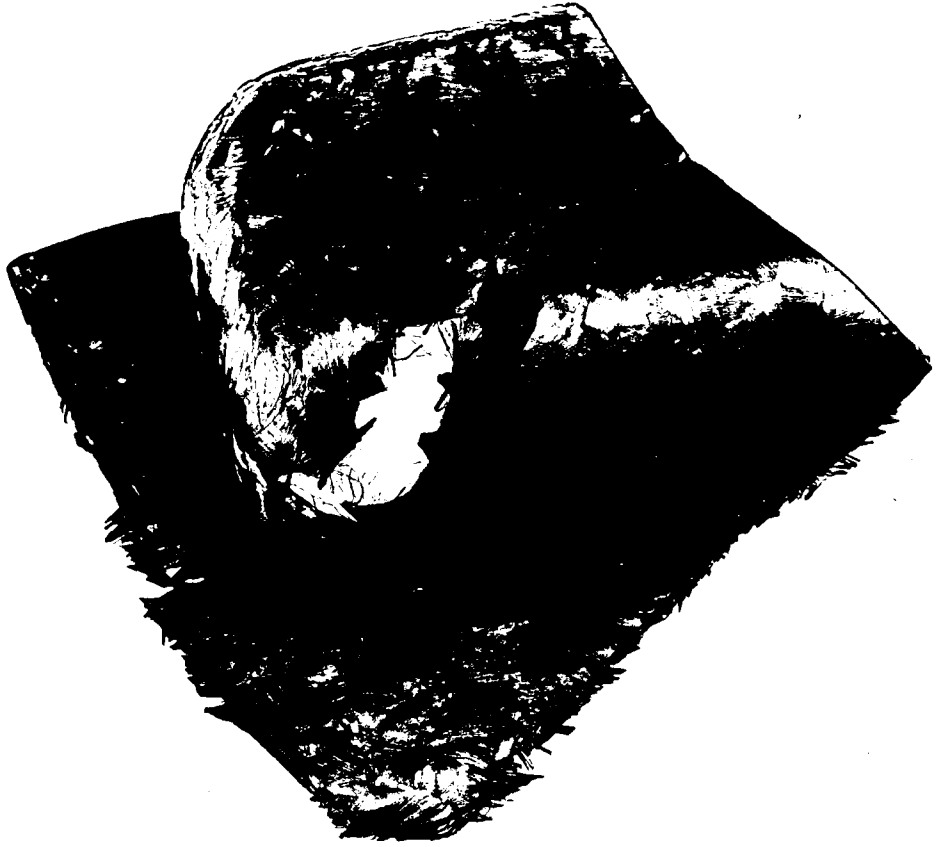
Figure 62
A moulding with a small radius of curvature
containing 6·35mm square particles, with
pronounced tearing and slight wrinkling.
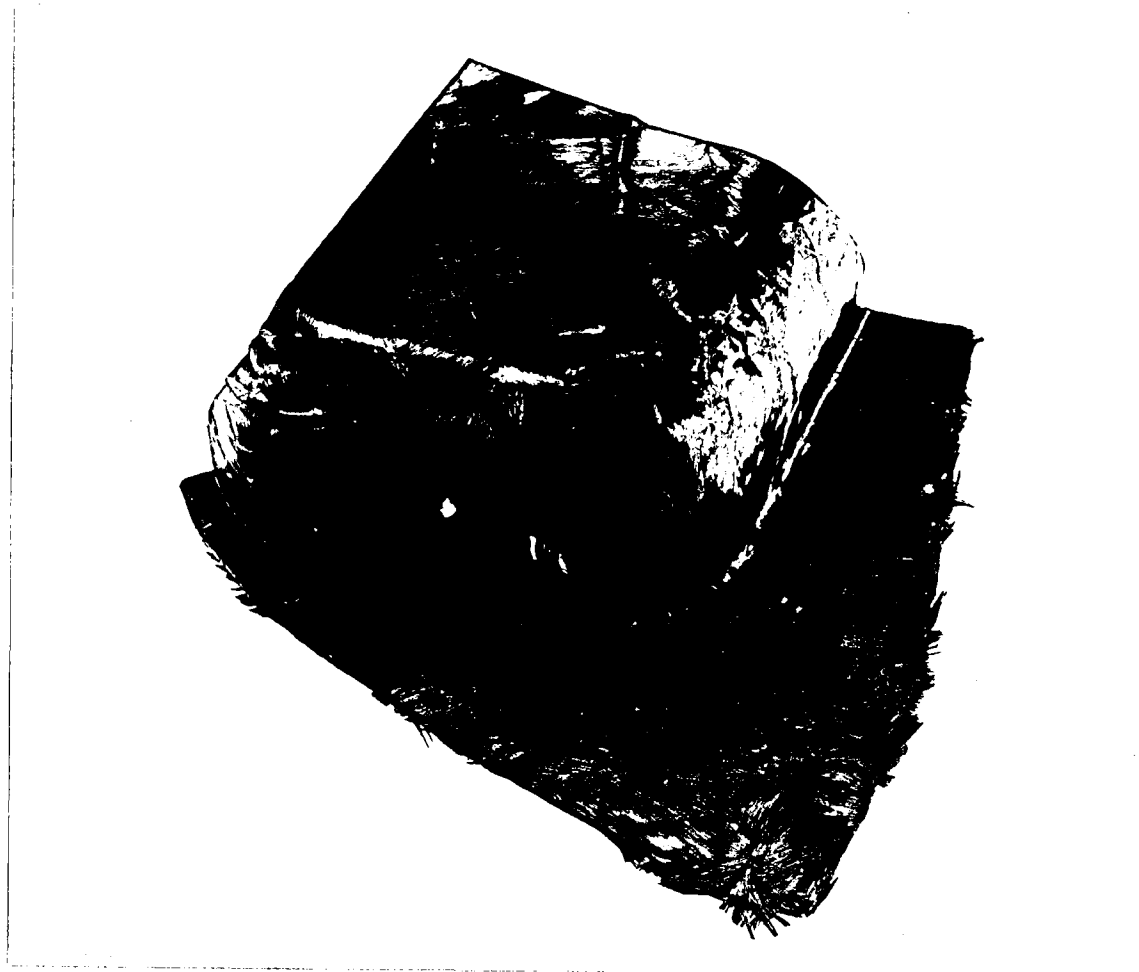
Figure 63
A moulding with a small radius of curvature
containing 12·7mm square particles, with
slight tearing and wrinkling.

Figure 64

Effect of PEEK content 12.7mm sq
APC-2 particles -Flexural strength
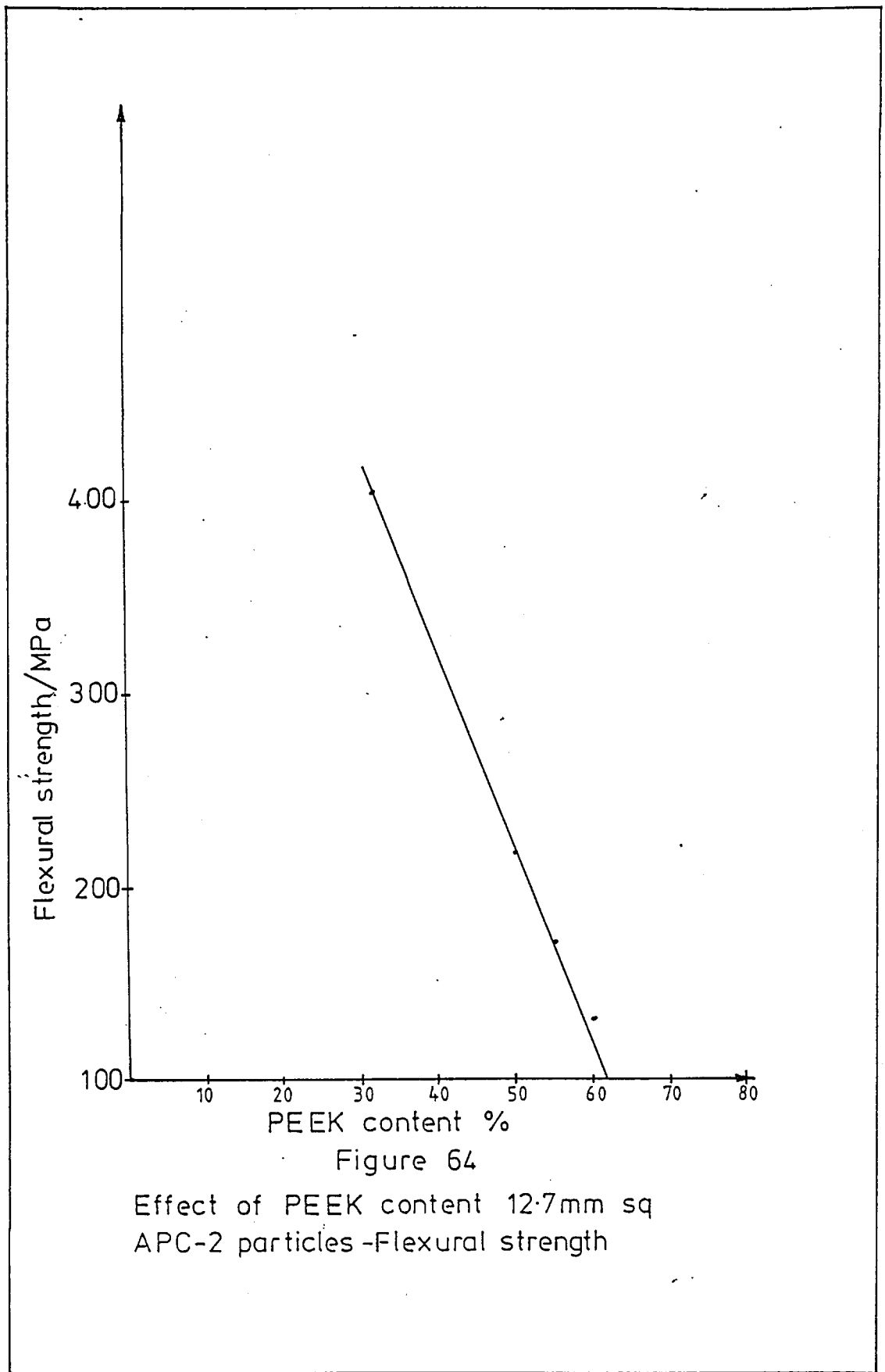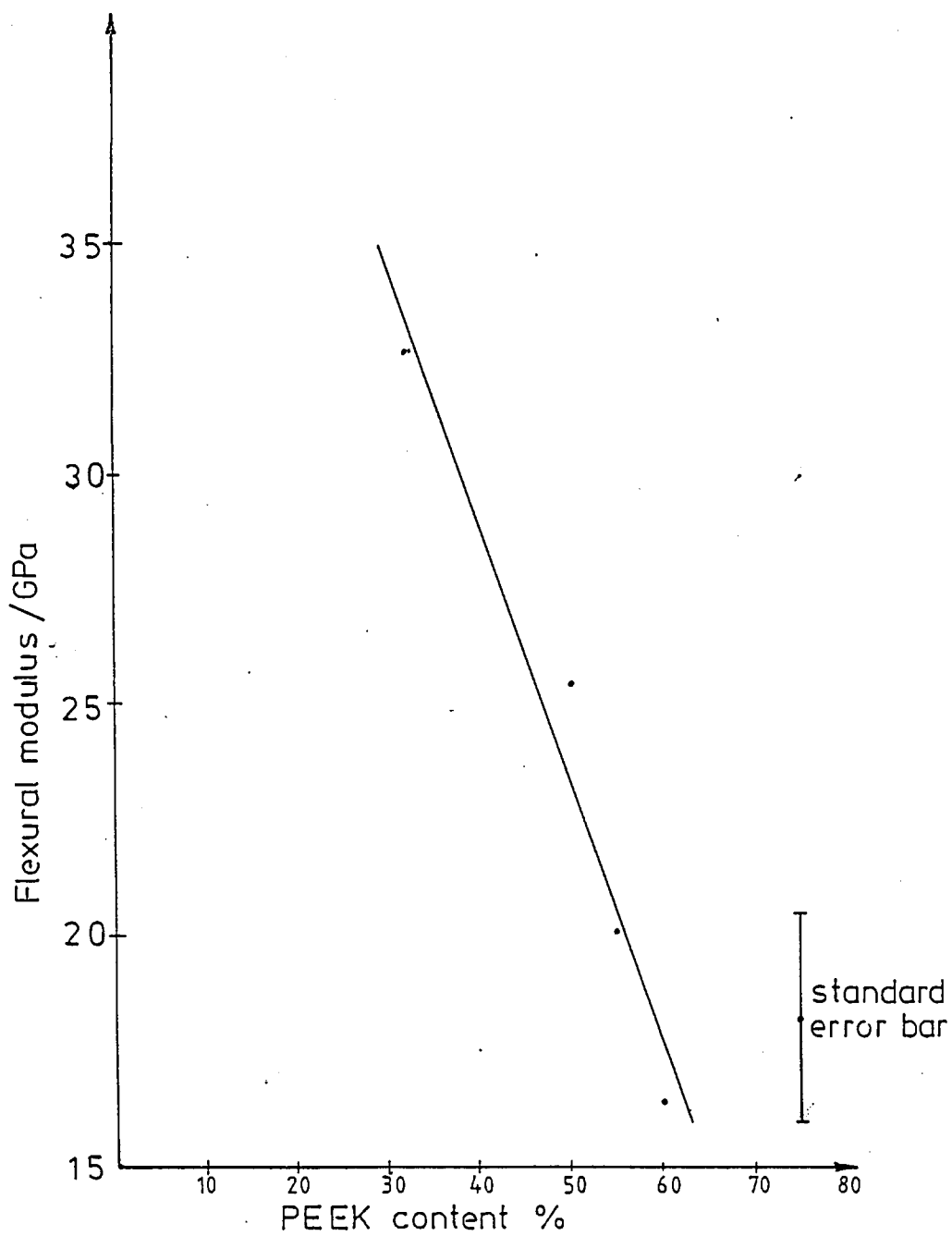
Figure 65

Effect of PEEK content 12·7mm sq
APC-2 particles -Flexural modulus

Figure 66
The effect of particle size with 8 ply APC2 as a
source for the particles Flexural strength
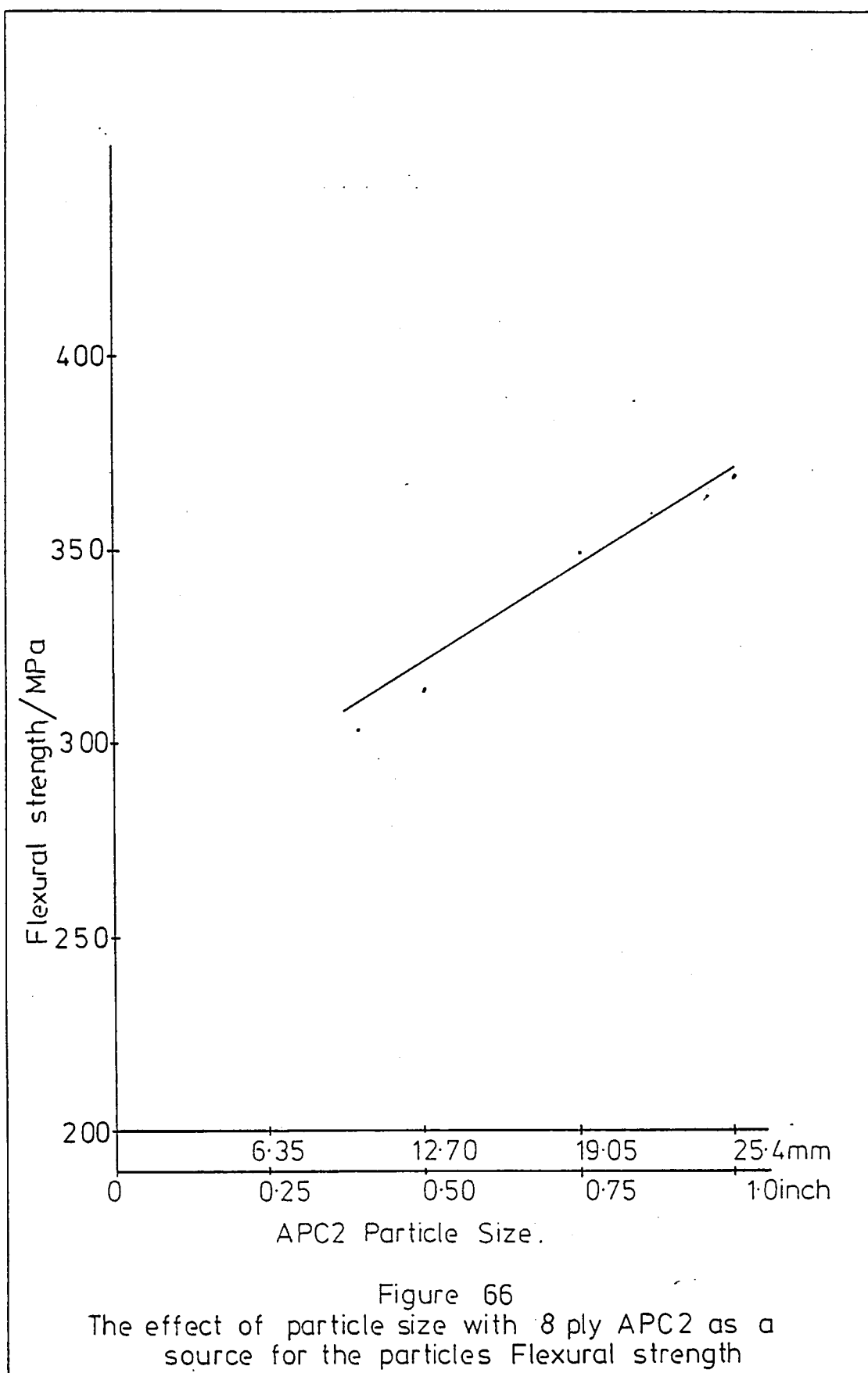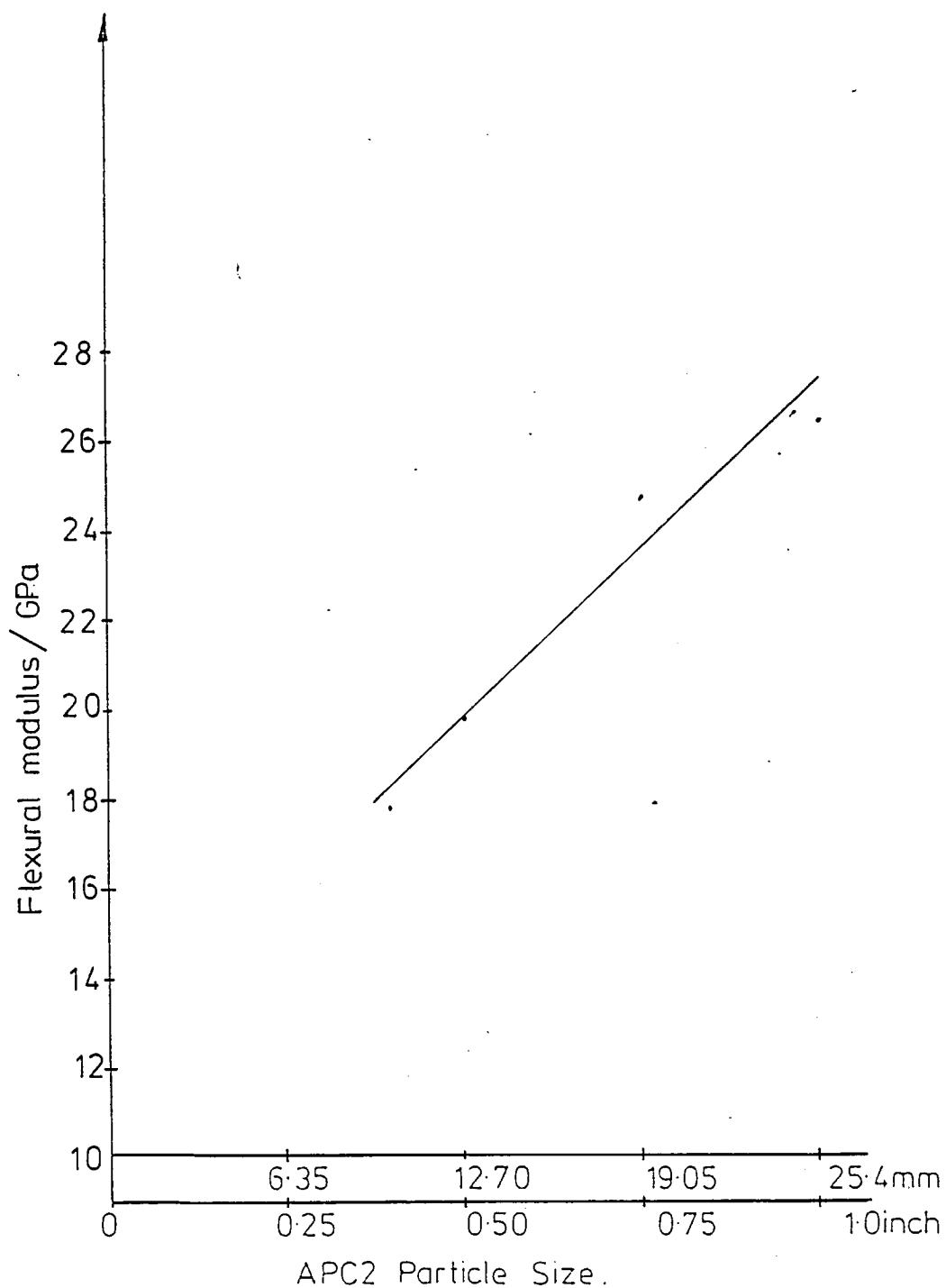
Figure 67
Effect of particle size with 8 ply APC2 as a
source for the particles Flexural modulus

Figure 68
Effect of particle size with 8 ply APC2 as a
source for the particles Tensile strength

Figure 69
Effect of particle size with 8 ply APC2 as a
source for the particles Tensile modulus
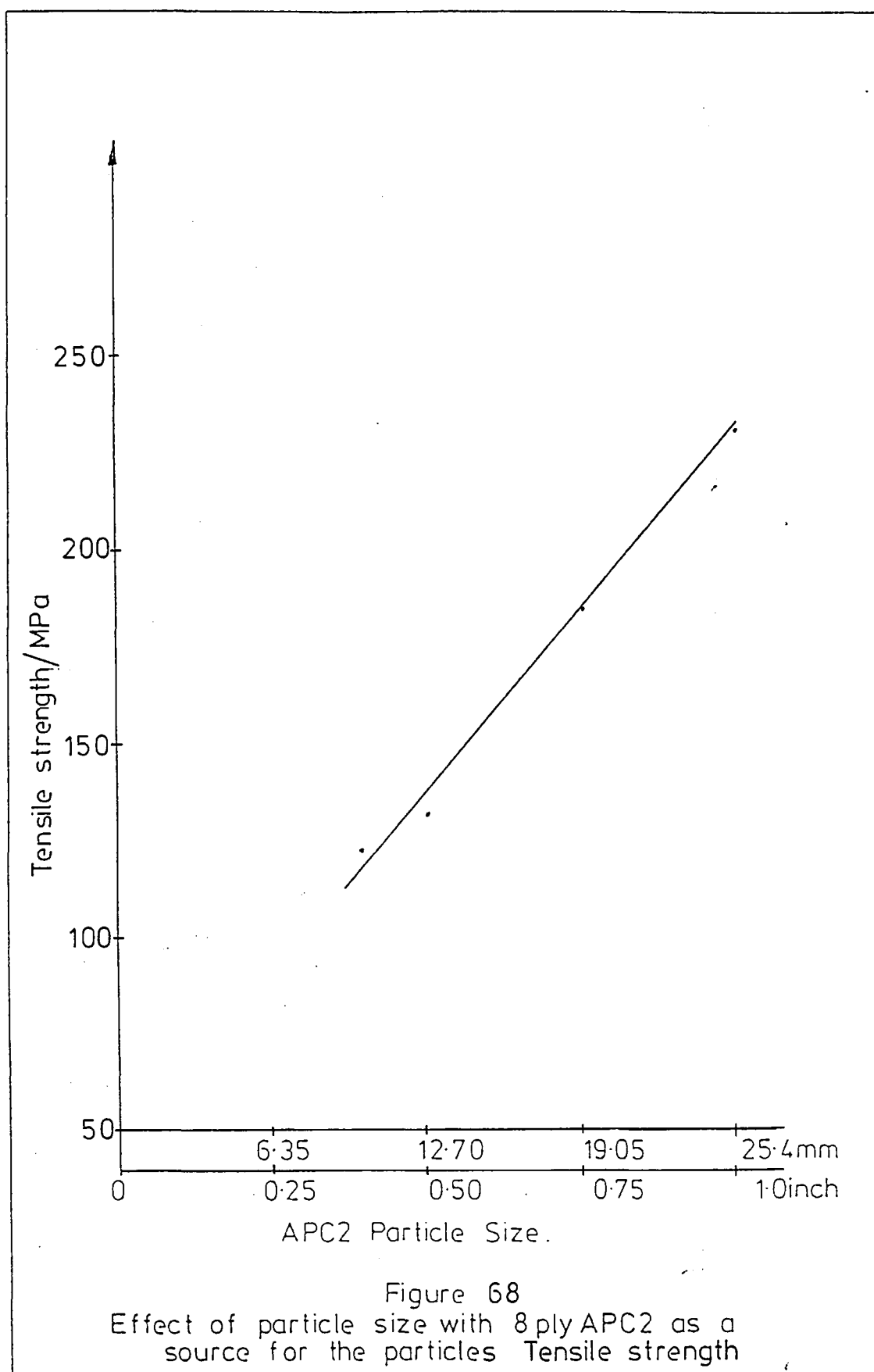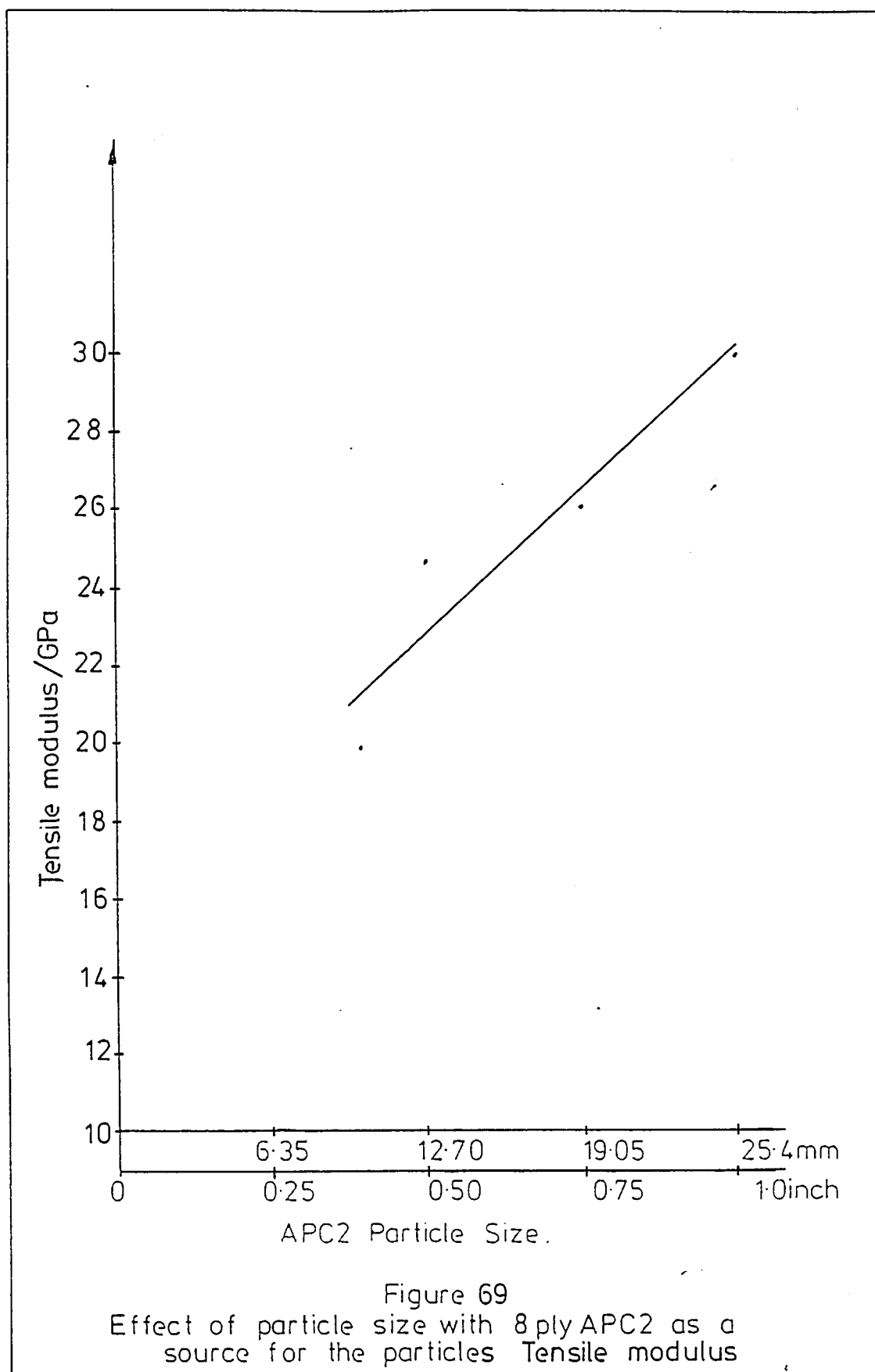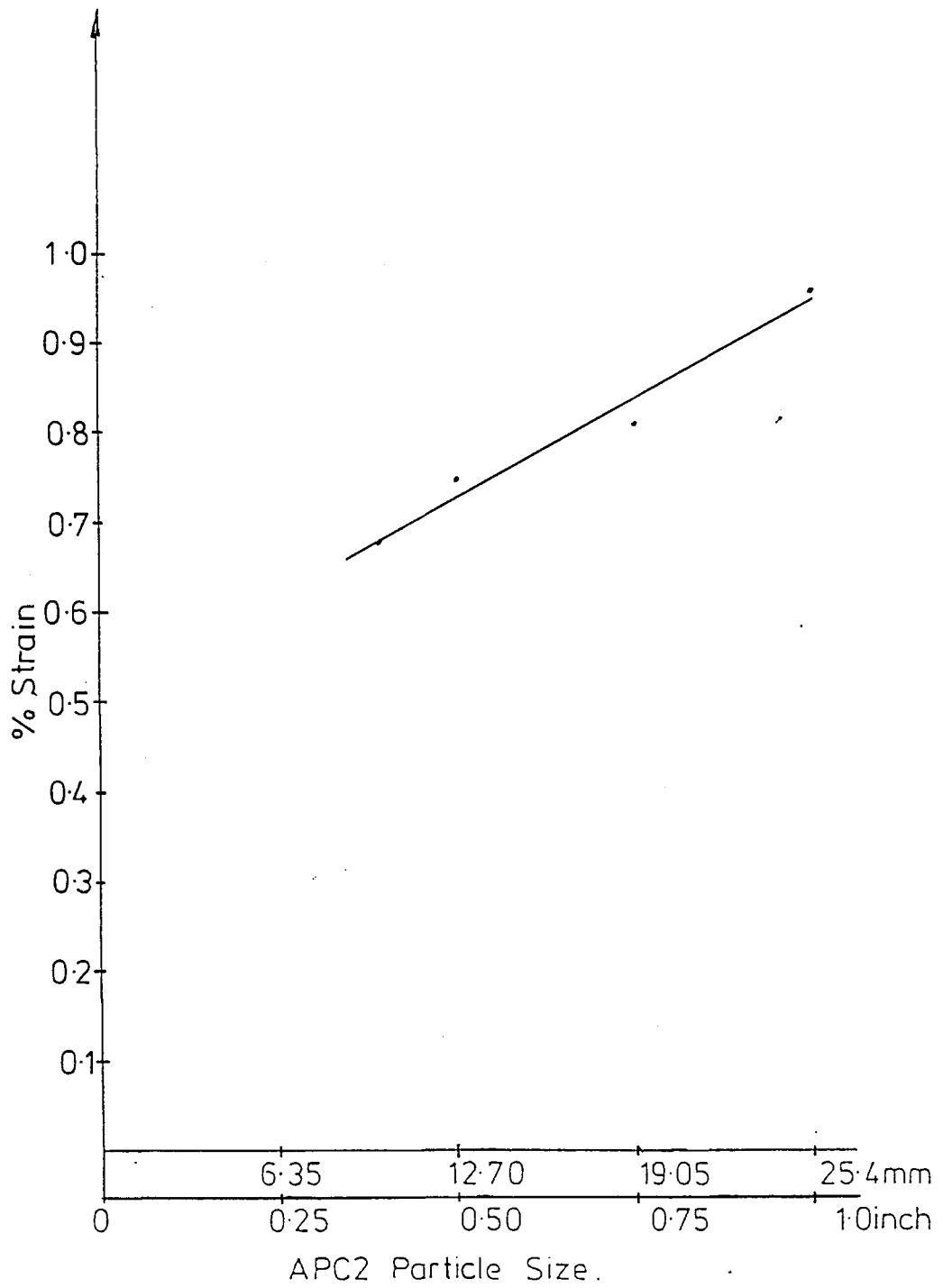
Figure 70
Effect of particle size with 8 ply APC2 as a
source for the particles Tensile strain at failure

Figure 71
Effect of particle size with 8 ply APC2 as a
source for the particles Compression strength
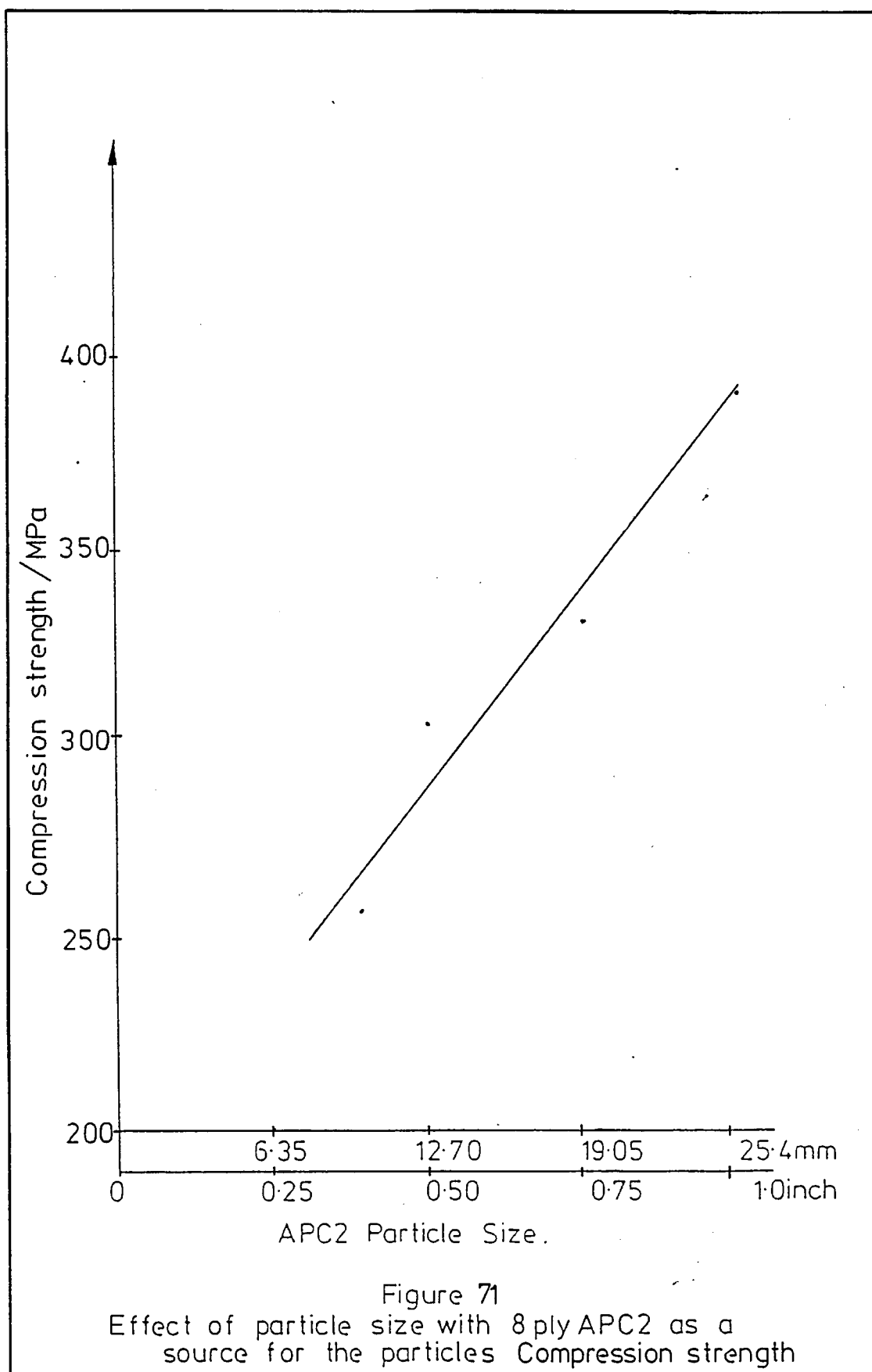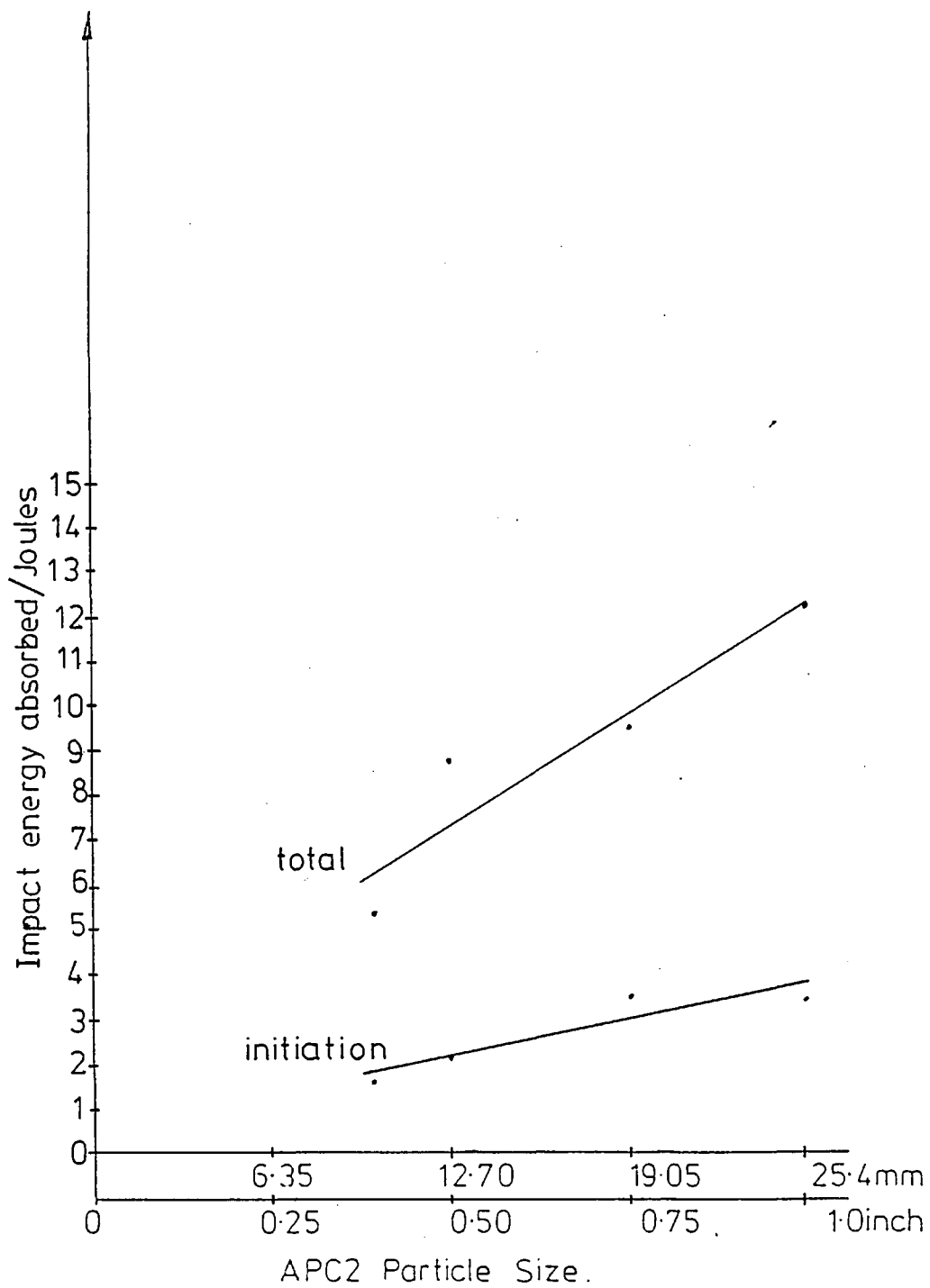
Figure 72

Effect of particle size with 8 ply APC2 as a
source for the particles Impact toughness

Figure 73
Effect of particle size with 8 ply APC2 as a
source for the particles Fracture toughness

Figure 74

Figure 75

Time held at 400°C during processing /mins
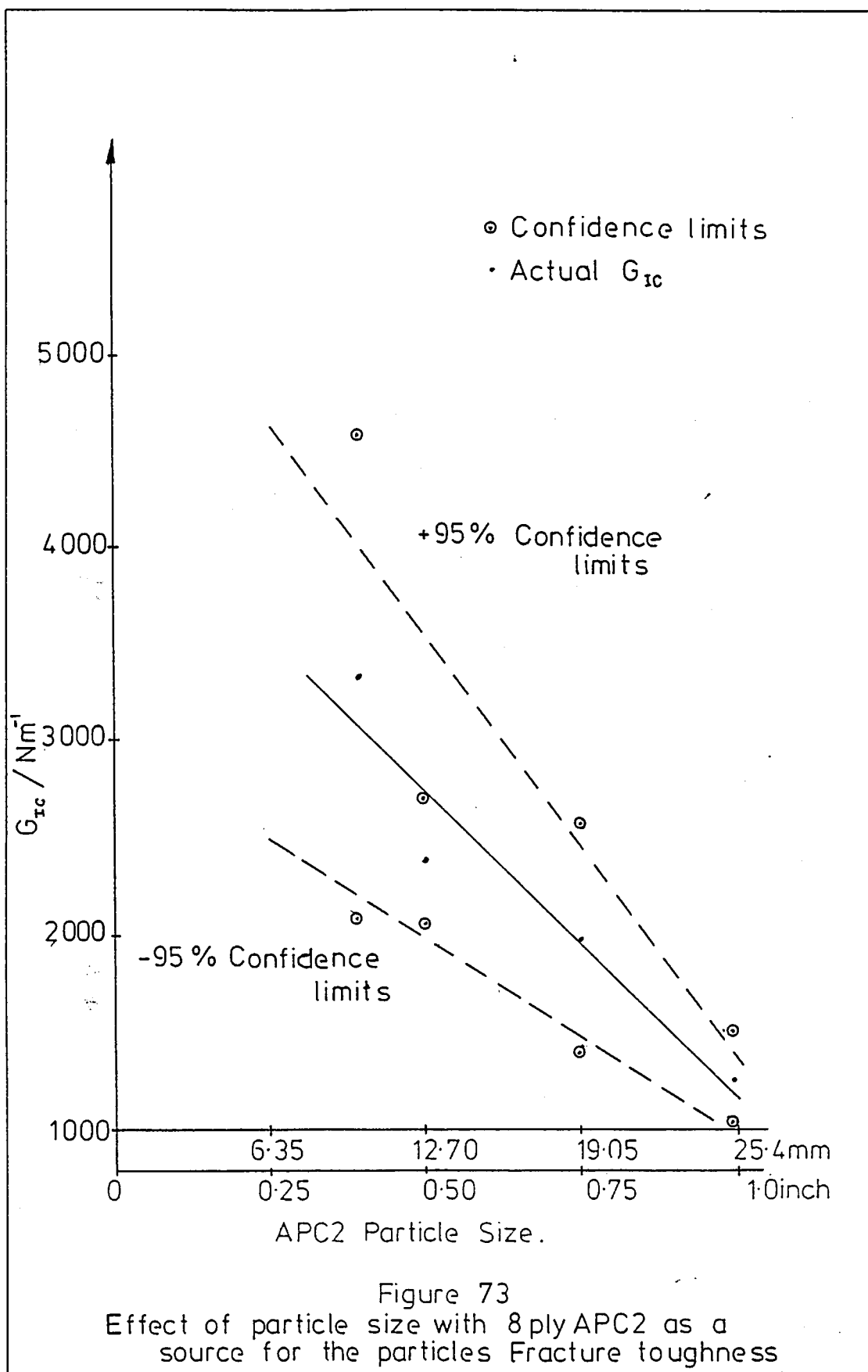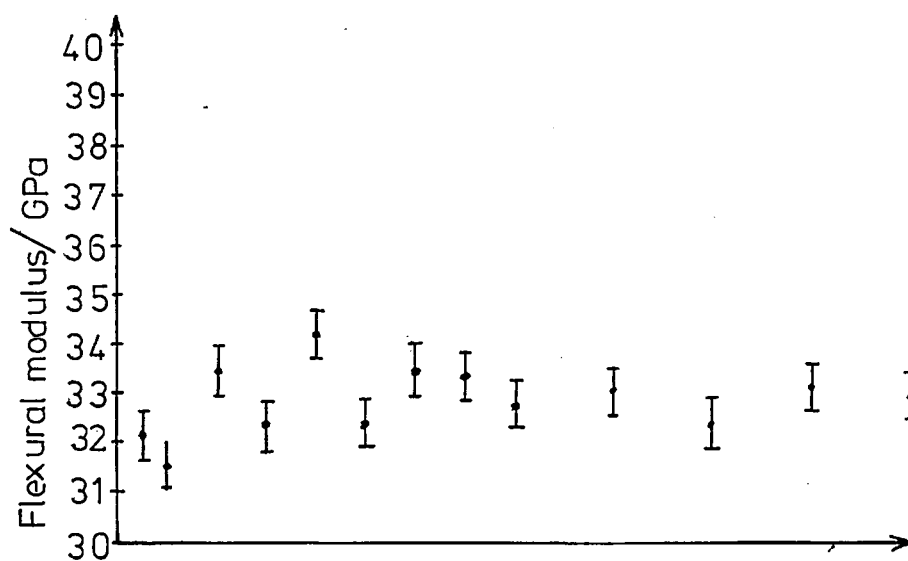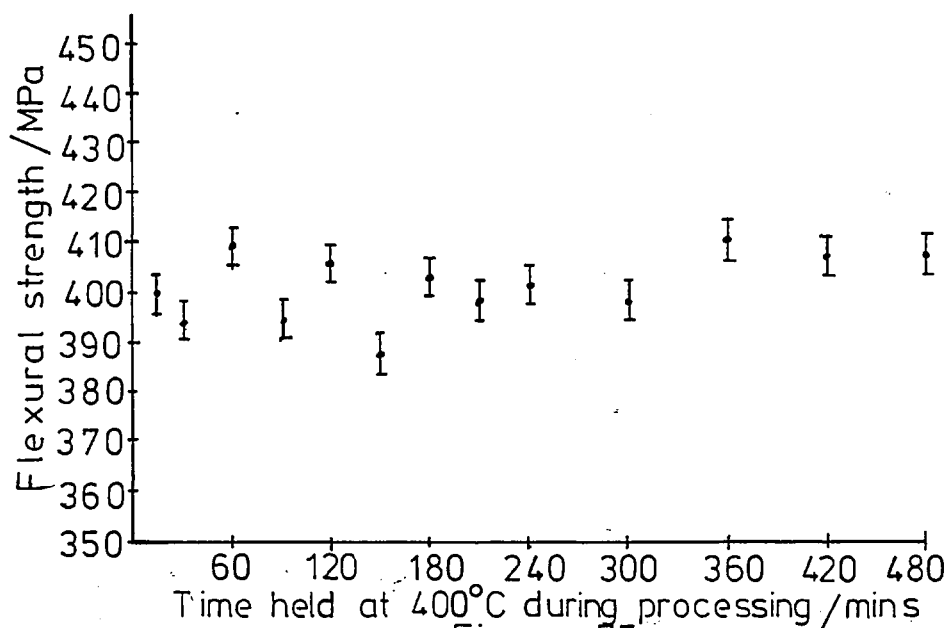
Effect of prolonged time at moulding temperature (400°C) upon the flexural properties of reclaimed APC 2
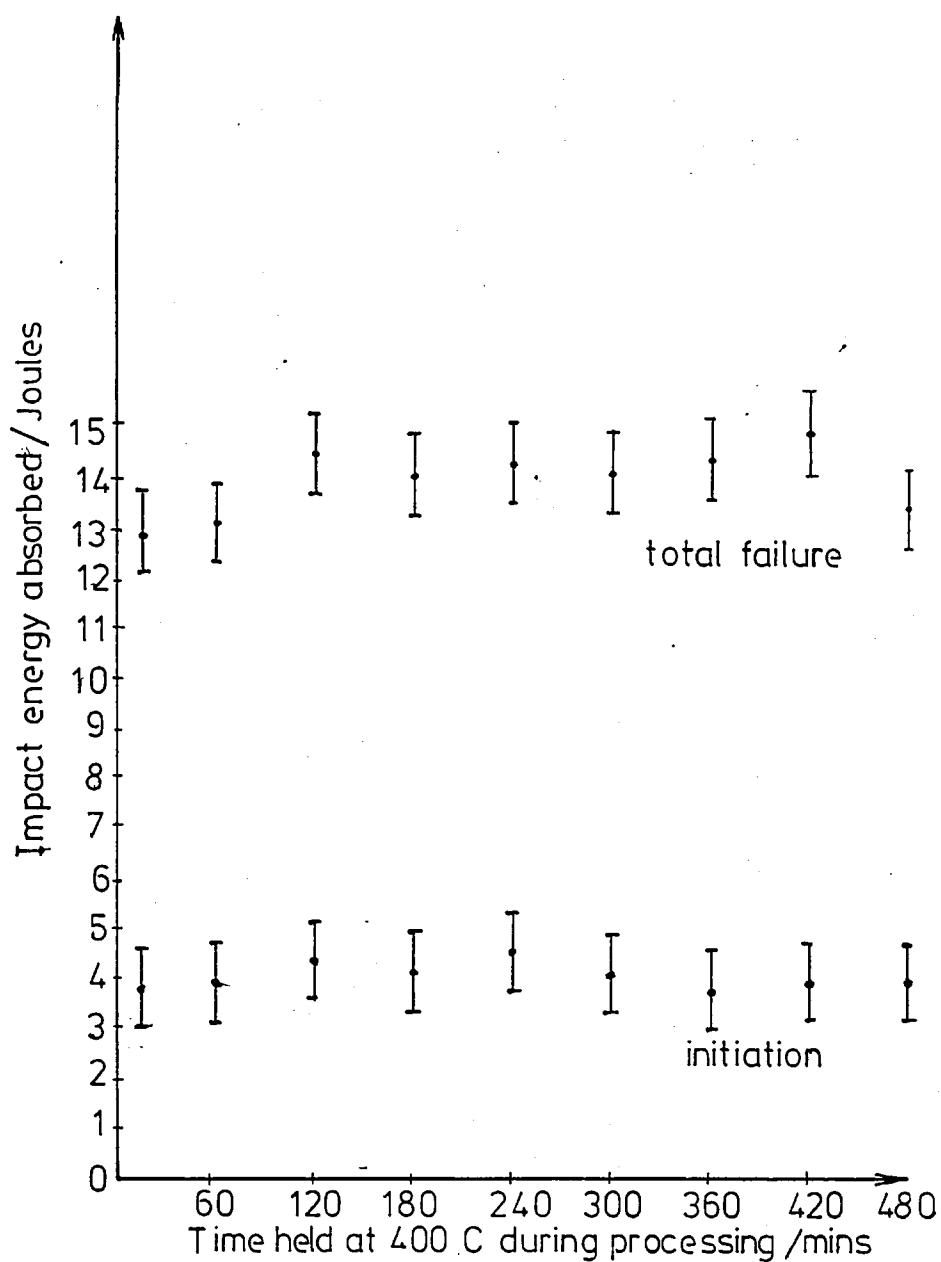
Figure 76

The effect of prolonged time at moulding temperature (400°C) upon the impact toughness of reclaimed APC2

Figure 77

Theoretical modulus predictions
v's particle size - Tensile

Figure 7 8
Theoretical modulus predictions
v's particle size - Flexure
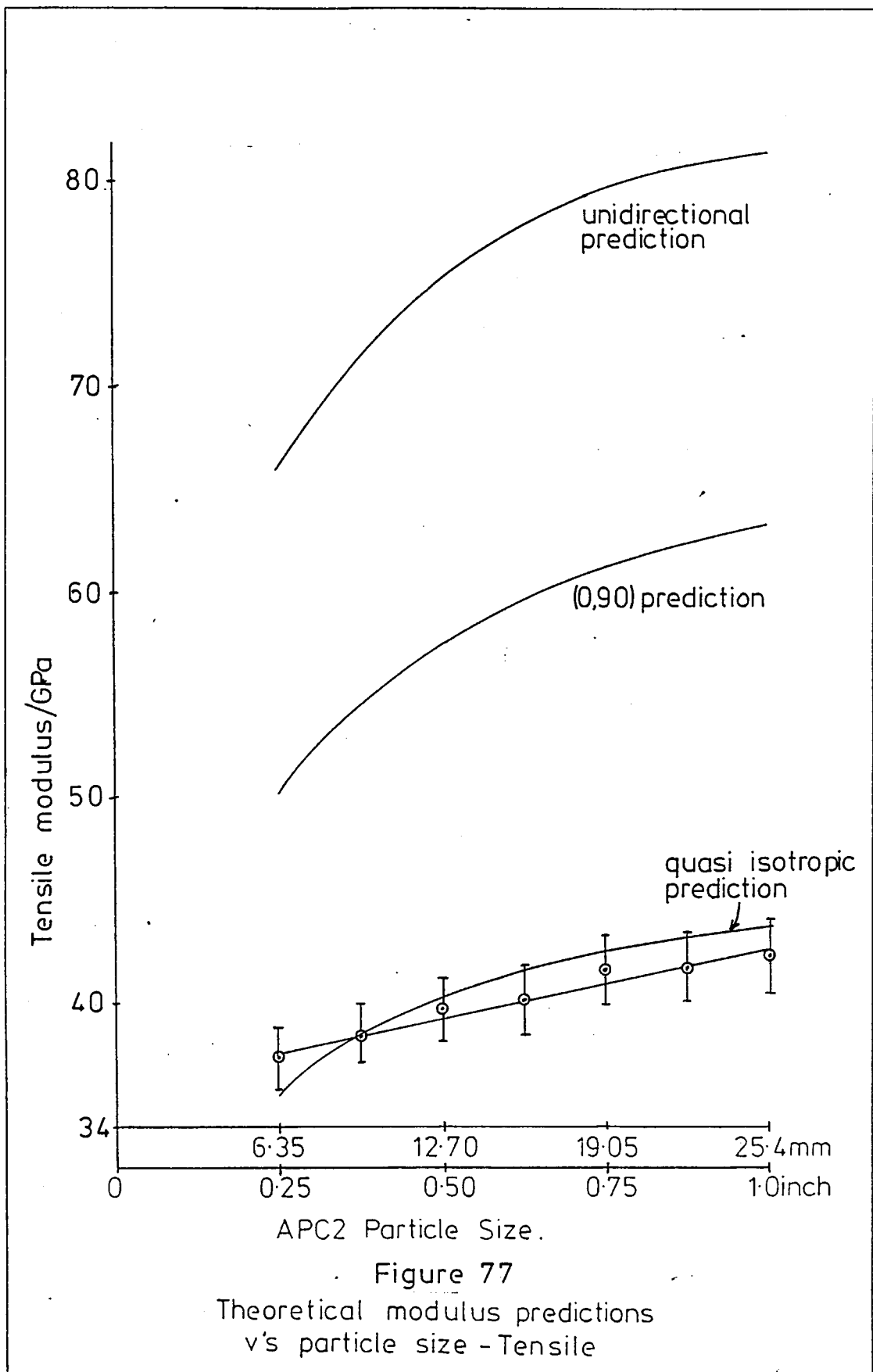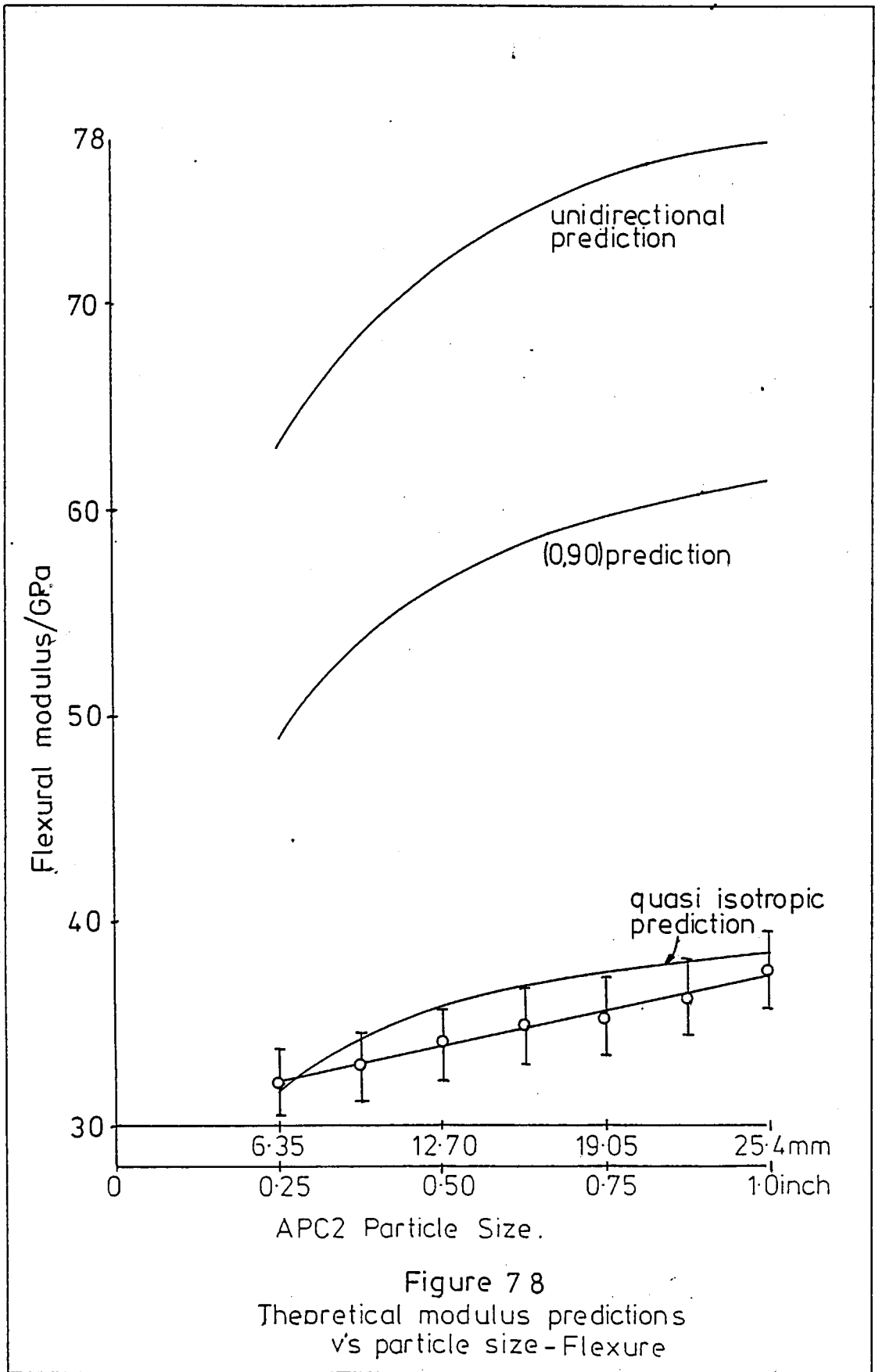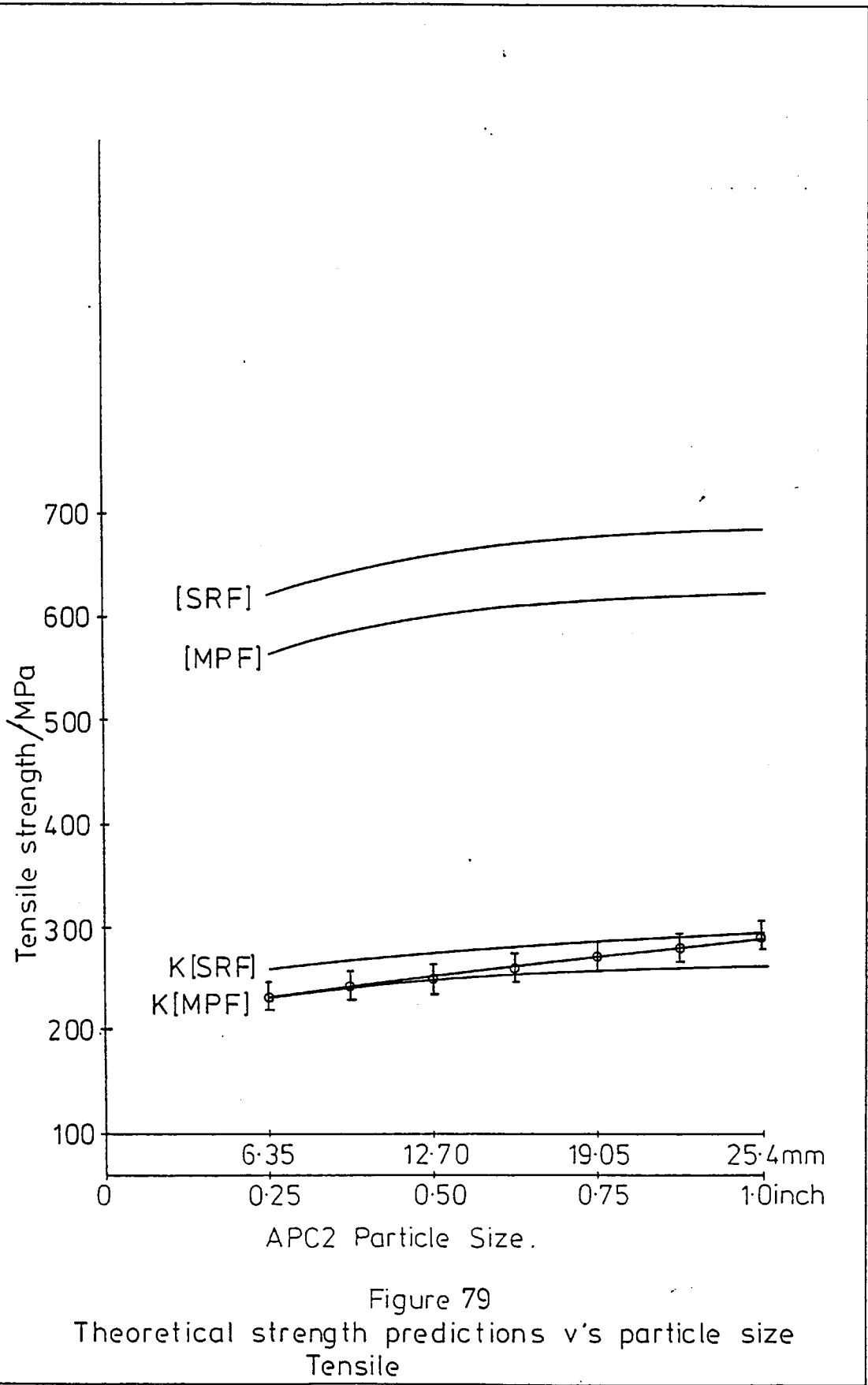
Figure 79

Theoretical strength predictions v's particle size
Tensile

Figure 80
Theoretical strength predictions v's particle size
Flexure

Figure 81
Theoretical strength predictions v's particle size
Compression
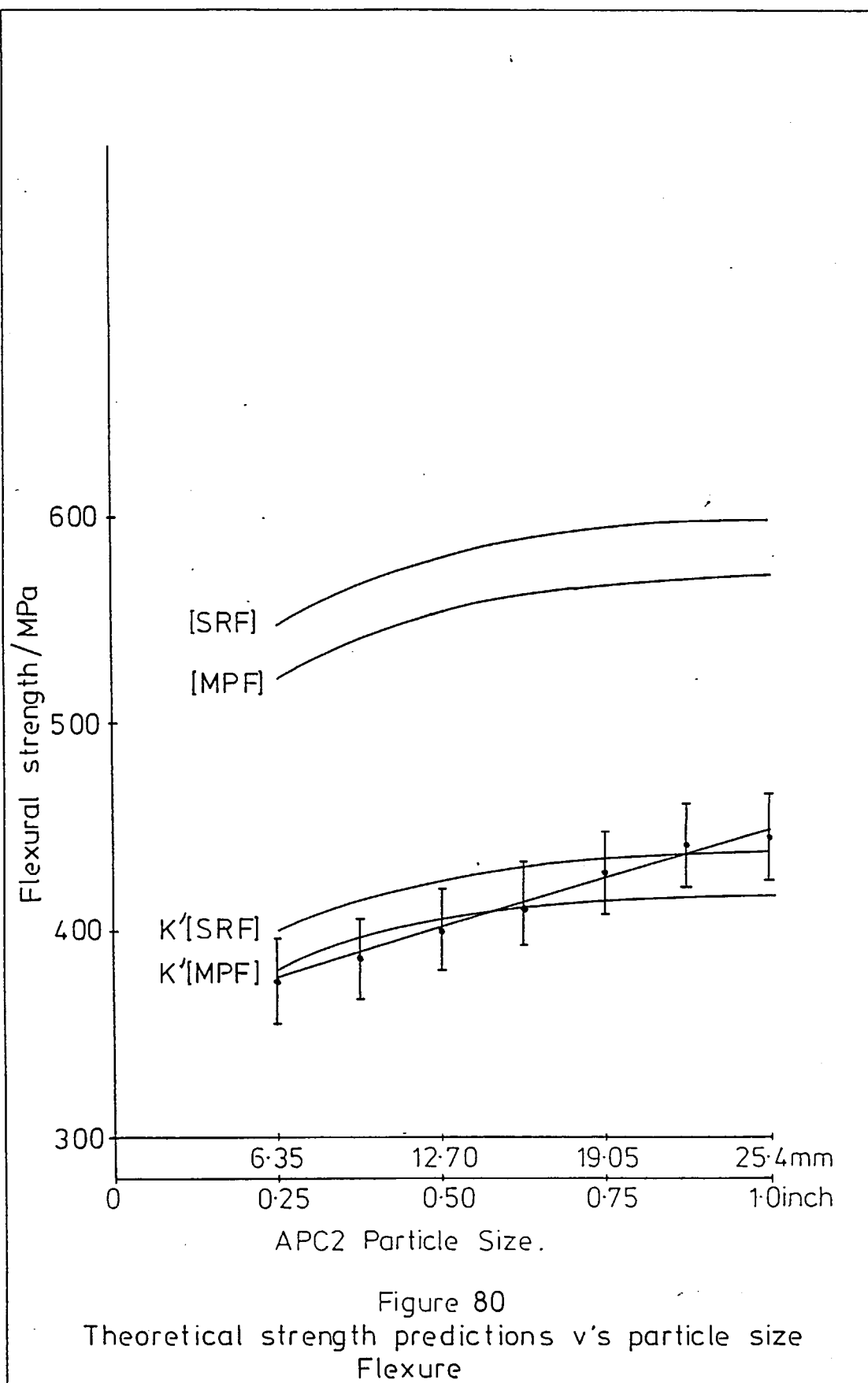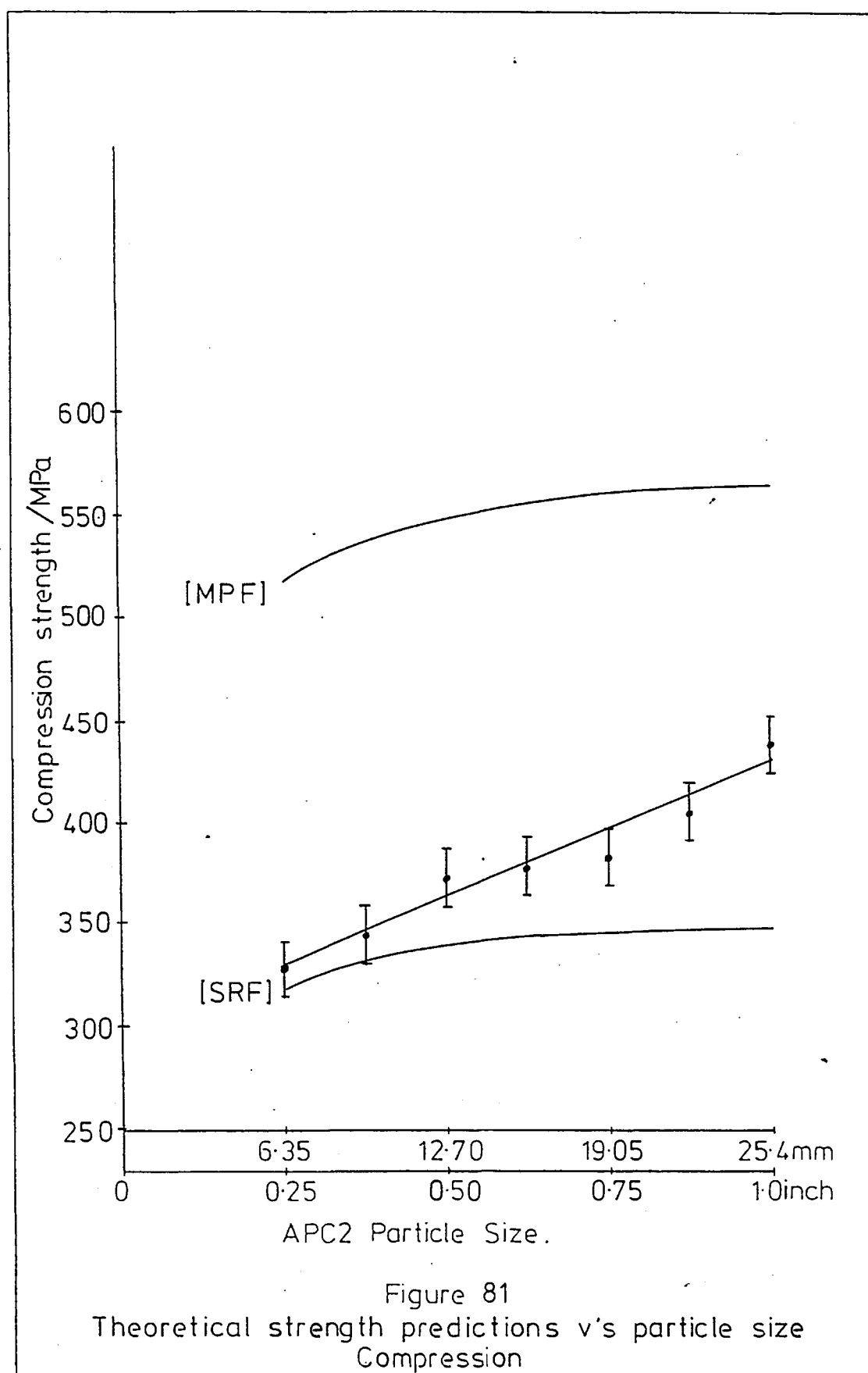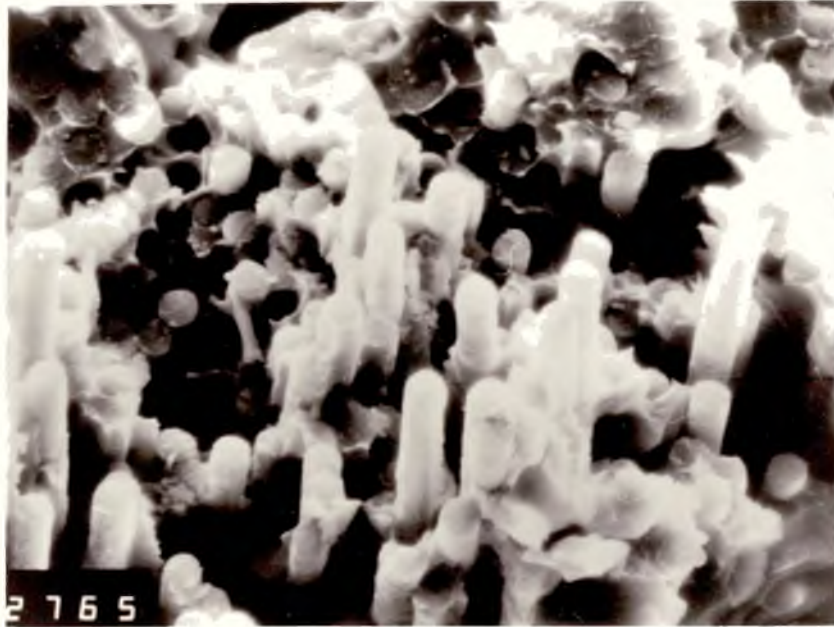
Figure 82   10μ

The combination of failure mode
X 880
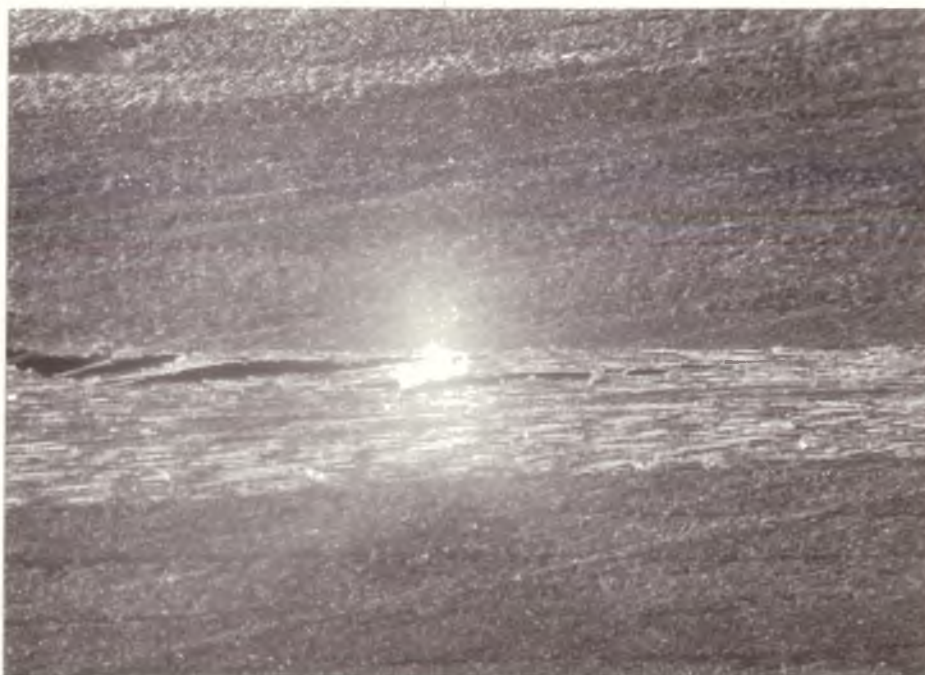
Figure 83
Straight crack growth through parallel fibres.
X 25
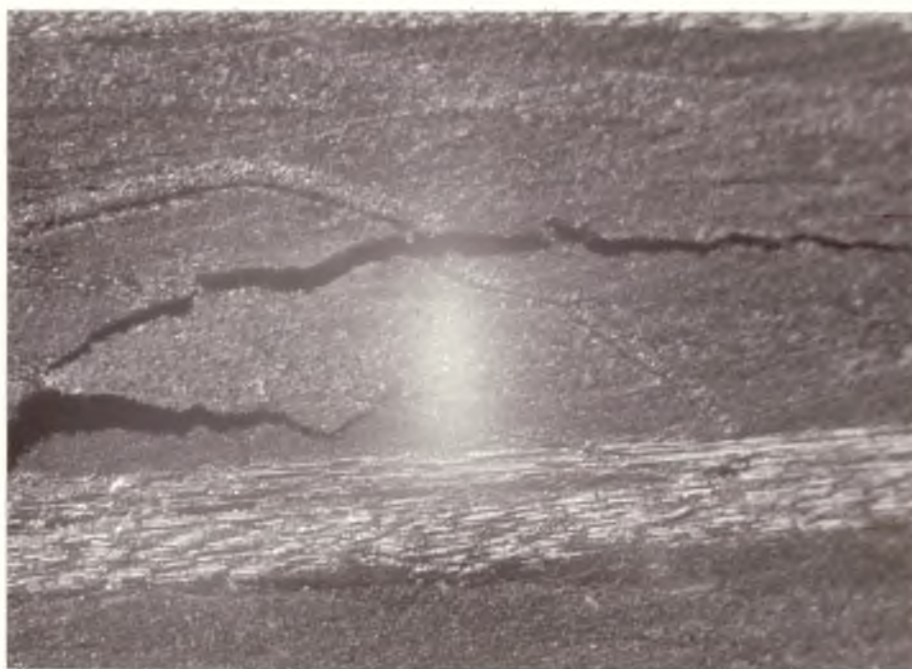
Figure 84
Uneven crack growth through transverse fibres
and secondary crack formation . X 25
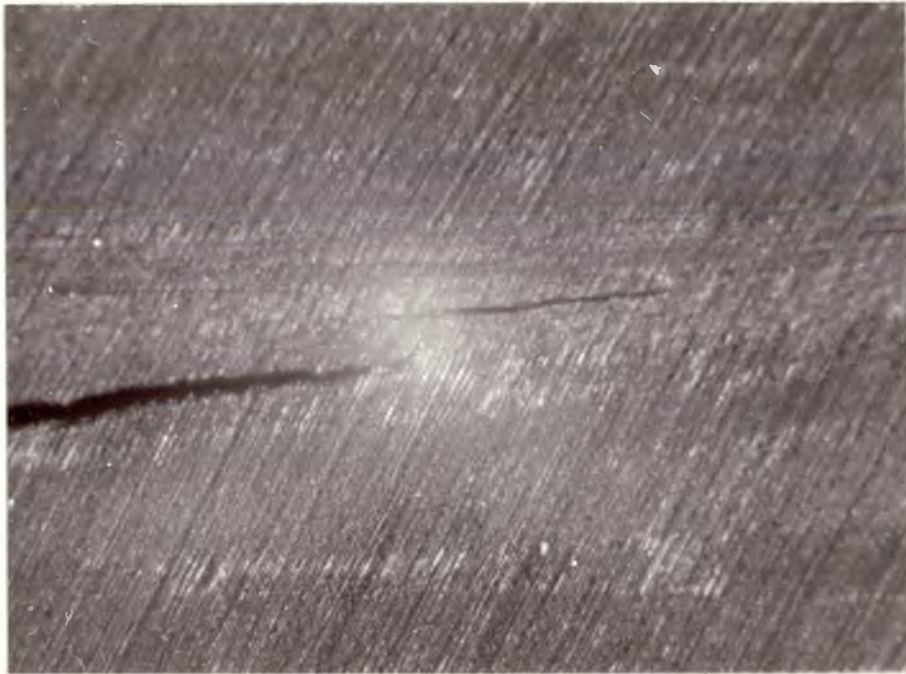
Figure 85
Cracks opening in front of main crack.
X 25
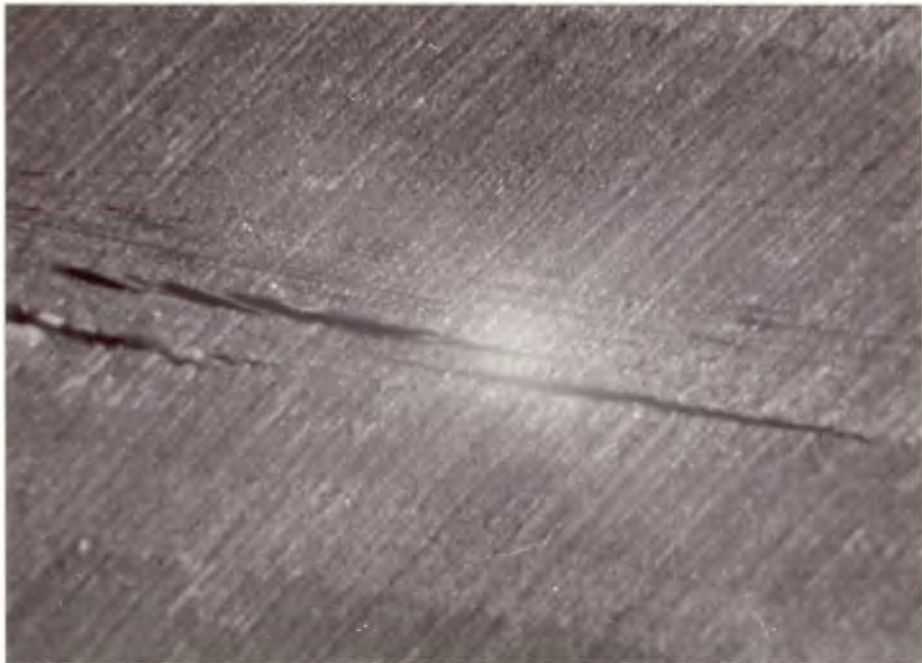
Figure 86
Cracks in front of and adjacent to main
crack . X 25
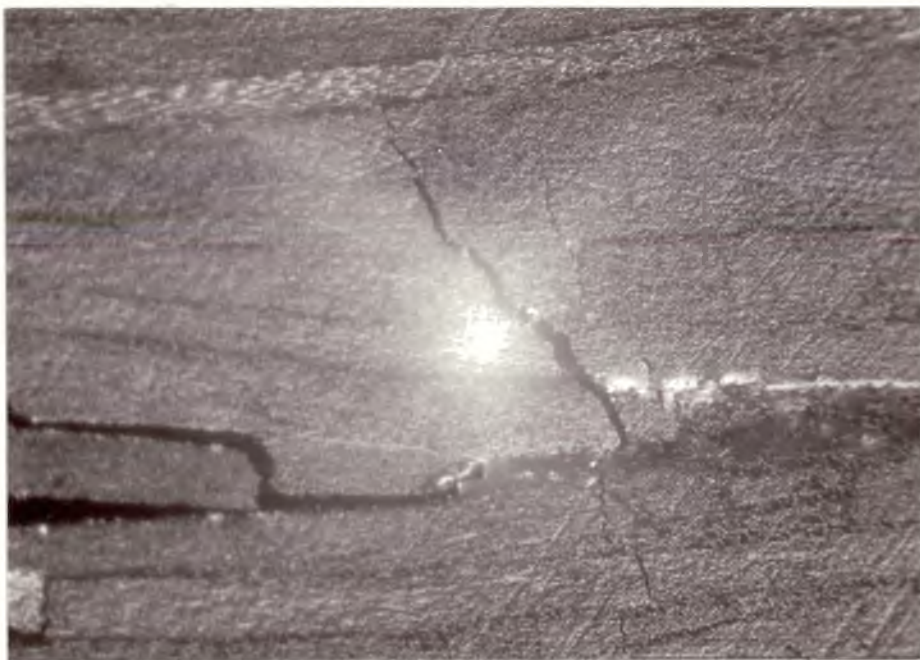
Figure 87
Crack blunting effect of PEEK rich zone. X 25
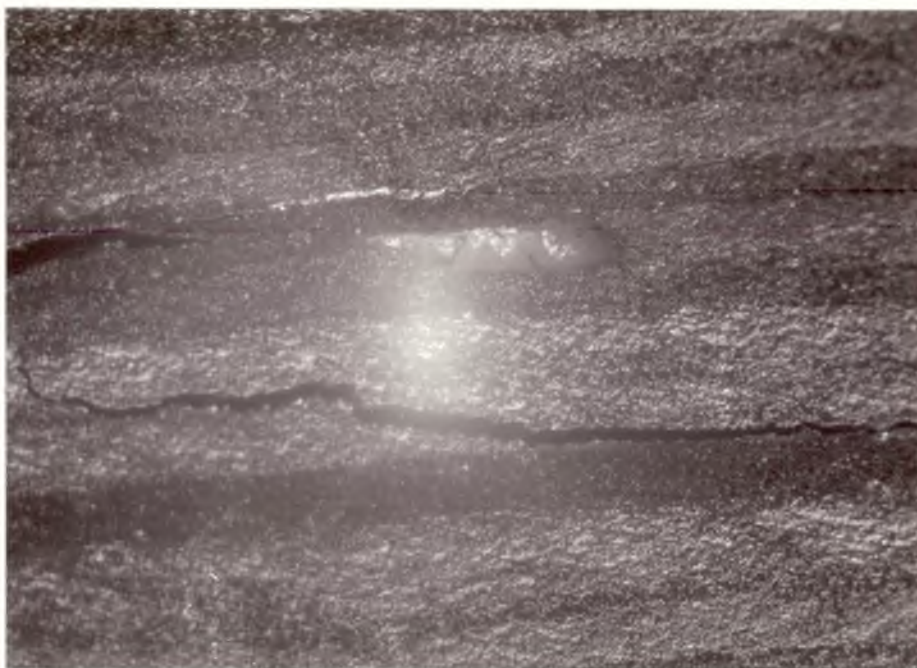
Figure 88
Crack blunting of a PEEK rich zone and secondary
crack formation . X 25
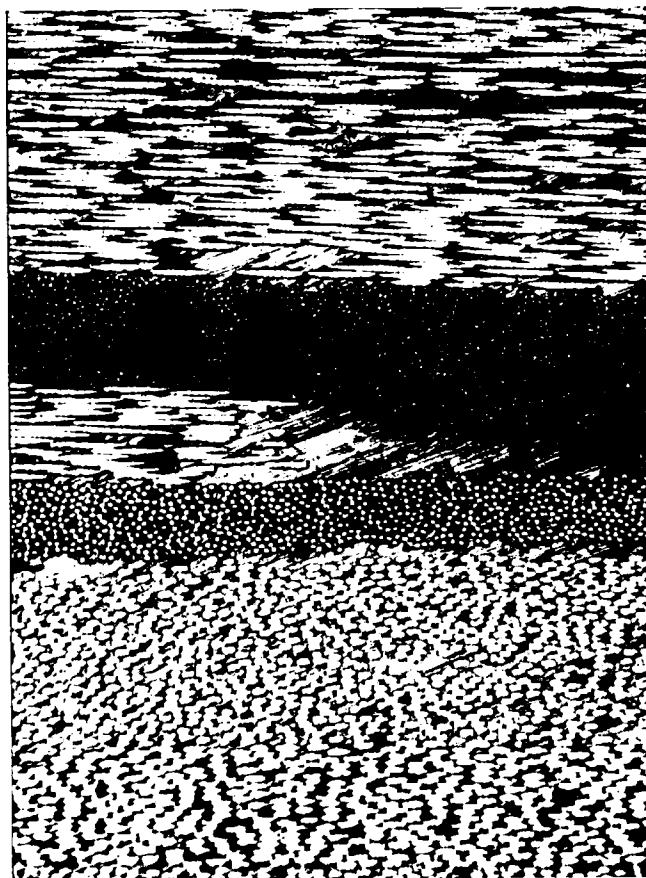
Figure 89

Side view of a polished DCB specimen.

X80

Formation of a PEEK rich zone at the
confluence of three particles.
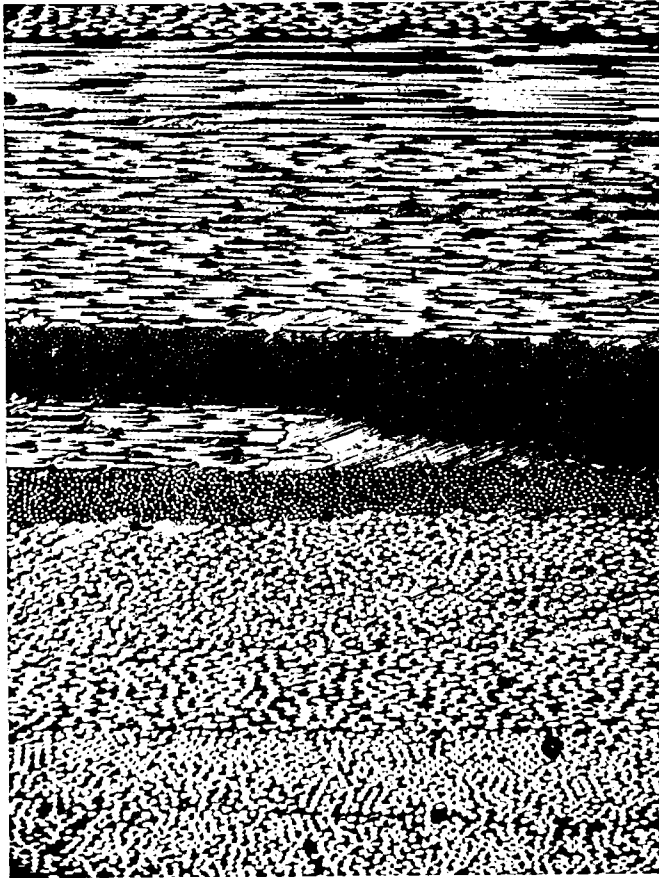
Figure 90
As Figure 89.
X40
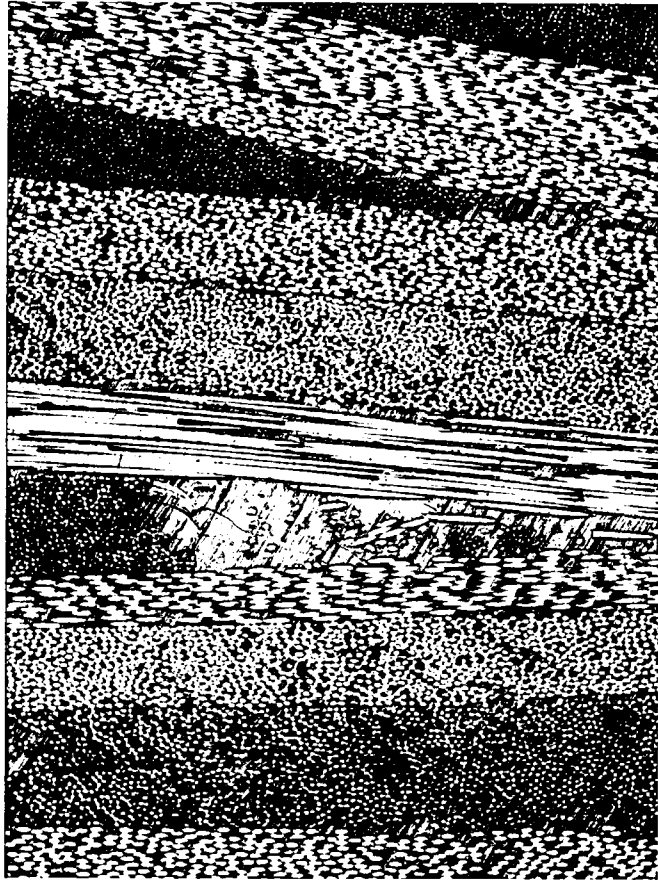
Figure 91

Side view of a polished DCB specimen. X80
Again, a PEEK rich zone but also showing the
random orientation of the particles - giving
varied fibre directions.
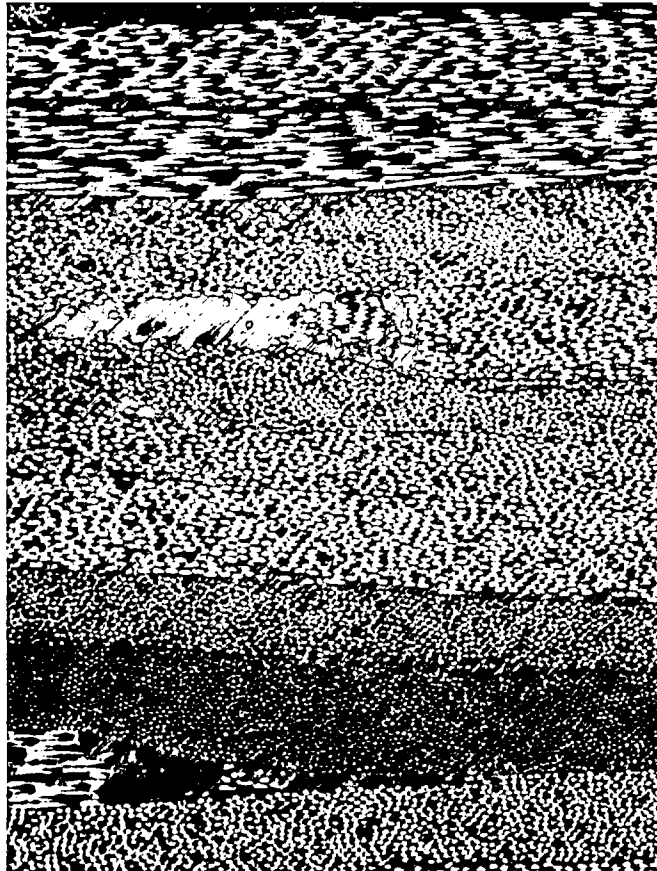
Figure 92

Another representation of PEEK rich zones.

X 80
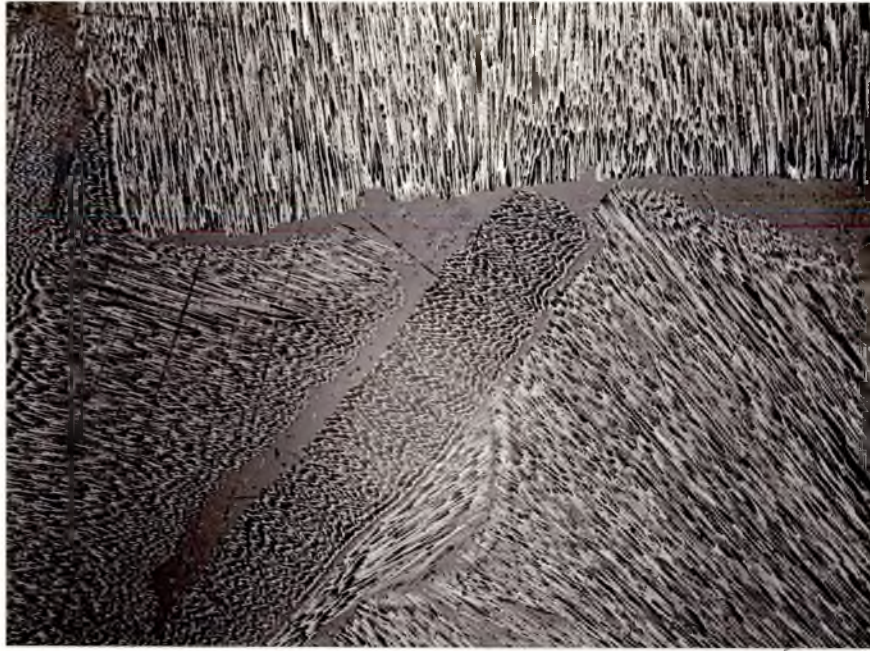
Figure 93
Top view of a polished 12·7mm sample . X20
PEEK rich area at the ends of particles
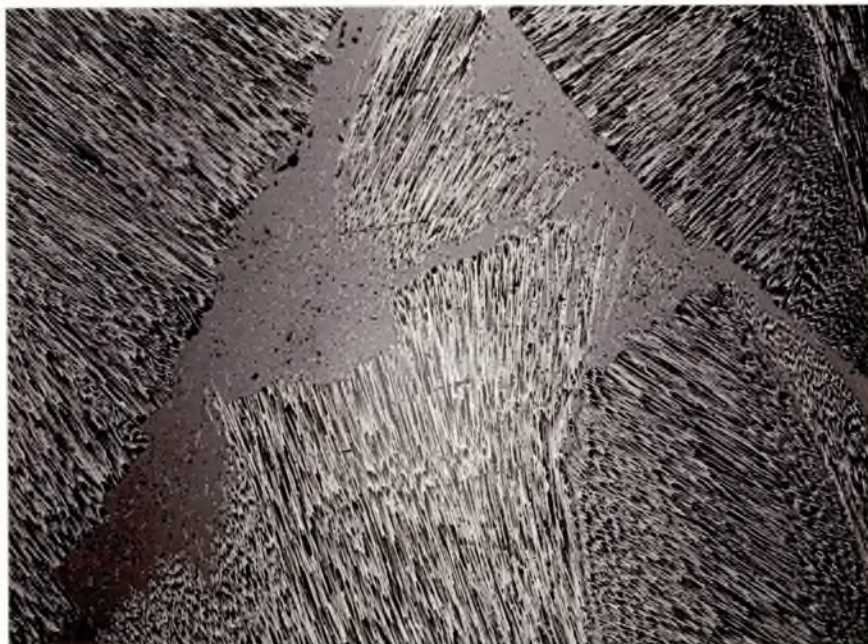
Figure 94
Top view of a polished 12·7mm sample. X20
Enlarged PEEK rich area with flakes
of smaller fibres.
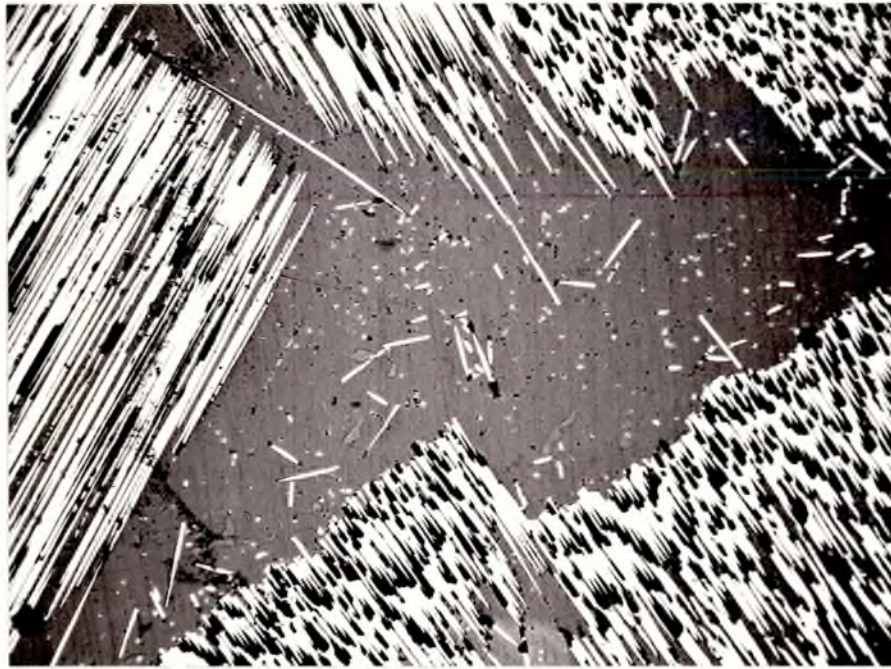
Figure 95
Top view of a polished 9·5mm sample . X80
Closer view of the small flakes of fibre in PEEK
rich zones.
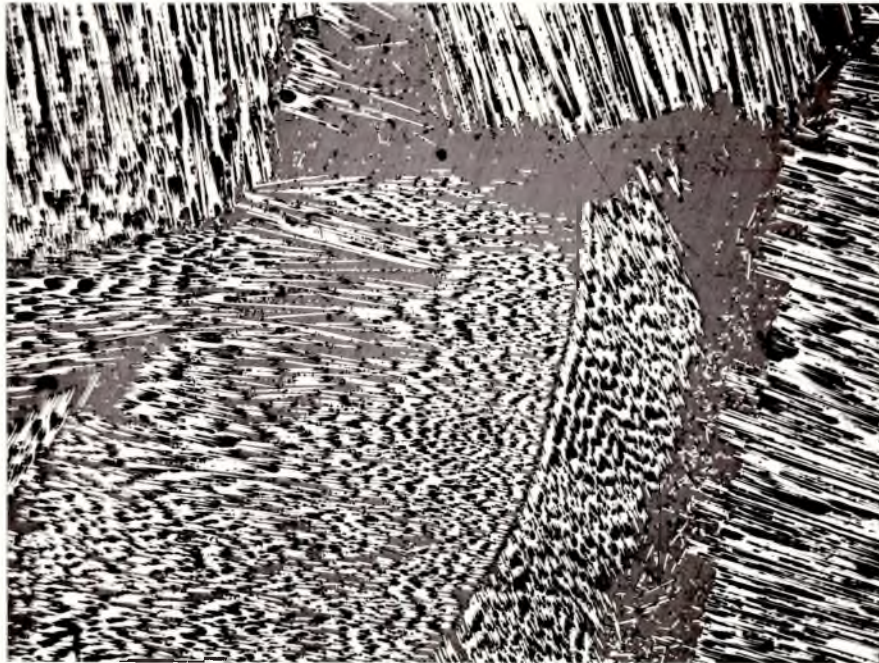
Figure 96
Top view of a polished 12·7mm sample . X40
Again showing small flakes in PEEK rich regions.

Figure 97
Side view of a polished 25·4mm sample. X20
Showing relatively few PEEK rich zones for
this size of particle.
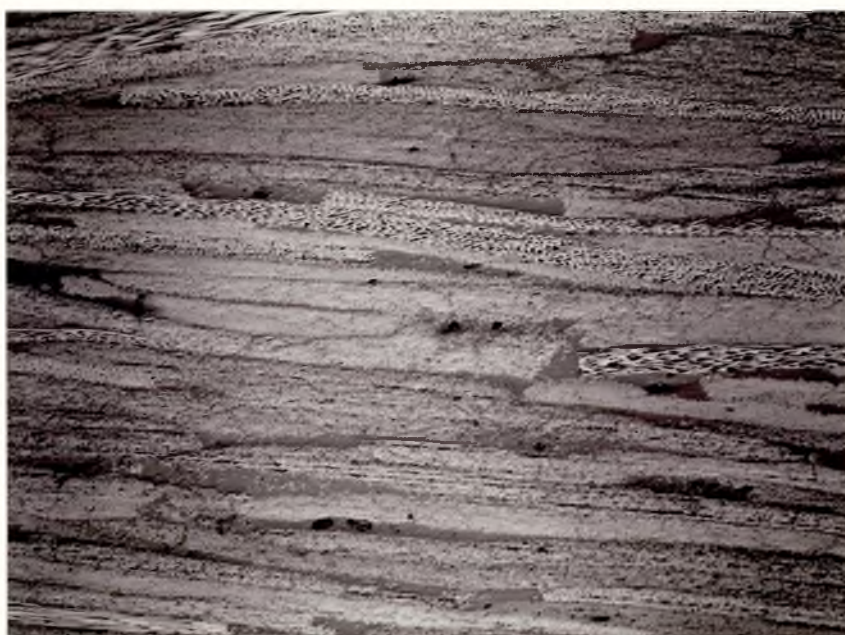
Figure 98
Side view of a polished 6·35mm sample. X 20
Showing many more PEEK rich zones compared
to above.

Figure 99 . X20

The same presentation as Figure 98, but taken
on an oblique light microscope to give greater
contrast between the light PEEK regions and
dark particle regions.

Figure 100

Macrograph of the fracture surfaces of DCB
specimens decreasing particle size from left
to right i)continuous fibre beam,
ii) 22.2mm particulate beam,iii)19.1mm particulate
beam, iv)12.7mm particulate beam v)6.35mm
particulate beam.
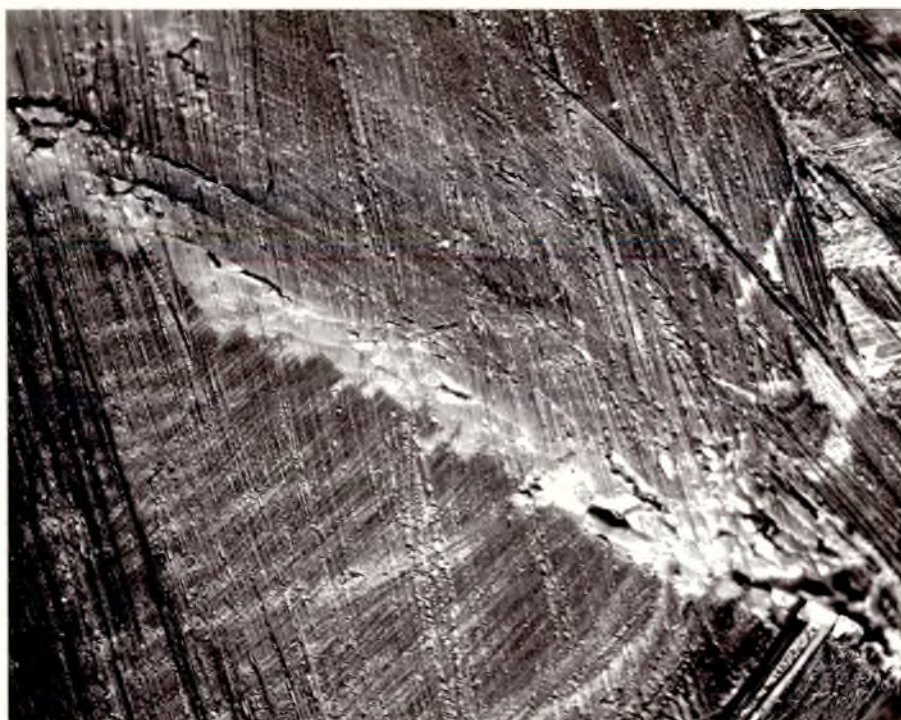
Figure 101
Oblique light micrograph of the fracture surface
of a 22·2mm sample. X 25
PEEK rich zone at particle boundary.

Figure 102
Oblique light micrograph of the fracture surface
of a 6·35mm sample. X25
Several particles meeting with a central PEEK rich region.
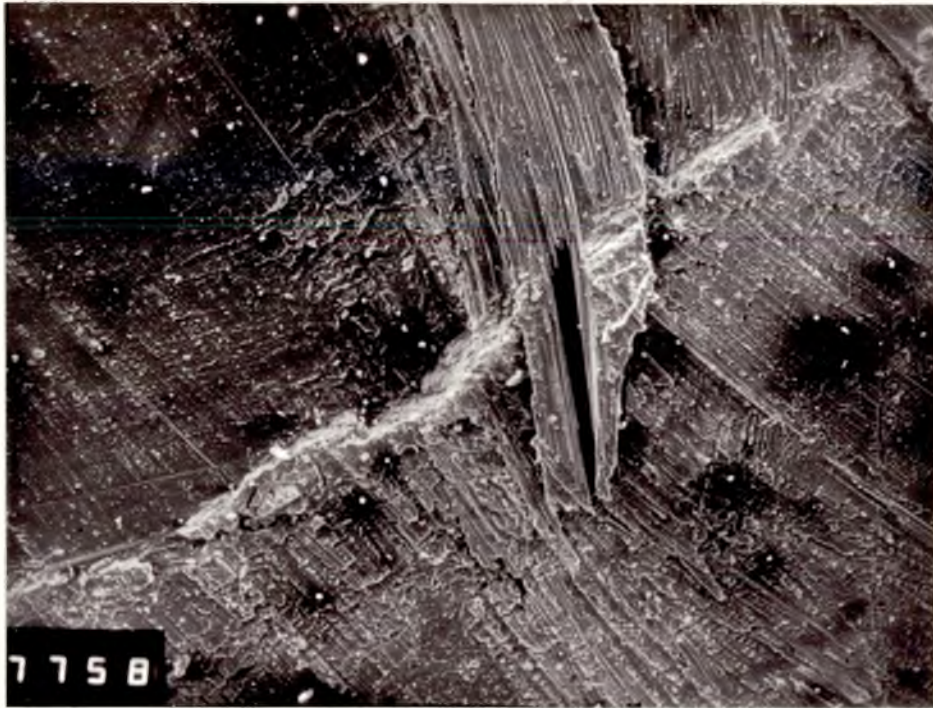
Figure 103
SEM micrograph of a 22·2mm sample showing boundary
between two particles. X 30
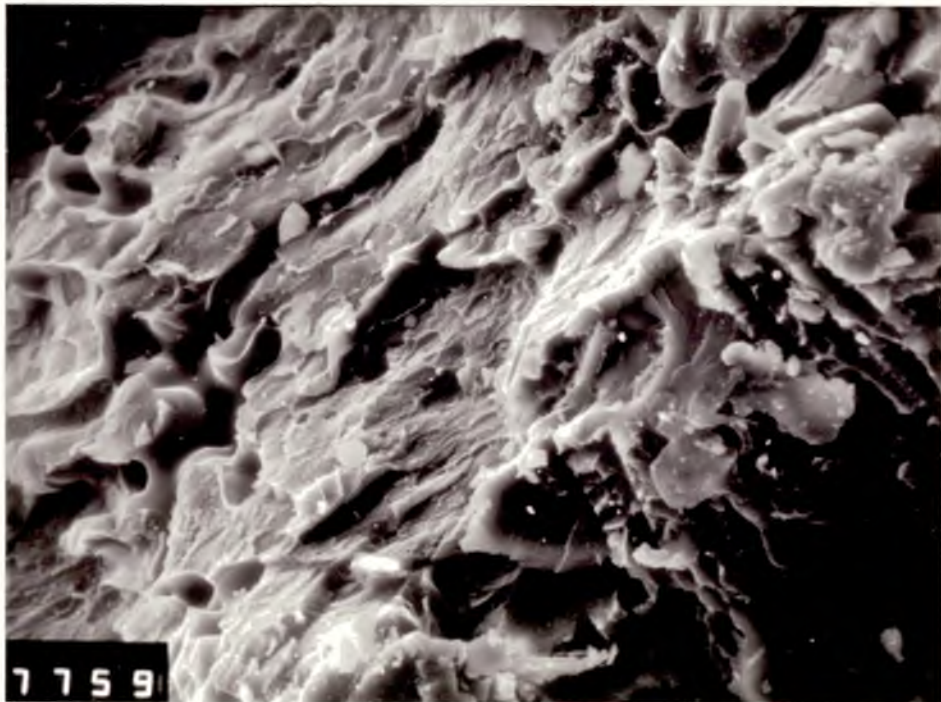
Figure 104 10ᴍ   X480
High magnification fractograph. The boundary region of
Figure 103 showing PEEK dominated fracture surface at
these boundary regions.
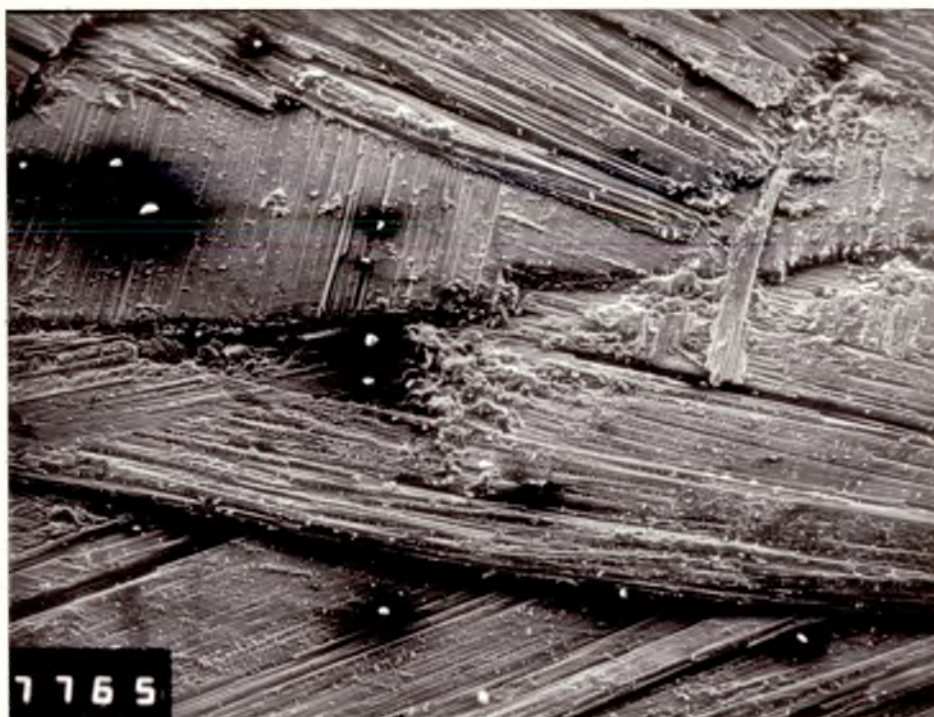
Figure 105
SEM fractograph of a 6·35mm sample X30
showing the meeting of several particles.
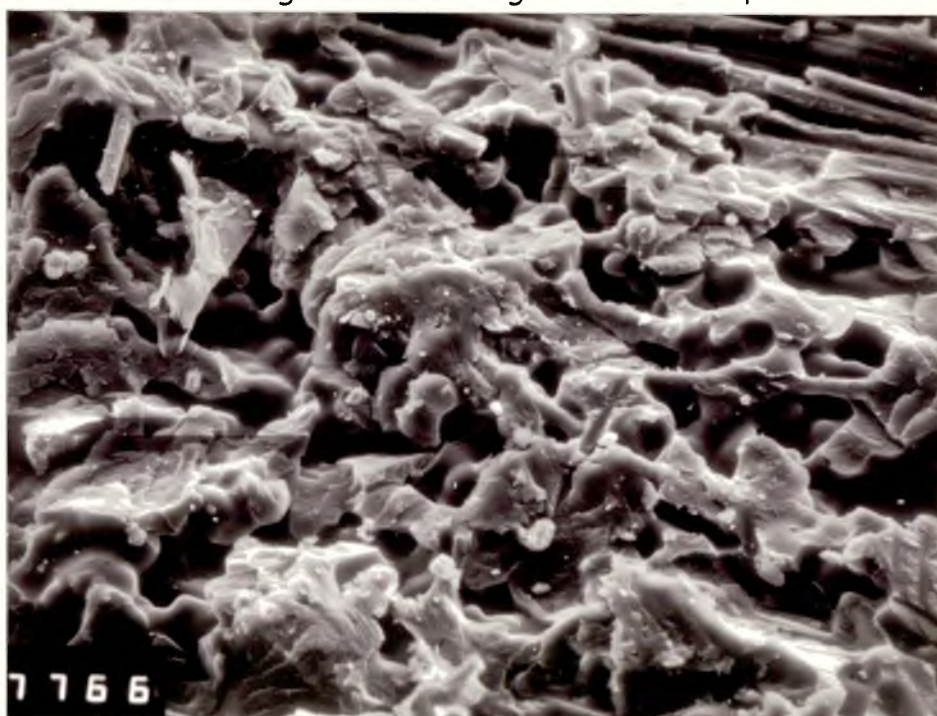
Figure 106   20μ   X260
Higher magnification fractograph
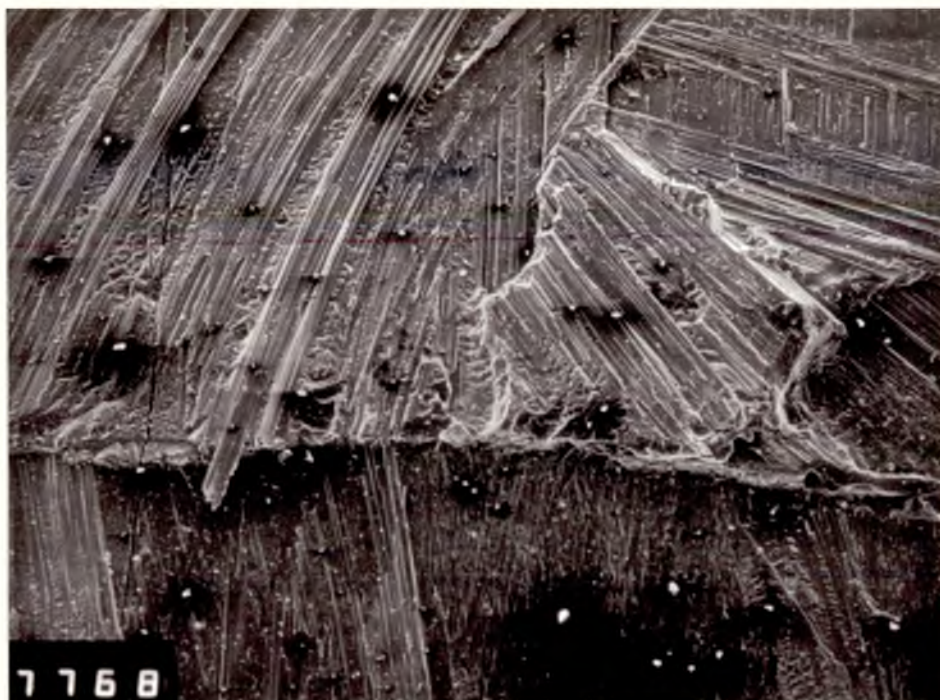showing the PEEK rich region in Figure 105. Massive
ductile fracture is apparent.

-250-

Figure 107
Fractograph of a 12·7mm sample . X 30
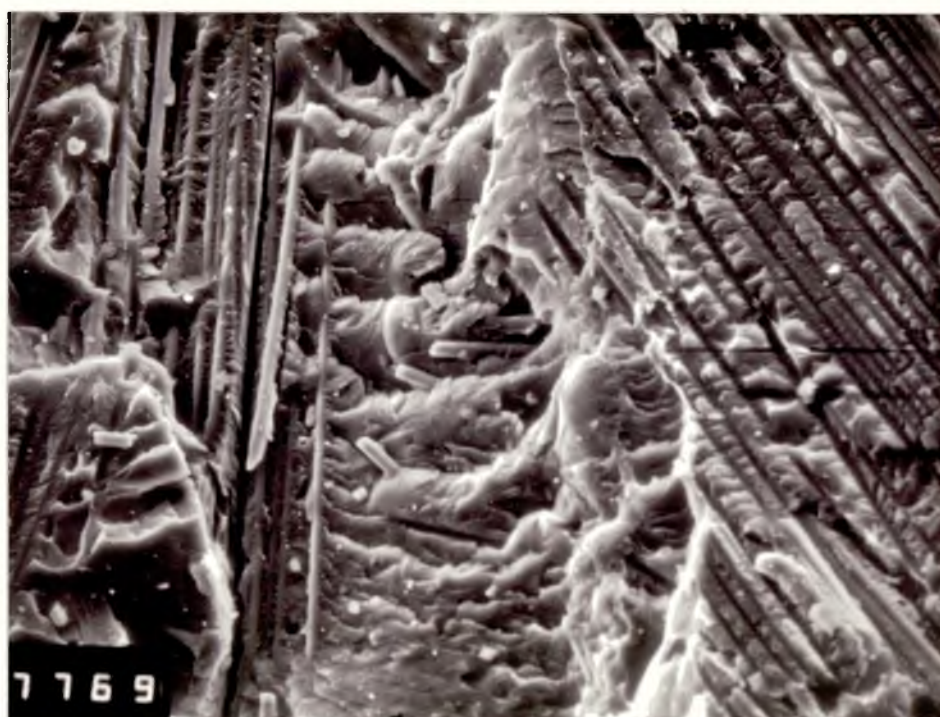
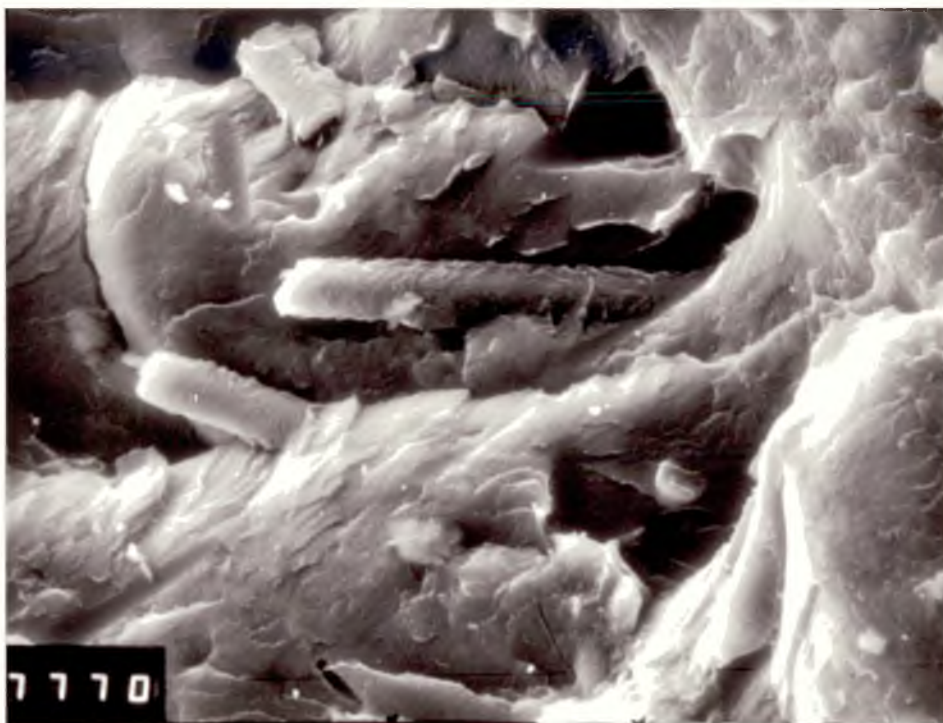Figure 108   20µ   X220
Higher magnification of Figure 107

-251-

Figure 109   10μ   X 880
Figures 107 and 108 together with this
fractograph present the small fibres in the
PEEK rich zone and how they are pulled
from the graph.
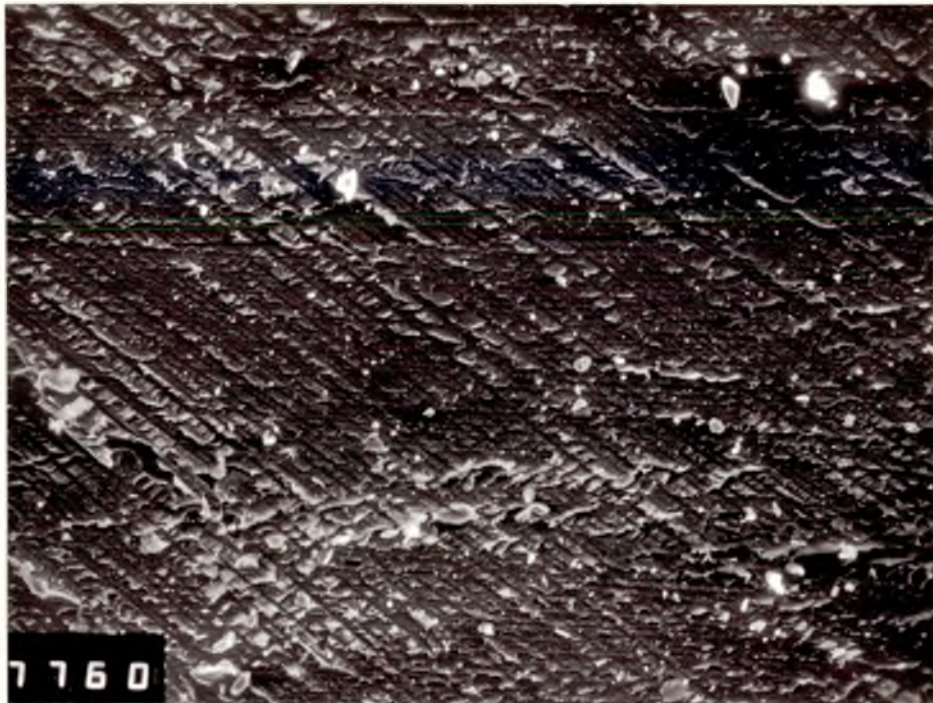
Figure 110
SEM fractograph of a 22·2mm sample   X55
showing the most common cleavage type of fracture
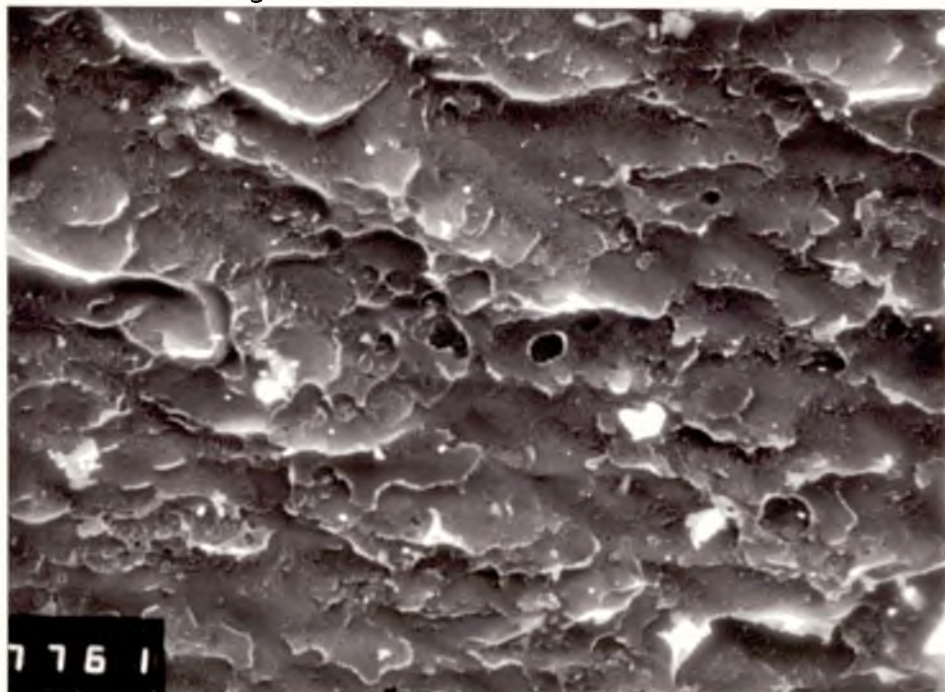through the PEEK matrix.

Figure 111   10μ   X880
As Figure 110 showing very slight deformation of
the PEEK matrix during fracture.
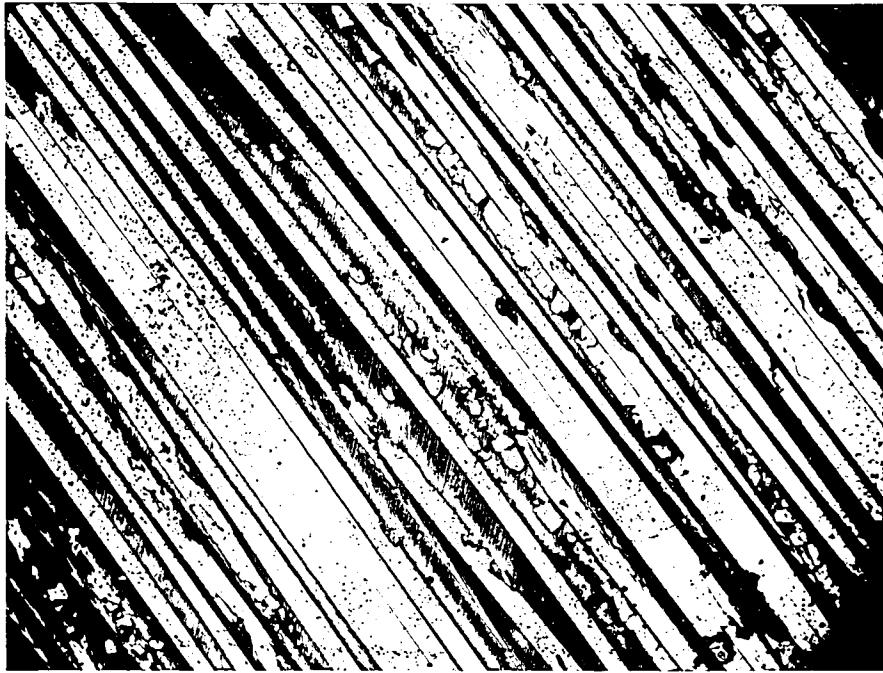
Figure 112
Top view of a polished 25·4mm sample , X400
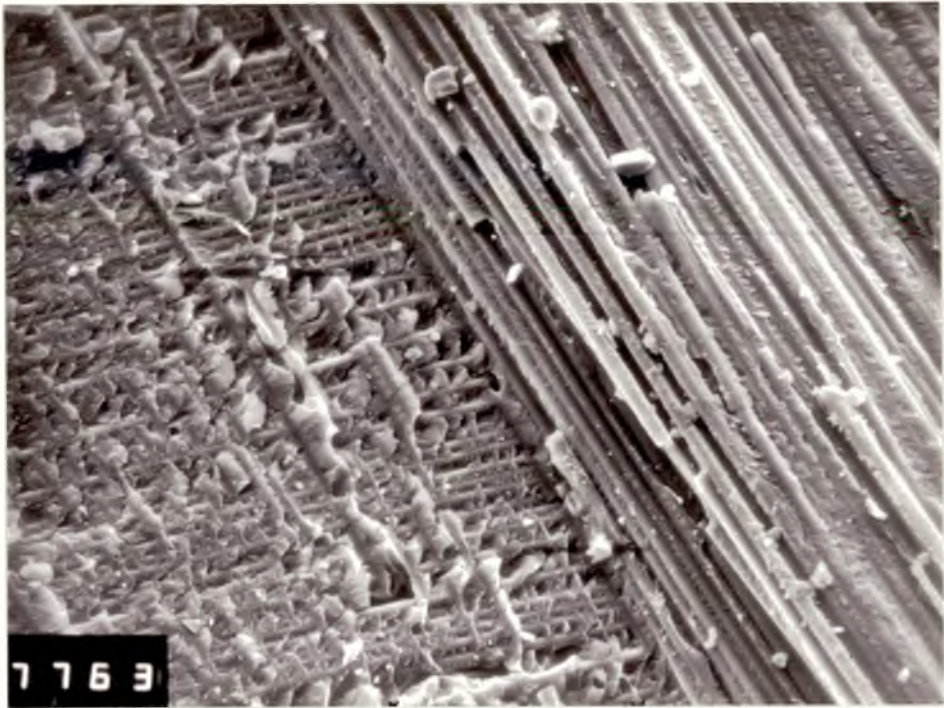showing the small gaps of PEEK between fibres.

Figure 113
SEM fractograph of a 6.35mm sample   20μ
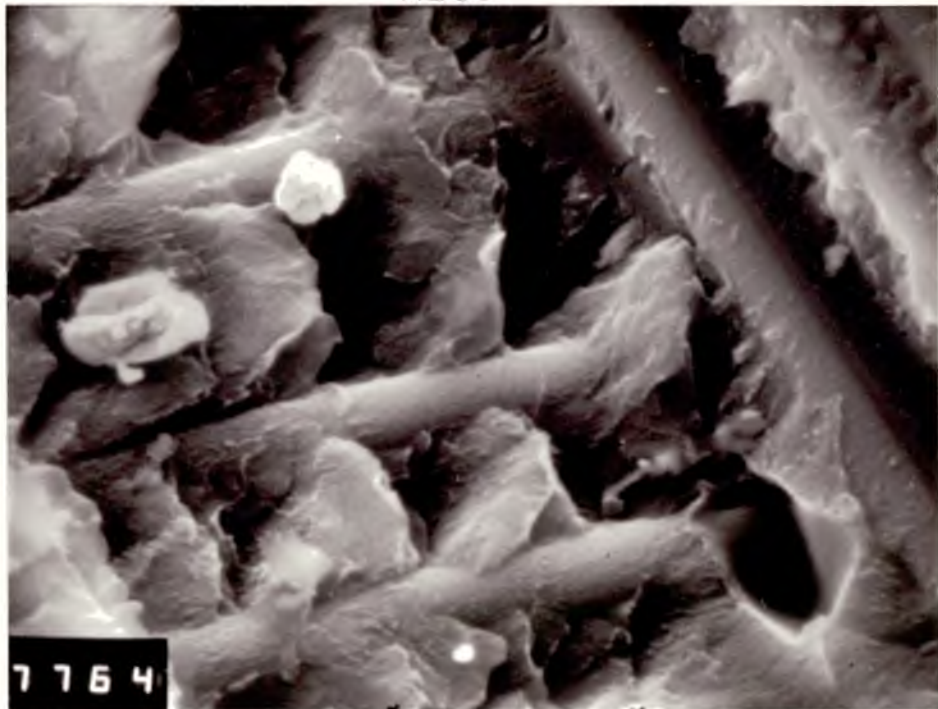showing an alternative mode of failure.
X260

Figure 114
Higher magnification view of Figure 113   10μ
showing ductile type fracture between fibres.
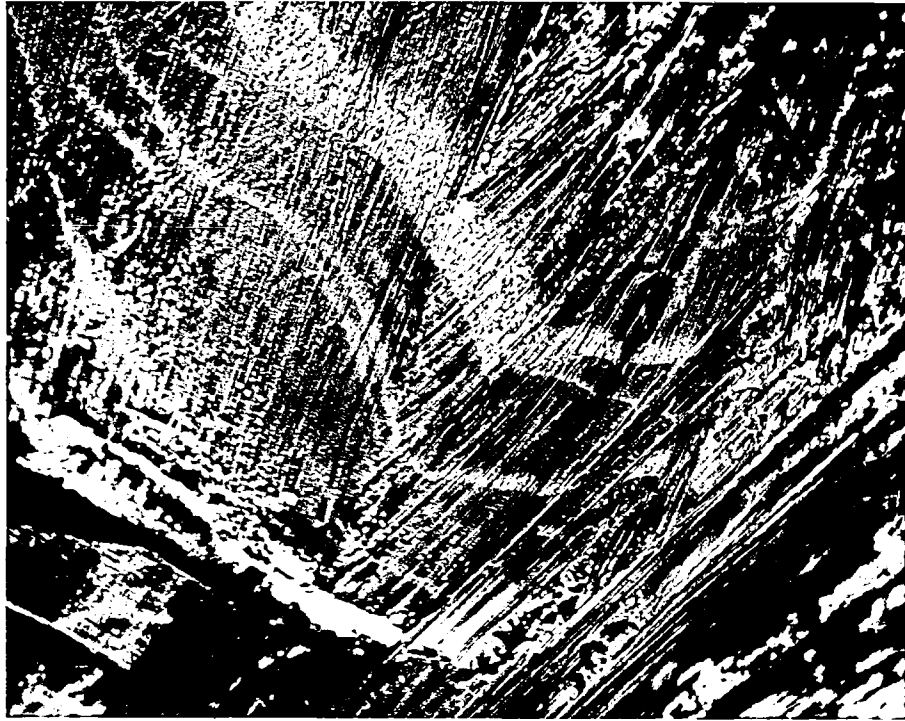X2000

Figure 115
Oblique light fractograph of a 22.2mm sample   X25
showing white areas not at particle boundaries
and forming across the fibre direction.

Figure 116   20μ   X400
Higher magnification view of white region showing
more massive deformation than the cleavage mode.
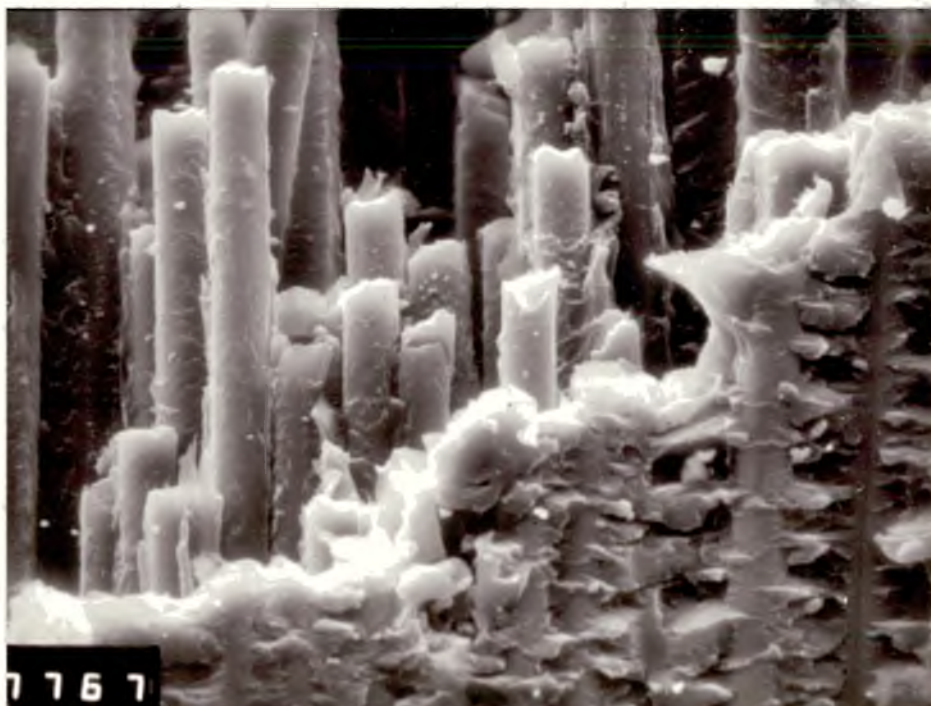
Figure 117   10μ   X 880
A combination of toughening modes.
The matrix at the fibre ends undergoes
ductile drawing, and fibre ends are pulled
through the matrix.

Figure 118

Theoretical modulus prediction for quasi isotropic
particulate APC   Tensile

Figure 119

Theoretical modulus prediction for quasi isotropic
particulate APC Flexure

Figure 120

Theoretical strength prediction for quasi isotropic particulate APC Tensile

Figure 121
Theoretical strength prediction for quasi isotropic
particulate APC   Flexural

Figure 122

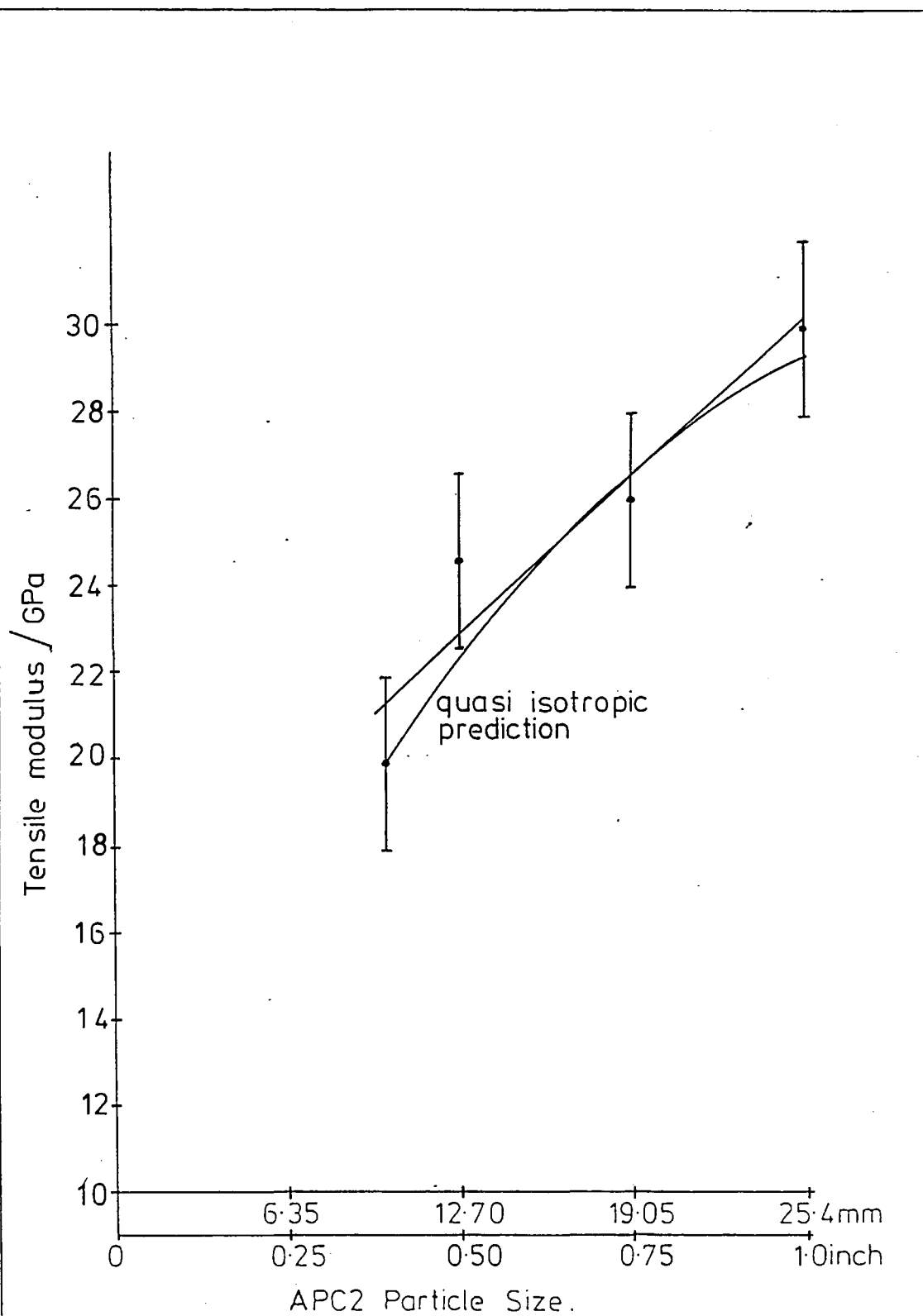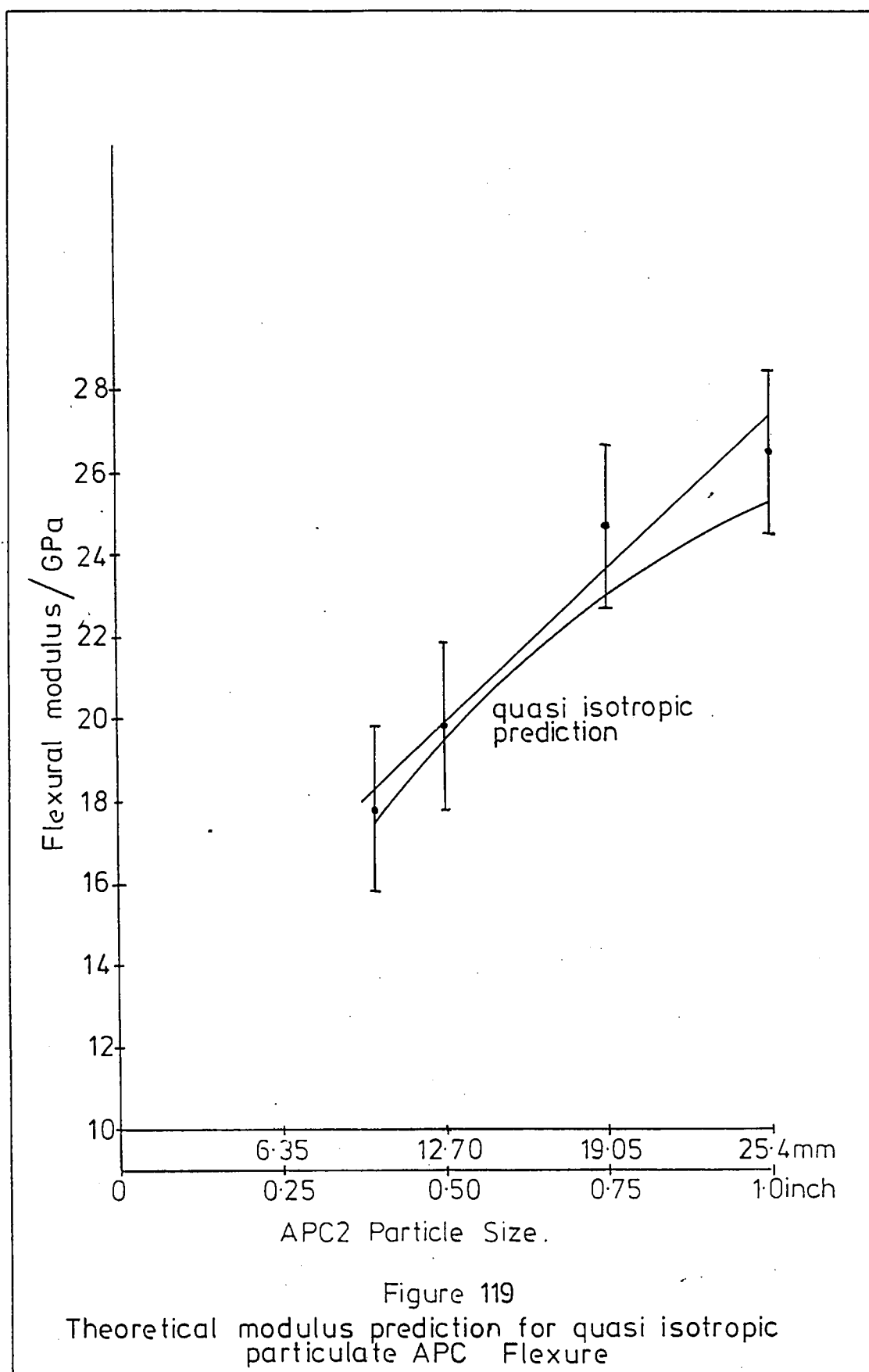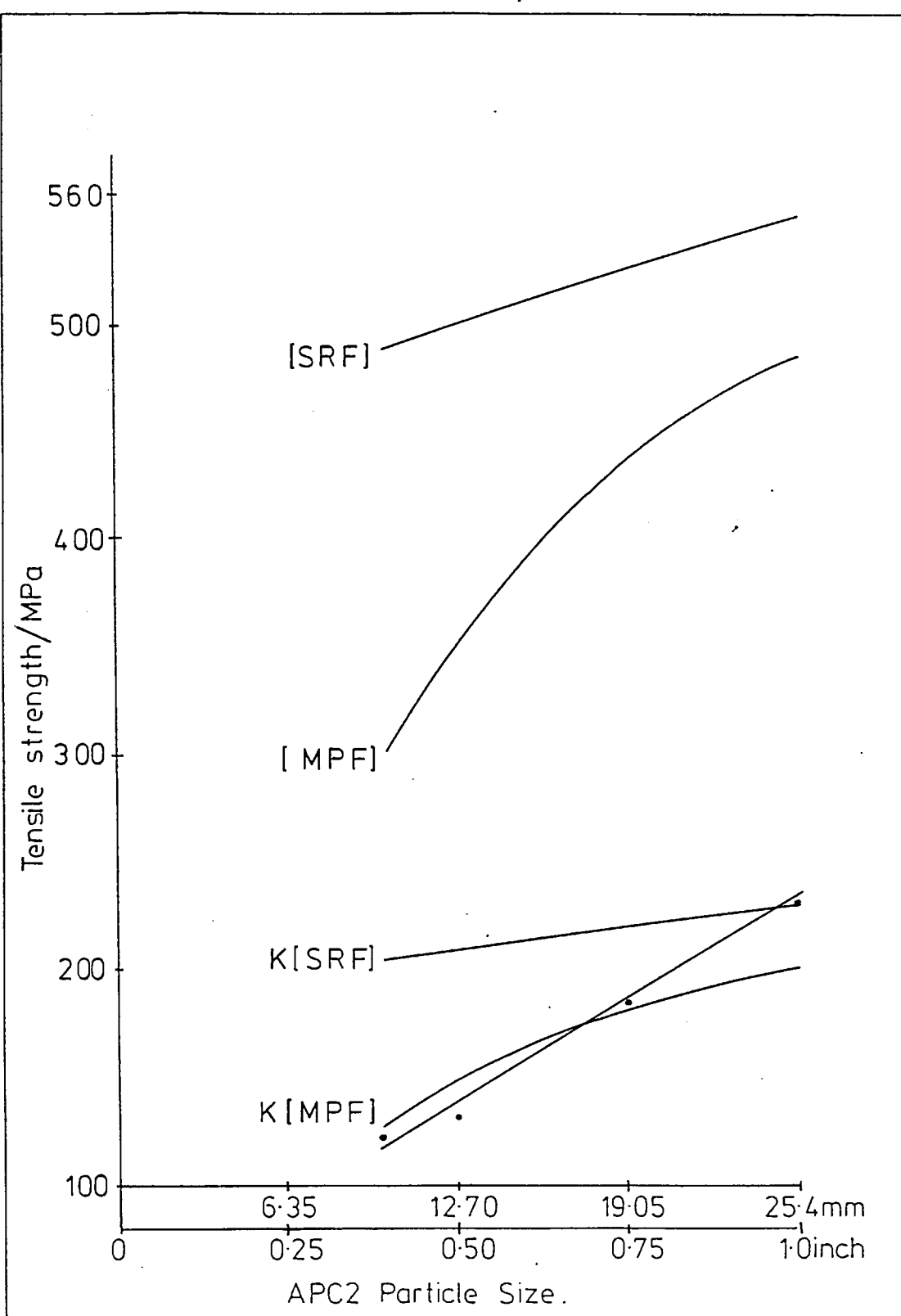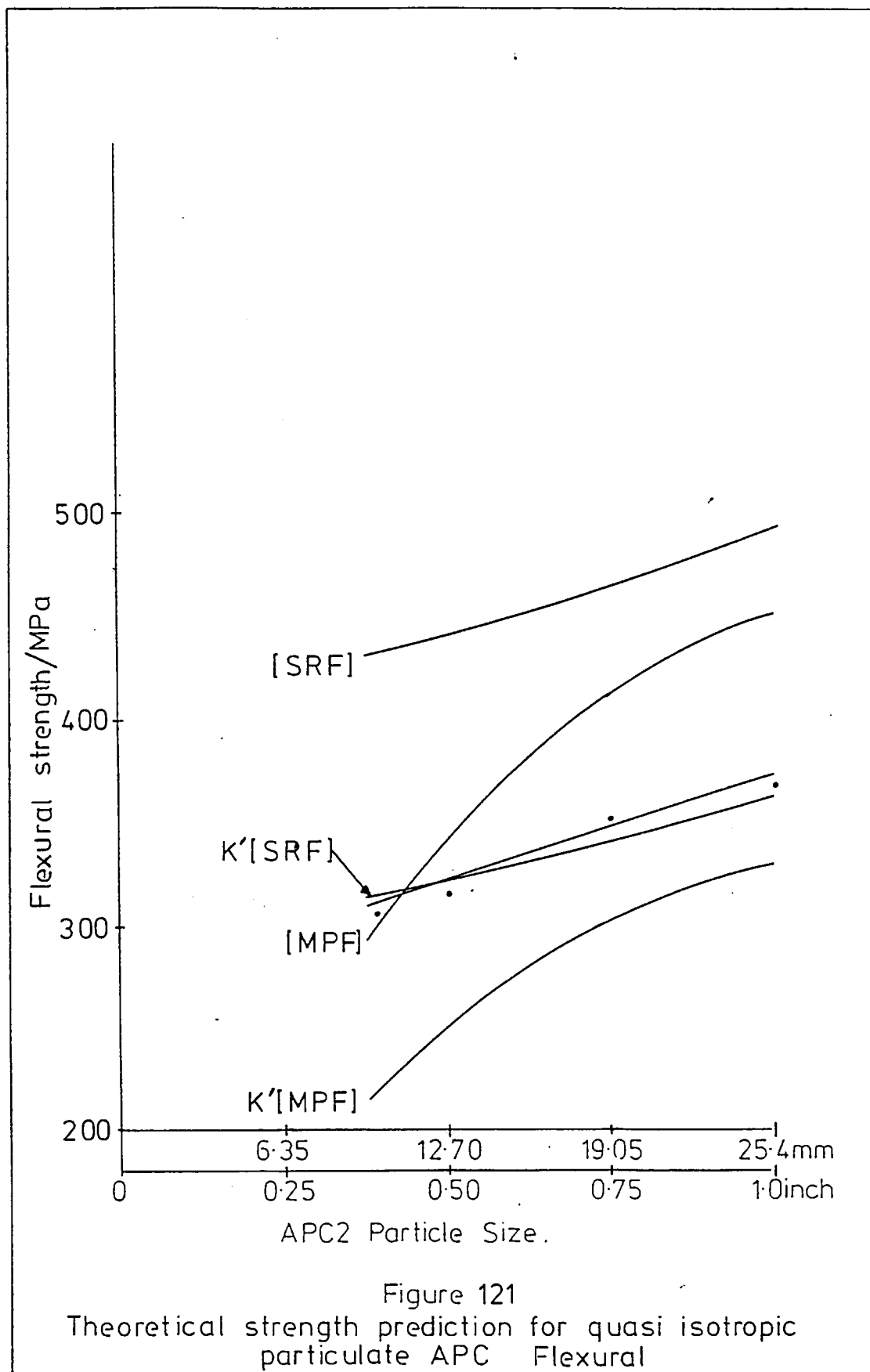Theoretical strength prediction for quasi isotropic
particulate APC Compression
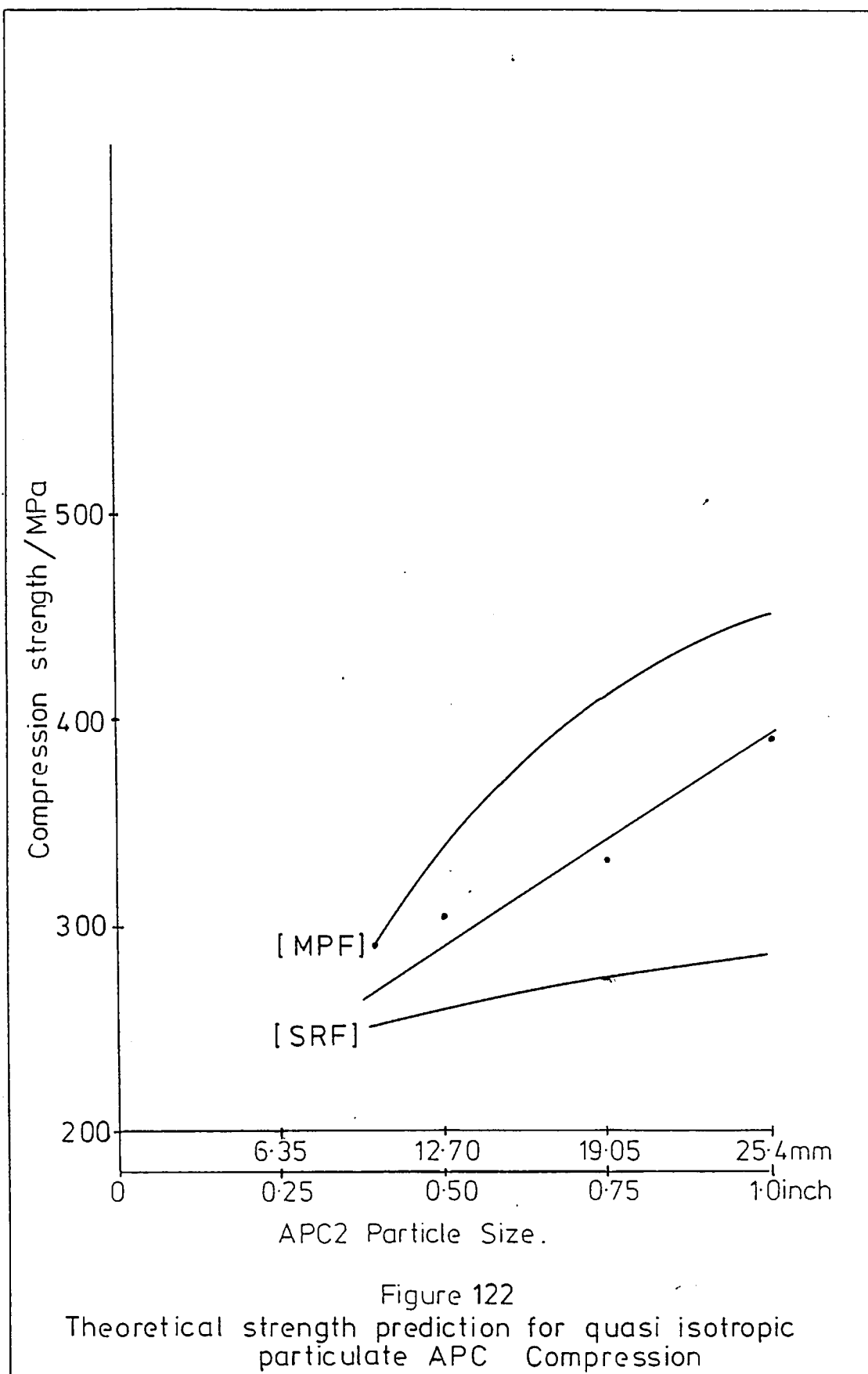
In-Plane shear modulus, G_{12}			23°C(73°F)	5.1 GPa	0.74 msi
Open-Hole tensile strength [- 45/0/+45/90]$_s$	Specimen width 38mm (1.50in)		23°C(73°F)	429 MPa	62 ksi
[(-45/90/+45/0$_s$)$_s$ /-45/+45]$_s$	Hole diameter 6.35mm (0.250in.)		23°C(73°F)	843 MPa	122ksi
Short beam shear strength	ASTM D-2344		23°C(73°F)	105 MPa°	15.2 ksi°
° Specimens do not fail in shear.					

MODE I INTERLAMINAR FRACTURE TOUGHNESS (G_{IC}) Test method	Temperature	Cleavage Mode kJ/m²	Ductile Mode kJ/m²	Cleavage Mode in lb/in²	Ductile Mode in lb/in²
Straight-sided double cantilever beam test. Data reduction by Area Method	23°C(73°F)	1.5	2.0	8.5	11.3

FIGURE I DAMAGE TOLERANCE

Lay-up: $[-45/0/+45/90]_{5S}$
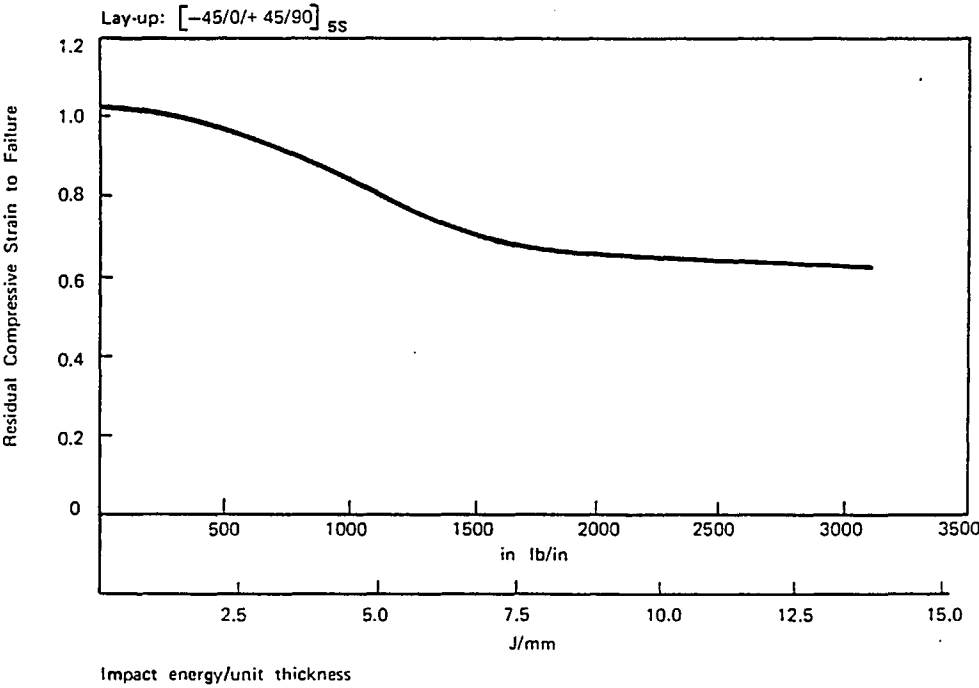
DAMAGE TOLERANCE
Residual compressive strain to failure vs applied impact energy/unit thickness

FIGURE II DAMAGE TOLERANCE

Lay-up [−45/0, +45/90]ss
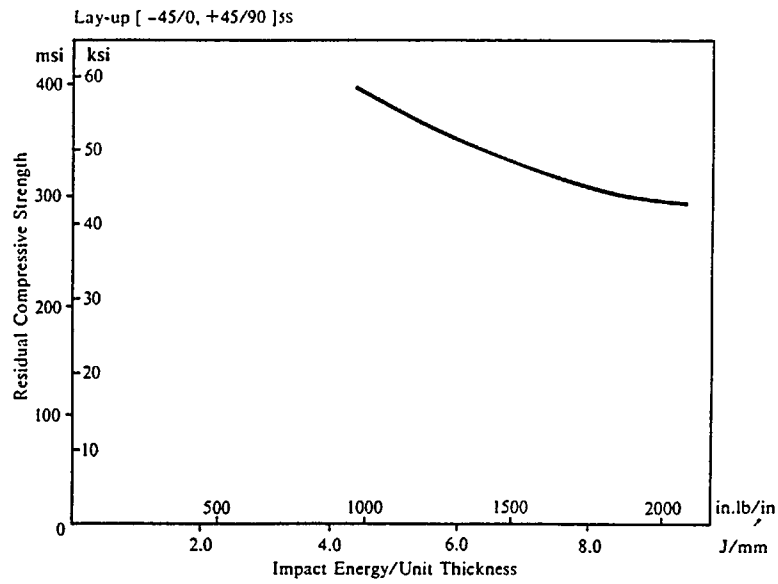
DAMAGE TOLERANCE
Residual compressive strength vs applied impact energy/unit thickness

FIGURE III INTERPOLATED CREEP DATA FOR ±45° LAY-UP AT 23°C(73°F)

± 45° CREEP DATA
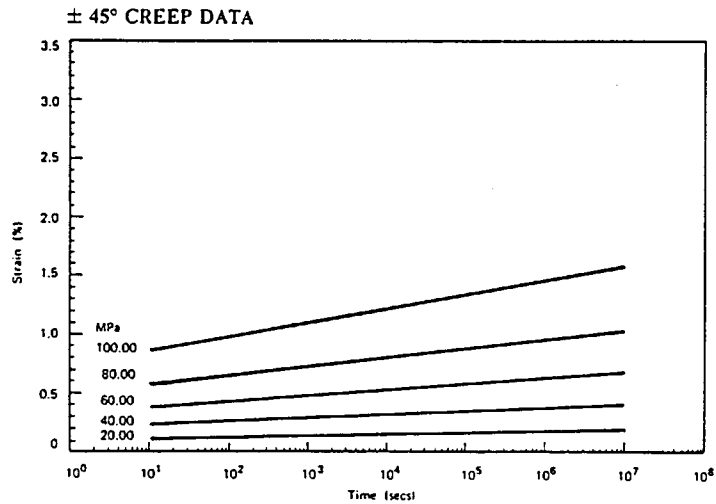
FIGURE IV INSTRUMENTED FALLING WEIGHT IMPACT TOUGHNESS
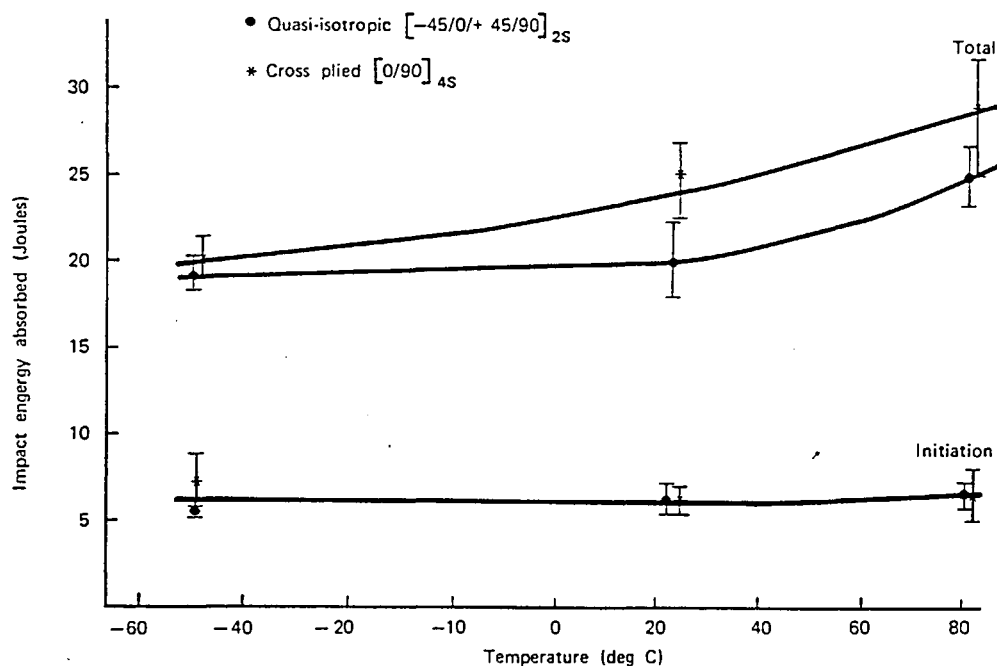
INSTRUMENTED FALLING WEIGHT IMPACT DATA VERSUS TEMPERATURE

(75mm x 75mm) plaques, 50mm diameter support, 12.5mm impactor nose, impact velocity 5m/s

Test Method: A Versatile System of Impact Tests and Data, C J Hooley, et al Kunstoffe, 72 (1982) 9.

All values quoted for properties of Fiberite's Aromatic Polymer Composites are results of tests on representative samples and do not constitute a specification.

Information contained in this publication (and otherwise supplied to users) is based on our general experience and is given in good faith, but we are unable to accept responsibility in respect of factors which are outside our knowledge or control. Freedom under patents, copyright and registered designs cannot be assumed.

*PEEK is an ICI product sold under the trade mark Victrex®

© Fiberite Corporation, 1987

Data Sheet 3a

For further information, please contact:

USA

Fiberite Corporation
28271 Verdugo
Suite A
Laguna Hill, CA 92653
Tel: (714) 472-4227
Fax: (714) 472-4353

EUROPE

Fiberite Europe GmbH
Erkelenzer Strasse, 20
D-4050 Mönchengladbach
West Germany

Tel: (02161) 58929
Fax: (02161) 570657
Telex: 8529202 TRIB

Under these high temperature fire conditions, APC-2 sheets 3 mm (0.120in) thick show significant advantages over aluminium sheets of the same thickness:-

(i) APC-2 sheets have much lower thermal conductivity than aluminium; it takes 3 times longer for the back of the APC-2 sheet to glow red compared with aluminium sheet. With the front face of APC-2 at 1100°C (2000°F) the rear face temperature was 275°C. (530°F).

(ii) APC-2 sheets resist flame penetration much longer.

APC-2 sheets were still unpenetrated after 15 minutes whereas the aluminium sheet was punctured at 5 minutes. Under the definitions of ISO/DIS2685, aluminium sheet is fire-resistant but APC-2 probably satisfies both categories of fire resistant (5 minutes) and fireproof (15 minutes).

(iii) APC-2 sheets retain their mechanical properties in the high temperature flame whilst the aluminium sheet softens at 600°C, (1100°F) and is rapidly reduced to a weak oxide film at the higher temperatures (1000°C, 1830°F) used in these tests.

TYPICAL FIRE PROPERTIES OF APC-2*

Property	Method	Units	Results
Thickness		mm	3.1
		(in)	(0.120)
Density		kg m^{-3}	1657
		lb ft m^{-3}	104
Ignitability:-			
Oxygen Index	ASTM D2863	%	67
	ISO/IS4589		,
Self-ignition temperature	ASTM D1929	°C	595
(PEEK resin)		(°F)	(1100)
Flash-ignition temperature	ASTM D1929	°C	575
(PEEK resin)		(°F)	(1070)
Flammability:-			
UL 94 Vertical			V-0
Fire resistance:-			
Flame penetration time at 1100°C	ICI propane torch	Minutes	15
Smoke:-			
NBS Smoke chamber	ASTM E662		1
Optical Density D$_m$			
(corr) in flaming mode			

* Tests were carried out under ISO standard conditions, but as yet not by ISO appointed test laboratories.

All values quoted for properties of Fiberite's Aromatic Polymer Composites are results of tests on representative samples and do not constitute a specification.

Information contained in this publication (and otherwise supplied to users) is based on our general experience and is given in good faith, but we are unable to accept responsibility in respect of factors which are outside our

For further information, please contact:

knowledge or control. Freedom under patents, copyright and registered designs cannot be assumed.

*PEEK is an ICI product sold under the trade mark Victrex®

© Fiberite Corporation, 1987

Data Sheet 4

USA

Fiberite Corporation
28271 Verdugo
Suite A
Laguna Hill, CA 92653
Tel: (714) 472-4227
Fax: (714) 472-4353

EUROPE

Fiberite Europe GmbH
Erkelenzer Strasse, 20
D-4050 Mönchengladbach
West Germany

Tel: (02161) 58929
Fax: (02161) 570657
Telex: 8529202 TRIB

APC-2
PEEK/CARBON FIBRE COMPOSITE
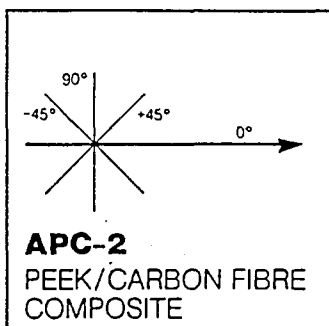
(ICI) **FIBERITE**®

DATA SHEET 3a:

Property data of aromatic polymer composite, APC-2/Hercules Magnamite® AS4 carbon fibre

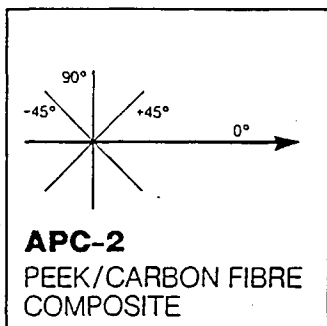APC-2: PEEK*/carbon fibre composite is an advanced structural composite of a proprietary high strength, unidirectional continuous carbon fibre in a PEEK matrix.

PHYSICAL PROPERTIES

Density	1.6 g/cm³ (0.058 lb/in³)
Carbon fibre volume fraction	61%
Carbon fibre weight fraction	68%
Carbon fibre areal weight	145 g/m³

COEFFICIENT OF THERMAL EXPANSION

Fibre Orientation	Temperature	
0°	23°C-143°C (73°F-289°F)	0.5x10⁻⁶/°C (0.28x10⁻⁶/°F)
	143°C-343°C (289°F-649°F)	1.0x10⁻⁶/°C (0.56x10⁻⁶/°F)
90°	23°C-143°C (73°F-289°F)	30x10⁻⁶/°C (17x10⁻⁶/°F)
	143°C-343°C) (289°F-649°F)	75x10⁻⁶/°C (42x10⁻⁶/°F)

MECHANICAL PROPERTIES

Property	Test Method	Temperature		
0°	ASTM D-3039	23°C(73°F)		
Tensile strength			2130 MPa	309 ksi
Tensile modulus			134 GPa	19.4 msi
Tensile strain to failure			1.45 %	
Compressive strength	IITRI Test	23°C(73°F)	1100 MPa	160 ksi
Flexural strength	ASTM D-790 Span-to-depth ratio 60:1	23°C(73°F)	1880 MPa	273 ksi
Flexural modulus			121 GPa	17.5 msi
90°	ASTM D-3039	23°C(73°F)		
Tensile strength			80 MPa	11.6 ksi
Tensile modulus			8.9 GPa	1.29 msi
Tensile strain to failure			1.0 %	
Flexural strength	ASTM D-790 Span-to-depth ratio 25:1	23°C(73°F)	137 MPa	19.9 ksi
Flexural modulus			8.9 GPa	1.29 msi
± 45°	ASTM D-3518			
Tensile strength		−73°C(−99°F)	267 MPa	38.7 ksi
		23°C(73°F)	300 MPa	43.5 ksi
		120°C(248°F)	221 MPa	32.0 ksi
Tensile modulus		−73°C(−99°F)	21.9 GPa	3.18 msi
		23°C(73°F)	19.2 GPa	2.78 msi
		120°C(248°F)	12.9 GPa	1.87 msi
Tensile strain to failure		−73°C(−99°F)	19.9%	
		23°C(73°F)	17.2%	
		120°C(248°F)	18.0%	

Fire property data of aromatic polymer composite, APC-2

SUMMARY

APC-2: PEEK*/carbon fibre composite has very good resistance to burning. It is difficult to ignite and exhibits low flame propagation rates by standard laboratory tests. The smoke emission from APC-2 during a fire is amongst the lowest of all plastics.

Sheets of APC-2 material show significantly longer flame penetration times than aluminium sheets at temperatures above 1000°C (1830°F).

Values quoted for properties are the result of limited tests on representative samples. These values do not constitute design data. Additional and more comprehensive data will be published in due course after further testing.

IGNITABILITY*

A commonly used test method for determining ignitability is the Oxygen Index Test (ASTM D2863, ISO/IS4589). This measures the minimum percentage of oxygen necessary in an atmosphere to support combustion. APC-2 has an Oxygen Index of 67%. This value is high by comparison with other composites.

The difficult ignitability of PEEK resin alone has also been demonstrated in other tests. Self-ignition and flash-ignition temperatures were determined using the Setchkin hot-air ignition furnace (ASTM D1929-75). Results in the range 575°—600°C (1070°—1100°F) were obtained in these tests.

FLAME PROPAGATION*

The Underwriters Laboratories Standard 94 is used to evaluate the flammability of materials. APC-2 readily achieves the lowest flammability rating of V-0 when tested in accordance with UL94, Vertical Burning Test.

The flame spread characteristics have been measured in accordance with FAR 25.853. The results obtained from this test carried out on APC-2 are:

Horizontal mode: burn rate	: 0
Vertical mode : Average burn length	: 14 mm (0.6 in)
Average flaming time after removal of test flame	: 0 secs

SMOKE*

APC-2 is one of the lowest smoke emitting materials evaluated in the NBS Smoke Chamber. This test (ASTM E662, BS 6401) provides a measure of the obscuration of visible light by smoke in units of specific optical density. The NBS smoke test is normally carried out in two modes; flaming and non-flaming. Under the conditions of the flaming mode, the maximum specific optical density obtained for APC-2 was:-

$$D_m(corr.) = 1$$

FIRE RESISTANCE*

Many components of an aircraft structure are required to be fire-resistant. As defined by the ISO Standard DIS2685, this means that structural material should have a flame penetration time at 1100 ± 50°C (2000° ± 120°F) which is at least equal to aluminium alloy sheet. Experiments have been carried out to determine the penetration times of APC-2 versus aluminium alloy sheet to a propane-air burner at 1050°C (1900°F). (Fig. 1).

Figure 1

APC-2 PEEK/CF COMPOSITE FAA FLAME PENETRATION TEST

28 in. Square (700 mm)
Front Surface 2000°F (1090°C)
Propane Flame 2000°F (1090°C)
Rear Surface 700°F (370°C)
0.080 in. thick (2 mm)
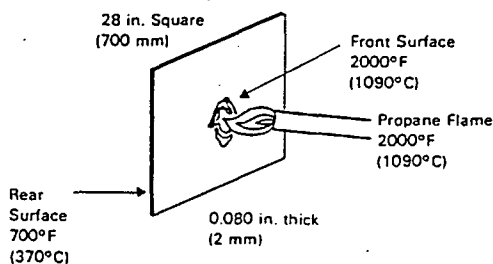
Burn through time 15—18 mins.

ULTRASONIC PRINCIPLES

The Model FTS MARK IV Mainframe generates ultrasonic vibrations and sends them through the object tested in a beam of short bursts of energy. Any discontinuity in the path of the ultrasonic beam, as well as the far side of the test object, reflects the vibrations back to the instrument. The time required for the initial pulse to travel through this material and subsequently return as an echo is displayed on a cathode ray tube (CRT) as a thickness or distance measurement.

The sound waves are generated as recurrent changes in electrical voltage occurring at an ultrasonic rate, since they are above the audible range. Ultrasonic vibrations of lower frequencies act in essentially the same manner as do audible sound waves. Ultrasonic waves of the higher frequencies behave somewhat like light waves. Ultrasonic vibrations have two basic characteristics:

a. They are reflected by mechanical discontinuities occuring in the medium through which they are traveling:

b. They tend to travel in a straight line, as do light waves, due to the shortness of the wave lengths employed.

Ultrasonic waves can be propagated to some extent in any elastic material. This propagation, or traveling, of the waves occurs as a displacement of the successive elements of the medium. In any elastic substance there is a restoring force which tends to restore each element of material back to its original position after movement.

Since all elastic substances also possess inertia, the particle continues to move after it returns to the location from which it started and finally reaches another location past the original one. It will then continue to bounce back and forth with a constantly diminishing amplitude. The particles of the material will execute different movements, or orbits, as the wave passes through them. The overall effect is to attenuate the strength of the ultrasonic energy traveling through this medium.

Longitudinal, or compression, waves exist when the motions of the particles of a medium are parallel to the direction of waves traveled. It is the type used when employing the straight beam technique of testing. This type wave is most often used in ultrasonic testing, since it will travel in liquids or solids, and is easily generated and detected. Longitudinal waves have a high velocity of travel in most materials, and the wave lengths in common materials are usually very short in comparison with the cross sectional area of the crystal used. This property allows the ultrasonic energy to be directed into a sharp beam, a fact which permits accurate location of defects.

When shear waves are generated in a material, the movements of the particles in that medium are at right angle to the direction of wave propagation. They usually travel in a beam form of small cross section. Shear waves have a velocity that is approximately one-half that of longitudinal waves. The shear wave is the type that is generated when using the angle beam technique of testing.

Because of their lower velocity, the wave length of shear waves is much shorter than that of longitudinal waves. This shorter wave length makes them more sensitive to small discontinuities and they are more easily scattered within a material. Shear waves will not travel in gases or liquids, these materials being inelastic to shear and therefore incapable of supporting shear waves.

APPLICATION OF ULTRASONIC PRINCIPLES

All ultrasonic testers manufactured by Sonic Instruments generate an electrical signal that changes at an ultrasonic frequency. A transducer utilizes the Piezoelectric principle to convert the electrical energy into mechanical vibrations that penetrate through the material. Energy passing through the material is reflected partially by any discontinuities in its path or almost totally by the back surface. The vibrations sensed by the transducer are treated in a reverse manner to convert back to electrical energy, which is processed and displayed by the tester. The vibrations can be from discontinuities in the energy path or the multiple reflections from the back surface.

The tester will detect any appreciable discontinuity or lack of elasticity in a material under test. It will detect and locate holes or cracks within a solid mass of elastic material within the sensitivity limits. The nature of the discontinuity which causes a variation in material elasticity does not influence the ability of the instrument to detect. A drilled hole or a flaw such as a blow hole of equal projected area will indicate in the same manner.

The defect size which can be detected is also dependent upon the grain size of the material. If a part has a natural grain size of one-eighth inch diameter, it will be difficult to distinguish a one-eighth inch defect. The ultrasonic wave will be affected by all of these segregations without regard to the difference in size. To summarize, if the material is homogeneous except for the defects, or if the defects are larger than any natural discontinuity within the material, the tester will detect them, provided that there are not so many defects that the sound beam cannot penetrate the material.
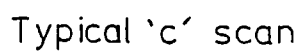
Typical 'c' scan

The mechanical properties of compression moulded reconstituted carbon fibre reinforced PEEK (APC-2)

G. C. McGRATH*, D. W. CLEGGt, A. A. COLLYER‡

(*Royal Aircraft Establishment/tUniversity of Nottingham/‡Sheffield City Polytechnic, UK)

Results from tensile and flexural tests on reconstituted carbon fibre-reinforced PEEK show that the variations in the tensile and flexural moduli of the composites increase linearly with the size of the particles in the moulding. Quasi-isotropic theory enables an accurate prediction of the experimental values from the modulus reduction factor relationship. A similar approach with respect to experimental strength can only be applied if the mode of failure is known.

Key words: composite materials; carbon fibre reinforcements; polyetheretherketone; mechanical properties; recycling; reconstituted composites

Aromatic Polymer Composite (APC-2) is a continuous carbon fibre reinforced polyetheretherketone (PEEK), containing 68% by weight carbon fibre. It is available from Fiberite Europe. Like all carbon fibre composite materials it is inherently expensive and, as such, any waste material from pattern cutting that could be re-used would be extremely valuable. One method that has been tried is to fragment the material and to compression mould it into a sophisticated chipboard. This fragmentation was achieved by a 'monomuncher', which is based on two parallel, inwardly rotating shafts each fitted with intermeshing cutting teeth. The shafts rotate at different speeds so that as well as a nip by the teeth there is a tearing and shearing action between the opposing teeth. The fragments are ragged and of variable length and very little regularity, which is necessary for mathematical modelling, is achieved. Therefore, a more suitable method is to cut the waste material into platelets of uniform size and to compression mould these into a composite sheet that can be mathematically analysed. Thus, a composite material can be manufactured from planar particles.

In the present work, squares of various sizes from 6.35 to 25.4 mm (0.25–1 in) were cut from APC-2 pre-preg of thickness 0.125 mm and compression moulded into plaques 150 mm square and 2 mm thick. The flexural, tensile, and compression behaviours of these materials were determined as a function of particle size and their performance was compared with theoretical values calculated from the theory of planar reinforcement.

THEORY

The main difference between fibre and planar reinforcements should be a numerical factor that will account for the different geometry and the effects of stress transfer between the different planes of the flakes. The theory of planar reinforcement is based on fibre reinforcement theory with flake reinforcement being analogous to short fibre reinforcement. The details of the theory are given by McGrath and Collyer[1] and the resulting equations are derived in terms of a Modulus Reduction Factor [MRF]; Strength Reduction Factor [SRF] and Matrix Performance Factor [MPF].

$$[\text{MRF}] = 1 - \frac{\ln(u+1)}{u} \qquad (1)$$

where

$$u = \left[\frac{G_m \phi_f}{E_f(1-\phi_f)}\right]^{1/2} \qquad (2)$$

where G_m is the matrix shear modulus, E_f is the tensile modulus of the fibre, and ϕ_f is the volume fraction of the flakes.

The rule of mixtures becomes:

$$E_c = \phi_f E_f [\text{MRF}] + (1 - \phi_f)E_m \tag{3}$$

where E_c is the modulus of the composite and E_m is the modulus of the matrix. Strength predictions are more complex, and the validity of the theory depends on the failure mode, which itself depends on the aspect ratio and interfacial shear strength,[2] τ:

$$\frac{W_c}{t} = \frac{\sigma_f}{\tau} \tag{4}$$

Where t is the flake thickness, σ_f is the rupture strength and W_c is the critical flake width.

Only if the flake width is greater than W_c will the composite fail by fracture of the reinforcements, otherwise a lower level flake pull-out occurs, without full utilization of the reinforcement because the flakes are too small to enable transfer of stress up to their breaking strengths[3].

Flake fracture

The strength reduction factor [SRF] accounts for the discontinuous nature of the reinforcement:

$$\sigma_c = \phi_f \sigma_f [\text{SRF}] + \phi_m \sigma'_m \tag{5}$$

where

$$[\text{SRF}] = \left\{ \frac{1 - \dfrac{\tanh(u)}{u}}{1 - \text{sech}(u)} \right\} \tag{6}$$

σ'_m is the tensile strength in the matrix at rupture $\sigma'_m = \sigma_m/3$, where σ_m is the tensile strength of the matrix.

Flake pull-out

Failure of the matrix results in pull-out of flakes, the matrix performance factor [MPF] characterizes this type of failure:

$$\sigma_c = \phi_f \tau_m [\text{MPF}] + \phi_m \sigma''_m \tag{7}$$

where

$$[\text{MPF}] = \frac{\alpha}{u} \left\{ \frac{1}{\tanh(u)} - \frac{1}{(u)} \right\} \tag{8}$$

where τ_m is the shear rupture stress of the matrix or interface, whichever is the lower, σ''_m is the tensile strength in the matrix at rupture and α is the aspect ratio. In this mode of failure, σ''_m approximates to σ_m.

EXPERIMENTAL

Samples were prepared using a matched metal mould in conjunction with a twelve inch ($\approx$300 mm) Moore's press at 390°C (platen temperature) and a consolidation pressure of 5.5 MPa. High temper aluminium sheet was used as a release ply, with both the mould and aluminium being coated with a suitable release agent.

Unless otherwise stated, the particles of prepreg were scattered by hand into the mould to obtain approximate random fibre directions and so produce isotropic sheet. The plaque was moulded as described above and post consolidation cooling was effected by an air quench

through the platens at 7°C min⁻¹ to 300°C, followed by a water quench to 70°C.

Initial isotropic samples, each containing a single particle size, were manufactured using a matched metal mould in conjunction with a press at 390°C. A range of single ply particle sizes was employed, from 6.35 mm square to 25.4 mm square; a final choice being randomly sized particles from 'monomunching'. Thus a series of samples were available for evaluation, and the properties of initial interest were those derived from tensile, flexure and compression tests. The test methods were in accordance with the recommendations of ASTM standards.

Before testing, the homogeneity of the samples was assessed by ultrasonic C-scanning.

Flexure

The advantages of flexure as compared with tension for strength evaluation on brittle materials are that the results are less sensitive to slight misalignment of the specimen–apparatus assembly, and the stress field is such as to limit the region in which failure is likely to initiate.[4]

The classical elasticity formula can be used and the maximum stress, σ, presumably the breaking stress, is given by:

$$\sigma = \frac{3\,PL}{2\,b\,d^2} \tag{9}$$

where L, is the span, b is the width, d is the thickness and P is the maximum force recorded during the test.

The modulus of elasticity E_f, is the ratio within the elastic limit of stress corresponding to strain. This was calculated by drawing a tangent to the steepest initial linear portion of the load/deflection curve and:

$$E_f = \frac{L^3 m}{4\,b\,d^3} \tag{10}$$

where m is the slope of the tangent to the initial linear portion of the load/deflection curve.

Tension

Tensile testing machines seldom apply an accurate axial stress to the specimen at low elongations, which are experienced with APC-2; some bending is usually superimposed on the tension and the maximum stress in one face of the specimen is, therefore, greater than the recorded average stress. A brittle specimen, therefore, breaks at a recorded stress that is lower than that which actually initiated failure.

The tensile strengths, S, was calculated from:

$$S = \frac{P}{b\,d} \tag{11}$$

The modulus of elasticity being:

$$E_t = \frac{m\,l}{b\,d} \tag{12}$$

where l is the gauge length of the extensometer.

Compression

For continuous fibres aligned in one direction it has been found that the strength under compression in one direction is less than that under tension. The basis of the failure, when it occurs, has been attributed to shear yield in the resin, debonding of the fibres, voids and differential effects arising from differences in Poissons ratio.[5]

APC-2, as engineering materials, is used in compressive loading applications, therefore, there has been an interest in the compressive strength. The test method used for compressive strength was the Illinois Institute of Technology Research Institute IITRI Test Method.[6]

RESULTS AND DISCUSSION

The mechanical properties of continuous fibre reinforced PEEK, APC-2, were determined as a control and these are presented in Table 1.

The flexural, tensile and compressive properties of the reclaimed material are presented as a function of particle size, in Figs 1–5; and linear relationships were found to exist between the variables, within experimental error.

In trying to develop a model to explain the mechanical properties it is necessary to examine the fracture process. Wherever it occurs, whether by flexure, tension, or compression it is for one or more of the following reasons: (i) cohesive failure of the matrix; (ii) cohesive failure of the reinforcement; or (iii) adhesive failure at the interface or interfacial region.

Reinforcement failure occurs when the stress in the direction of the particle axis exceeds a certain value, and usually precedes total failure where matrix cracking or interfacial debonding takes place. In some instances it is believed that the origin of fracture cracking is through microcracks produced by differential expansion effects attendant on cooling after moulding, or in subsequent thermal cycling.

An idea of failure mode can often be gained from the appearance of the fracture surface. For example, if fracture takes place at an interface, then flakes are pulled out with little or no polymer adhering to them. Conversely, in matrix failure, the flake will be pulled out with the polymer adhering to the flakes. In cases

where there is strong interfacial bonding flake fracture may be observed, with very few platelet ends being visible.

The two graphs of modulus have uniform gradients of $0.26\,\mathrm{GPa\,mm^{-1}}$, and so it is assumed that there is a relationship between particle size and modulus.

However, the strength graphs show no such relationship because the mode of failure changes with particle size.

Tensile modulus

The application of the Modulus Reduction Factor [MRF] depends upon successful intepretation of its various components given in Equations (1) and (2).

The matrix shear modulus of PEEK, G_m, is 1.3 GPa, and so this term is constant. The aspect ratio, α, varies only with particle size; but there are two ways in which the tensile modulus, E_f, of the flake could vary with volume fraction, ϕ_f.

This gives rise to two approaches:

- Analysis of the data by simple volume fraction considerations and assuming the modulus of a unidirectional reinforcement. If this is so:

$$u = \alpha(0.1436)$$

- Alternatively, a novel approach would be to propose that E_f takes account of the anisotropy within the flake and takes the modulus of a quasi-isotropic lay-up or a $(0, 90)_s$ lay-up, such an arrangement would mean that $\phi_f/(1 - \phi_f)$ is unity. Then:

  for quasi-isotropic, $u = \alpha(0.1636)$
  or for $(0, 90)_s$ lay-up, $u = \alpha(0.1346)$

These predictions are presented in Fig. 1 and they suggest that the most applicable approach to the problem is the quasi-isotropic prediction.

It is readily observed that it is virtually impossible for the reinforcement theory based on a unidirectional lay-up to be effective as this predicts a modulus greater than that of a quasi-isotropic lay-up at a particle size less than 6.35 mm square. Of the other two lay-ups, it is suggested that the $(0, 90)_s$ predictions are more relevant to an ordered and therefore, anisotropic lay-up.

Table 1. Characterization of APC-2

	Macrostructure of the APC-2 samples							
	$(0)_{16}$		$(90)_{16}$		$(0, 90)_{4S}$		$(+45, 90, -45, 0)_{2S}$	
Flexural strength (MPa)	1876	(49.0)	140	(6.4)	1163	(30)	616	(34.7)
Flexural modulus (GPa)	130	(1.7)	10.3	(0.3)	68.8	(2.4)	40.9	(2.1)
Tensile strength (MPa)	2125	(31.0)	80.0	(1.6)	1023	(47.0)	704	(26.0)
Tensile modulus (GPa)	135	(2.1)	9.3	(0.4)	71.8	(1.6)	48.6	(2.9)
Tensile strain (%)	1.45	(0.2)	1.0	(0.2)	1.35	(0.15)	1.69	(0.1)
Compression strength (MPa)	1094	(46.0)			742	(29.3)	361	(20.1)

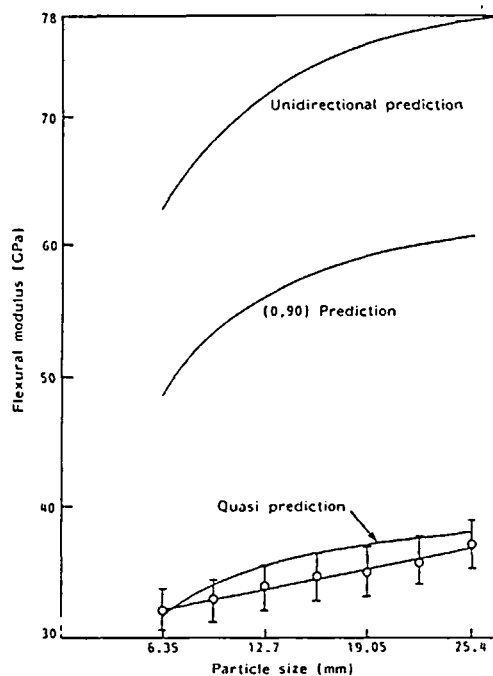(Standard deviations are given in parentheses)
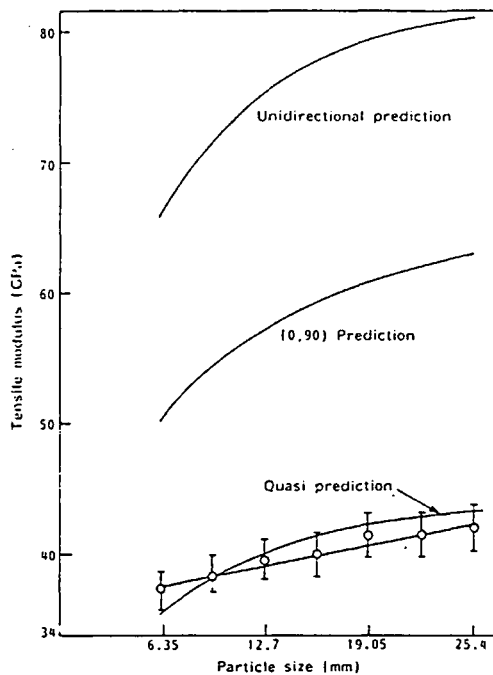
Fig. 1 Theoretical modulus predictions versus particle size (tensile loading)

This leaves the predictions of a quasi-isotropic property profile. Practical results are superimposed onto Fig. 1 to confirm this.

Flexural modulus

To substantiate the previous prediction, the same analysis is applied to the flexural modulus equation, giving the following values:

unidirectional, $u = \alpha(0.1458)$
quasi-isotropic, $u = \alpha(0.1783)$
$(0, 90)_s$ lay-up, $u = \alpha(0.1375)$

The subsequent predictions are presented in Fig. 2 from which the quasi-isotropic predictions would appear to be experimentally justified.

Strength

The strength predictions where flake fracture occurs are dependent upon the [SRF] as in Equation (6), whereas, if flake pull-out is the cause of failure, then the [MPF] applies, as in Equation (8).

The quasi-isotropic theory previously applied to explain the modulus variation may also be applied to the strength behaviour, bearing in mind a possible complication caused by a fracture mode dependent on particle sizes.

Presented in Figs 3–5 are the three strengths which have been examined in a thoeretical model. There are two relevant observations to be made from this:
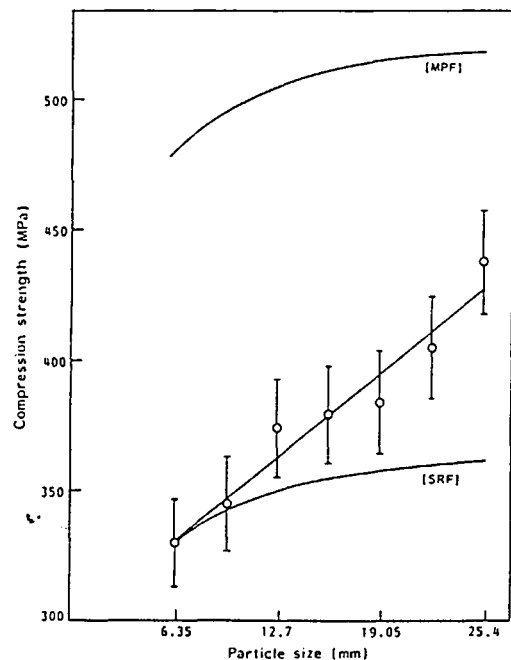

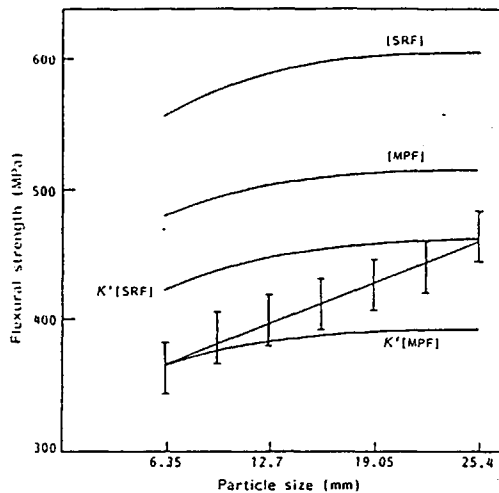Fig. 2 Theoretical modulus predictions versus particle size (flexural loading)

Fig. 3 Theoretical strength predictions versus particle size (compressive loading)

214

Fig. 4 Theoretical strength predictions versus particle size (flexural loading)

Fig. 6 Scanning electron micrograph of a fracture surface showing flake pull out and flake fracture (×1260)

- Predicted strengths are generally very much higher than measured strengths. This is explained by Padawer and Beecher,[7] who propose a constant in Equation (5) such that:

$$\sigma_c = \phi_f \sigma_f \, [\text{SRF}] \, K + \phi_m \sigma'_m \qquad (13)$$

K, being less than unity represents the strength loss due to material inhomogeneities and fabricating defects. Equation (5) thus represents an upper bound.

- The predicted gradient is considerably less than the measured gradient. This is explained by consideration of the failure mode. When mouldings are made from small particles flake pull-out
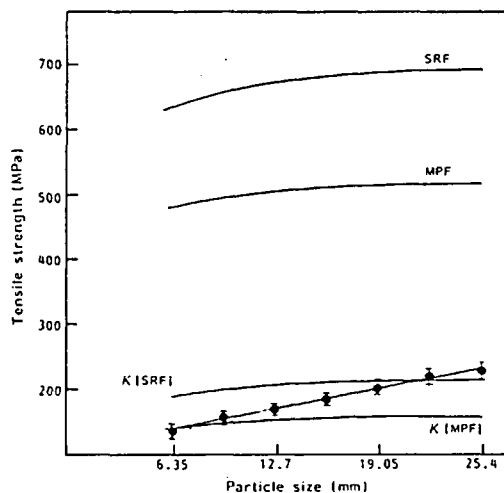

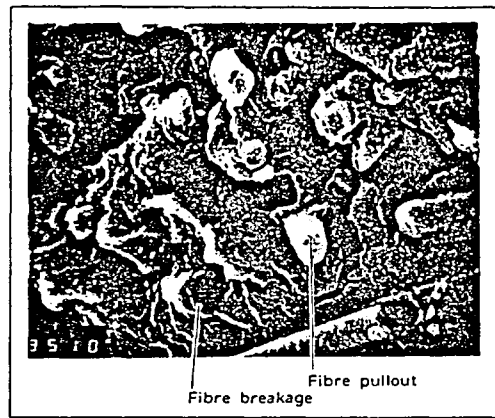Fig. 5 Theoretical strength predictions versus particle size (tensile loading)

predominates and [MPF] is applicable. Conversely, at larger particle sizes flake fracture predominates and [SRF] applies and between the two extremities, failure mechanism is a combination of flake fracture and flake pull-out. This is confirmed by microscopic and macroscopic examination of the fractures, which reveals partial flake pull-out and flake fracture. Fig. 6 presents a microscopic section showing both systems.

If the [MPF] is under consideration then a constant must also be employed such that Equation (7) becomes:

$$\sigma_c = \phi_f \tau_m \, [\text{MPF}] \, K + \phi_m \sigma''_m \qquad (14)$$

Combination of particle sizes

The production of a moulding from varying particle sizes produced mechanical properties based on a combination of the properties of the constituent particle sizes.

In the case of the two particle sizes examined, the mechanical properties are predicted by the application of 'rule-of-mixtures' theory, emphasizing satisfactory moulding techniques.

The 'monomunched' material produces mouldings that are very disappointing with respect to the modulus property. This is due to the fact that the base particle shape can be needle-like or rectangular, and the width is therefore considerably reduced. This lowers the value of the aspect ratio, decreasing the [MRF].

An apparent anomally observed in the property profile presented in Table 2 is the improved tensile strength of random-sized particles compared with the regular particle sized mouldings. It is suggested that this is due to a degree of interplanar reinforcement, promoted by the angular particles, which encourages a network of reinforcements within the moulding.

Table 2. Mechanical properties of APC-2 made from a combination of particle sizes

	Particle size					
	12.7–25.4 mm		Random		3 mm Random	
Flexural strength (MPa)	432.6	(2.6)	396.2	(41.2)	439.0	(41.8)
Flexural modulus (GPa)	34.3	(1.2)	31.0	(2.8)	33.5	(2.5)
Tensile strength (MPa)	200.1	(3.6)	215.9	(11.9)	215.6	(11.6)
Tensile modulus (GPa)	40.5	(1.6)	37.6	(2.1)	40.6	(2.3)
Tensile strain (%)	0.72	(0.14)	0.77	(0.03)	0.77	(0.09)
Compression strength (MPa)	395.0	(10.1)	382.0	(15.3)	423.3	(15.6)

(Standard deviations are given in parentheses)

CONCLUSIONS

The modulus of reclaimed APC-2 can be predicted by application of a Modulus Reduction Factor [MRF], but the strength is less predictable, and use of a defect factor must be made. This permits prediction of the strength provided that the mode of failure is observed, with flake pull-out predominating at small particle sizes and flake fracture becoming progressively more dominant as particle size increases.

REFERENCES

1 Rayson, H. W., McGrath, G. and Collyer, A. A. *Mechanical Properties of Reinforced thermoplastics* (Elsevier, Applied Science Publishers, 1986) Chapter 2
2 Kelly, A. and Davies, G. J. *Metal Reviews* 10 (1965) pp 1–77
3 Riley, V. R. 'Fibre/fibre interaction' *J Comp Mater* 2 (October 1968) pp 436–446
4 Turner. S) *Mechanical Testing of Plastics, 2nd Edition* (George Goodwin in association with The Plastics and Rubber Institute, 1983)
5 Sheldon, R. P. 'Composite Polymeric Materials' (Applied Science Publishers, 1982)
6 Hofer, B. et al 'Development of Engineering Data on Mechanical Properties of Advanced Composite Materials' *US Air Force Technical Report AFML-TR-72-205, Part 1* (September 1972)
7 Padawer, E. and Beecher, N. 'On the strength and stiffness of planar reinforced plastic resins' *Polym Eng Sci* 10 (May, 1970) pp 185–192

AUTHORS

Dr Clegg, to whom inquiries should be addressed, is with the Department of Metallurgy and Materials Science, University of Nottingham, University Park, Nottingham, NG7 2RD, UK.